The Dissertation Committee for Kyunghaeng Lee

certifies that this is the approved version of the following dissertation:

Impact of Fracture Creation and Growth on Well Injectivity and Reservoir Sweep during Waterflooding and Chemical EOR Processes

Committee:

Mukul M. Sharma, Supervisor

Chun Huh, Co-Supervisor

Gary A. Pope

Matthew T. Balhoff

Roger T. Bonnecaze

Impact of Fracture Creation and Growth on Well Injectivity and Reservoir Sweep during Waterflooding and Chemical EOR Processes

by

Kyunghaeng Lee, B.S.; M.S.E.

Dissertation

Presented to the Faculty of the Graduate School of

the University of Texas at Austin

in Partial Fulfillment

of the Requirements

for the Degree of

Doctor of Philosophy

The University of Texas at Austin

May 2012

Dedication

To my wife, Seung Hyun Bae, and my daughter, Cheny Lee,

who both supported me as ever in my studies

and

To my mother, Myung Sook Kang, my father, Jai Poong Lee, and all my other family,

for their devoted and endless love.

Acknowledgements

I would like to express my deepest gratitude to my supervisor, Dr. Mukul M. Sharma, for his continuous guidance and support throughout all these years. As a truly talented supervisor and professor, he allowed me to explore my academic potential and exposed me to the exciting world of research. I also would like to acknowledge Dr. Chun Huh, as my co-supervisor, for this warm-hearted guidance and sincere advice. His supervision over the last 5 years truly guided me to a right path, and encouraged me, especially during the difficult process of research. Dr. Gary A. Pope must also be acknowledged for his invaluable contribution to the understanding of polymer flooding, which is major part of my dissertation. Drs. Balhoff and Bonnecaze are also acknowledged for their constructive comments on fracturing and polymer flooding as committee members.

I am grateful to my fellow colleagues for their comments and suggestions: Sukkyoon Choi, Choongyoung Han, Myeonghwan Noh, Nam-Su Park, Hyun-Il Cho, and Hee-Jae Lee. Also, I want express my gratitude to Dr. Sharma's group members. I offer my special thanks to Jin Kyung Lee for her sincere support. Additionally, I would like to extend my gratitude to those who always supported and encouraged me: Hee-Song, Byungjoon, Jong-Soo, Kiyoul, Kyungwon, Yonghwee, Changmin, Hoonyoung, Hyun-Tae, Hyungjoo, Kwangjin, Dongkeun, Wonjin, and Youngwoong.

Impact of Fracture Creation and Growth on Well Injectivity and Reservoir Sweep during Waterflooding and Chemical EOR Processes

Kyunghaeng Lee, Ph.D.

The University of Texas at Austin, 2012

Supervisor: Mukul M. Sharma, Chun Huh

During waterflooding, or chemical EOR processes with polymers, fractures are frequently generated in injectors. This can have a profound impact on the process performance and reservoir management. A fracture growth model was developed and linked to a reservoir simulator that incorporates the effect of (i) particle plugging due to filtration of solids and oil droplets in the injected fluids; (ii) non-Newtonian polymer rheology (shear-thinning and -thickening) for polymer injection; and (iii) thermal stresses induced by cold water injection. Dynamic fracture growth, which results from the pore pressure increase due to particle plugging or complex polymer rheology, affects the well injectivity and reservoir sweep significantly. With the fracture growth model, simulations can be made not only to make more accurate reservoir sweep and oil recovery predictions, but also to help identify well patterns that may improve reservoir performance.

In homogeneous reservoirs, the injectivity is significantly affected by the propagation of an injection induced fracture; but the ultimate oil recovery and reservoir sweep are relatively unaffected. In multi-layered reservoirs, however, reservoir sweep and oil recovery are impacted significantly by the fracture growth. The oil recovery results from our fracture growth model differ substantially from those obtained based on the assumption of no fracture generation or a static fracture. For polymer injection processes, the shear rate dependence of the polymer viscosity is critical in determining the injectivity, fracture growth, and oil recovery.

In addition to vertical injection well fractures, horizontal injection well fractures have been simulated by using the fracture growth model. The reservoir stress distribution determines the fracture orientation near a horizontal well. When the minimum horizontal stress orientation is perpendicular to the horizontal injector, a longitudinal fracture is generated, while with the minimum horizontal stress orientation parallel to the injector, a transverse fracture is developed. The impact of static and dynamic transverse/longitudinal fractures on well injectivity and reservoir sweep has been investigated. The impacts of (i) lengths of horizontal injector and producer; (ii) location of water oil contact; (iii) sizes of transverse and longitudinal fractures; (iv) particle concentration in the water, were further investigated.

The well injectivity model was validated successfully by history matching injection of water (with particles) and shear rate dependent polymer injection. The history match was performed by adjusting the effective particle concentration in the injected water or the shear rate dependent polymer rheology. Based on history matching the long-

term injection rates and pressures, estimates of the fracture length were made. These fracture dimensions could not be independently measured and verified. Based on the simulation results recommendations were made for strategies for drilling well patterns, water quality and injection rates that will lead to better oil recovery.

Table of Contents

List of Tables xii

List of Figures xii

Chapter 1: Introduction 1

1.1 Background 1

1.2 Problem Statement 3

1.3 Research Objectives 4

1.4 Approach and Methodology 5

1.4.1 Development of Fracture Growth Model for Water and Polymer Injection 5

1.4.2 Simulation of Static Fractures with Water and Polymer Injection 6

1.4.3 Development of Model for Fracture Growth with Water Injection 6

1.4.4 Simulation of Polymer Injection EOR Processes with Fracture Growth 8

1.4.5 Simulation of Water and Polymer Injection with Horizontal Wells 9

1.4.6 Comparison with the Field Data 9

1.5 Outline of the Dissertation 10

Chapter 2: Models for Water and Polymer Injection 14

2.1 Introduction 14

2.2 Injection of Water with Particles 15

2.2.1 Particle Plugging in Porous Media 15

2.2.2 Particle Retention 15

2.2.3 Flow of Particle Suspensions in Porous Media 16

2.2.4 Permeability Reduction Model 19

2.3 Injection of Polymer 21

2.3.1 Power-law Model 21

2.3.2 Carreau Model 22

2.3.3 Unified Model 23

2.3.4 Effect of Polymer Concentration on Polymer Viscosity 26

2.3.5 Effect of Effective Salinity on Polymer Viscosity 28

2.4 Summary 28

Chapter 3: Water and Polymer Injection with Static Fractures 34
3.1 Introduction.....34
3.2 Reservoir Heterogeneity and Fracture Orientation.....35
3.3 Water Injection with Static Fracture in Single Layer 36
3.3.1 Injectivity Increase due to Static Fracture 36
3.3.2 Reservoir Sweep Efficiency due to Fracture 36
3.3.2.1 Effect of Mobility Ratio on Oil Recovery and Reservoir Sweep37
3.3.3 Water Breakthrough due to Static Fracture 39
3.4 Water Injection with Static Fracture in Two Layers.....40
3.4.1 Effect of Mobility Ratio.....40
3.5 Polymer Injection with Static Fracture in Single Layer.....52
3.6 Polymer Injection In Wells with Static Fracture in Two Layers 59
3.7 Summary.....61

Chapter 4: Water and Polymer Injectivity in Wells with Dynamic Fractures 122
4.1 Introduction.....122
4.2 Fracture Generation/Growth Mechanisms.....122
4.3 Water and Polymer Injection Wells with Dynamic Fracture In Single Layer133
4.4 Water and Polymer Injection Wells with Dynamic Fracture In Two Layers 136
4.5 Summary.....140

Chapter 5: Simulation of Water and Polymer Injection with Horizontal Wells.....160
5.1 Introduction.....160
5.2 Water Injection in Horizontal Wells with Static Transverse Fractures 161
5.3 Water Injection in Horizontal Wells with Static Longitudinal Fracture.....163
5.4 Water Injection in Horizontal Wells with Various Static Transverse Fracture Conductivities 165
5.5 Water Injection in Horizontal Wells with Various Longitudinal Fracture Conductivities 166
5.6 Dynamic Longitudinal Fracture with Horizontal Wells - Water Injection 168
5.7 Dynamic Transverse Fracture with Horizontal Wells, Different Fracture Conductivities – Water Injection 169
5.8 Sensitivity Study for Locations of Horizontal Injector and Producer.....169

5.9 Summary 174

Chapter 6: Comparison with the Field Data 203

6.1 Introduction 203

6.2 Comparison Of Field Data with Simulation Results 204

6.3 Shear Rate Dependent Polymer Injection in Brookshire Dome Field 210

6.3.1 Intoduction to the Field Data 211

6.3.2 Development of the Simulation Model 211

6.3.3 Screening Simulations before History Match 211

6.3.4 History Matching Simulations 214

6.4 Summary 217

Chapter 7: Conclusions and Recommendations for Future Work 240

7.1 Conclusion 240

7.2 Recommendations for Future Work 247

Abbreviations and Nomenclature 248

Bibliography 251

List of Tables

Table 3.1: Input data for water injection with static fracture 64

Table 3.2: Input data for water injection with static fracture 65

Table 3.3: Input data for water injection with static fracture 66

Table 3.4: Input data for water injection with static fracture 67

Table 3.5: Impact of fracture and particles in the water on oil recovery 67

Table 3.6: Input data for polymer injection to estimate polymer injectivity 68

Table 4.1: Input parameters for effective stress calculation 142

Table 4.2: Input parameters for fracture growth simulation 143

Table 5.1: Input data for water injection with static fracture 176

Table 5.2: Impact of transverse fractures on well injectivity and oil recovery with constant injection BHP constraint (4,500 psi) 177

Table 5.3: Impact of transverse fractures on well injectivity and oil recovery with constant injection rate constraint (30,000 bbl/D).....177

Table 5.4: Impact of longitudinal fractures on well injectivity and oil recovery with constant injection BHP constraint (4,500 psi) 177

Table 5.5: Impact of longitudinal fractures on well injectivity and oil recovery with constant injection rate constraint (30,000 bbl/D).....178

Table 5.6: Impact of transverse fracture conductivity on well injectivity and oil recovery with constant injection BHP constraint (4,500 psi) 178

Table 5.7: Impact of transverse fracture conductivity on well injectivity and oil recovery with constant injection BHP constraint (4,500 psi) 178

Table 5.8: Impact of longitudinal fracture conductivity on well injectivity and oil recovery with constant injection BHP constraint (4,500 psi) 179
Table 5.9: Impact of longitudinal fracture conductivity on well injectivity and oil recovery with constant injection BHP constraint (4,500 psi) 179
Table 6.1: Reservoir properties for history matching 219
Table 6.2: Input well properties for Brookshire Dome Field.....219
Table 6.3: Reservoir permeabilities in Brookshire Dome Field 219

List of Figures

Figure 1.1: Flowchart of tasks for impact of injection well fractures on well injectivity and reservoir sweep during waterflooding and chemical EOR processes 12

Figure 1.2: Flowchart of fracture growth model 13

Figure 2.1: Particle plugging in a fractured injection well, particle concentration 20 ppm, initial porosity 0.2, initial permeability 100 md, injection rate 100 bbl/D 30

Figure 2.2: Porosity decreases after particle plugging in a fractured injection well, particle concentration 20 ppm, initial porosity 0.2, initial permeability 100 md, injection rate 100 bbl/D, fracture permeability 100 D.....30

Figure 2.3: Permeability decreases after particle plugging in a fractured injection well, particle concentration 20 ppm, initial porosity 0.2, initial permeability 100 md, injection rate 100 bbl/D, fracture permeability 100 D.....31

Figure 2.4: Effect of injected particle concentration on injection BHP for un-fractured wells, initial porosity 0.3, initial permeability 500 md, and injection rate 100 bbl/D 31

Figure 2.5: Effect of injected particle concentration on injectivity for un-fractured wells, initial porosity 0.3, initial permeability 500 md, injection rate 100 bbl/D ...32

Figure 2.6: Shear rate dependent polymer viscosity, power-law polymer $\mu = 70\gamma^{0.3}$, unified model, and Carreau model: Flopaam 3330S polymer viscosity vs. shear rate (1500 ppm; 1.6 % NaCl; 25ºC) 32

Figure 2.7: Shear rate dependent polymer viscosity with various polymer concentration, unified model: Flopaam 3330S polymer viscosity vs. shear rate (1500 ppm; 1.6 % NaCl; 25ºC) 33

Figure 2.8: Shear rate dependent polymer viscosity with various polymer concentration, Carreau model: Flopaam 3330S polymer viscosity vs. shear rate (1500 ppm; 1.6 % NCl; 25ºC) 33
Figure 3.1: Five-spots geometry – (a) Favorable and (b) unfavorable orientation.....69
Figure 3.2: Impact of static fracture during water injection on injectivity 69
Figure 3.3: Impact of static fracture during water injection on injectivity ratio.....70
Figure 3.4: Water saturation with fractured reservoir after 13 months, favorable direction70
Figure 3.5: Water saturation with un-fractured reservoir after 13 months, favorable direction 71
Figure 3.6: Water saturation with fractured reservoir after 23 months, favorable direction71
Figure 3.7: Water saturation with fractured reservoir after 23 months, favorable direction72
Figure 3.8: Water breakthrough with fractured and un-fractured reservoirs (favorable mobility ratio), injected fluid viscosity 30 cp, and oil viscosity 10 cp 72
Figure 3.9: Oil recovery with fractured and un-fractured reservoirs (favorable mobility ratio), injected fluid viscosity 30 cp, and oil viscosity 10 cp.....73
Figure 3.10: Water breakthrough with fractured and un-fractured reservoirs (unfavorable mobility ratio), injected fluid viscosity 1cp, oil viscosity 10 cp.....73
Figure 3.11: Oil recovery with fractured and un-fractured reservoirs (unfavorable mobility ratio), injected fluid viscosity 1 cp, oil viscosity 10 cp.....74
Figure 3.12: Oil recovery of un-fractured reservoirs with various mobility ratios.....74
Figure 3.13: Oil recovery with various fracture length, water viscosity 1cp, oil viscosity 30 cp.....75
Figure 3.14: Water cut with various fracture lengths, water viscosity 1cp, oil viscosity 30 cp.....75
Figure 3.15: Oil recovery with various injected fluid viscosities without fracture 76

Figure 3.16: Water Cut with various injected fluid viscosities without fracture 76
Figure 3.17: Impact of mobility ratio on flow allocation into fractured layer 77
Figure 3.18: Impact of mobility ratio and fracture on cumulative oil production 77
Figure 3.19: Impact of mobility ratio on oil recovery 78
Figure 3.20: Oil recovery for fractured and un-fractured cases (*Case 1.1*) 78
Figure 3.21: Flow allocation into the fractured and un-fractured layers in the fractured reservoir (*Case 1.1*).....79
Figure 3.22: Water cut for fractured and un-fractured cases (*Case 1.1*).....79
Figure 3.23: Water cut for the fractured and un-fractured layers in the fractured reservoir case (*Case 1.1*) 80
Figure 3.24: Oil recovery for fractured and un-fractured cases (*Case 1.2*) 80
Figure 3.25: Flow allocation into the fractured and un-fractured layers in the fractured reservoir (*Case 1.2*).....81
Figure 3.26: Water cut for fractured and un-fractured cases (*Case 1.2*).....81
Figure 3.27: Water cut for the fractured and un-fractured layers in the fractured reservoir case (*Case 1.2*) 82
Figure 3.28: Oil recovery for fractured and un-fractured cases (*Case 1.3*) 82
Figure 3.29: Flow allocation into the fractured and un-fractured layers in the fractured reservoir (*Case 1.3*).....83
Figure 3.30: Water cut for fractured and un-fractured cases (*Case 1.3*).....83
Figure 3.31: Water cut for fractured and un-fractured layers in the fractured reservoir case (*Case 1.3*) 84
Figure 3.32: Oil recovery for fractured and un-fractured cases (*Case 1.4*) 84
Figure 3.33: Water cut for fractured and un-fractured cases (*Case 1.4*).....85
Figure 3.34: Oil recovery for fractured and un-fractured cases (*Case 1.5*) 85

Figure 3.35: Flow allocation into the fractured and un-fractured layers in the fractured reservoir (*Case 1.5*)....86
Figure 3.36: Water cut for fractured and un-fractured cases (*Case 1.5*)....86
Figure 3.37: Water cut for the fractured and un-fractured layers in the fractured reservoir case (*Case 1.5*)....87
Figure 3.38: Oil recovery for fractured and un-fractured cases (*Case 1.6*)....87
Figure 3.39: Flow allocation into the fractured and un-fractured layers in the fractured reservoir (*Case 1.6*)....88
Figure 3.40: Water cut for fractured and un-fractured cases (*Case 1.6*)....88
Figure 3.41: Oil recovery for fractured and un-fractured cases (*Case 2.1*)....89
Figure 3.42: Flow allocation into the fractured and un-fractured layers in the fractured reservoir (*Case 2.1*)....89
Figure 3.43: Water cut for fractured and un-fractured cases (*Case 2.1*)....90
Figure 3.44: Water cut for the fractured and un-fractured layers in the fractured reservoir case (*Case 2.1*)....90
Figure 3.45: Oil recovery for fractured and un-fractured cases (*Case 2.2*)....91
Figure 3.46: Flow allocation into the fractured and un-fractured layers in the fractured reservoir (*Case 2.2*)....91
Figure 3.47: Water cut for fractured and un-fractured cases (*Case 2.2*)....92
Figure 3.48: Water cut for the fractured and un-fractured layers in the fractured reservoir case (*Case 2.2*)....92
Figure 3.49: Oil recovery for fractured and un-fractured cases (*Case 2.3*)....93
Figure 3.50: Flow allocation into the fractured and un-fractured layers in the fractured reservoir (*Case 2.3*)....93
Figure 3.51: Water cut for fractured and un-fractured cases (*Case 2.3*)....94

Figure 3.52: Water cut for the fractured and un-fractured layers in the fractured reservoir case (*Case 2.3*) 94
Figure 3.53: Oil recovery for fractured and un-fractured cases (*Case 2.4*) 95
Figure 3.54: Flow allocation into the fractured and un-fractured layers in the fractured reservoir (*Case 2.4*) 95
Figure 3.55: Water cut for fractured and un-fractured cases (*Case 2.4*) 96
Figure 3.56: Water cut for the fractured and un-fractured layers in the fractured reservoir case (*Case 2.4*) 96
Figure 3.57: Oil recovery for fractured and un-fractured cases (*Case 2.5*) 97
Figure 3.58: Flow allocation into the fractured and un-fractured layers in the fractured reservoir (*Case 2.5*) 97
Figure 3.59: Water cut for fractured and un-fractured cases (*Case 2.5*) 98
Figure 3.60: Water cut for the fractured and un-fractured layers in the fractured reservoir case (*Case 2.5*) 98
Figure 3.61: Oil recovery for fractured and un-fractured cases (*Case 2.6*) 99
Figure 3.62: Flow allocation into the fractured and un-fractured layers in the fractured reservoir (*Case 2.6*) 99
Figure 3.63: Water cut for fractured and un-fractured cases (*Case 2.6*) 100
Figure 3.64: Water cut for the fractured and un-fractured layers in the fractured reservoir case (*Case 2.6*) 100
Figure 3.65: Injectivity with different power-law n values and injection rate, without fracture 101
Figure 3.66: Injectivity with different power-law n values and fracture conductivity 101
Figure 3.67: Injectivity of power-law fluid $\mu = 70\gamma^{-0.5}$, injection rate and fracture length 102

Figure 3.68: Injectivity of Newtonian fluid (70 cp) with different fracture conductivity and fracture length 102
Figure 3.69: Injectivity of power-law fluid $\mu = 70\gamma^{0.5}$ with different fracture conductivity and fracture length 103
Figure 3.70: Injectivity of power-law, Newtonian, and unified model with different injection rate and without fracture 103
Figure 3.71: Injectivity of unified model with different injection rate and fracture length104
Figure 3.72: Injectivity of unified model with different injection rate and without fracture104
Figure 3.73: Injectivity of unified model with different injection rate and 124 ft fracture105
Figure 3.74: Injectivity of unified model with different injection rate and 384 ft, 544 ft, 704 ft fractures 105
Figure 3.75: Injectivity of unified model with different injection rate and fracture conductivity, and 124 ft fracture length 106
Figure 3.76: Injectivity of unified model with different injection rate and fracture conductivity, and 384 ft fracture length 106
Figure 3.77: Relation between injection rate and shear rate with power-law different flow behavior index n values and unified model, un-fractured reservoir 107
Figure 3.78: Relation between injection rate and shear rate with power-law different flow behavior index n values and unified model, $L/r_e = 0.12$.....107
Figure 3.79: Relation between injection rate and shear rate with different fracture length, power-law fluid $\mu = 70\gamma^{-0.5}$ 108
Figure 3.80: Relation between injection rate and polymer viscosity with different fracture length, power-law fluid $\mu = 70\gamma^{0.5}$ 108
Figure 3.81: Relation between injection rate and shear rate, un-fractured case, unified model, Flopaam 3330S polymer (1,500 ppm; 1.6% NaCl; 25 ºC) 109

Figure 3.82: Injectivity of Newtonian, power-law, Viscoelastic model, injection rate = 500 bbl/D, without fracture, Newtonian model viscosity 70 cp, power-law model viscosity $\mu = 70\gamma^{0.5}$, unified model, Flopaam 3330S polymer (1,500 ppm; 1.6% NaCl; 25 ºC) 109

Figure 3.83: Injectivity of Newtonian, power-law, Viscoelastic model, injection rate = 500 bbl/D, fracture length 384 ft, Newtonian model viscosity 70 cp, power-law model viscosity $\mu = 70\gamma^{0.5}$, unified model, Flopaam 3330S polymer (1,500 ppm; 1.6% NaCl; 25 ºC).....110

Figure 3.84: Injectivity of Newtonian, power-law, Viscoelastic model, injection rate = 1,000 bbl/D, without fracture, Newtonian model viscosity 70 cp, power-law model viscosity $\mu = 70\gamma^{0.5}$, unified model, Flopaam 3330S polymer (1,500 ppm; 1.6% NaCl; 25 ºC) 110

Figure 3.85: Injectivity of Newtonian, power-law, Viscoelastic model, injection rate = 1,000 bbl/D, fracture length 384 ft, Newtonian model viscosity 70 cp, power-law model viscosity $\mu = 70\gamma^{0.5}$, unified model, Flopaam 3330S polymer (1,500 ppm; 1.6% NaCl; 25 ºC).....111

Figure 3.86: Oil recovery for fractured and un-fractured cases (*Case 3.1*), unified model Flopaam 3330S polymer (1,500 ppm; 1.6% NaCl; 25 ºC) 111

Figure 3.87: Flow allocation into the fractured and un-fractured layers in the fractured reservoir (*Case 3.1*), unified model Flopaam 3330S polymer (1,500 ppm; 1.6% NaCl; 25 ºC) 112

Figure 3.88: Water cut for fractured and un-fractured cases (*Case 3.1*), unified model Flopaam 3330S polymer (1,500 ppm; 1.6% NaCl; 25 ºC) 112

Figure 3.89: Water cut for the fractured and un-fractured layers in the fractured reservoir case (*Case 3.1*), unified model Flopaam 3330S polymer (1,500 ppm; 1.6% NaCl; 25 ºC).....113
Figure 3.90: Oil recovery for fractured and un-fractured cases (*Case 3.2*), unified model Flopaam 3330S polymer (1,500 ppm; 1.6% NaCl; 25 ºC) 113
Figure 3.91: Flow allocation into the fractured and un-fractured layers in the fractured reservoir (*Case 3.2*), unified model Flopaam 3330S polymer (1,500 ppm; 1.6% NaCl; 25 ºC) 114
Figure 3.92: Water cut for fractured and un-fractured cases (*Case 3.2*), unified model Flopaam 3330S polymer (1,500 ppm; 1.6% NaCl; 25 ºC) 114
Figure 3.93: Water cut for the fractured and un-fractured layers in the fractured reservoir case (*Case 3.2*), unified model Flopaam 3330S polymer (1,500 ppm; 1.6% NaCl; 25 ºC).....115
Figure 3.94: Oil recovery for fractured and un-fractured cases (*Case 3.3*), unified model Flopaam 3330S polymer (1,500 ppm; 1.6% NaCl; 25 ºC) 115
Figure 3.95: Flow allocation into the fractured and un-fractured layers in the fractured reservoir (*Case 3.3*), unified model Flopaam 3330S polymer (1,500 ppm; 1.6% NaCl; 25 ºC) 116
Figure 3.96: Water cut for fractured and un-fractured cases (*Case 3.3*), unified model Flopaam 3330S polymer (1,500 ppm; 1.6% NaCl; 25 ºC) 116
Figure 3.97: Water cut for the fractured and un-fractured layers in the fractured reservoir case (*Case 3.3*), unified model Flopaam 3330S polymer (1,500 ppm; 1.6% NaCl; 25 ºC).....117
Figure 3.98: Oil recovery for fractured and un-fractured cases (*Case 3.4*), unified model Flopaam 3330S polymer (1,500 ppm; 1.6% NaCl; 25 ºC) 117

Figure 3.99: Flow allocation into the fractured and un-fractured layers in the fractured reservoir (*Case 3.4*), unified model Flopaam 3330S polymer (1,500 ppm; 1.6% NaCl; 25 ºC) 118
Figure 3.100: Water cut for fractured and un-fractured cases (*Case 3.4*), unified model Flopaam 3330S polymer (1,500 ppm; 1.6% NaCl; 25 ºC) 118
Figure 3.101: Water cut for the fractured and un-fractured layers in the fractured reservoir case (*Case 3.4*), unified model Flopaam 3330S polymer (1,500 ppm; 1.6% NaCl; 25 ºC) 119
Figure 3.102: Oil recovery for fractured and un-fractured cases (*Case 3.5*), unified model Flopaam 3330S polymer (1,500 ppm; 1.6% NaCl; 25 ºC) 119
Figure 3.103: Flow allocation into the fractured and un-fractured layers in the fractured reservoir (*Case 3.5*), unified model Flopaam 3330S polymer (1,500 ppm; 1.6% NaCl; 25 ºC) 120
Figure 3.104: Water cut for fractured and un-fractured cases (*Case 3.5*), unified model Flopaam 3330S polymer (1,500 ppm; 1.6% NaCl; 25 ºC) 120
Figure 3.105: Water cut for the fractured and un-fractured layers in the fractured reservoir case (*Case 3.5*), unified model Flopaam 3330S polymer (1,500 ppm; 1.6% NaCl; 25 ºC) 121
Figure 4.1: Fracture growth mechanism during water and polymer injection 144
Figure 4.2: Effective stress distribution with fluid temperature 175 ºF, particle concentration 20 ppm, injection rate 900 bbl/D, reservoir temperature 175 ºF 145
Figure 4.3: Effective stress distribution with fluid temperature 75 ºF, particle concentration 20 ppm, injection rate 900 bbl/D, reservoir temperature 175 ºF 146

Figure 4.4: Effective stress distribution with different injection fluid temperature, particle concentration 20 ppm, injection rate 900 bbl/D, reservoir temperature 175 ºF 146
Figure 4.5: Fracture length with different injection fluid temperature, particle concentration 20 ppm, injection rate 900 bbl/D, reservoir temperature 175 ºF 147
Figure 4.6: Oil recovery for fractured and un-fractured cases (*Case 4.1*) 147
Figure 4.7: Water cut for fractured and un-fractured cases (*Case 4.1*).....148
Figure 4.8: Injectivity for fractured and un-fractured cases (*Case 4.1*).....148
Figure 4.9: Oil recovery for fractured and un-fractured cases (*Case 4.2*), unified model, Flopaam 3330S polymer (1,500 ppm; 1.6% NaCl; 25 ºC) 149
Figure 4.10: Injection BHP for fractured and un-fractured cases (*Case 4.2*), unified model, Flopaam 3330S polymer (1,500 ppm; 1.6% NaCl; 25 ºC) 149
Figure 4.11: Water cut for fractured and un-fractured cases (*Case 4.2*), unified model, Flopaam 3330S polymer (1,500 ppm; 1.6% NaCl; 25 ºC) 150
Figure 4.12: Injectivity for fractured and un-fractured cases (*Case 4.2*), unified model, Flopaam 3330S polymer (1,500 ppm; 1.6% NaCl; 25 ºC) 150
Figure 4.13: Relation between shear rate and polymer viscosity (*Case 4.2*), unified model, Flopaam 3330S polymer (1,500 ppm; 1.6% NaCl; 25 ºC) 151
Figure 4.14: Oil recovery for fractured and un-fractured cases (*Case 5.1*) 151
Figure 4.15: Flow Allocation for fractured and un-fractured layers (*Case 5.1*) 152
Figure 4.16: Water Cut for fractured and un-fractured cases (*Case 5.1*).....152
Figure 4.17: Water Cut for fractured and un-fractured layers (*Case 5.1*).....153
Figure 4.18: Injectivity for fractured and un-fractured cases (*Case 5.1*).....153
Figure 4.19: Oil recovery for polymer and water injection cases (*Case 6.1*) 154

Figure 4.20: Water Cut for polymer and water injection cases (*Case 6.1*).....154
Figure 4.21: Oil recovery for fractured and un-fractured cases (*Case 7.1*) 155
Figure 4.22: Flow allocation for fractured and un-fractured layers (*Case 7.1*) 155
Figure 4.23: Water cut for fractured and un-fractured cases (*Case 7.1*).....156
Figure 4.24: Water cut for fractured and un-fractured layers (*Case 7.1*) 156
Figure 4.25: Injectivity for fractured and un-fractured cases (*Case 7.1*).....157
Figure 4.26: Oil recovery for fractured and un-fractured cases (*Case 8.1*), unified model, Flopaam 3330S polymer (1,500 ppm; 1.6% NaCl; 25 ºC) 157
Figure 4.27: Flow allocation for fractured and un-fractured layers (*Case 8.1*), unified model, Flopaam 3330S polymer (1,500 ppm; 1.6% NaCl; 25 ºC) 158
Figure 4.28: Water cut for fractured and un-fractured cases (*Case 8.1*), unified model, Flopaam 3330S polymer (1,500 ppm; 1.6% NaCl; 25 ºC) 158
Figure 4.29: Water cut for fractured and un-fractured layers (*Case 8.1*), unified model, Flopaam 3330S polymer (1,500 ppm; 1.6% NaCl; 25 ºC) 159
Figure 4.30: Injectivity for fractured and un-fractured layers (*Case 8.1*), unified model, Flopaam 3330S polymer (1,500 ppm; 1.6% NaCl; 25 ºC) 159
Figure 6.1: Relative permeability curves for water and oil 220
Figure 6.2: Shear rate dependent polymer viscosity, unified model: Flopaam 3330S polymer viscosity vs. shear rate (1500 ppm; 1.6 % NaCl; 25 ºC) 220
Figure 6.3: Field data comparison with simulated results of Well #1 221
Figure 6.4: Field data (Injectivity) comparison with simulated results of Well #1 221
Figure 6.5: Field data comparison with simulated results of Well #2 222
Figure 6.6: Field data (Injectivity) comparison with simulated results of Well #2 222
Figure 6.7: Field data comparison with simulated results of Well #3 223
Figure 6.8: Field data (Injectivity) comparison with simulated results of Well #3 223

Figure 6.9: Field data comparison with simulated results of Well #4 224
Figure 6.10: Field data (Injectivity) comparison with simulated results of Well #4 224
Figure 6.13: Relation between shear rate and polymer viscosity, unified polymer model: Flopaam 3330S polymer viscosity vs. shear rate (1500 ppm; 1.6 % NaCl; 25 ºC) 226
Figure 6.14: Injectivity with different injection rate, unified polymer model: Flopaam 3330S polymer viscosity vs. shear rate (1500 ppm; 1.6 % NaCl; 25 ºC) ...226
Figure 6.15: Injectivity with different injection rate with/without fracture growth, unified polymer model: Flopaam 330S polymer viscosity vs. shear rate (1500 ppm; 1.6 % NaCl; 25 ºC) 227
Figure 6.16: Fracture growth during water and polymer injection, unified polymer model: Flopaam 330S polymer viscosity vs. shear rate (1500 ppm; 1.6 % NaCl; 25 ºC) 227
Figure 6.17: Injectivity decline during water and polymer injection, unified polymer model: Flopaam 3330S polymer viscosity vs. shear rate (1500 ppm; 1.6 % NaCl; 25 ºC).....228
Figure 6.18: Injection BHP increase during water and polymer injection, unified polymer model: Flopaam 3330S polymer viscosity vs. shear rate (1500 ppm; 1.6 % NaCl; 25 ºC).....228
Figure 6.19: Shear rate dependent polymer viscosity with different temperature and shear rate.....229
Figure 6.20: Shear rate dependent polymer viscosity with different temperature and shear rate.....229
Figure 6.21: Well Head Pressure with various perforation densities.....230
Figure 6.22: Impact of shear rate coefficient on well head pressure 230

Figure 6.23: Impact of shear rate coefficient on polymer viscosity 231
Figure 6.24: Tubing head pressure and injection rate during polymer injection with difference C value and fracture.....231
Figure 6.25: Impact of reservoir thickness on well head pressure.....232
Figure 6.26: Impact of shear rate coefficient, perforation density, and reservoir thickness.....232
Figure 6.27: Grid block refinement near injector 233
Figure 6.28: Impact of grid block refinement on injection BHP 233
Figure 6.29: Impact of grid block refinement on well injectivity during polymer injection.....234
Figure 6.30: Impact of grid block size on polymer injection rate.....234
Figure 6.31: Impact of grid block size on well injectivity during polymer injection 235
Figure 6.32: Impact of grid block size and shear rate coefficient on well injectivity during polymer injection.....235
Figure 6.33: Injection Rate and well head pressure field data.....236
Figure 6.34: Polymer concentration profile in Brookshire field.....236
Figure 6.35: Shear rate dependent polymer viscosity with different polymer concentration.....237
Figure 6.36: Well head pressure with different grid block sizes 237
Figure 6.37: Polymer viscosity near injector with different grid block sizes 238
Figure 6.38: Wellhead pressure with different shear rate coefficients 238
Figure 6.39: Wellhead pressure with different polymer concentrations.....239

Chapter 1: Introduction

After the primary production of oil which generally can recover only about 10~20% of original oil in place, all subsequent oil production relies on injection of water or other fluids through a wellbore into the reservoir. The understanding of the rock–fluid interactions and their dynamics at and near the wellbore is, therefore, critically important. The purpose of this dissertation is twofold: (a) to model injection-induced fractures that may propagate during water or polymer injection and implement it in a reservoir simulator; and (b) to investigate the impact of injection well fractures on well injectivity and reservoir sweep during waterflooding and polymer EOR processes. The fracture growth model developed in this dissertation enables us to estimate the dimensions of the fracture in injection wells during injection of water and polymer, thereby allowing the optimization of injection conditions that maximize reservoir sweep and oil recovery.

1.1 BACKGROUND

Water injection has been widely used to maintain reservoir pressure and to displace oil (Eduin *et al.*, 2007, Genbao *et al.*, 2000; Hustedt *et al.*, 2005; Suri and Sharma, 2007) and polymer injection is increasingly employed as a low-cost method of recovery bypassed oil from un-swept zones (Demin *et al.*, 2000; Fulin and Xizhi, 2004; Huifen *et al.*, 2001; Van den Hoek *et al.*, 1996; Sorbie, 1991; Vossoughi, 2000; Zerpa *et al.*, 2005). During the water injection process, pore plugging caused by suspended solids and oil droplets in the injected water leads to a decline in well injectivity (Pang and

Sharma, 1997; Sharma *et al.*, 1997). During the polymer flooding, its injectivity can decrease because of increased fluid viscosity and also because high flow velocity near injectors may cause the polymer to shear-thicken (Delshad *et al.*, 2008). With injectivity decline during water/polymer injection, an increased injection pressure is required to maintain a given injection rate. If the increased injection pressure exceeds a certain minimum rock stress condition around the wellbore, fractures are initiated (Azeemuddin *et al.*, 2002; Gadde and Sharma, 2001; Ji *et al.*, 2004). In cases where the well has been fractured, the injection of water with fines over extended periods of time or the injection of polymer which shows high viscosity near the injector due to shear-thickening, causes the bottom-hole pressure (BHP) to increase above the formation breakdown pressure and extends the existing fracture. If the temperature of the injected fluid is different from that of the formation, a thermal front propagates from the injection well. This change in temperature causes the rock to contract or expand, thereby altering the stresses both in the region of changed temperature and in the surrounding rock (Perkins and Gonzalez, 1995). For example, injection of cold water into a high temperature reservoir can induce thermal stress, thereby reducing the minimum horizontal stress, which facilitates fracturing. The above three processes – pore plugging, high polymer viscosity and changes in temperature of the rock – are the main mechanisms that drive injection well fractures. This thesis addresses how the above three mechanisms influence the fracture generation, and in turn, how the fracture influences the oil recovery process.

1.2 PROBLEM STATEMENT

When a fracture develops at the injection wellbore, an accurate understanding of its development is important because the extent of fracture growth and its orientation significantly affects the sweep efficiency and oil recovery for a given well pattern. In a reservoir with complicated well patterns, optimizing the fracture growth and its orientation is, therefore, essential in maximizing the oil recovery. Appropriate selection of an injection rate and accurate knowledge of particle concentration in the water, polymer rheology, and temperature of the injected fluid, are key factors that determine the fracture growth dynamics, and knowledge of them thereby allows for specification of optimum well injection patterns to maximize oil recovery.

An accurate oil recovery simulation, therefore, requires a detailed description of fracture growth during water and polymer injection. However, there has not yet been any reservoir simulator that explicitly considers “dynamic” fracture growth during waterflood or EOR processes, even though most available simulators are capable of simulating a static fracture in the reservoir. Because a fracture may grow continuously as water and polymer are injected, a proper mechanistic consideration of the fracture growth is necessary for a more accurate reservoir simulation.

Developing a mechanistic model that accounts explicitly for the fracture growth in a reservoir simulator during water and polymer injection is the initial focus of this research. The model is then implemented into a reservoir simulator, so that dynamic growth of fractures and changes in fracture orientation can be calculated during the oil displacement simulations. This allows us to evaluate the impacts of different parameters such as well patterns, complex well trajectories and injection rates on oil recovery.

The fracture growth during water and polymer injection was investigated for fractures in both vertical and horizontal wells. Different fracture geometries with horizontal wells, transverse and longitudinal fractures were investigated under static and dynamic fracture conditions. For the case of induced transverse fracture, the impact of the number of the transverse fractures was investigated.

1.3 RESEARCH OBJECTIVES

The primary objective of this research is to determine the impact of fractures in vertical and horizontal wells on oil recovery by waterflooding and chemical EOR processes that use polymer. To that end, we developed the fracture growth model and linked to a reservoir simulator, so that the physics of fracture growth can be modeled accurately during simulation. This model incorporates the effects of (i) particle plugging due to solids and oil droplets in the injected fluid, (ii) non-Newtonian polymer rheology; and (iii) thermal stress induced by fluid injection.

The results of the research provide an improved understanding of the impact of dynamically growing injection well fractures. Simulations also help to identify conditions under which certain well geometry/placement, and controlled fracture generation, can enhance oil production in waterflooding and polymer-based EOR processes.

By carrying out process evaluation simulations with this fracture growth model, the role played by the injected fluid properties, and reservoir properties such as pressure,

porosity, permeability and stress distribution, can be predicted, which may optimize the injection conditions to maximize reservoir sweep and oil recovery.

1.4 APPROACH AND METHODOLOGY

To successfully accomplish the above research objectives, a detailed workflow was designed, as shown in **Figure 1.1**. The research is carried out in six broad categories: (1) development of the fracture growth model for water and polymer injection, and the model linkage to a reservoir simulator; (2) simulation of a static fracture with water and polymer injection; (3) simulation of water injection with the fracture growth model; (4) simulation of polymer injection processes with the fracture growth model; (5) simulation of water and polymer injection with horizontal wells; and (6) comparison of simulation results with the field data.

1.4.1 Development of Fracture Growth Model for Water and Polymer Injection

When water or polymer is injected into the reservoir, a fracture may be generated because the minute particles dispersed in the injection water plug the formation; or because polymer shear-thickens during polymer injection. Particle plugging during water injection reduces porosity and permeability, which causes the BHP to increase. Also, because of the shear-thickening behavior of polymers at high flow velocity, the pressure near the injector may increase sharply during polymer injection. The injection well fractures due to these two factors are first modeled with the appropriate consideration of pore pressure increase and the accordant changes in rock stress.

1.4.2 Simulation of Static Fractures with Water and Polymer Injection

In order to gain preliminary insight on the impact of a fracture on reservoir performance, the first set of simulations were conducted in simple reservoir patterns such as a five-spots or inverted five-spots with both un-fractured and statically fractured injectors. Simple waterflooding and polymer flooding were considered with representative process and reservoir model parameters. The oil recovery and the injectivity were compared for various cases as a function of fracture orientation, fracture length, and other relevant reservoir and fluids properties

1.4.3 Development of Model for Fracture Growth with Water Injection

After the above preliminary tasks are completed, a method for simulating dynamic fracture growth in a reservoir simulator was developed. The detailed strategy for allowing a reservoir simulator to simulate fracture growth is shown in **Figure 1.2**. Based on the initial rock stress distribution prescribed and pore pressure distribution calculated by the reservoir simulator for a given time step, the incremental fracture growth length and orientation near injector is calculated using the fracture growth model. This new module communicates with the reservoir simulator through an interface. This interface allows the simulator to calculate and provide the key input parameters for the module such as the reservoir permeability change due to increasing pore pressure and decreasing effective stress. The updated set of grid block properties such as permeability and porosity due to fracture growth is then used to simulate the fluid flow distribution for the next time step in the reservoir simulator. For the case of water injection with suspended particles, the fracture growth is driven by the new particle deposition near the new

fracture tip and face. In the case of polymer injection, increased viscosity near the fracture tip and face because of its shear rate dependence generates the fracture and makes it grow. The different fluid temperature altered the rock stress due to change of reservoir temperature, which accelerates or delays the fracture generation and growth.

Such modifications of the reservoir and fluids properties are applied to heterogeneous reservoirs that undergo waterflood and polymer flood processes. A reservoir with heterogeneous rock stress distribution could produce different fracture orientation, length and width in each layer. When different layers of a reservoir have different extents of fracture generation, the fluid injectivity and the degree of reservoir sweep in each layer will change with time. For oil recovery prediction for a heterogeneous reservoir, the dynamic fracture growth for each layer is calculated with the developed fracture growth model for a more accurate simulation of oil recovery. Unlike current reservoir simulators which consider static fractures only, the new simulation option implemented in this manner accounts for the effects of the growing fracture with different reservoir properties in each layer.

After completing the reservoir simulator integration, a detailed investigation is conducted to obtain the optimum fracture length and orientation. Also, the optimum location of injectors and producers during the water and polymer injection is considered to exploit fracture generation and growth for improved oil recovery. The variables that are altered for the optimization study include injection rate, concentration of solids in the injected water, and temperature of injected fluid. The fracture growth rate is a function of injection rate, temperature of injected fluid and concentration of solids in the injected water. Fracture orientation can be changed by altering the location of producers. Water is

injected at various temperatures, and a sensitivity study for injection water temperature is conducted.

A comparison between vertical and horizontal wells is performed for various reservoir geometries. Fracture growth in both types of wells is studied to determine when it may be appropriate to fracture these injection wells. The possibility of optimizing well spacing and well pattern for maximum reservoir sweep and injectivity is demonstrated with simulation examples.

1.4.4 Simulation of Polymer Injection EOR Processes with Fracture Growth

Chemical EOR processes that employ a polymer for mobility control have been simulated in order to study the impact of fractures with polymer injection. The shear rate dependent viscosity of the polymer during its injection is fully incorporated in the new fracture growth model. The effects – especially shear-thinning and shear-thickening behaviors of polymer viscosity – are investigated to simulate more accurately the pore pressure and rock stress distribution near the injection well during polymer injection. Both static and dynamic fractures during polymer injection are studied to see how oil recovery and reservoir sweep can be maximized. It is expected that the oil recovery with the fractured injection wells yields results significantly different from the cases where fractures are not present. Accordingly, by giving flexibility to the injection conditions for the injected polymer, the mobility condition in the reservoir could potentially altered for improved benefit. This research is the first systematic polymer-injection simulation study that accounts for fracture generation and growth near injectors.

1.4.5 Simulation of Water and Polymer Injection with Horizontal Wells

Horizontal wells are now more commonly used to inject both water and chemicals into reservoirs (Suri and Sharma, 2009). We carried out our study of polymer injection, as well as water injection, by investigating the role of horizontal well trajectories on oil recovery efficiency. It is shown that significant acceleration of oil production can be accomplished by using a combination of horizontal wells and hydraulic fractures. **Figure 1.3** shows an example of a wellbore geometry that takes advantage of combining horizontal wells with hydraulic fractures to significantly accelerate the oil production from reservoirs in both waterflooding and polymer flooding processes.

1.4.6 Comparison with the Field Data

The simulation results from the combined model were compared with results obtained from polymer flooding pilots conducted in the past. Previously, it was generally assumed that no fracture is generated during polymer injection. However, there are some recent reports of field polymer injection that have resulted in very high injectivity presumably due to the creation of fractures. An attempt has been made to compare the simulation predictions based on our model, with the field results assuming both un-fractured and fractured injection wells. The advantage or disadvantage of using horizontal wells with and without fractures also has been studied in specific instances in the field where polymer injection is proposed for mobility control, which is also briefly addressed.

1.5 OUTLINE OF THE DISSERTATION

This dissertation is organized as follows: the impact of injection well fractures on well injectivity and reservoir sweep during waterflooding and chemical EOR processes is briefly reviewed in Chapter 1. Chapter 2 presents the fracture generation and growth models for water and polymer injection. The mechanisms for fracture creation and growth – particle plugging during water injection and high viscosity of polymer during polymer injection – are described in detail.

In Chapter 3, the impact of static fracture during water injection and polymer injection on well injectivity, reservoir sweep, water breakthrough, and oil recovery is discussed. A heterogeneous reservoir case as well as a homogeneous reservoir case is used to show the impact of heterogeneity on well injectivity, reservoir sweep, and oil recovery.

In Chapter 4, the mechanisms for dynamic fracture growth during water and polymer injection are first described and the fracture growth model is then employed to predict dynamic fracture length and width. Flow allocation into dynamically fractured and un-fractured layers is also investigated with the fracture growth model.

In Chapter 5, the use of horizontal wells to maximize oil recovery during water and polymer injections is investigated. Longitudinal and transverse fractures are discussed, which are related to rock stress condition and well geometry.

History matching and a sensitivity study are performed in Chapter 6. The impact of polymer rheology and fracture growth on oil recovery and well injectivity is investigated. Polymer viscosity behavior, fracture growth, particle plugging, and

stimulation in a field case are simulated and analyzed in detail using fracture growth model.

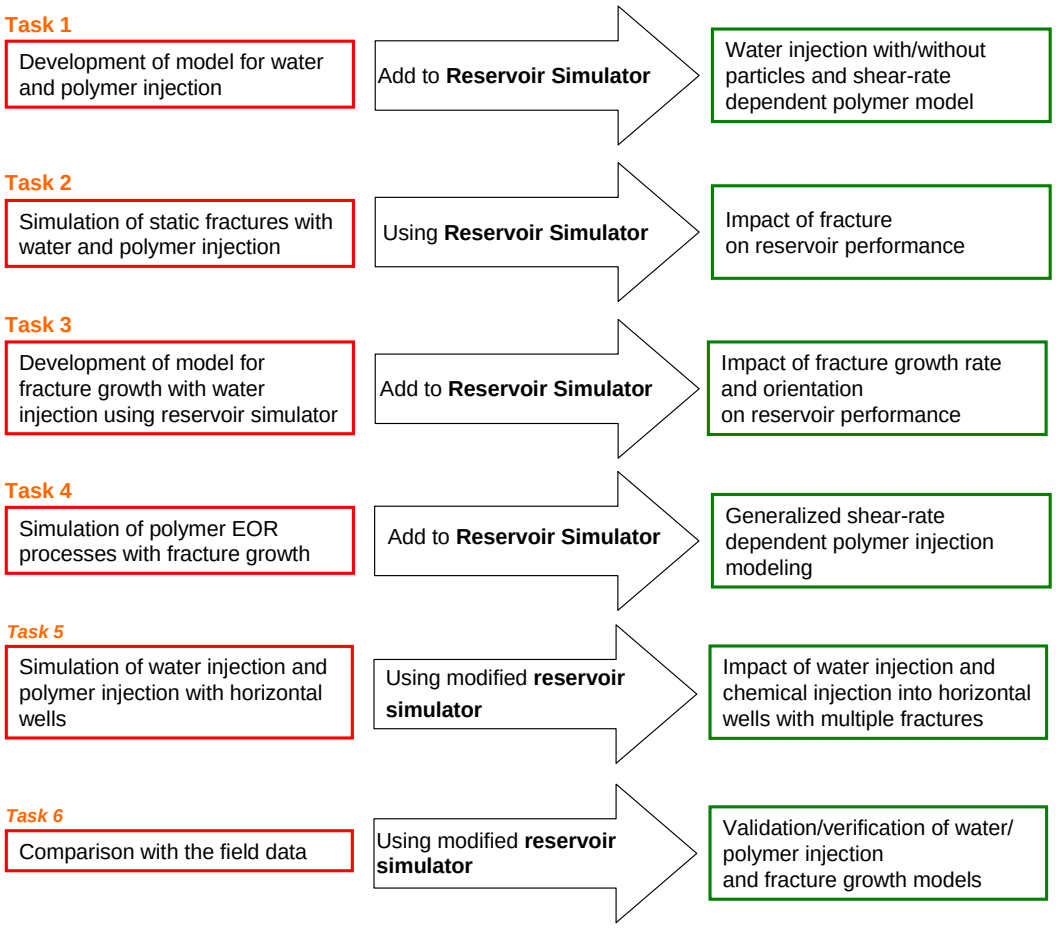

Figure 1.1: Flowchart of tasks for impact of injection well fractures on well injectivity and reservoir sweep during waterflooding and chemical EOR processes

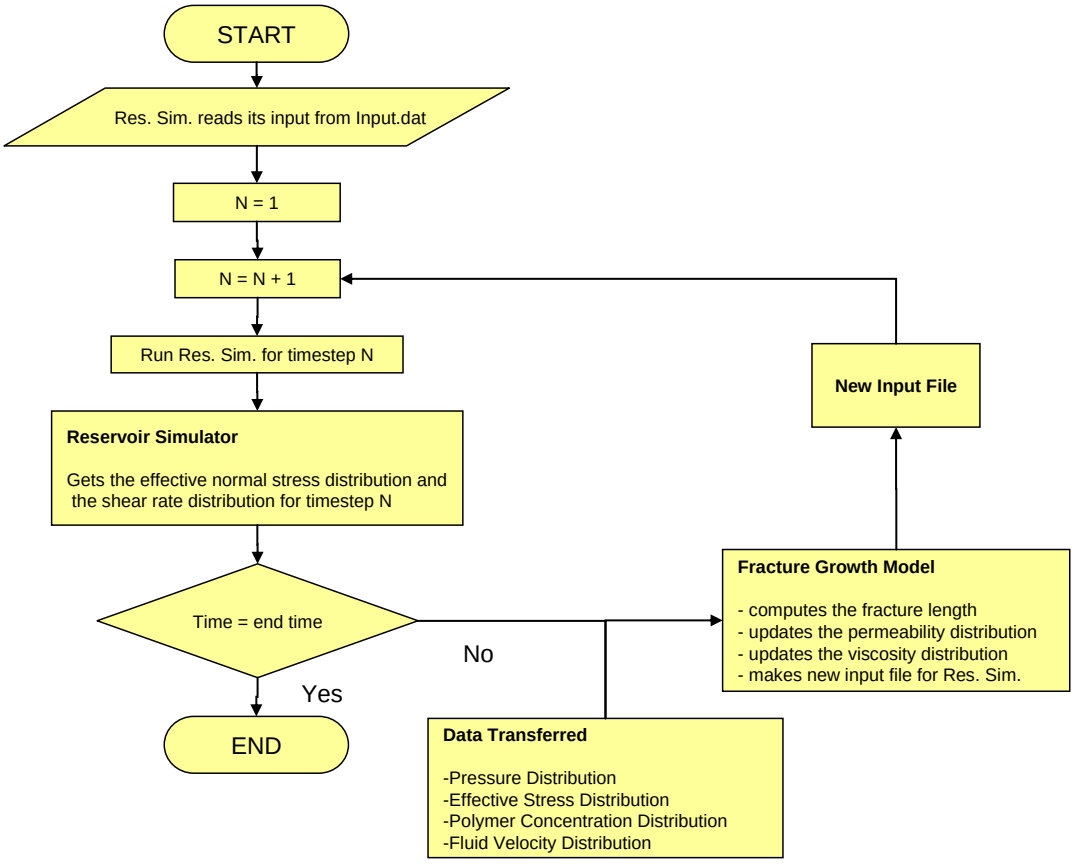

Figure 1.2: Flowchart of fracture growth model

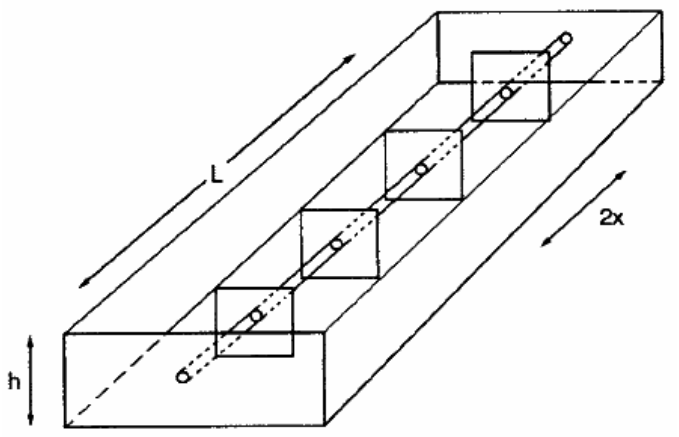

Figure 1.3: Horizontal well geometry with transverse fractures

Chapter 2: Models for Water and Polymer Injection

2.1 INTRODUCTION

Injection wells are sensitive to formation damage induced by water injection. Injectivity decline during water injection could occur due to the plugging near the wellbore of suspended particles in the injected water; precipitation resulting from incompatible injected and formation water; swelling of clay minerals; fines migration; or the growth of bacteria. Injectivity decline can have a significant impact on the water injection operations and their economics. Therefore, it is necessary to develop reliable models to predict the injectivity decline of water injection wells.

Along with water injection, polymer injection is also widely used to displace bypassed oil from un-swept zones after water injection (Fulin *et al.*, 2006; Garrouch, 1999; Huifen *et al.*, 2004; Liu *et al.*, 2002; Taber *et al.*, 1997; Wang *et al.*, 2007). If the viscosity of the injected water is much lower than the viscosity of oil in the reservoir, this unfavorable mobility ratio results in viscous fingering and channeling in the reservoir, which causes early water breakthrough, low oil recovery, and low reservoir sweep. To maximize the reservoir sweep, polymer injection is now widely used. With its increased viscosity, polymer prevents viscous fingering/channeling and early water breakthrough (Fernando *et al.*, 1985; Huifen *et al.*, 2004).

During polymer injection, injectivity decreases as the size of the high-viscosity polymer zone increases. The shear-thickening behavior of polymer near the injector at high injection rates especially intensifies injectivity decline (Yin *et al.*, 2006). To model

the polymer injection process, different polymer rheology models are employed in this chapter (Heemskerk *et al.*, 1984).

2.2 INJECTION OF WATER WITH PARTICLES

2.2.1 Particle Plugging in Porous Media

Water is injected into a subsurface reservoir for waterflooding, pressure maintenance and produced fluids management. In mature fields, a substantial amount of oil recovery is achieved through waterflooding. In offshore operations, the injection of produced water for waterflooding and pressure maintenance has increased. However, because produced water has suspended solids and oil droplets, injectivity decline can occur during produced water injection. Even though filtration before injection can reduce injectivity decline by decreasing the concentration of suspended solids, its cost is substantial. For these reasons, it is critical to develop reliable models to predict the injectivity of water injection wells. To predict injectivity decline due to particle plugging, the nature of this impairment needs to be modeled first.

2.2.2 Particle Retention

To understand particle plugging during water injection, the main mechanism for particle retention needs to be investigated. Based on experiments reported in the literature, it has been proposed (Pang *et al.*, 1997) that particle retention occurs mostly by four mechanisms: size exclusion, surface deposition, bridging and log-jam. Size exclusion takes place when the particle size is bigger than the size of the pore throat and the particles are strained out. With the second mechanism of surface deposition, particles

are retained by attractive surface forces acting on particles that are transported to the vicinity of the grains. The third mechanism, bridging, refers to the dynamic process in which particles are retained by previously retained particles, and form bridges. However, this mechanism and the fourth mechanism of log-jam are not significant in injection wells because the concentration of injected particles is low and is usually below the critical concentration needed for forming bridges and log-jams.

The retention mechanism and the extent of solids retained depend on various factors such as: (i) size distribution, concentration, shape and surface properties of the injected particles, (ii) grain or pore size distribution, shape, structure and surface properties of the formation, and (iii) fluid properties – interstitial velocity or physico-chemical properties.

2.2.3 Flow of Particle Suspensions in Porous Media

Any model for particle plugging during water injection must enable us to predict the porosity and permeability reduction during water injection with particles. During injection, some particles are deposited on the pore walls by various forces that act between particles and grains. A mass conservation equation for the flowing particles can be written as:

$$\nabla(uc - D\nabla c) + \frac{\partial}{\partial t}(\phi c + \sigma) = 0 \qquad (2.1)$$

where u is the Darcy velocity, c is the concentration of suspended particles (volume of particles per unit fluid volume), D is the dispersion coefficient, ϕ is the porosity and σ is the specific deposit (volume of deposited particles per unit bulk volume).

To simplify Equation (2.1), several assumptions are made. First, the flow is assumed to be incompressible. Second, dispersion and diffusion are neglected for particles larger than 1μm (Herzig *et al.*, 1970). With these assumptions, Equation (2.1) becomes:

$$u \cdot \nabla c + \frac{\partial}{\partial t}(\phi c + \sigma) = 0 \tag{2.2}$$

Assuming particle plugging to be the only mechanism decreasing porosity, we have:

$$\frac{\partial}{\partial t}\phi = -\frac{\partial \sigma}{\partial t} \tag{2.3}$$

The deposition rate can be defined to be proportional to particle concentration and the Darcy velocity, as proposed by Iwasaki (1937):

$$\frac{\partial \sigma}{\partial t} = \lambda u c \tag{2.4}$$

where λ is the filtration coefficient. With the above assumptions, Equation (2.2) in one dimension simplifies to

$$u\frac{\partial c}{\partial x} + \phi\frac{\partial}{\partial t}c + \lambda u c = 0 \tag{2.5}$$

where λ is assumed to be a constant equal to λ_o. The injection velocity u and porosity ϕ are also assumed to be constant with time. Equation (2.5) can be solved analytically for the one-dimensional case.

The initial and boundary conditions are:

$$c(x,0) = 0 \tag{2.6}$$

$$c(0,t) = c_{in} \tag{2.7}$$

where c_{in} is the injected particle concentration.

Solving Equation (2.5) with the above initial and boundary conditions in one dimension yield:

$$c(x,t) = 0 \qquad t < \frac{\phi x}{u} \qquad (2.8)$$

$$c(x,t) = c_{in} \exp(-\lambda_o x) \qquad t > \frac{\phi x}{u} \qquad (2.9)$$

Equation (2.8) and Equation (2.9) specify the concentration profile of suspended particles at any instant. Introducing the above equations into Equation (2.4) and solving the differential equation

$$\sigma(x,\theta) = \lambda_0 u \theta c_{in} \exp(-\lambda_o x) \qquad \theta > 0 \qquad (2.10)$$

$$\sigma(x,\theta) = 0 \qquad \theta \le 0 \qquad (2.11)$$

where θ is the corrected time measured from the time the suspension reaches a location x.

$$\theta(x) = t - \int_0^x \frac{dx'}{u(x')/\phi(x')} \qquad (2.12)$$

θ can be replaced by t because the difference between t and θ is important for the first few pore volumes (PV) only. Therefore,

$$\sigma(x,\theta) = \lambda_0 u t c_{in} \exp(-\lambda_o x) \qquad t >> 1\,\mathrm{PV} \qquad (2.13)$$

The corresponding decrease in porosity is expressed as:

$$\phi(x,t) = \phi_0 - \sigma(x,t) \qquad (2.14)$$

Therefore, the particle plugging during water injection decreases porosity in the reservoir. The decreased porosity affects the permeability reduction, which affects the stress reduction and fracture generation/growth during water injection.

2.2.4 Permeability Reduction Model

As particles are trapped in the pore walls and reduce porosity and permeability, the injectivity declines. There are various relationships available in the literatures which relate the decline in permeability to the concentration of deposited particles. Based on the Kozeny equation, Pang and Sharma (1997) proposed the following relation way of relating the permeability reduction to the particle plugging.

$$k = \frac{\phi^{1/3}}{K_K (1-\phi)^2 S^2 \tau} \tag{2.15}$$

where k is the permeability, S is the specific surface area, K_K is the Kozeny constant and τ is the tortuosity. The best-fit value for factor $k' = K_K \tau$ has been found by Carman to be 5. The ratio of permeability at any instant to the initial permeability is

$$\frac{k}{k_o} = \frac{\phi^3 (1-\phi_0)^2 S_o{}^2 k_o'}{\phi_0{}^3 (1-\phi)^2 S^2 k'} \tag{2.16}$$

Pang and Sharma proposed that the permeability reduction could be divided into three factors: reduced porosity (k_{dp}), increased surface area (k_{ds}), and increased tortuosity (k_{dt}).

$$k / k_o = k_{dp} k_{ds} k_{dt} \tag{2.17}$$

where

$$k_{dp} = \frac{\phi^3 (1-\phi_0)^2}{\phi_0^{\,3} (1-\phi)^2} \tag{2.18}$$

In calculating the permeability reduction due to increased surface area (k_{ds}), the particles are assumed to be spheres with their entire surface exposed to flow.

$$k_{ds} = \left(\frac{1+\sigma/(1-\phi_0)}{1+(d_g/d_p)\sigma/(1-\phi_0)} \right)^2 \tag{2.19}$$

The reduction in permeability due to increased tortuosity is difficult to evaluate. This has been accounted for by the introduction of an empirical parameter β>0, which is dependent on the pore structure and is called damage factor.

$$k_{dt} = \frac{1}{1+\beta} \tag{2.20}$$

During experiments with injection of water with suspended particles, particle trapping occurs very near the fracture face (Suarez-Rivera *et al.*, 2002). Particle deposition occurring near the fracture face is shown in **Figure 2.1**. The initial permeability is 100 md and the initial porosity is 20 %. The injection rate is 100 bbl/D. The particle concentration is 20 ppm and the fracture permeability and length are 100 D and 100 ft. Therefore, even though the particle concentration in the injected water is not large (of the order of 10 ppm), the impact of particle trapping on porosity and permeability is very severe after an extended period of injection.

The reduced porosity due to particle plugging could be up to 20~30% of the original porosity, which decreases permeability significantly as shown in **Figure 2.2** and **Figure 2.3**. Because of reduced porosity and permeability, BHP increases under constant injection rate conditions. If the permeability is reduced by a multiple of 5, the injection

pressure increases by 5 with constant injection rate. The effect of particle concentration on injection BHP and injectivity is shown in **Figure 2.4** and **Figure 2.5**. These two figures are obtained by using '*Fines Migration Model*' in reservoir simulator, *STARS* in *CMG*. By specifying the particle concentration and deposition rate, the particle plugging during water injection with particles can be simulated. These two figures show that high particle concentration increases the increase of injection BHP and the decrease of injectivity. As a result, accumulation of trapped particles induces fracture creation and growth during continuous water injection with particles, as described in Chapter 4.

2.3 INJECTION OF POLYMER

The polymers employed for polymer flooding show non-Newtonian rheological behavior, their viscosity depending on the shear rate (Han *et al.*, 1995; Ranjbar *et al.*, 1992). To represent the polymer solution viscosity in its bulk state, the Carreau model is commonly employed, as described below. When a polymer solution flows in a porous medium at a high shear rate, a "shear-thickening" phenomenon occurs, and the Carreau model cannot adequately represent such a behavior. A so-called "unified model" has recently been developed (Delshad *et al.*, 2008) to remedy the problem, as also described below. Both of these models are employed for our fracture dynamics study.

2.3.1 Power-law Model

There are several polymer rheology models, the simplest of which is the power-law model. This model is first employed here because of its simplicity, but it only

approximately describes the behavior of partially hydrolyzed polyacrylamide (HPAM) polymers used in EOR applications.

$$\mu_{eff} = K\left(\frac{\partial u}{\partial y}\right)^{n-1} \tag{2.21}$$

where

K = flow consistency index (SI unit $Pa \cdot s^n$)

$\frac{\partial u}{\partial y}$ = shear rate or velocity gradient perpendicular to the plane of shear (SI unit s^{-1})

n = flow behavior index (dimensionless)

2.3.2 Carreau Model

A model that describes the shear-thinning behavior of polymer better than the power-law model is the Carreau model. At low shear rates, the polymer shows shear-thinning behavior. At high velocities, the apparent viscosity approaches a Newtonian value of μ_∞ at infinite shear rate:

$$\mu_{app} = \mu_\infty + \left(\mu_p^o - \mu_\infty\right)\left[1 + \left(\lambda\gamma_{eff}\right)^\alpha\right]^{(n_1-1)/\alpha} \tag{2.22}$$

where μ_∞ is liming Newtonian viscosities at the high shear limit, μ_p^o is the limiting Newtonian viscosities at the low shear limit, λ is the polymer-specific empirical constant, γ_{eff} is effective stress, and α and n_1 are polymer-specific empirical constants.

One of the difficulties in applying the above model to polymer flow in porous media is that the shear rate in the pores cannot be directly defined. The most common

equation relating the effective porous media shear rate and the fluid Darcy velocity is (Cannela *et al.*, 1988):

$$\gamma_{eff} = C\left(\frac{3n_p+1}{4n_p}\right)^{n_p/(n_p-1)}\left[\frac{u_w}{\sqrt{kk_{rw}S_w\phi}}\right] \tag{2.23}$$

where k and ϕ represent the absolute permeability and porosity, and u_w, k_{rw}, S_w show the water phase Darcy velocity, relative permeability, and saturation respectively. Cannela *et al.* (1988) suggest that C=6.0 in Equation (2.23) matches various coreflood data sets well. Others have suggested that this value is too low and can change depending on the polymer properties and pore size (Delshad *et al.*, 2008).

2.3.3 Unified Model

For partially hydrolyzed polyacrylamide (HPAM) and related polymers, their apparent viscosity in porous media generally deceases as flow velocity increases; however, beyond a certain critical velocity, the apparent viscosity sharply increases, showing shear-thickening behavior. A procedure to predict both the shear-thinning and shear-thickening apparent viscosities, from the rheometer-measured shear and oscillatory viscosities, has been developed earlier and validated with corefloods (Delshad *et al.*, 2008).

To develop a comprehensive model for apparent viscosity, Delshad *et al.* (2008) assumed that its dependence on the Darcy velocity (or effective shear rate) consists of two parts: shear-viscosity-dominant part μ_{sh} and the elongational-viscosity-dominant part μ_{el} :

$$\mu = \mu_{sh} + \mu_{el} \tag{2.24}$$

A composite apparent viscosity model is then proposed in which the shear-viscosity-dominant part is represented by the Carreau equation, as given in Equation (2.22) above, and the elongational-viscosity-dominant part is represented in terms of the Deborah number, as modeled by Hirasaki and Pope (1974).

Apparent Viscosity for the Shear-Thickening Regime

As the polymer molecules flow through series of pore bodies and pore throats in reservoir rock, flow field elongation and contraction occur repetitively. Accordingly, the polymer molecules repeatedly stretch and re-coil to adjust to the flow field. If the flow velocity is too high, the polymer molecules do not have sufficient relaxation time to stretch and re-coil while adjusting to the flow. The resulting elastic strain causes the polymer's apparent high viscosity represented as shear-thickening behavior (Huh and Rossen 2008).

The polymer's shear-thickening behavior is generally correlated with Deborah number N_{Deb}, as was done by Hirasaki and Pope (1974). The Deborah number is a ratio of the characteristic period for elongation and contraction (τ_r) to the fluid's residence time going through pore throat and a pore body (τ_E). Delshad *et al.* (2008) thus proposed

$$\mu_{el} = \mu_{\max}\left[1-\exp\left(-\left(\lambda_2 N_{Deb}\right)^{n_2-1}\right)\right] \tag{2.25}$$

where $\mu_{\max}$, λ_2 and n_2 are empirical constants. One notable distinction between the earlier models and the proposed model is that, while the values from the earlier models

could increase indefinitely as N_{Deb} increases, the proposed model provides the plateau value of $\mu_{\max}$.

In the above equation, the Deborah number may be defined as

$$N_{Deb} \equiv \frac{\tau_r}{\tau_E} = \tau_r \gamma_{eff} \tag{2.26}$$

assuming, as Masuda *et al.* (1992) did, the inverse of the effective shear rate Equation (2.23) is a good approximation for the average residence time τ_E. Hirasaki and Pope (1974), Durst *et al.* (1981), and Haas and Durst (1981) approximated the average residence time with the inverse of the rate of flow elongation and contraction in the reservoir rock, ε:

$$\frac{1}{\tau_E} = \varepsilon = \frac{v}{d} = \frac{u_w}{(1-\phi S_w)\sqrt{150 k k_{rw}/\phi S_w}} \tag{2.27}$$

where v is the interstitial velocity and the latter expression of Equation (2.27) is obtained with the use of Kozey-Carman equation for d, the average pore size. Note that the effective shear rate, Equation (2.23), and Equation (2.27) have the same dependence on the key parameters, u_w, k, and k_{rw}, but the coefficient values are different.

Equation (2.24) thus becomes (Delshad *et al.*, 2008), covering the entire range of the Darcy velocity:

$$\mu = \mu_\infty + \left(\mu_p^0 - \mu_\infty\right)\left[1+\left(\lambda\gamma_{eff}\right)^\alpha\right]^{(n-1)/\alpha} + \mu_{\max}\left[1-\exp\left(-\left(\lambda_2\tau_r\gamma_{eff}\right)^{n_2-1}\right)\right] \tag{2.28}$$

To examine the effects of the polymer rheology on fracture generation and growth, the three viscosity models described above were employed: the power-law model; the Carreau model, and the unified model, as shown in **Figure 2.6**. With a low

shear rate region, the shear rate dependent polymer behavior of the Carreau model and the unified model is exactly the same as at a moderate injection rate. However, the high rate polymer-injection case shows the difference in polymer rheology between the Carreau and unified models. The shear-thickening behavior of polymer critically affects the BHP, and fracture growth, because shear-thickening behavior of polymer may develop at the fracture tip.

2.3.4 Effect of Polymer Concentration on Polymer Viscosity

A unified model of polymer viscosity includes polymer concentration as well as shear rate (Delshad *et al.*, 2008). Basically, a high polymer concentration shows high polymer viscosity. **Figure 2.7** and **Figure 2.8** show the effect of polymer concentration on polymer effective viscosity.

In the equation of unified polymer injection model, shear-thinning plateau viscosity (μ_p^0) is computed as a function of polymer concentration (*Cp*) and effective salinity (C_{sep}) as follows.

$$\mu_p^0 = \mu_w \left(1+\left(A_{p1}C_p + A_{p2}C_p^2 + A_{p3}C_p^3\right)C_{sep}^{S_p}\right) \tag{2.29}$$

where A_{p1}, A_{p2}, A_{p3} and S_p are constant model input parameters. The effective salinity for polymer (C_{sep}) taking into account both anion and divalent cation concentrations is defined as

$$C_{SEP} = \frac{C_{51} + \left(\beta_P - 1\right)C_{61}}{C_{11}} \tag{2.30}$$

where C_{51} is the total anion concentration in water (Eq/l), C_{61} is total divalent cation concentration in water (Eq/l), C_{11} represents aqueous phase water concentration (volume fraction), and β_P is a constant input model parameter.

The implementation of the Viscoelastic model follows Equation (2.28) assuming $\alpha = 2$ and the high shear viscosity (μ_∞) approaches the water viscosity (μ_w).

$$\mu_{app} = \mu_w + \left(\mu_p^0 - \mu_w\right)\left[1+\left(\lambda\gamma_{eff}\right)^2\right]^{(n-1)/2} + \mu_{\max}\left[1-\exp\left(-\left(\lambda_2\tau_r\gamma_{eff}\right)^{n_2-1}\right)\right] \quad (2.31)$$

Similar to the shear-thinning plateau viscosity, the shear-thickening plateau viscosity ($\mu_{\max}$) is computed as a function of polymer (C_p) and effective salinity (C_{SEP}) as follows:

$$\mu_{\max} = \mu_w\left(1+\left(A_{p11}C_p + A_{p22}C_p^2\right)C_{sep}^{S_p}\right) \quad (2.32)$$

where A_{p11} and A_{p22} are model input parameters. **Figure 2.7** describes the impact of polymer concentration on the unified polymer viscosity.

Like in the unified polymer model, the Carreau model polymer viscosity also increases with increasing polymer concentration. **Figure 2.8** shows the impact of polymer concentration and shear rate on polymer viscosity. The calculation of shear-thinning plateau viscosity and effective salinity is exactly same as in the unified model equation.

2.3.5 Effect of Effective Salinity on Polymer Viscosity

Effective salinity for polymer, while taking into accounts both anion and divalent cation concentrations, is defined in Equation (2.30) and affects polymer viscosity. The implementation of the viscoelastic model follows Equation (2.31), and shear-thickening plateau viscosity is computed by Equation (2.32). **Figure 2.7** shows the shear rate dependent viscosity of the unified model. The red curve shows the shear rate dependent polymer viscosity of the unified model with 0.33 effective salinity for polymer. The blue curve shows the shear rate dependent polymer viscosity of the unified model with 0.033 effective salinity for polymer. **Figure 2.8** describes the shear rate dependent viscosity of the Carreau model. Like the unified model, the Carreau model polymer viscosity is also affected by effective salinity.

2.4 SUMMARY

Water and polymer injection are widely used in the field to maintain reservoir pressure, improve reservoir sweep and enhance oil recovery and to dispose produced water. Even though the concentration of particles or oil droplets is usually small – for example, the order of 10 ppm – the impact of particle trapping on porosity and permeability is very significant after an extended period or injection. Due to reduced porosity and permeability, injection BHP increases continuously during water injection.

The high fluid viscosity during polymer injection also increases injection BHP. Especially when injection rate is high enough to show shear-thickening behavior near the

injector, polymer viscosity can increase significantly, which also increases injection BHP.

Particle plugging during water injection and high polymer viscosity including shear-thickening behavior during polymer injection can increase injection BHP, and induce fracture generation and growth. Therefore, models for particle trapping and shear-rate-dependent polymer rheology are the first step in investigating static and dynamic fracture growth during water and polymer injection.

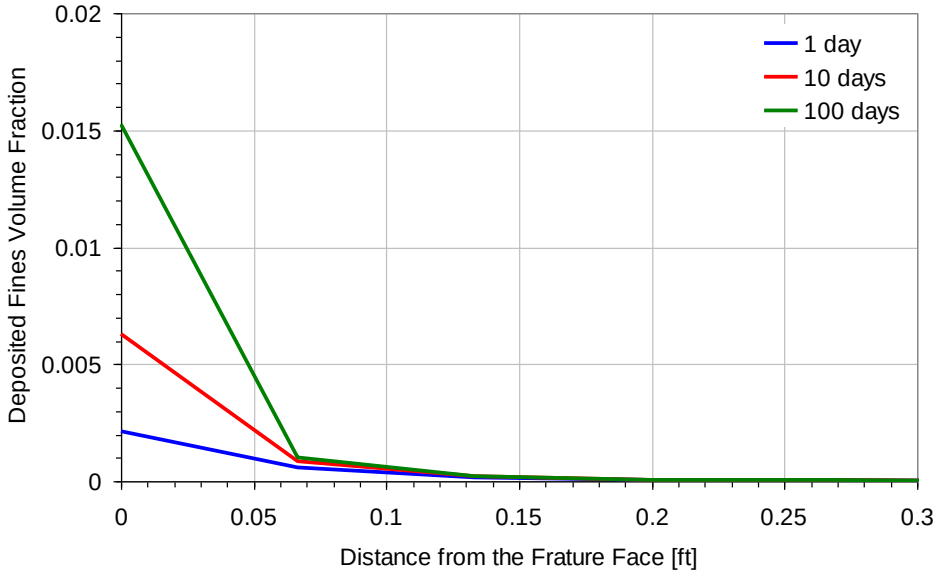

Figure 2.1: Particle plugging in a fractured injection well, particle concentration 20 ppm, initial porosity 0.2, initial permeability 100 md, injection rate 100 bbl/D

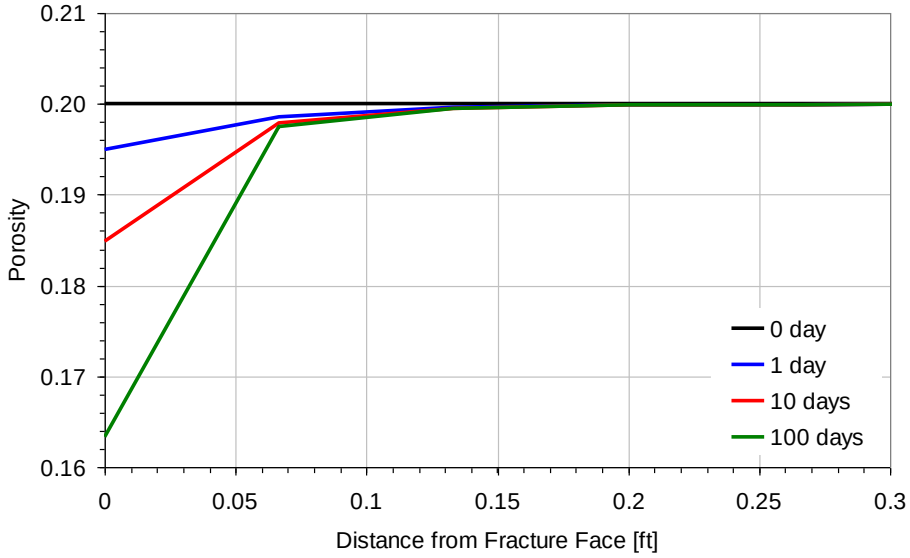

Figure 2.2: Porosity decreases after particle plugging in a fractured injection well, particle concentration 20 ppm, initial porosity 0.2, initial permeability 100 md, injection rate 100 bbl/D, fracture permeability 100 D

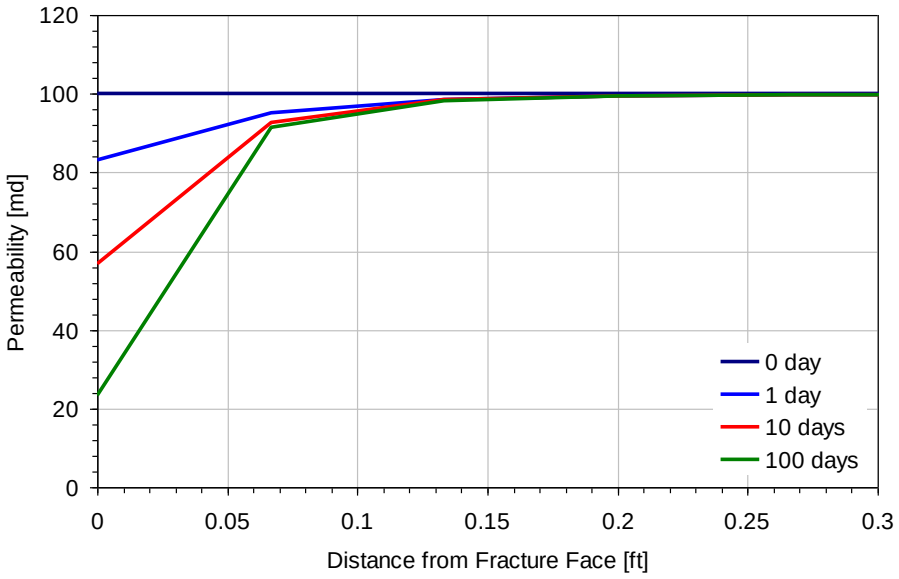

Figure 2.3: Permeability decreases after particle plugging in a fractured injection well, particle concentration 20 ppm, initial porosity 0.2, initial permeability 100 md, injection rate 100 bbl/D, fracture permeability 100 D

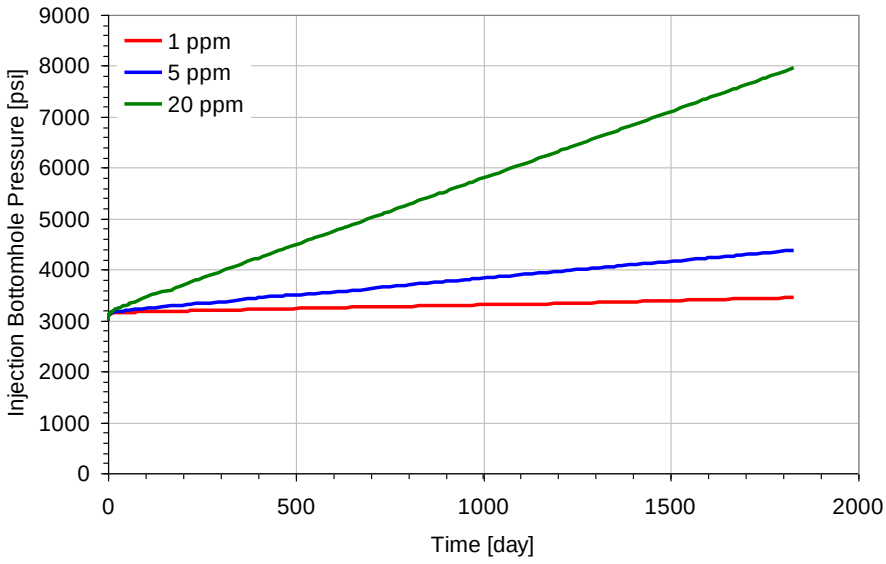

Figure 2.4: Effect of injected particle concentration on injection BHP for un-fractured wells, initial porosity 0.3, initial permeability 500 md, and injection rate 100 bbl/D

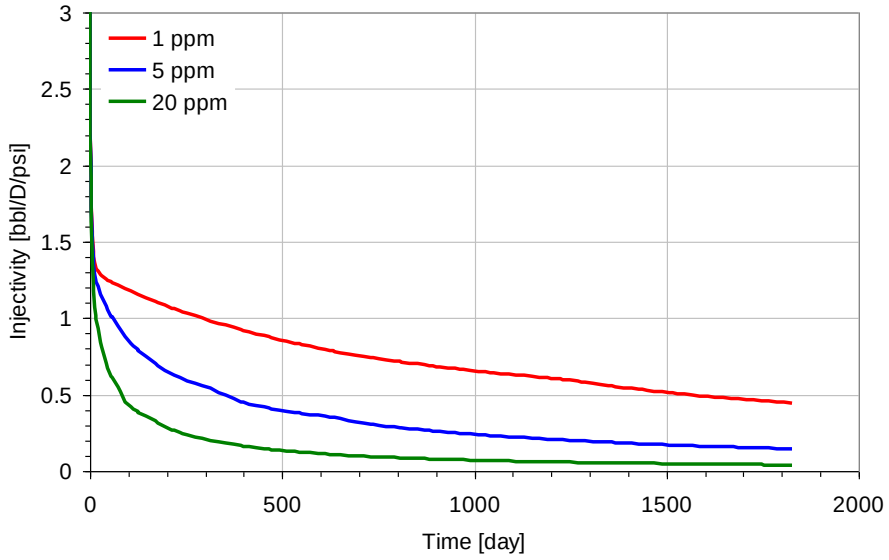

Figure 2.5: Effect of injected particle concentration on injectivity for un-fractured wells, initial porosity 0.3, initial permeability 500 md, injection rate 100 bbl/D

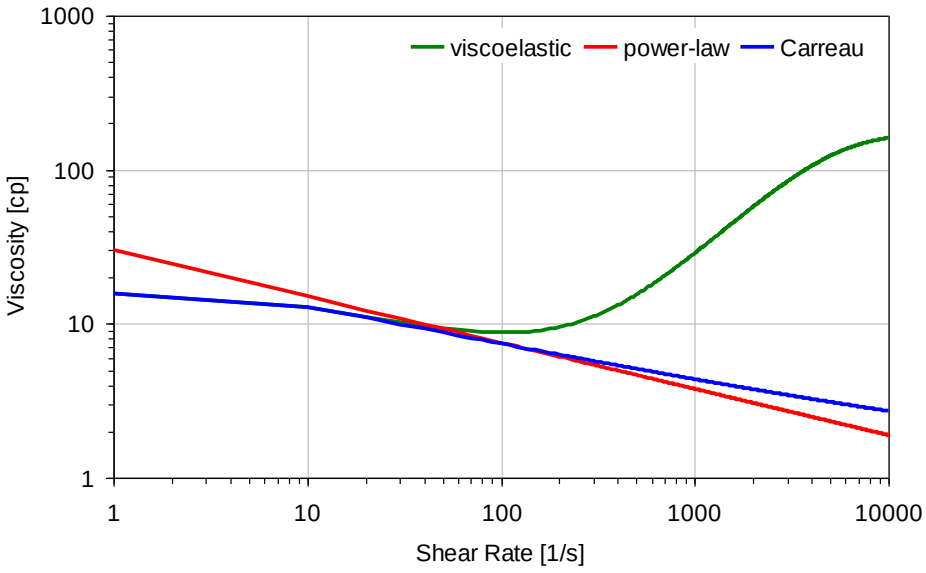

Figure 2.6: Shear rate dependent polymer viscosity, power-law polymer $\mu = 70\gamma^{0.3}$, unified model, and Carreau model: Flopaam 3330S polymer viscosity vs. shear rate (1500 ppm; 1.6 % NaCl; 25ºC)

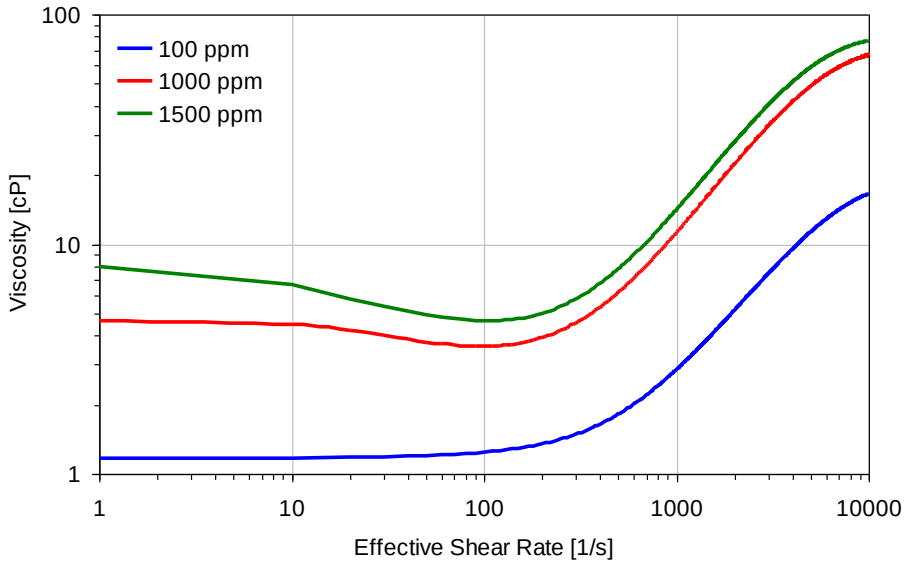

Figure 2.7: Shear rate dependent polymer viscosity with various polymer concentration, unified model: Flopaam 3330S polymer viscosity vs. shear rate (1500 ppm; 1.6 % NaCl; 25ºC)

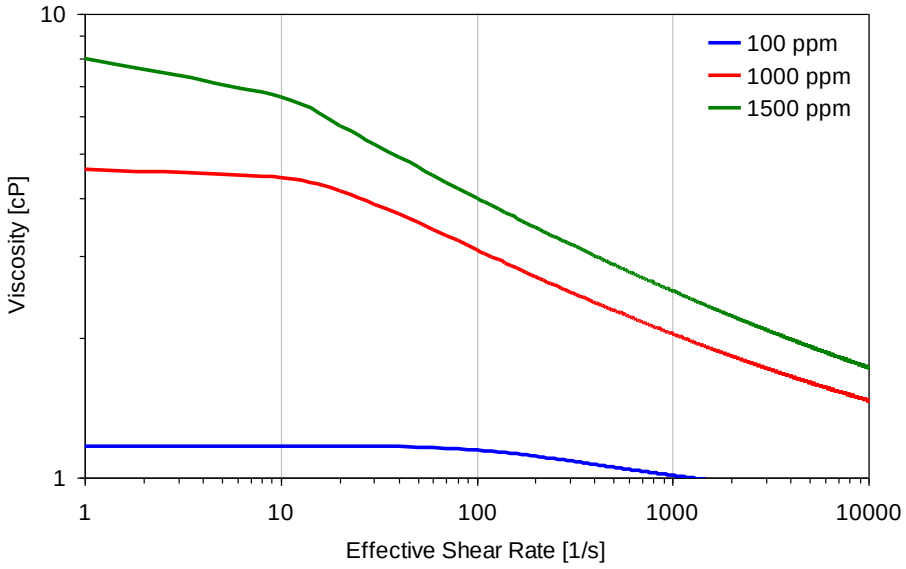

Figure 2.8: Shear rate dependent polymer viscosity with various polymer concentration, Carreau model: Flopaam 3330S polymer viscosity vs. shear rate (1500 ppm; 1.6 % NaCl; 25ºC)

Chapter 3: Water and Polymer Injection with Static Fractures

3.1 INTRODUCTION

During water injection, the injector BHP increases gradually due to particle plugging. This particle plugging occurs at the fracture face and tip and decreases porosity and permeability there. The reduced porosity and permeability in turn increases BHP (Gadde and Sharma, 2001). During polymer injection, high polymer viscosity also induces injection BHP to increase continuously (Wang *et al.*, 2006; Liu and Seright, 2000). The objectives of the simulation study described in this chapter are (i) to demonstrate the importance of fracture at the injection well during waterflood and polymer-based EOR processes; (ii) by carrying out simulations using simple static fracture models to identify the important fracture and flow parameters that govern the behavior of more complex dynamic fracture model studied in Chapter 4, and (iii) to explore the impact of an injection well fracture on well injectivity and reservoir sweep during water and polymer injection. The commercial reservoir simulator *CMG-STARS* was used in this research to simulate waterflood and polymer flood performance. Water injection with/without particles is modeled by using the *Fines Migration Model* in *CMG*, and polymer injection is simulated by using the *Shear Rate Dependent Model* in *CMG*. The *Fines Migration Model* has the capability to specify injected particle concentration, particle deposition rate, and porosity/permeability reduction due to particle plugging. The *Shear Rate Dependent Model* is capable of modeling polymer injection, and simulating polymer viscosity as a function of shear rate and polymer concentration. Prior to

investigating the dynamically induced fracture, the static fracture is examined in this chapter as the first step to understand injection well fractures. Chapter 4 then presents a qualitative study of dynamic fracture behavior related to particle plugging and shear rate dependent polymer injection.

3.2 RESERVOIR HETEROGENEITY AND FRACTURE ORIENTATION

The impact of static fracture on well injectivity, reservoir sweep, and oil recovery depends on reservoir geometry as well as fracture geometry. In this chapter, the effects of the static fracture are studied employing a simple five-spot element reservoir model in which a fracture is generated at the injector. Two representative fracture orientations are considered for the five-spot injector-producer geometry. The first one is the "favorable" fracture orientation, shown in **Figure 3.1 (a)**, which allows an areal sweep better than the no-fracture case. The second one, **Figure 3.1 (b)** is the "unfavorable" fracture orientation, which causes an areal sweep worse than the no-fracture case. The favorable fracture orientation causes slow water breakthrough, while the unfavorable fracture causes the injected fluid break through quickly into the producer.

Reservoir heterogeneity also plays an important role in the fracture's impact on reservoir sweep and oil recovery. In this preliminary study, the reservoir heterogeneity is represented by the simplest case of two layers of different stress distribution. Two-layered reservoir can have a different stress distribution within each layer, which may induce a fracture at the well in only one layer. The flow allocation into the layers will then be significantly affected by fracture geometry, thereby influencing breakthrough

timing and reservoir sweep. For a systematic investigation on the effects of fracture, four different set of simulations are carried out in this chapter: (a) water injection into a homogeneous reservoir (sub-section 3.3); (b) water injection into a two-layer reservoir (sub-section 3.4); (c) polymer injection into single layer (sub-section 3.5); and (d) polymer injection into two layers (sub-section 3.6).

3.3 WATER INJECTION WITH STATIC FRACTURE IN SINGLE LAYER

During water injection, fracture length (x_f) and permeability (k_f) are the main parameters that affect well injectivity, which was examined with a series of waterflood simulations for a simple five-spot element model. The conditions for the waterflood simulations are listed in **Table 3.1**.

3.3.1 Injectivity Increase due to Static Fracture

Figure 3.2 shows injectivity as a function of time and fracture length. **Figure 3.3** is same as **Figure 3.2**, except that the injectivity is normalized with the no-fracture case, to emphasize the injectivity increase. As fracture length increases from 0 to 800 ft with reservoir size 1,000×1,000×40 ft, the injectivity increases up to about 6 times from 0.6 bbl/D/psi to 3.5 bbl/D/psi. The distance between injector and producer is 1,000 ft and the fracture orientation is favorable.

3.3.2 Reservoir Sweep Efficiency due to Fracture

Before we handle the dynamic fracture growth and its impacts in the next chapter, the impact of static fracture on well injectivity, reservoir sweep, and oil recovery is first investigated here. A high permeability fracture facilitates injection of water and polymer.

For an unfavorable fracture orientation, a static fracture, which direction is favorable or not, near the injector decreases the distance between injector fracture tip and producer, which results in earlier water breakthrough and lower oil recovery, even when the fracture orientation is favorable.

3.3.2.1 Effect of Mobility Ratio on Oil Recovery and Reservoir Sweep

The impact of static fracture on oil recovery and reservoir sweep depends on mobility ratio. If the mobility ratio is favorable, which means injected fluid mobility is lower than reservoir fluid mobility, the impact of static fracture is not significant, because the injected fluid breaks out through the producer after already completing oil production. There is no channeling of injected fluid with a favorable mobility ratio. On the other hand, if the mobility ratio is unfavorable, injected fluid breaks out through the producer during oil production and the distance between fracture tip and producer plays a significant role in oil recovery. Shorter distance between fracture tip and producer with an unfavorable mobility ratio induces early water breakthrough and less reservoir sweep. **Figure 3.4**~**Figure 3.7** illustrate the impact of static fracture on reservoir sweep with various mobility ratios. The variables investigated are shown in **Table 3.2**.

Figure 3.4 and **Figure 3.5** show water saturation distributions after 13 months with unfavorable mobility ratios (M = 10). The injected fluid viscosity (1 cp) is much lower than the existing fluid viscosity (10 cp) Because of the decreased distance between the injection well fracture tip and the producer at this mobility ratio, water breakthrough with static fracture is earlier, and water breakthrough without static fracture is later. Therefore, static fracture is harmful on oil recovery with an unfavorable mobility ratio.

On the other hand, if a mobility ratio is favorable and there is only one homogeneous layer, the impact of static fracture on oil recovery is negligible, as shown in **Figure 3.6** and **Figure 3.7**. Most of the injected fluid breaks through after oil production is complete, regardless of the static fracture. The red-colored area, which represents the un-swept zone, is almost the same for statically fractured and un-fractured cases.

Figure 3.8 and **Figure 3.9** compare water breakthrough and oil recovery with and without a fracture, when a high viscosity fluid is injected. There is not much difference in reservoir sweep and oil recovery between these two cases because water breakthrough timing is almost the same (at the 700^{th} day) without viscous fingering. However, in the case of unfavorable mobility in **Figure 3.10** and **Figure 3.11**, water breakthrough time is reduced (at the 500^{th} day) with a fracture because static fracture reduces distance between injector fracture tip and producer. Therefore, oil recovery with a static fracture should be slightly lower than without a static fracture as shown in **Figure 3.11**. The unfavorable mobility ratio accelerates water breakthrough. Water breakthrough timing with high viscous injected fluid is at the 380^{th} day and one with low viscous injected fluid is at the 240^{th} day (**Figure 3.10)**.

The viscosity of the reservoir oil is very important for oil recovery during water injection. Low oil viscosity facilitates oil recovery and high oil viscosity delays and reduces oil recovery. **Figure 3.15** shows the impact of mobility ratio on oil recovery. The oil viscosity ranges from 1 cp to 1,000 cp. The corresponding mobility ratio is from 0.001 to 1. The low-viscosity oil can be produced much more easily than the high-viscosity oil. According to Darcy's law, a 10-fold increase in viscosity requires a 10-fold increase in pressure drop near the producer. With the same pressure drop, 10 times more viscous

fluid shows a 10 times lower production rate. Therefore, a lower mobility ratio results in a greater ultimate recovery, and a more rapid oil recovery rate.

3.3.3 Water Breakthrough due to Static Fracture

Static fracture length is one of the key factors in oil recovery. Static fracture near an injector decreases distance between injector fracture tip and producer, which results in earlier water breakthrough and less reservoir sweep. The variables investigated are shown in **Table 3.3**.

Figure 3.13 shows the impact of static fracture and fracture length (0 ft, 95 ft, and 195 ft) on oil recovery in the single layer case. This result is obtained under the following conditions: constant injection rate, static fracture in single layer, and fracture direction is favorable (fracture direction towards between two producers). Regardless of fracture orientation, favorable or unfavorable, longer fracture decreases the distance between fracture tip and producer, which induces early water breakthrough. Therefore, earlier water breakthrough with a longer fracture results in less oil recovery. The static fracture induces the early water breakthrough, poor reservoir sweep and low oil recovery.

Figure 3.14 shows the impact of fracture length on water cut. The varying distance between fracture tip and producer induces different water breakthrough timing, which determines oil recovery. A static fracture expedites water breakthrough, which lowers oil recovery as shown in **Figure 3.13** and **Figure 3.14**.

As well as fracture length, mobility ratio is a critical parameter for oil recovery and reservoir sweep. **Figure 3.15** shows the impact of mobility ratio on oil recovery in the un-fractured case. A high mobility ratio with low injected fluid viscosity shows the

viscous fingering and early water breakthrough. As a result, the rate of oil recovery in the case of a high mobility ratio (unfavorable mobility ratio) is much lower than in the case of a low mobility ratio (favorable mobility ratio). **Figure 3.16** describes the water cut. This early water breakthrough with a high mobility ratio slows the oil recovery in comparison to one with low mobility ratio.

3.4 WATER INJECTION WITH STATIC FRACTURE IN TWO LAYERS

To investigate the impact of a static fracture, waterflooding into single layer reservoir has been carried in sub-section 3.3. The impact of a fracture can be intensified with a two-layer reservoir case. When there is fracture in only one layer, flow allocation, reservoir sweep and oil recovery can be affected by fracture geometry. The impact of a fracture in a two-layer reservoir on waterflood performance is shown in sub-section 3.4.

3.4.1 Effect of Mobility Ratio

The impact of fracture on injectivity is relatively small with injection of a high-viscosity fluid into the reservoir filled with a lower viscosity fluid. On the other hand, with a lower viscosity fluid injection, the impact of fracture on injectivity is large.

In the case of a two-layered reservoir, the flow allocation into both layers is again affected by the mobility ratio between the injected fluid and the fluid already in the reservoir, and by fracture conductivity. In **Figure 3.17**, the red line shows the flow allocation in the fractured layer with mobility ratio 0.1, which means that the viscosity of injected fluid is 10 times higher than the viscosity of oil in the reservoir. The lower

mobility ratio case shows that the flow allocation is much higher (90~100%) in the fractured layer because low viscosity oil serves as light resistance for an injected fluid. This preferential flow allocation would dramatically affect reservoir sweep and oil recovery. In the higher mobility ratio case (M = 10), the flow allocation into the fractured layer is about 50%, and the impact of having a fracture in only one layer is negligible in terms of reservoir sweep and oil recovery.

Figure 3.18 shows the cumulative oil production for each layer in a two-layer reservoir. The green and yellow-green curves show the cumulative oil production in the fractured and un-fractured layers with a mobility ratio of 1. In the case where the mobility ratio is 1, a smaller volume of the injected fluid flows into the fractured layer than in the case where the mobility ratio is 0.1. Therefore, oil recovery in the un-fractured layer with lower mobility case (M = 0.1) is much slower than one with higher mobility ratio case (M = 1). As well as flow allocation, viscous fingering affects the oil recovery. In the case of lower mobility ratio (M = 0.1), the viscous fingering cannot be observed. On the other hand, in the case of higher mobility ratio (M = 1), the oil recovery curve is more smooth than lower mobility ratio case because of viscous fingering.

The mobility ratio affects the flow allocation into the fractured and un-fractured layers, which affects the amount of oil recovery. **Figure 3.19** shows the overall oil recovery for the entire reservoir. At a low mobility ratio (M = 0.1), oil recovery is initially rapid, and water breakthrough is early, because the injected fluid is flowing through the fractured layer. However, after water breakthrough in the fractured layer, the rate of oil recovery slows, because most of the injected fluid still flows into the fractured layer. Also, at a lower mobility ratio, reservoir sweep is more efficient, and flow

allocation into fractured layer is higher, resulting in rapid reservoir sweep in the fractured layer and sluggish reservoir sweep in the un-fractured layer. When water breakthrough occurs in the un-fractured layer (around the 900th day), a lower mobility ratio case reaches the maximum oil recovery much more rapidly than a high mobility ratio case.

3.4.2 Effect of Fracture on Waterflood Performance

3.4.2.1 Pure Water Injection

Case 1.1
(a) Oil viscosity 0.5 cp (favorable mobility ratio)
(b) Favorable fracture orientation

Rock stress distribution in the reservoir can determine the fracture geometry in the reservoir. In the case of a two-layer reservoir, when there is a different rock stress distribution due to different geomechanical parameters (e.g., elastic modulus, Poisson's ratio, and yield stress), a static fracture can grow in one layer and not in the other layer. Flow allocation into the two layers during water injection is affected by the presence or absence of a fracture in each of the layers. When there is a fracture in one layer but not in the other layer, oil recovery and reservoir sweep are affected by the fracture because more injected fluid flows into the fractured layer. Also, flow allocation into the fractured layer is affected by the mobility ratio as well as the fracture conductivity. A simulation was run for water injection with a static fracture, two layers and where the fracture orientation is favorable (away from the producers). The variables investigated were shown in **Table 3.4**.

Oil viscosity is 0.5 cp, which means that the mobility ratio is 0.5, a favorable mobility ratio. In **Figure 3.20**, the red curve represents the oil recovery of the un-fractured case and the blue curve shows the oil recovery of the fractured case. The un-fractured case means there is no fracture either layer, and the fractured case means there is a static fracture in only one layer. The fractured case shows that more than half of the injected water flows into the fractured layer. Therefore, there is early water breakthrough in the fractured layer, which causes poor reservoir sweep and oil recovery in the un-fractured layer. However, overall oil recovery is similar in both fractured and un-fractured cases after water breakthrough. **Figure 3.21** shows the flow allocation into both fractured and un-fractured layers. With 0.5 mobility ratio and 100 D fracture permeability, about 80% of the injected fluid flows into the fractured layer. Early water breakthrough occurs in the fractured layer, and late water breakthrough in the un-fractured layer as shown in **Figure 3.22**. On the other hand, the un-fractured case has single water breakthrough around the 400^{th} day because exactly half of the injected water flows into each layer. **Figure 3.23** represents the water cut for each layer in the case of partially fractured reservoir. Even though the fracture orientation points away from the two producers, the water cut in the fractured layer is shown much earlier than in the un-fractured layer, which causes a lower oil recovery for the fractured case, because 80% of injected water flows into the fractured layer. Lower mobility ratio and higher fracture conductivity increases the flow allocation into the fractured layer, which significantly affects the oil recovery and reservoir sweep.

Case 1.2
(a) Oil viscosity 1 cp (neutral mobility ratio)
(b) Favorable fracture orientation

In this case, the mobility ratio is 1 (versus 0.5 in the previous case) which decreases the flow allocation into the fractured layer. **Figure 3.25** describes these different flow allocations. Where the mobility ratio is 1, the flow allocation into the fractured layer is only 75%, compared to 80% with a 0.5 mobility ratio; the fracture has a more significant impact when the mobility ratio is lower. Therefore, in the case where a mobility ratio is high due to higher existing fluid viscosity, the oil recovery between two cases – fractured and un-fractured cases – are very similar to each other (**Figure 3.24**). The slight difference between the fractured and un-fractured cases is shown in water breakthrough and oil production rate. The fractured case expedites water breakthrough and delays oil recovery. Also, water breakthrough timing where a mobility ratio is 1 is shown earlier than where a mobility ratio 0.5 even though the flow allocation where a mobility ratio is 0.5 into the fractured layer is much higher than where a mobility ratio is 1, because there is piston-like oil displacement with a lower mobility ratio and viscous fingering slightly occurs where a mobility ratio is 1.

Case 1.3
(a) Oil viscosity 30 cp (favorable mobility ratio)
(b) Favorable fracture orientation

This case shows a favorable mobility ratio in a two layer reservoir. The red curve in **Figure 3.28** represents the oil recovery in the un-fractured reservoir, and the blue curve shows the oil recovery in the fractured reservoir. With an unfavorable mobility

ratio, the impact of a static fracture on flow allocation is reduced, as shown in **Figure 3.29**. Therefore, the oil recovery of fractured and un-fractured cases is almost the same. **Figure 3.30** describes slightly different water breakthrough in both fractured and un-fractured cases, because the impact of a static fracture on the flow allocation with an unfavorable mobility ratio is lower than with a favorable mobility ratio. In the fractured case, the water breakthrough in the fractured and un-fractured layers is similar, as **Figure 3.31** illustrates. Also, due to viscous fingering, water breakthrough timing with a high mobility ratio is much earlier than with a low mobility ratio (***Case 1.1*** and ***Case 1.2***) even though the flow allocation with a low mobility ratio into the fractured layer is much higher than with a high mobility ratio. In brief, in the case of an unfavorable mobility ratio, the impact of a static fracture on oil recovery and reservoir sweep is minimized.

So far, the impact of a static favorable fracture orientation on water breakthrough, reservoir sweep, and oil recovery is discussed. ***Cases 1.4, 1.5, and 1.6*** describe a water injection with an unfavorable fracture orientation. An unfavorable fracture orientation means the fracture points directly to the producer. This orientation accelerates water breakthrough and reduces reservoir sweep and oil recovery.

Case 1.4
(a) Oil viscosity 0.5 cp (favorable mobility ratio)
(b) Unfavorable fracture orientation

The first three cases show the impact of a static fracture and a favorable mobility ratio on oil recovery and water breakthrough. Because of a favorable and low mobility ratio, the impact of static fracture on oil recovery and reservoir sweep is critical. An unfavorable fracture orientation facilitates earlier water breakthrough in the fractured

layer (**Figure 3.33)**, which lowers oil recovery in the fractured case. **Figure 3.32** shows slightly lower oil recovery with fracture for a season, but similar oil recovery between fractured and un-fractured cases after water breakthrough.

Case 1.5
(a) Oil viscosity 1 cp (favorable mobility ratio)
(b) Unfavorable fracture orientation

In ***Case 1.5***, the oil viscosity is altered to 1 cp. The mobility ratio increases from 0.5 to 1, and the impact of the static fracture on flow allocation decreases slightly because oil viscosity increases. Water breakthrough and oil recovery between the fractured and un-fractured cases are not different from each other. **Figure 3.35** shows the flow allocation into the fractured and the un-fractured layers. An increased mobility ratio induces slightly lower flow allocation into the fractured layer.

Case 1.6
(a) Oil viscosity 30 cp (unfavorable mobility ratio)
(b) Unfavorable fracture orientation

Because of high oil viscosity, the impact of a static fracture on flow allocation is not critical, and oil production rate is also slower than in previous cases (**Figure 3.39** and **Figure 3.38**). The water breakthrough time for the fractured and un-fractured cases is almost the same (**Figure 3.40**).

During pure water injection without particles, the impact of water injection on water breakthrough, reservoir sweep, and oil recovery has been investigated. Ultimate oil recovery for both fractured and un-fractured cases is not significantly different because

there is no formation damage, and oil in the un-fractured layer is swept. However, when there are particles in the injected water, particle plugging induces formation damage in both layers. Formation damage is much more severe with an un-fractured layer, but formation damage in a fractured layer is negligible, because there is enough fracture face to be plugged. Formation damage in an un-fractured layer, investigated in the next sections, significantly affects oil recovery and reservoir sweep.

3.4.2.2 Water Injection with Particles

In sub-section 3.4.1.2, simulations with pure water injection have been performed as the first step of a water injection study. However, in a real water flood, injected fluid often contains particles in the order of 10 ppm. Particles of this size play a significant role in well injectivity and reservoir sweep, therefore this section of the study incorporates the process of particle plugging during water injection, while systematically investigating the effects of mobility ratio and fracture orientation on reservoir sweep and oil recovery as in sub-section 3.4.1.1. During water injection without particles, a static fracture has a limited impact on flow allocation, and ultimate oil recovery. However, water injection with particles exhibits a different relationship between oil recovery, reservoir sweep, and flow allocation.

If sea water or reproduced water is used for waterflooding, there are particles or oil droplets in the injected water. Even though the fraction of particles or oil droplets in the water is negligible, continuous injection of water damages the matrix near the wellbore by particle plugging. Reduced permeability and porosity due to particle plugging affect well injectivity and flow allocation. More and more injected fluid flows

into the fractured layer due to formation damage in the un-fractured layer. Of course, formation damage occurs in the fractured layer also. However, a spacious fracture face in the fractured layer minimizes formation damage. Therefore, after formation damage progresses in the un-fractured layer, most of the injected fluid, more than 99%, flows into the fractured layer. The reservoir sweep can no longer be conducted in the un-fractured layer, which lowers reservoir sweep. On the other hand, if there is no fracture in both layers during water injection with particles, exactly the same amount of injected water flows into both layers and reservoir sweep and oil recovery are much higher than in a partially fractured reservoir. However, the un-fractured case can not occur in the field because injection BHP increases continuously due to formation damage. Fracture generation and growth are discussed in Chapter 4. In brief, water injection with particles in a partially fractured reservoir causes unequal flow allocation, poor reservoir sweep, and oil recovery.

Case 2.1
(a) Oil viscosity 0.5 cp (favorable mobility ratio)
(b) Favorable fracture orientation

An un-fractured case results in a much higher oil recovery than a fractured case due to better reservoir sweep and equal flow allocation into both layers (**Figure 3.41**). **Figure 3.42** describes the flow allocation into each layer (fractured and un-fractured) in the fractured case. As formation damage progresses in the un-fractured layer, most of the injected fluid flows into the fractured layer, resulting in poor reservoir sweep. The water breakthrough timing with the un-fractured case is much later than with the fractured case, because most of the injected fluid in the fractured case flows into the fractured layer

(**Figure 3.43**). In the fractured case, because more than 99% of the injected fluid flows into the fractured layer, there is no reservoir sweep or water breakthrough in the un-fractured layer (**Figure 3.44**).

Case 2.2
(a) Oil viscosity 1 cp (favorable mobility ratio)
(b) Favorable fracture orientation

The increased oil viscosity in this scenario reduces the flow allocation into the fractured layer (**Figure 3.46**), and induces viscous fingering in both layers. However, the flow allocations into the fractured layer in ***Case 2.1*** and ***Case 2.2*** become almost 100% after formation damage in the un-fractured layer. A high fraction of the injected water flows into the fractured layer, which facilitates water breakthrough in the fractured layer (**Figure 3.47** and **Figure 3.48**).

Case 2.3
(a) Oil viscosity 30 cp (unfavorable mobility ratio)
(b) Favorable fracture orientation

At this unfavorable mobility ratio, reservoir sweep efficiency becomes significantly low; it takes much longer to reach maximum oil recovery with high oil viscosity (**Figure 3.49**). Even though the impact of a static fracture on flow allocation decreases due to the high oil viscosity, most of the injected fluid flows into the fractured layer because of particle plugging (**Figure 3.50**). Similar to the results of previous cases (***Case 2.1*** and ***Case 2.2***), most of the injected fluid flows into the fractured reservoir and the reservoir sweep efficiency in the un-fractured layer is low (**Figure 3.51** and **Figure 3.52**)

Case 2.4
(a) Oil viscosity 0.5 cp (favorable mobility ratio)
(b) Unfavorable fracture orientation

During water injection without particles, an unfavorable fracture orientation induces early water breakthrough, and, at a favorable mobility ratio, most of the injected fluid flows into the fracture. This results in poor reservoir sweep efficiency. Also, in the fractured case, with particle-free injection, early water breakthrough occurs in the fractured layer, which facilitates water breakthrough and lowers oil recovery. **Figure 3.54** describes the flow allocation for both fractured and un-fractured cases. Water breakthrough is earlier for the fractured case (**Figure 3.55**) due to higher flow allocation into the fractured layer and there is no water breakthrough in the un-fractured layer (**Figure 3.56**) due to severe formation damage. This results in very poor reservoir sweep and oil recovery in the fractured case (**Figure 3.53**).

Case 2.5
(a) Oil viscosity 1 cp (favorable mobility ratio)
(b) Unfavorable fracture orientation

As the mobility ratio increases from 0.5 to 1, the impact of a static fracture on flow allocation into the fractured layer decreases slightly (**Figure 3.58**). With particle-free injection water breakthrough occurs for both layers (**Figure 3.48**). However, with particle-laden injection, formation damage eventually inhibits flow in the un-fractured layer (**Figure 3.58**), and there is no reservoir sweep or water breakthrough in the un-fractured layer, (**Figure 3.60**). The unfavorable fracture orientation accelerates water breakthrough, and particle-laden water decreases the reservoir sweep in the un-fractured

layer. Because of these phenomena, oil recovery in the fractured case is much lower than in the un-fractured case (**Figure 3.57**).

Case 2.6
(a) Oil viscosity 30 cp (unfavorable mobility ratio)
(b) Unfavorable fracture orientation

If the viscosity of existing fluid in the reservoir, such as oil in this case, is high, the impact of static fracture on well injectivity decreases. Flow allocation into the fractured layer is relatively low initially (**Figure 3.62**). However, as particle plugging progresses, more injected fluid flows into the fractured reservoir. After two or three years, most of the injected fluid flows into the fractured layer, which lowers reservoir sweep in the un-fractured layer (**Figure 3.64**). Oil recovery in the fractured case is much lower than in the un-fractured case (**Figure 3.61**). There is water breakthrough in the fractured case at earlier than 100 days, and the oil recovery in the fractured case becomes much lower than the un-fractured case due to early water breakthrough. Initially, flow allocation into the fractured layer decreases up to 65% but as particle plugging progresses, more injected fluid injected into the fractured layer (**Figure 3.62**). **Figure 3.63** and **Figure 3.64** describe the water cut. In the fractured layer, there is early water breakthrough. Breakthrough in the un-fractured layer occurs very late, at 300 days, which lowers the oil recovery in the fractured reservoir.

In summary, this section demonstrates that fracture and mobility ratio play a significant role in oil recovery during waterflooding. When there are particles in injected water, the impact of fracture becomes more significant. **Table 3.5** shows the impact of particle plugging on oil recovery. When there are no particles in the injected water, the

presence of a fracture affects oil production rate, but has little effect on cumulative production. On the other hand, when there are particles (20 ppm) in the injected water, the oil recoveries with and without particles are significantly different.

3.5 POLYMER INJECTION WITH STATIC FRACTURE IN SINGLE LAYER

Polymer injection is widely used in the field to improve oil recovery. A high-viscosity polymer can be used to obtain a favorable mobility ratio. A favorable mobility ratio results in better reservoir sweep and oil recovery. However, the high polymer viscosity results in poor well injectivity. Also, the shear rate dependence of polymer viscosity complicates the estimation of well injectivity.

Because of the shear rate dependence of polymer viscosity, polymer injectivity with a static fracture depends on injection rate, polymer rheology, fracture conductivity, and fracture length. In this section, various kinds of input parameters are investigated to study the impact of injection rate, polymer rheology, fracture conductivity and fracture length.

3.5.1 Injectivity Increase due to Static Fracture

3.5.1.1 Power-law Model

Chemical EOR processes that employ polymer injection for mobility control are simulated to study the impact of fractures on polymer flood performance. The shear rate dependent viscosity polymer, which shows both shear-thinning and shear-thickening behavior, is fully incorporated in the new model. Both static and dynamic fractures with

vertical wells are investigated to better understand how oil production and reservoir sweep can be accelerated and improved. It is expected that oil recovery using fractured injection wells is significantly different from oil recovery using un-fractured injection wells. To the best of our knowledge, this is the first systematic simulation to study polymer injection EOR processes that account for fracture generation and growth near injectors.

Polymer injectivity is a very important issue in chemical EOR processes. A fluid with a low flow behavior index ($n < 1$) exhibits shear-thinning behavior. A fluid with a high flow behavior index ($n > 1$) exhibits shear-thickening behavior. A Newtonian fluid is represented with a flow behavior index that approaches unity ($n = 0.99$). **Figure 3.65** describes the impact of flow behavior index and injection rate on injectivity. A high injection rate provides a high shear rate near the injector. The viscosity of a shear-thinning power-law fluid decreases with increasing shear rate, thus its injectivity increases at a high injection rate.

Relative fracture conductivity (F_{cd}) is a dimensionless number defined by the relationship between fracture permeability (k_f), fracture width (w), fracture half length (x_f), and reservoir matrix permeability (k):

$$F_{CD} = \frac{k_f \cdot w}{k \cdot x_f} \tag{3.1}$$

Injectivity is higher when relative fracture conductivity is high and fluid flow behavior index is low (**Figure 3.66**). **Figure 3.67** shows the impact of fracture length and injection rate on well injectivity of a power-law fluid. An increase in injection rate induces a high shear rate near the injector. Also, as fracture length increases, the injectivity of the

polymer increases. **Figure 3.68** shows that longer fracture length and higher fracture conductivity result in higher injectivity for a Newtonian fluid. **Figure 3.69** shows a similar trend for a power-law fluid.

3.5.1.2 Unified Viscoelastic Model

Injectivity is affected by polymer rheology and injection rate. The shear-thinning and shear-thickening behavior of a polymer affects well injectivity during polymer injection. If the injection rate induces shear-thinning (low viscosity) behavior, it enhances well injectivity. However, if the injection rate induces shear-thickening (high-viscosity) behavior, it reduces well injectivity. The green curve in **Figure 3.70** compares the injectivity of a power-law fluid ($n = 0.5$), a Newtonian fluid ($n = 0.99$), and a fluid modeled using a unified approach. The unified approach (Equation (2.35)) models the fluid as shear-thinning at low injection rates (injectivity increase) and as shear-thickening at high injection rates (injectivity decrease). Due to shear-thinning polymer behavior, the injectivity only increases at the high injection rate. For comparison, the injectivity of a Newtonian fluid remains constant with various injection rates, because Newtonian fluid viscosity is independent of shear rate.

Figure 3.71 shows injectivity as a function of injection rate and fracture length for the unified model. If there is no injection well fracture, injectivity at injection rates from 5 bbl/D/ft to 40 bbl/D/ft follow the trend shown in **Figure 3.70**. With a short (124 ft) fracture (shown separately in **Figure 3.73**), the unified model predicts shear-thinning behavior at rates up to 17.5 bbl/D/ft (compared to 3 bbl/D/ft without fracture), and shear-thickening behavior at rates above 17.5 bbl/D/ft. Unified model fluids do not exhibit

shear-thickening behavior in longer fractures, because shear rates remain low even at high injection rates. **Figure 3.75** shows injectivity as a function of relative fracture conductivity and injection rate. With a low injection rate (5 bbl/D/ft), shear-thinning behavior is observed. However, with a high injection rate (above 25 bbl/D/ft), shear-thickening behavior lowers injectivity. On the other hand, a longer fracture (**Figure 3.76**) shows only shear-thinning behavior within the same range of injection rates. Also, higher fracture conductivity increases the injectivity as well.

In this manner, the unified model highlights the interplay between flow behavior index, fracture conductivity, and fracture length. Flow behavior index can be used to represent the relationship between shear rate and injection rate. The equation relating the effective porous media shear rate and the fluid Darcy velocity is

$$\gamma_{eff} = \frac{\dot{\gamma}_{fac} |u_l|}{\sqrt{k k_{rl} \phi S_l}} \tag{3.2}$$

where k and ϕ are the absolute permeability and porosity, u_l, k_{rl} and S_l are the liquid phase Darcy velocity, relative permeability, and saturation (Cannella *et al.*, 1988). The shear rate factor is given by

$$\dot{\gamma}_{fac} = C\left[\frac{3n+1}{4n}\right]^{\frac{n}{n-1}} \tag{3.3}$$

where n is the shear-thinning power exponent and C is a constant value, usually equal to 6. A shear rate factor of 4.8 (used in these models) corresponds to $C = 6$ and $n = 0.5$.

Figure 3.77 shows the relationship between the injection rate and the shear rate in an un-fractured reservoir. The shear rate is calculated 1.2 ft away from the injector and 1

ft away from the fracture face. The width of the grid block representing the fracture is 0.1 ft and the grid block size increases gradually as the distance from the injector increases (from 0.1 ft to 20 ft). In this simulation (reservoir permeability 500md, reservoir porosity 0.3), injection rates from 5 bbl/D/ft to 35 bbl/D/ft correspond to shear rates from 500 s^{-1} to 4500 s^{-1}. The grid block size is critical factor for calculating shear rate during polymer injection. Near wellbore region, shear rate could be higher than 10,000 s^{-1} in injection rate from 5 bbl/D/ft to 35 bbl/D/ft. The reason that shear rate ranges between 500 s^{-1} and 4500 s^{-1} with this injection rate is grid block size in reservoir simulation. The large grid block size induces lower shear rate near injector because there is large pressure drop near wellbore. When the injection rate is above 30 bbl/D/ft, the shear-thickening behavior of the unified model fluid is observed.

The presence of a fracture affects the relation between injection rate and shear rate. Most of the injected fluid flows into the fracture, which means that shear rate in the matrix decreases in the presence of a static fracture even at a high injection rate. Fracture width is 0.1 ft and the shape of fracture is assumed to be rectangular shape. Polymer rheology also affects the relation between injection rate and shear rate in the presence of a static fracture. **Figure 3.78** shows the relation between injection rate and shear rate in the power-law and unified models. Because the fluid velocity in the matrix is small due to high viscosity, shear rates in the case of the unified model are lower than in the other models. In the case of the power-law fluid, a lower flow index value, *n*, induces more fluid to flow in the fracture, which decreases the polymer velocity in the matrix. Therefore, a lower flow behavior index value lowers shear rate in the matrix near the injector. A comparison of **Figure 3.77** and **Figure 3.78** shows that the shear rates

induced in the presence of a static fracture are roughly ten times lower than in the un-fractured case, and this effect is more dramatic for a unified fluid than for a power-law fluid.

Polymer viscosity and shear rate are also affected by fracture length. **Figure 3.79** shows the relation between injection rate and shear rate for a power-law fluid ($n = 0.5$). More injected fluid flows into a longer fracture than into a shorter fracture, therefore the matrix shear rate at a given injection rate is lower in the presence of a longer fracture versus a shorter fracture. Power-law fluid viscosity is higher in the presence of a static fracture because so much of the flow is reallocated into the fracture, which decreases velocity and shear rate in the matrix (**Figure 3.80**). For this reason, the impact of a fracture on well injectivity with a power-law fluid is smaller than with a Newtonian fluid. **Figure 3.81** shows the shear rate increase for the unified model with an increasing injection rate. However, the increase of shear rate in a unified model fluid is much lower than the increase in a power-law fluid, because a higher injection rate induces shear-thickening behavior in the unified model.

Figure 3.82 shows polymer injectivity as a function of time for an un-fractured reservoir at an injection rate of 500 bbl/D. Injectivity decreases with time because the polymer viscosity is high relative to the existing fluid viscosity. The rate at which injectivity decreases depends on the polymer rheology model, injection rate, and injection well fracture (**Figure 3.82**~**Figure 3.85**). **Figure 3.82** shows that the injectivity of the power-law model remains the highest, and the injectivity of the Newtonian fluid remains the lowest. The unified model fluid exhibits a lesser degree of shear-thinning behavior than the power-law fluid.

Figure 3.83 shows polymer injectivity as a function of time for a fractured reservoir at an injection rate of 500 bbl/D. The unified model fluid injectivity is much higher than the power-law polymer injectivity. The injectivity for all three models is higher in the presence of a fracture, but the relationship between the unified model and the power-law model is reversed because of their contrasting responses to decreased shear rate (**Figure 3.78**).

Because power-law and unified model fluids are shear rate dependent polymers, injection rate affects polymer injectivity. **Figure 3.84** shows injectivity as a function of time for each for an un-fractured reservoir at an injection rate of 1,000 bbl/D. Comparing **Figure 3.82** and **Figure 3.84** shows that, at the higher injection rate of 1,000 bbl/D, the power-law fluid injectivity increases, while the unified model fluid injectivity decreases; at the increased injection rate, the power-law fluid exhibits shear-thinning behavior, while the unified model fluid exhibits shear-thickening behavior. Newtonian fluid injectivity is not affected by injection rate. Comparing **Figure 3.83** and **Figure 3.85** shows that at the higher injection rate of 1,000 bbl/D, the power-law fluid injectivity with a fracture is also higher, as it exhibits shear-thinning behavior. On the other hand, changing the injection rate from 500 bbl/D to 1,000 bbl/D has a negligible a negligible effect on the injectivity of the unified model fluid

Consequently, well injectivity depends on polymer rheology, fracture length, injection rate, fracture conductivity, and so on. A careful investigation of polymer injection well injectivity in a two-layer reservoir has been performed in the next section.

3.6 POLYMER INJECTION IN WELLS WITH STATIC FRACTURE IN TWO LAYERS

3.6.1 Unified Polymer Model Injection

Case 3.1
(a) Oil viscosity 1 cp (favorable mobility ratio)
(b) Favorable fracture orientation

Reservoir heterogeneity (e.g. multiple layers) affects oil recovery and reservoir sweep. In water injection with particles, particle plugging in an un-fractured layer causes very low flow allocation into the un-fractured layer, which induces early water breakthrough in the fractured layer and poor reservoir sweep and oil recovery in the un-fractured layer. In polymer injection, reservoir heterogeneity affects not only flow allocation, reservoir sweep, and oil recovery (as with water injection), but also affects polymer viscosity. An injection well static fracture induces higher flow allocation into the fractured layer (**Figure 3.87**), which promotes earlier water breakthrough in the fractured layer (fractured case, **Figure 3.88** and **Figure 3.89**). However, in this case, because there are no particles in the injected fluid, there is no formation damage near the injector regardless of whether the layer is fractured or un-fractured. Therefore, ultimate oil recovery after water breakthrough in both fractured and un-fractured layers is almost the same (**Figure 3.86**).

Case 3.2
(a) Oil viscosity 3 cp (favorable mobility ratio)
(b) Favorable fracture orientation

Well injectivity is affected by the viscosity of the fluid existing in the reservoir. A high viscosity reservoir fluid reduces the impact of a fracture on flow allocation into the

fractured and un-fractured layers (**Figure 3.91**). Therefore, the flow allocation with 1 cp of oil viscosity into the fractured layer is higher than with 3 cp of viscosity.

Case 3.3
(a) Oil viscosity 30 cp (unfavorable mobility ratio)
(b) Favorable fracture orientation

For this case, the high oil viscosity induces lower flow allocation into the fractured layer, which decreases the impact of injection well fractures on well injectivity and flow allocation. With high oil viscosity (30 cp), oil recovery, water breakthrough, and reservoir sweep do not show too much difference between fractured and un-fractured cases. **Figure 3.95** show that the flow allocation into the fractured layer is about 60~70% and **Figure 3.96** shows that water breakthrough occurs at the 780^{th} day with the fractured case and at the 980^{th} day with the un-fractured case. High oil viscosity minimizes the impact of a static fracture on injectivity and reservoir sweep.

Case 3.4
(a) Oil viscosity 1 cp (favorable mobility ratio)
(b) Unfavorable fracture orientation

For this simulation, although the mobility ratio is favorable, the unfavorable fracture orientation facilitates early water breakthrough, and lowers reservoir sweep and oil recovery. The ultimate fraction of oil recovered, however, is not significantly affected by the presence of a fracture in one layer. **Figure 3.98** shows the oil recovery for the fractured and un-fractured cases. Around the 200^{th} day, water breakthrough occurs in the fractured layer, as shown in **Figure 3.100** and **Figure 3.101**. As the unfavorable fracture orientation facilitates increased water production, oil production declines. Also, initially

more than 70% of the injected polymer flows into the fractured layer (**Figure 3.99**). However, the high viscosity of the injected polymer decreases the impact of static fracture by reducing the flow allocation to about 60%. Because there is no formation damage in the un-fractured layer due to particle plugging, efficient reservoir sweep can ultimately be completed in the un-fractured layer.

Case 3.5
(a) Oil viscosity 30 cp (unfavorable mobility ratio)
(b) Unfavorable fracture orientation

In this case, the high viscosity of the oil lowers the flow allocation into the fractured layer, and thus reduces the impact of a fracture on reservoir sweep and flow allocation (**Figure 3.103**). Therefore, there is little impact of injection well fractures on oil recovery and reservoir sweep with high oil viscosity during a unified polymer model injection (**Figure 3.102**~**Figure 3.105**).

3.7 SUMMARY

To investigate static injection well fractures during water and polymer injection, several sensitivity studies have been performed. This chapter explored the effect of mobility ratio, fracture orientation, reservoir heterogeneity, and rheological model parameters on well injectivity, reservoir sweep, and oil recovery. The impact of these parameters can be summarized as follows:

- The increase in injectivity due to the presence of a static fracture depends on fracture conductivity (fracture length and width). As fracture length increases,

the injectivity increases up to about 6 times the injectivity in an un-fractured well.

- A lower mobility ratio increases the effect of a static fracture on flow allocation in a two layer reservoir, which lowers reservoir sweep and oil recovery. As the viscosity of the existing fluid in the reservoir increases, flow allocation into the fractured layer decreases.
- When the mobility ratio is favorable, the presence of a fracture has a negligible effect on water breakthrough and oil recovery in a one-layer reservoir. However, when the mobility ratio is unfavorable, a fracture has a noticeable effect. In the presence of a fracture, water breakthrough occurs earlier, and oil recovery is lower than without a fracture.
- The oil recovery and reservoir sweep with and without a fracture in a two-layer reservoir show significant differences. A lower mobility ratio induces a higher flow allocation into the fractured layer, which results in poor reservoir sweep and lower oil recovery.
- Particle plugging intensifies the impact of a static fracture in a two-layer reservoir on oil recovery and reservoir sweep. The flow allocation into the fractured layer is up to 99% of the injected fluid. Therefore, reservoir sweep in the un-fractured layer is minimized and most of oil in the un-fractured layer cannot be recovered. As a result, reservoir sweep is poor and oil recovery is low when a fracture is present in only one layer.

- Injectivity during polymer injection depends on polymer rheology because the mobility ratio between injected polymer and oil in the reservoir is a function of injection rate and reservoir properties. Injectivity increases with increasing injection rate during injection of a shear-thinning polymer. As the degree of shear-thinning and the fracture conductivity increases, injectivity also increases.
- Viscoelastic fluid rheology affects well injectivity. A viscoelastic fluid shows shear-thinning behavior at low shear rate and shear-thickening behavior at high shear rate. In the low shear rate region, well injectivity increases with increasing injection rate, but in the high shear rate region, injectivity decreases with increasing injection rate due to shear-thickening behavior.

Table 3.1: Input data for water injection with static fracture in single layer

Reservoir Properties

Reservoir Size (ft)	$1000\times1000\times40$
Reservoir Porosity and Permeability (md)	0.3; 500
Initial Water Saturation	0.65
Initial Oil Saturation	0.35
Compressibility of Formation (psi^{-1})	6.7×10^{-7}

Rock and Fluid Data

Relative Permeability End Points for Water and Oil	0.3; 0.7
Irreducible Water Saturation	0.3
Residual Oil Saturation	0.35
Compressibility of Formation, Water, and Oil (psi^{-1})	6.7×10^{-7}; 3.03×10^{-6}; 8.32×10^{-6}

Well Properties

Well Type	Vertical
Injection Rate (bbl/D)	500
Injection Well Radius (in)	3

Table 3.2: Input data for water injection with static fracture in sub-section 3.3.2

Reservoir Properties

Reservoir Size (ft)	$500 \times 500 \times 40$ (Single Layer)
Reservoir Porosity and Permeability (md)	0.2; 100
Initial Oil Saturation	0.7
Fracture Half Length (ft)	220
Fracture Permeability (D)	100

Rock and Fluid Data

Relative Permeability End Points for Water and Oil	0.3; 0.7
Irreducible Water Saturation	0.3
Residual Oil Saturation	0.35
Compressibility of Formation, Water, and Oil (psi^{-1})	6.7×10^{-7}; 3.03×10^{-6}; 8.32×10^{-6}

Well Properties

Well Type	Vertical
Injection Rate (bbl/D)	200
Injection Well Radius (in)	3

Table 3.3: Input data for water injection with static fracture in sub-section 3.3.3

Reservoir Properties

Reservoir Size (ft)	1000 × 1000 × 40
Reservoir Porosity and Permeability (md)	0.2; 100
Fracture Permeability (D)	100
Fracture Half Length (ft)	220

Rock and Fluid Data

Irreducible Water Saturation	0.3
Residual Oil Saturation	0.35

Well Properties

Well Type	Vertical
Injection Rate (bbl/D)	200
Injection Well Radius (in)	3

Table 3.4: Input data for water injection with static fracture in two layers

Reservoir Properties	
Reservoir Size (ft)	300 × 300 × 40
Reservoir Porosity and Permeability (md)	0.2; 100
Fracture Permeability (D)	100
Fracture Half Length (ft)	150
Rock and Fluid Data	
Irreducible Water Saturation	0.3
Residual Oil Saturation	0.35
Well Properties	
Well Type	Vertical
Injection Rate (bbl/D)	500
Injection Well Radius (in)	3

Table 3.5: Impact of fracture and particles in the water on oil recovery

	Mobility Ratio (M)	Oil Recovery with Fractured/Un-fractured Reservoirs at 500 days	Oil Recovery with Fractured/Un-fractured Reservoirs at 1,800 days
Without Particle Plugging	0.5	36 / 44	46 / 46
	1	36 / 39	46 / 46
	30	16 / 17	27 / 28

With Particle Plugging	0.5	25 / 46	26 / 59
	1	19 / 23	26 / 44
	30	15 / 20	23 / 42

Table 3.6: Input data for polymer injection to estimate polymer injectivity

Reservoir Properties

Reservoir Size (ft)	$1000 \times 1000 \times 40$ (Single Layer)
Reservoir Porosity and Permeability (md)	0.3; 500
Initial Oil Saturation	0.35
Fracture Permeability (D)	100

Rock and Fluid Data

Relative Permeability End Points for Water and Oil	0.3; 0.7
Irreducible Water Saturation	0.3
Residual Oil Saturation	0.35
Compressibility of Formation, Water, and Oil (psi^{-1})	6.7×10^{-7}; 3.03×10^{-6}; 8.32×10^{-6}

Well Properties

Well Type	Vertical
Polymer Concentration in Injected Water (ppm)	1500
Injection Well Radius (in)	3

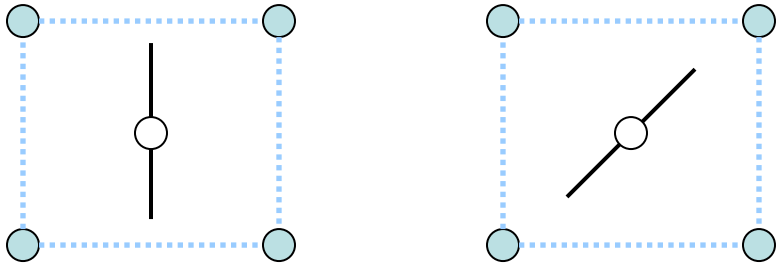

Figure 3.1: Five-spots geometry – (a) Favorable and (b) unfavorable orientation

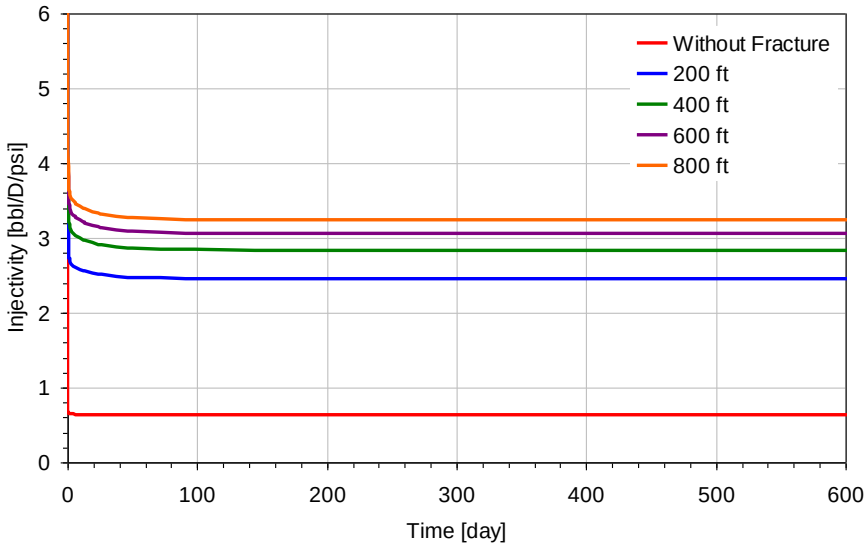

Figure 3.2: Impact of static fracture during water injection on injectivity

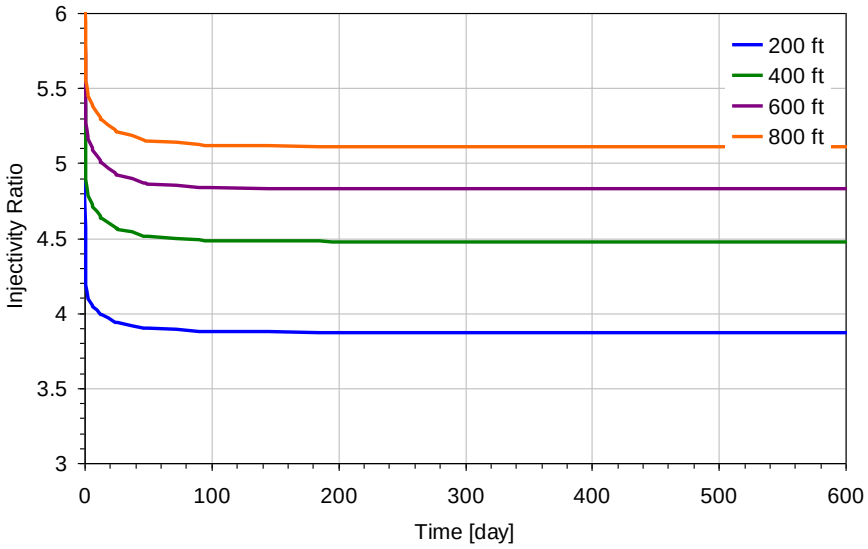

Figure 3.3: Impact of static fracture during water injection on injectivity ratio

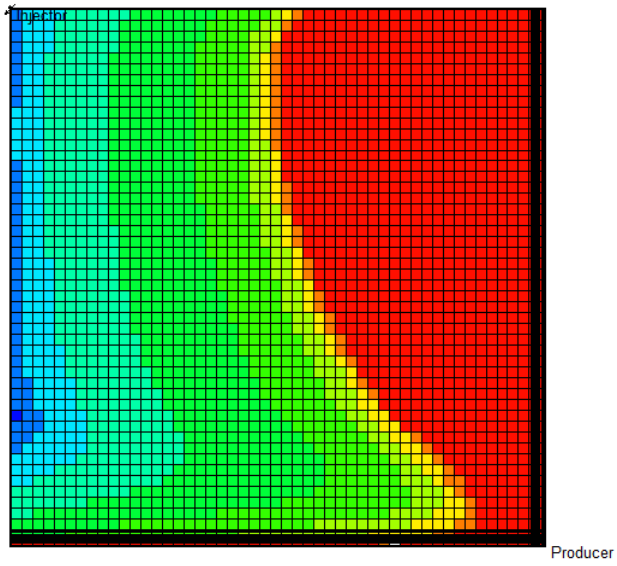

Figure 3.4: Water saturation with fractured reservoir after 13 months, favorable direction

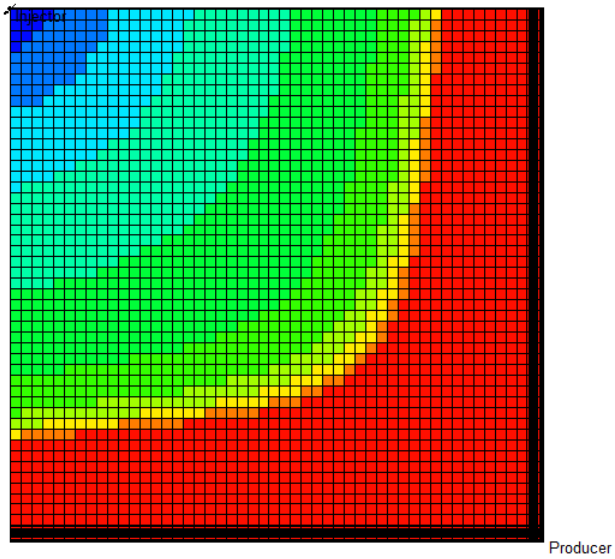

Figure 3.5: Water saturation with un-fractured reservoir after 13 months, favorable direction

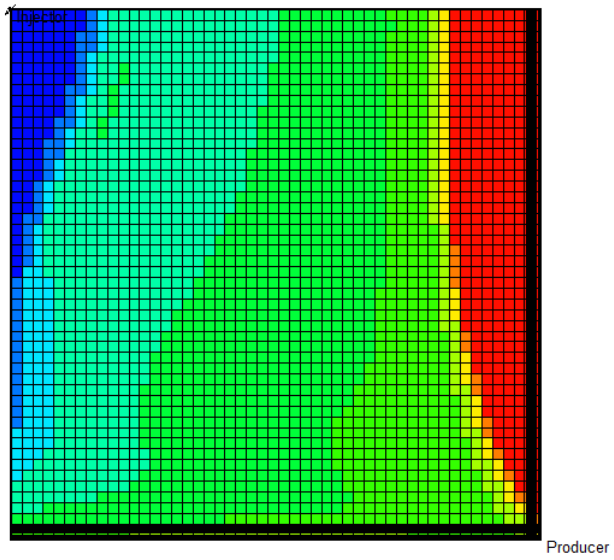

Figure 3.6: Water saturation with fractured reservoir after 23 months, favorable direction

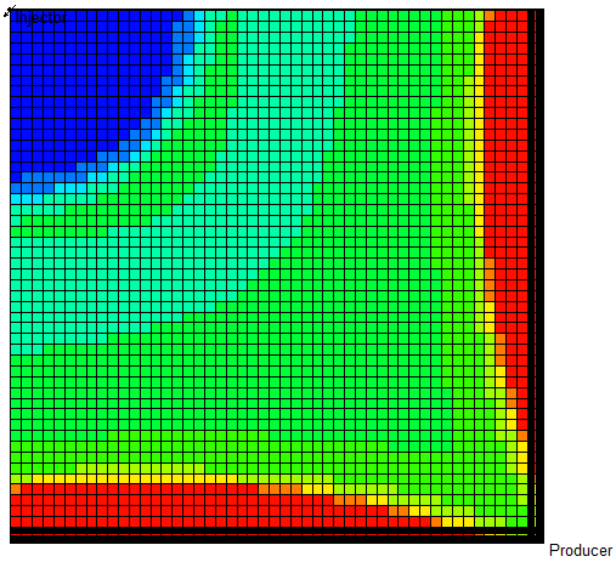

Figure 3.7: Water saturation with fractured reservoir after 23 months, favorable direction

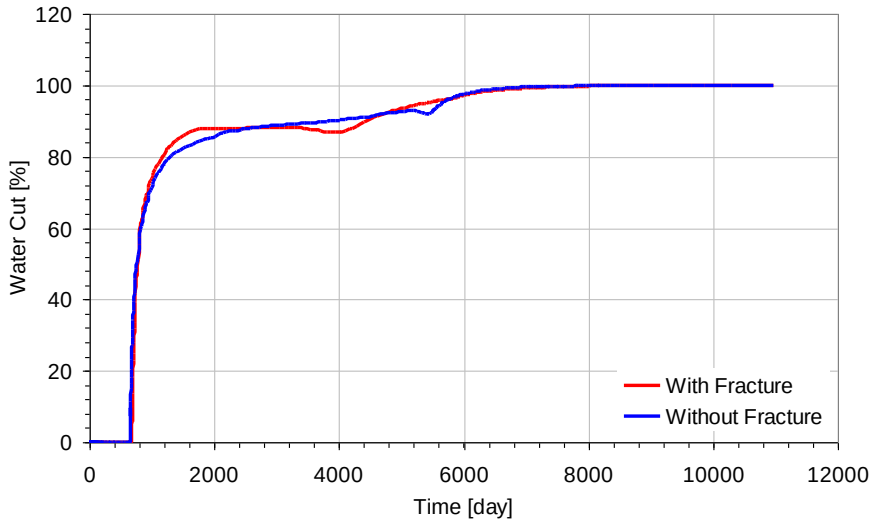

Figure 3.8: Water breakthrough with fractured and un-fractured reservoirs (favorable mobility ratio), injected fluid viscosity 30 cp, and oil viscosity 10 cp

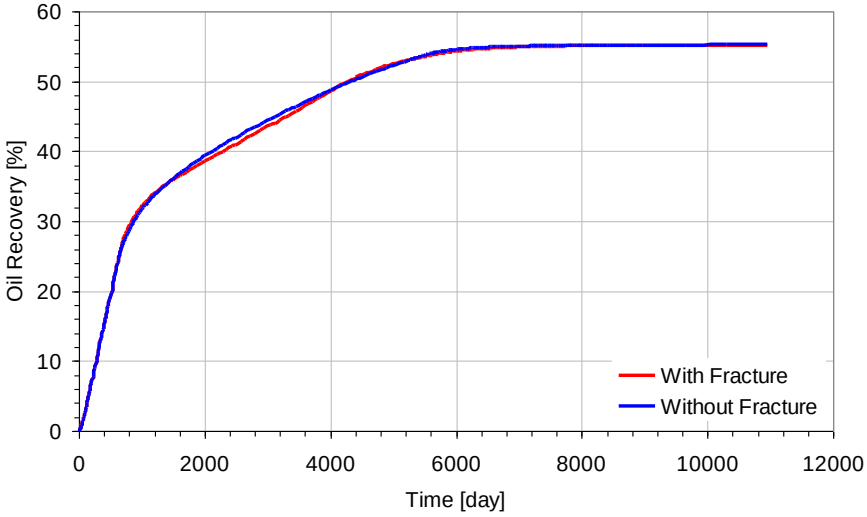

Figure 3.9: Oil recovery with fractured and un-fractured reservoirs (favorable mobility ratio), injected fluid viscosity 30 cp, and oil viscosity 10 cp

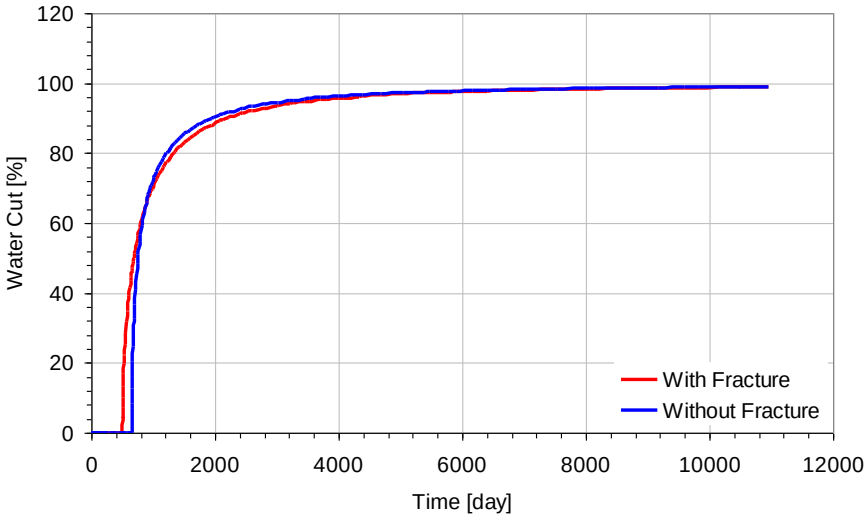

Figure 3.10: Water breakthrough with fractured and un-fractured reservoirs (unfavorable mobility ratio), injected fluid viscosity 1cp, oil viscosity 10 cp

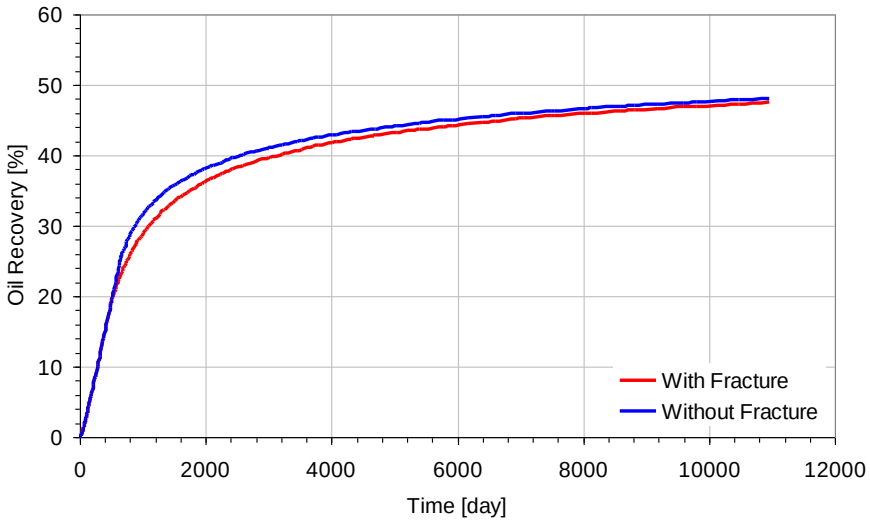

Figure 3.11: Oil recovery with fractured and un-fractured reservoirs (unfavorable mobility ratio), injected fluid viscosity 1 cp, oil viscosity 10 cp

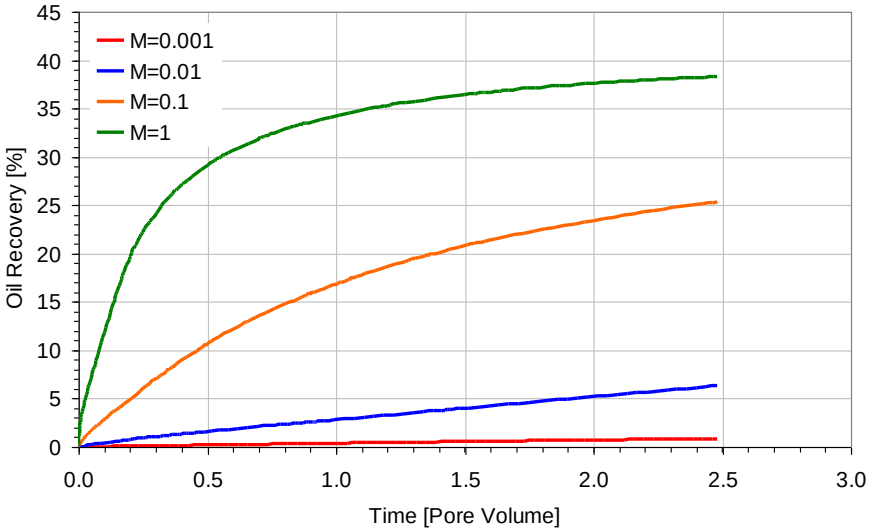

Figure 3.12: Oil recovery of un-fractured reservoirs with various mobility ratios

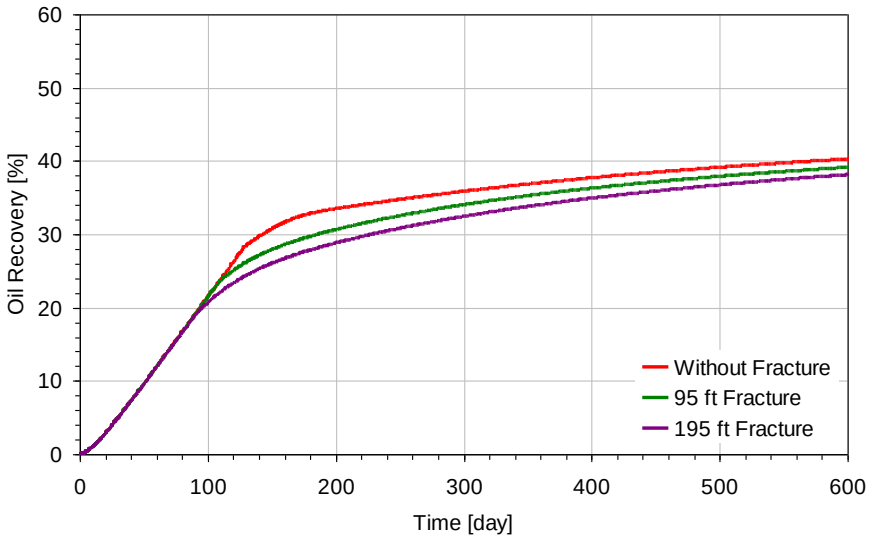

Figure 3.13: Oil recovery with various fracture length, water viscosity 1cp, oil viscosity 30 cp

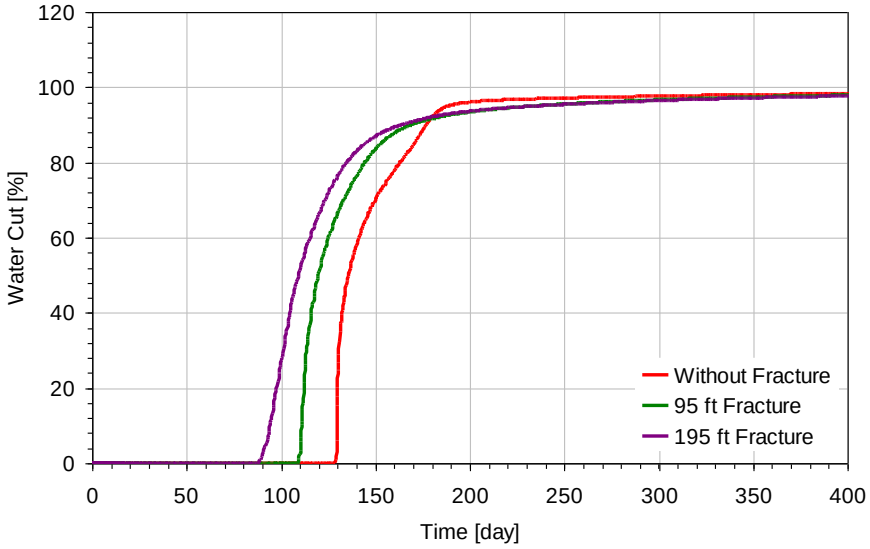

Figure 3.14: Water cut with various fracture lengths, water viscosity 1cp, oil viscosity 30 cp

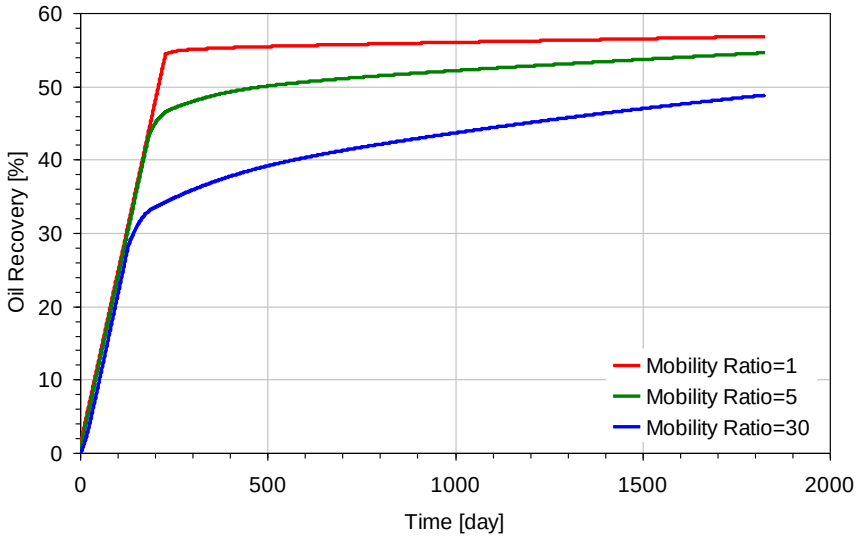

Figure 3.15: Oil recovery with various injected fluid viscosities without fracture

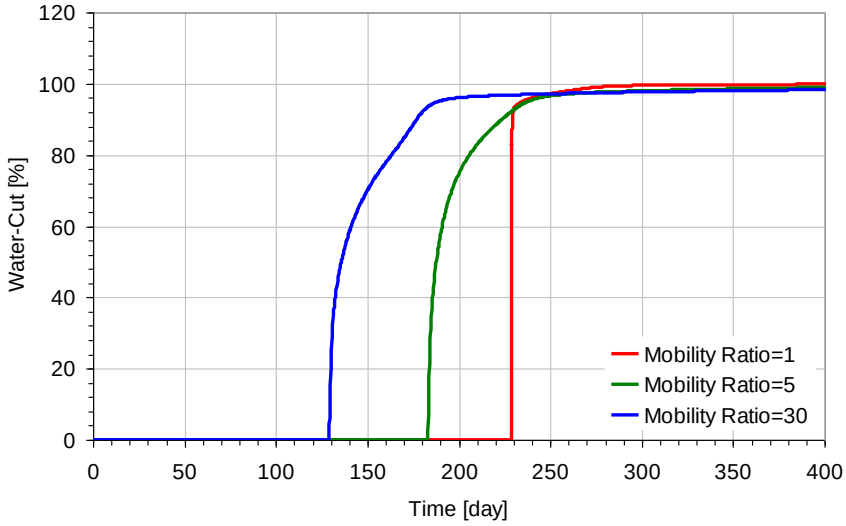

Figure 3.16: Water Cut with various injected fluid viscosities without fracture

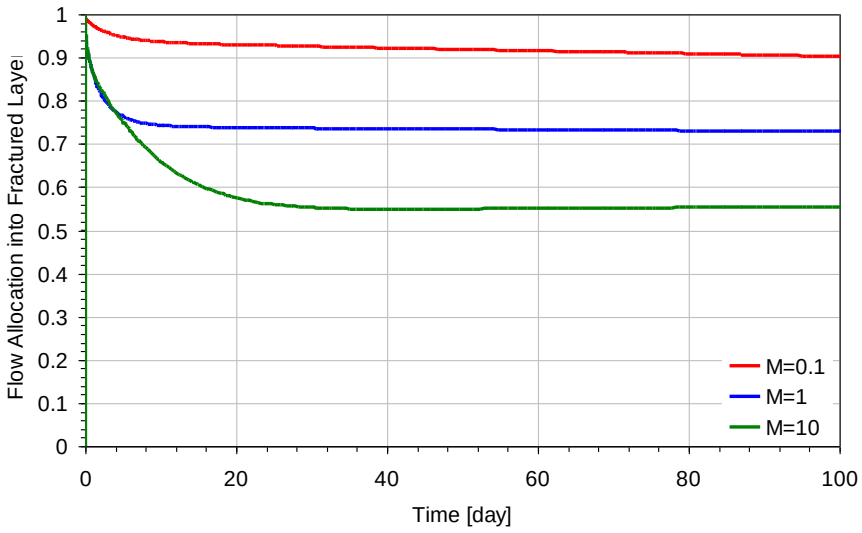

Figure 3.17: Impact of mobility ratio on flow allocation into fractured layer

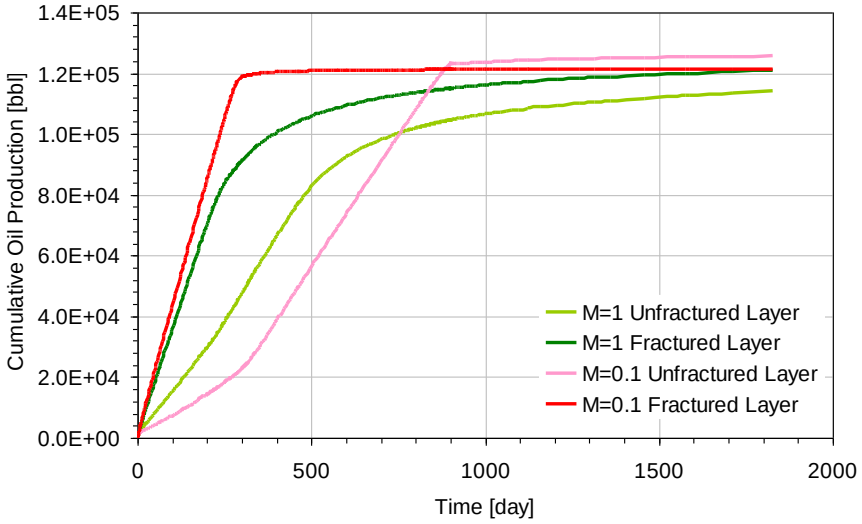

Figure 3.18: Impact of mobility ratio and fracture on cumulative oil production

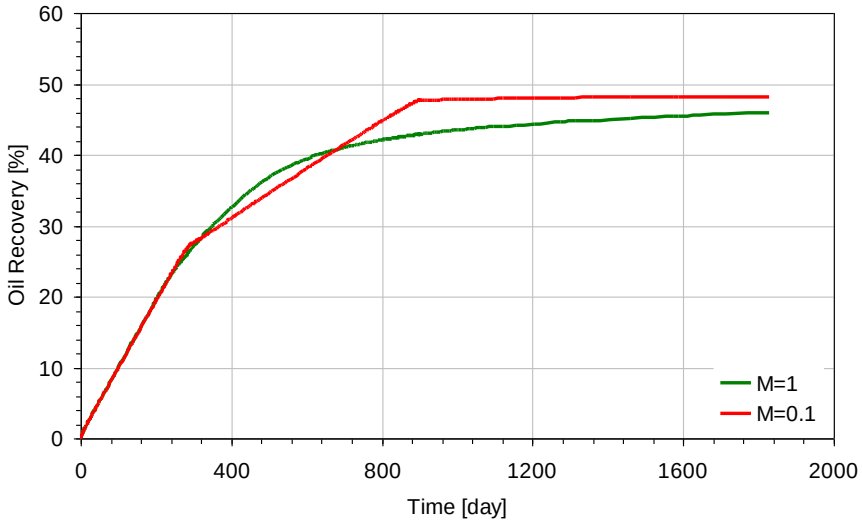

Figure 3.19: Impact of mobility ratio on oil recovery

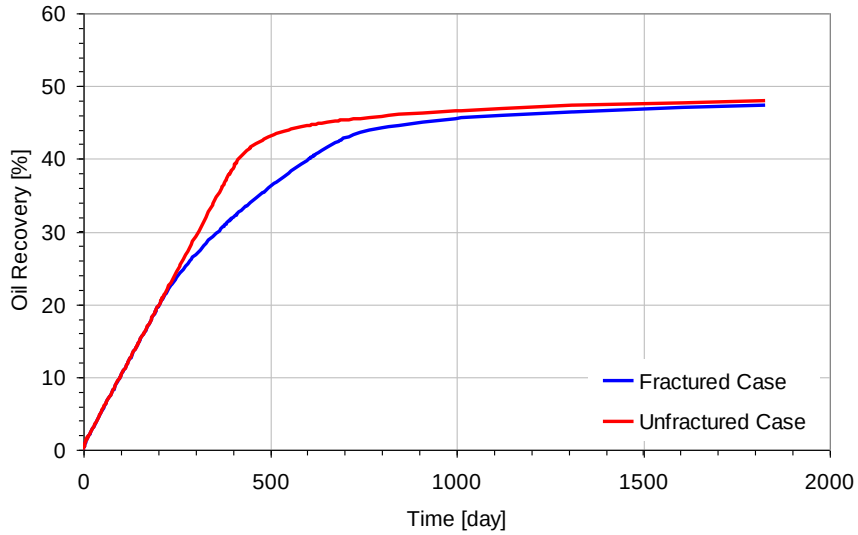

Figure 3.20: Oil recovery for fractured and un-fractured cases (*Case 1.1*)

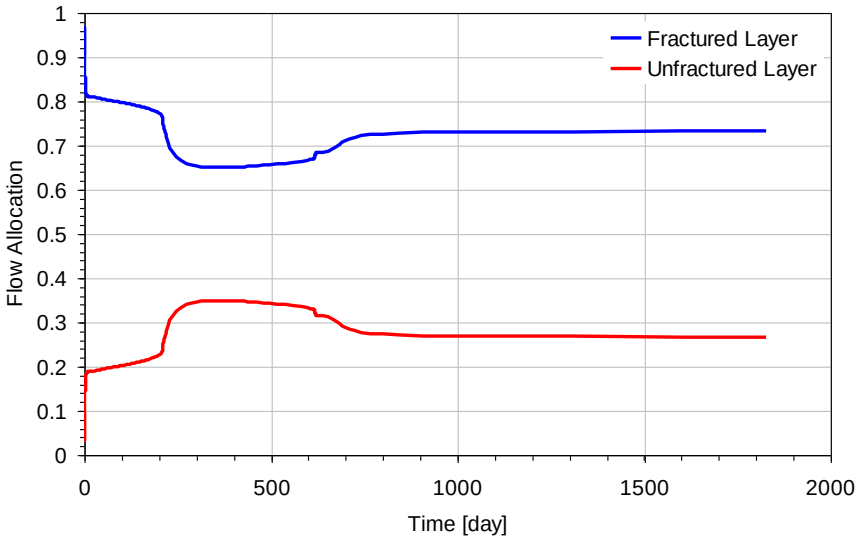

Figure 3.21: Flow allocation into the fractured and un-fractured layers in the fractured reservoir (*Case 1.1*)

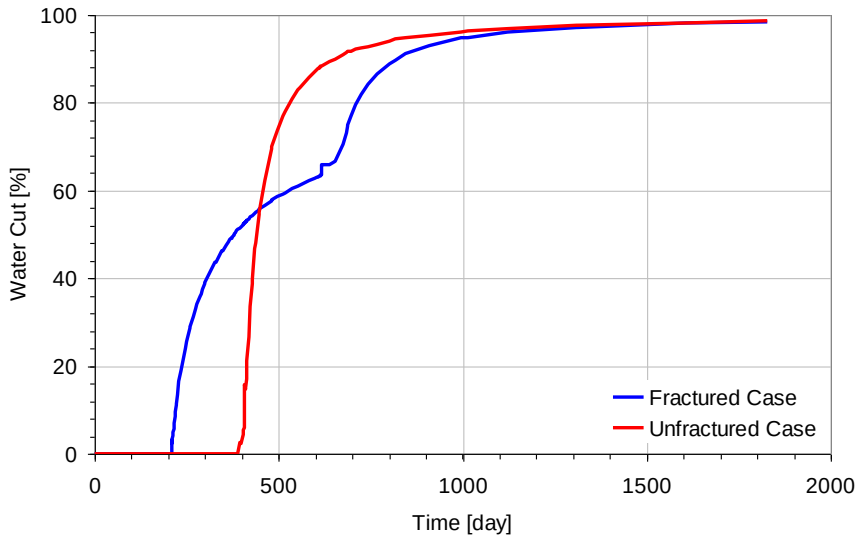

Figure 3.22: Water cut for fractured and un-fractured cases (*Case 1.1*)

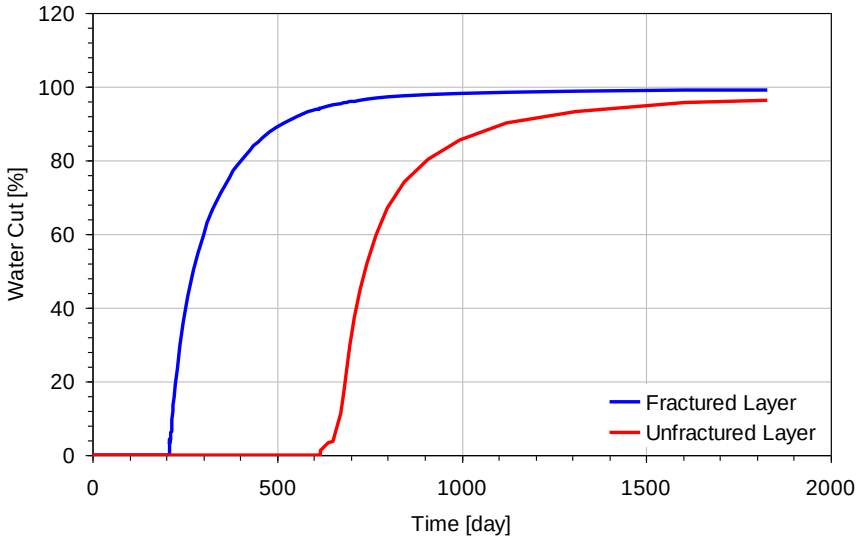

Figure 3.23: Water cut for the fractured and un-fractured layers in the fractured reservoir case (*Case 1.1*)

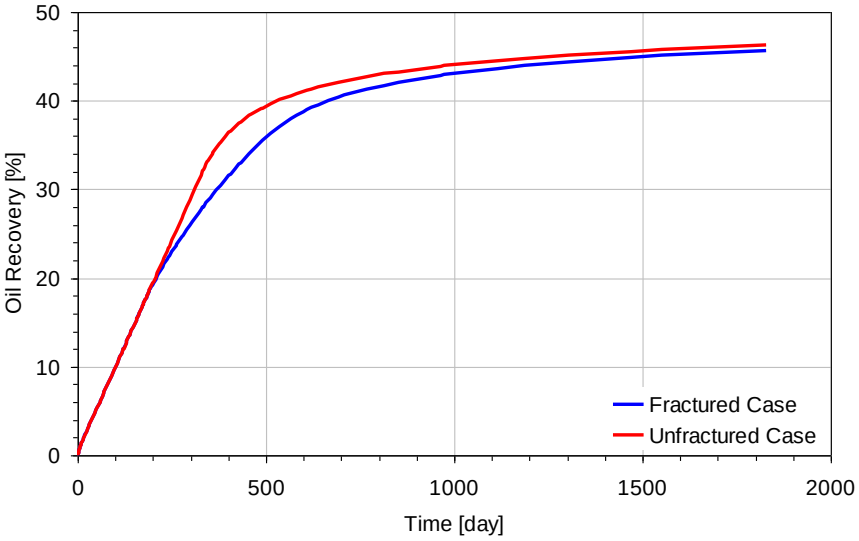

Figure 3.24: Oil recovery for fractured and un-fractured cases (*Case 1.2*)

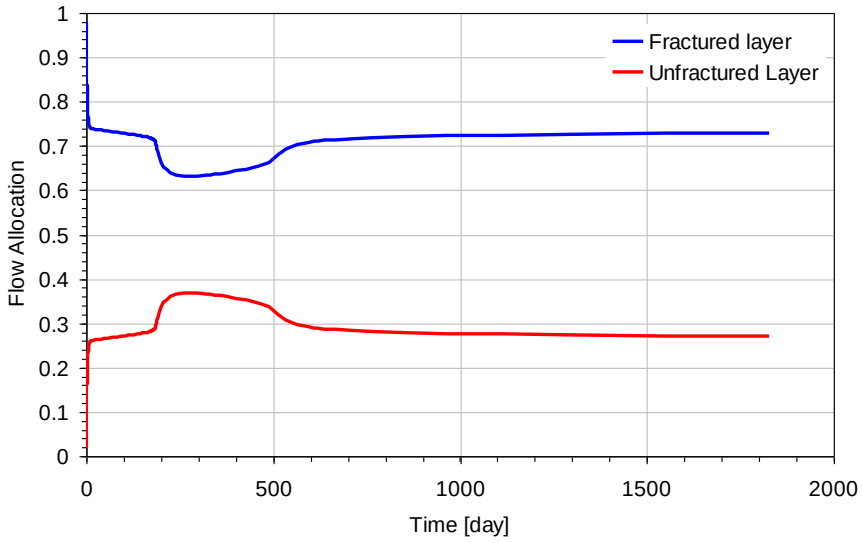

Figure 3.25: Flow allocation into the fractured and un-fractured layers in the fractured reservoir (*Case 1.2*)

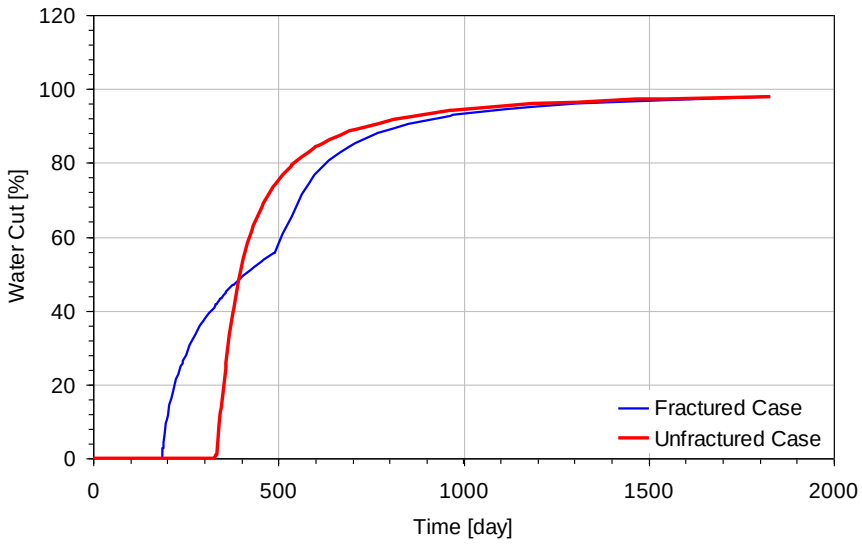

Figure 3.26: Water cut for fractured and un-fractured cases (*Case 1.2*)

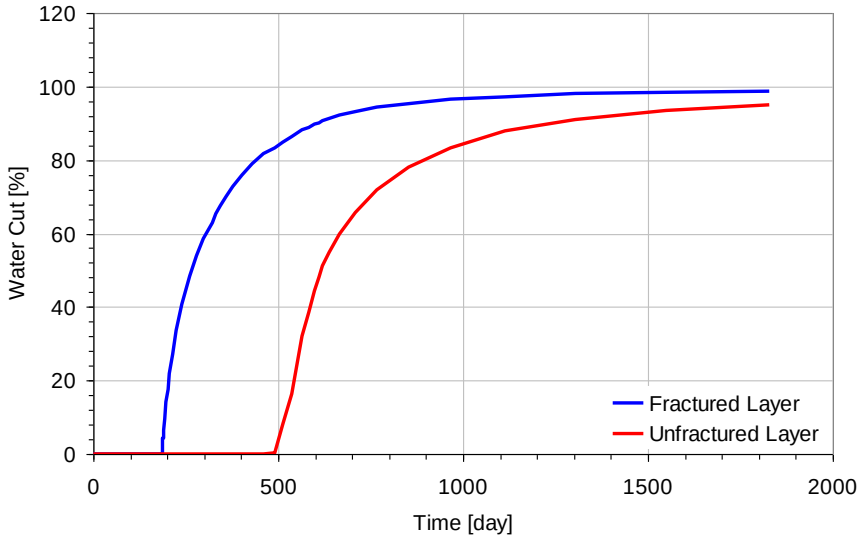

Figure 3.27: Water cut for the fractured and un-fractured layers in the fractured reservoir case (*Case 1.2*)

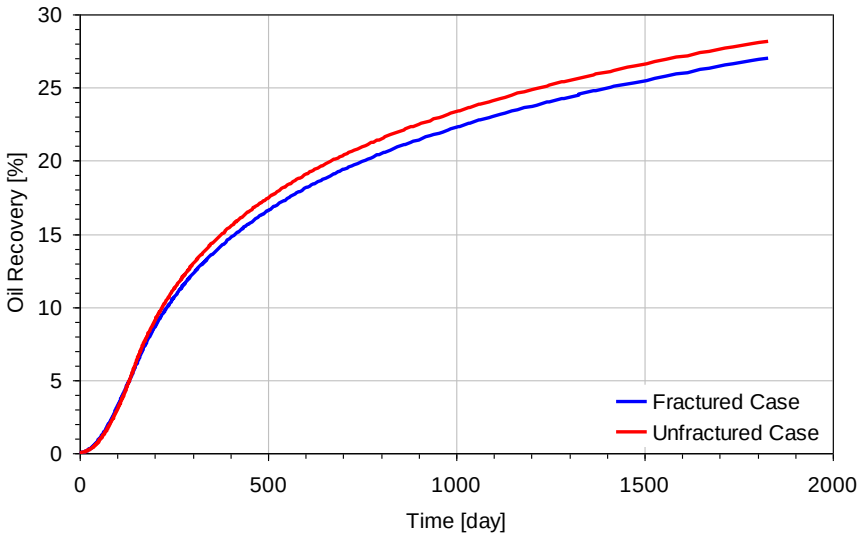

Figure 3.28: Oil recovery for fractured and un-fractured cases (*Case 1.3*)

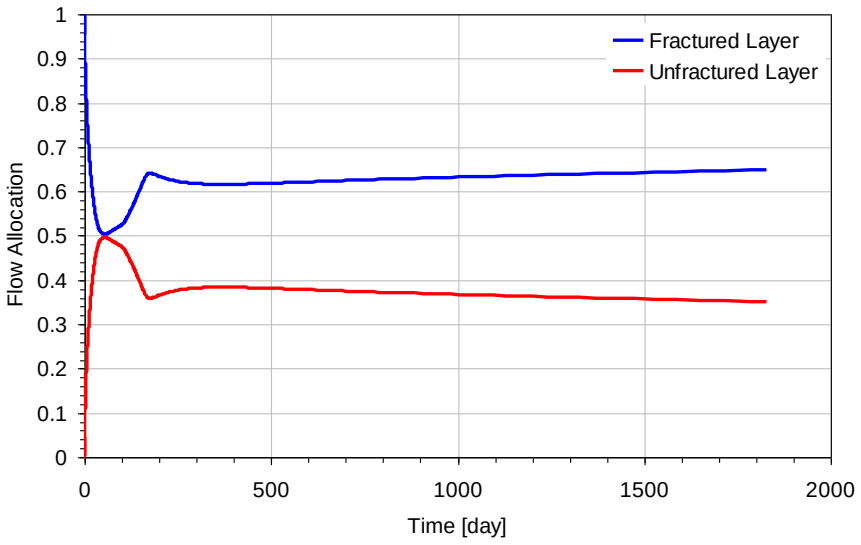

Figure 3.29: Flow allocation into the fractured and un-fractured layers in the fractured reservoir (*Case 1.3*)

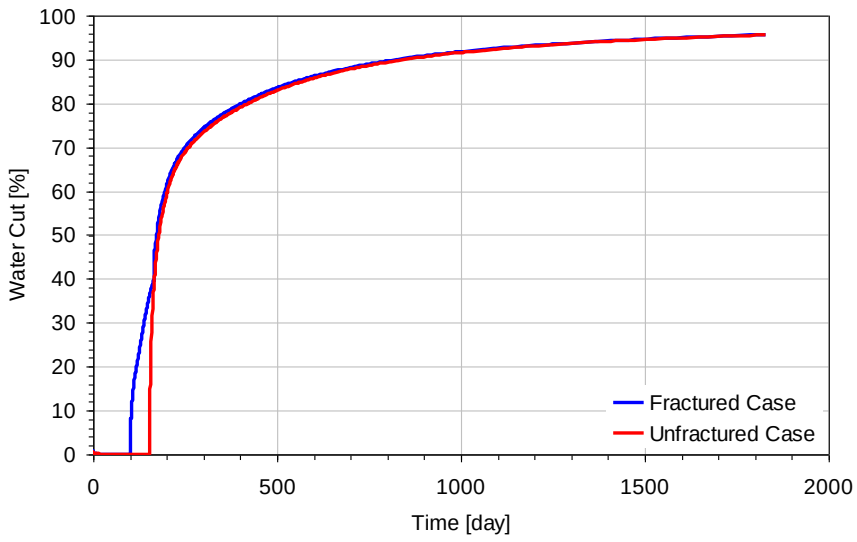

Figure 3.30: Water cut for fractured and un-fractured cases (*Case 1.3*)

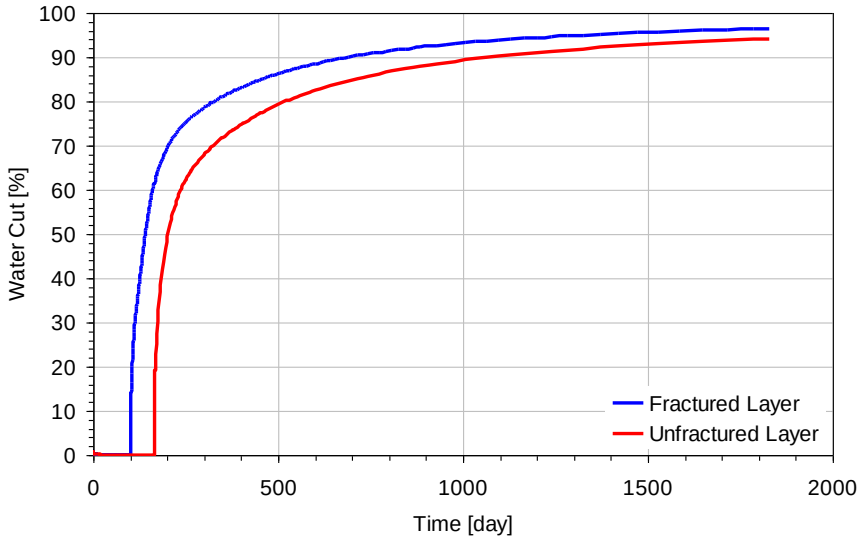

Figure 3.31: Water cut for fractured and un-fractured layers in the fractured reservoir case (*Case 1.3*)

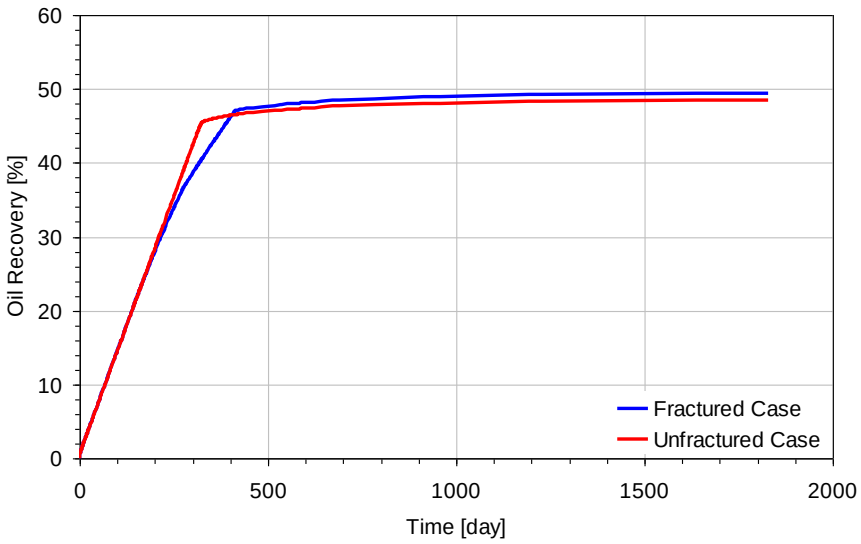

Figure 3.32: Oil recovery for fractured and un-fractured cases (*Case 1.4*)

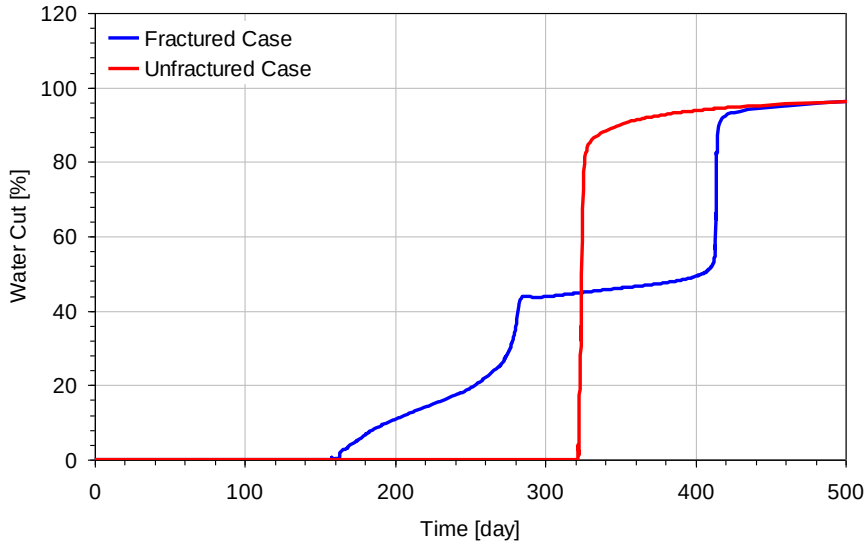

Figure 3.33: Water cut for fractured and un-fractured cases (*Case 1.4*)

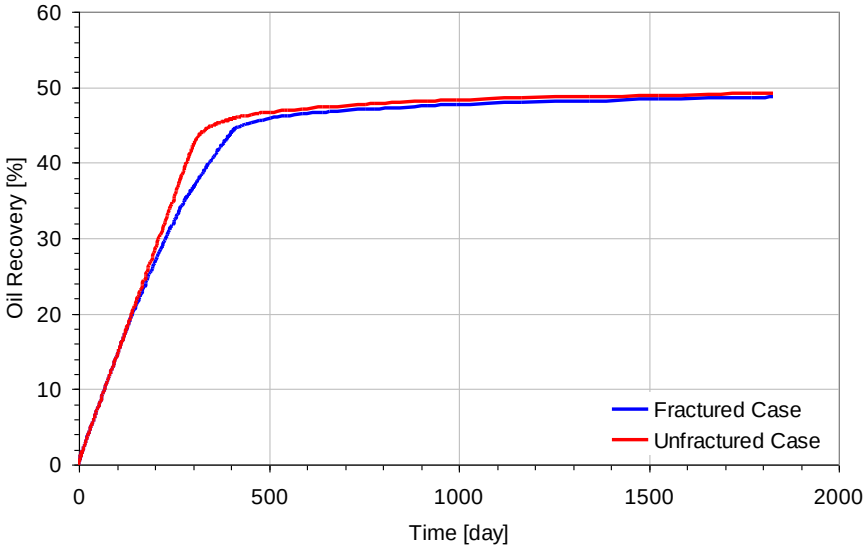

Figure 3.34: Oil recovery for fractured and un-fractured cases (*Case 1.5*)

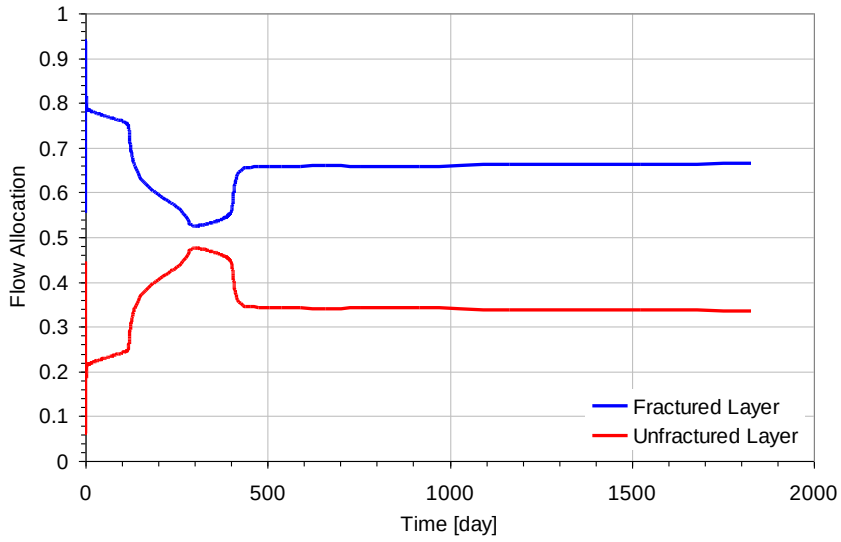

Figure 3.35: Flow allocation into the fractured and un-fractured layers in the fractured reservoir (*Case 1.5*)

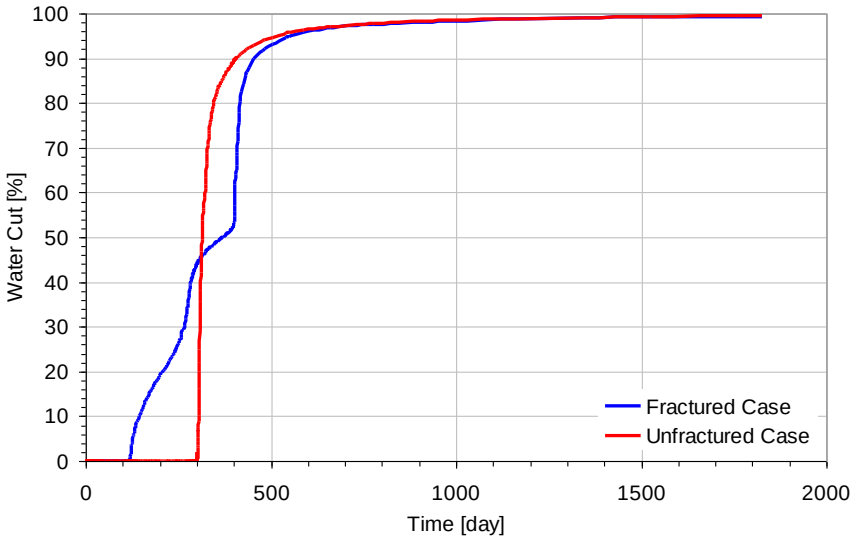

Figure 3.36: Water cut for fractured and un-fractured cases (*Case 1.5*)

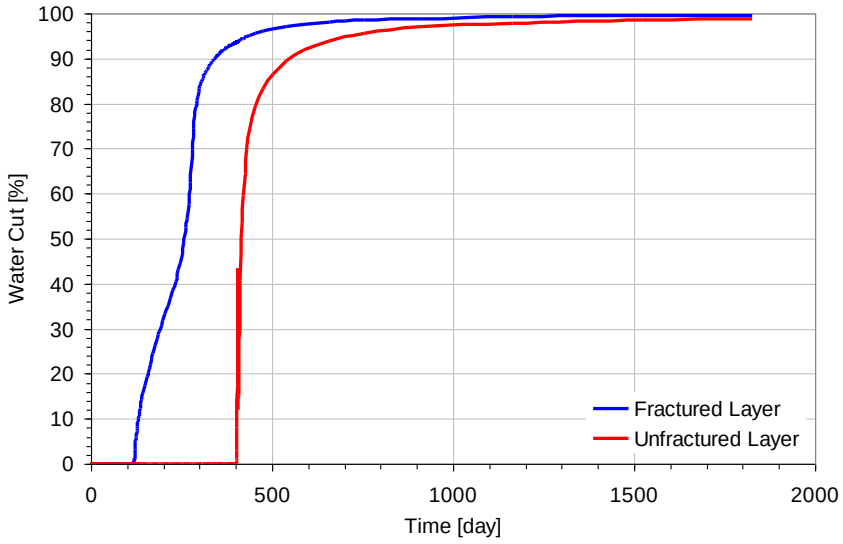

Figure 3.37: Water cut for the fractured and un-fractured layers in the fractured reservoir case (*Case 1.5*)

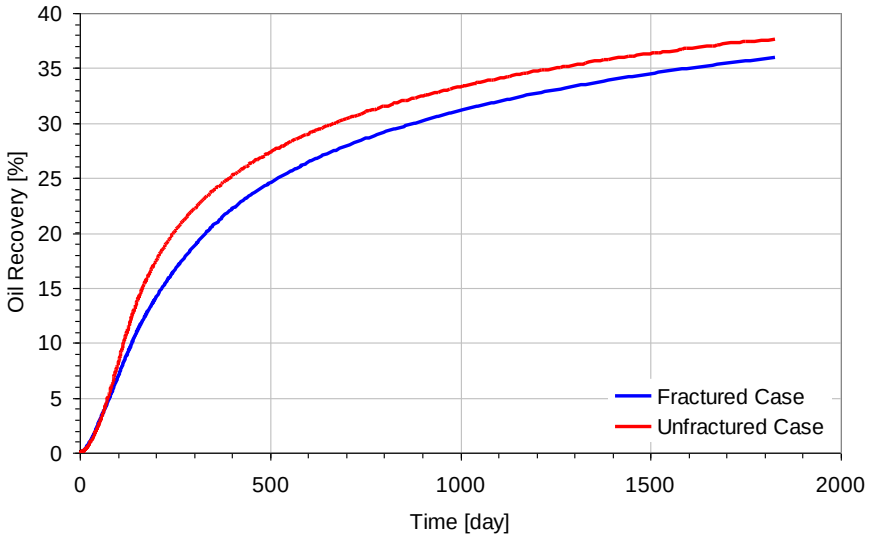

Figure 3.38: Oil recovery for fractured and un-fractured cases (*Case 1.6*)

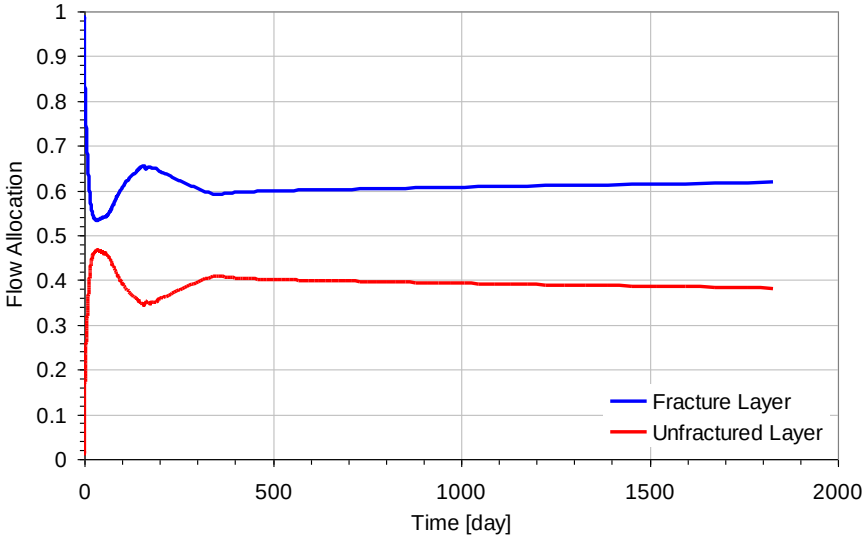

Figure 3.39: Flow allocation into the fractured and un-fractured layers in the fractured reservoir (*Case 1.6*)

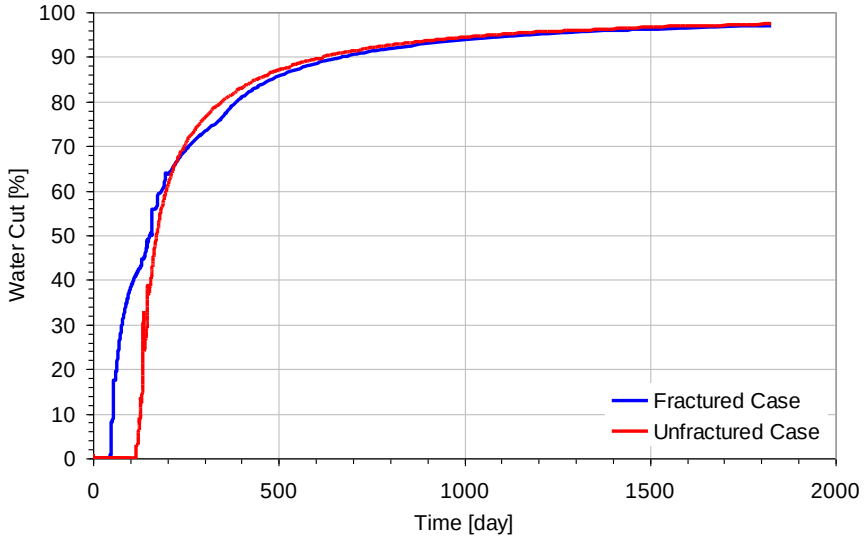

Figure 3.40: Water cut for fractured and un-fractured cases (*Case 1.6*)

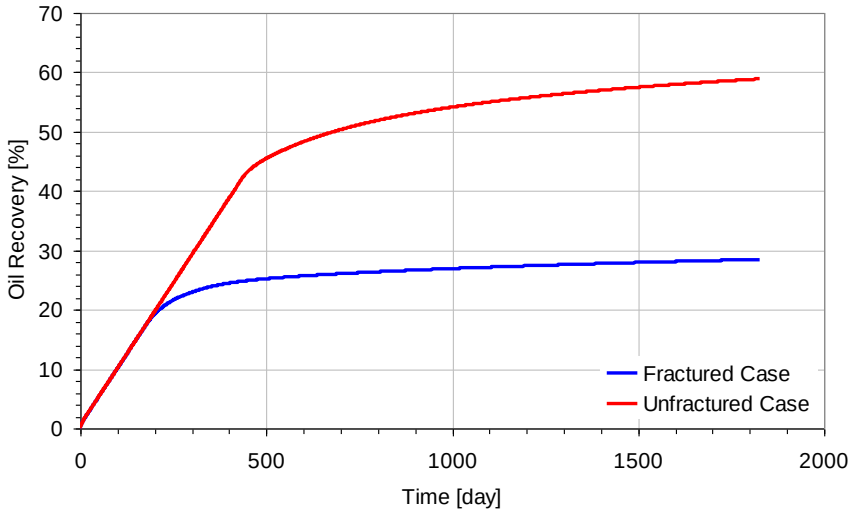

Figure 3.41: Oil recovery for fractured and un-fractured cases (*Case 2.1*)

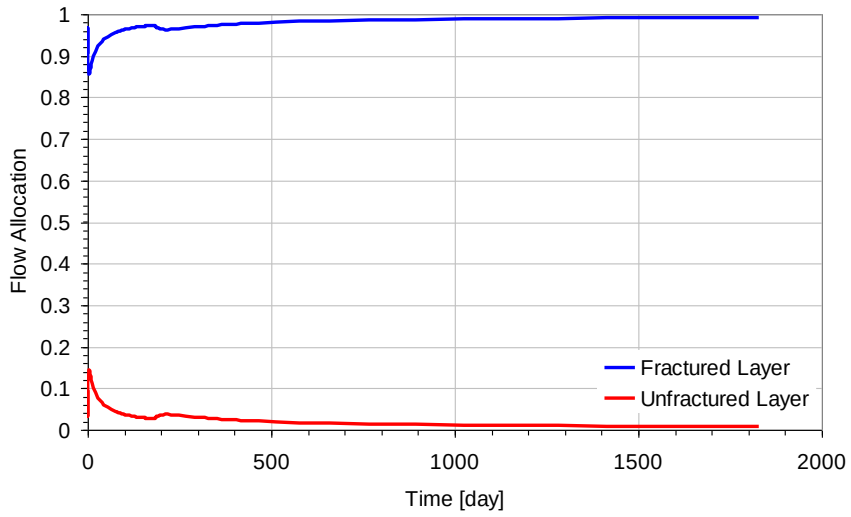

Figure 3.42: Flow allocation into the fractured and un-fractured layers in the fractured reservoir (*Case 2.1*)

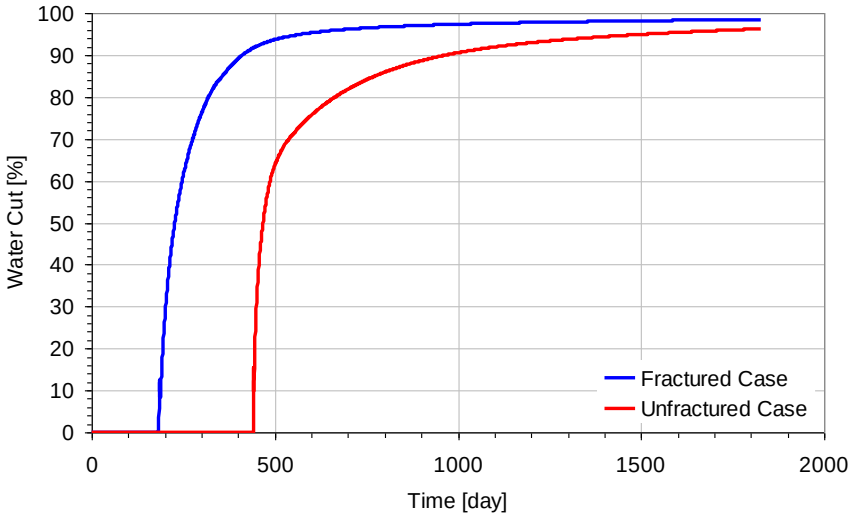

Figure 3.43: Water cut for fractured and un-fractured cases (*Case 2.1*)

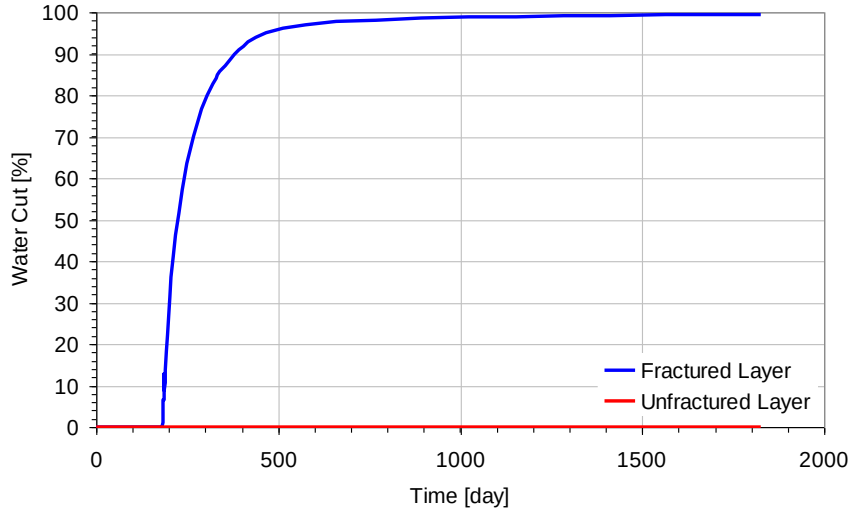

Figure 3.44: Water cut for the fractured and un-fractured layers in the fractured reservoir case (*Case 2.1*)

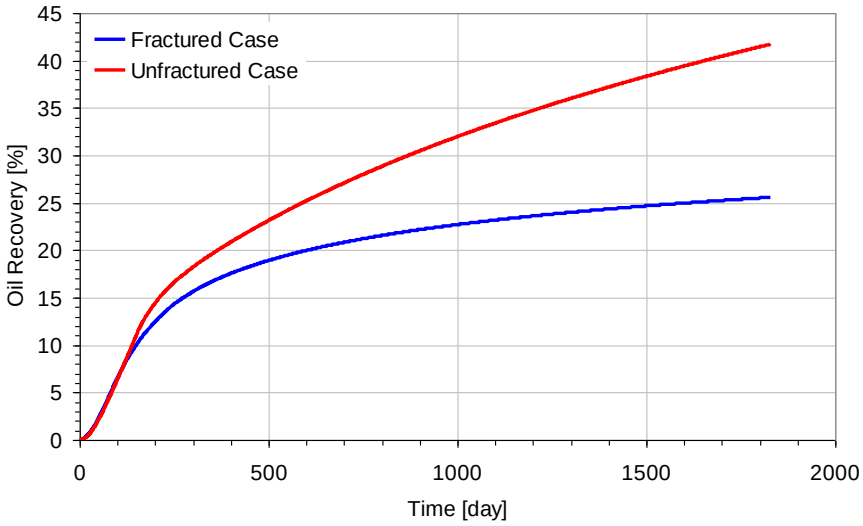

Figure 3.45: Oil recovery for fractured and un-fractured cases (*Case 2.2*)

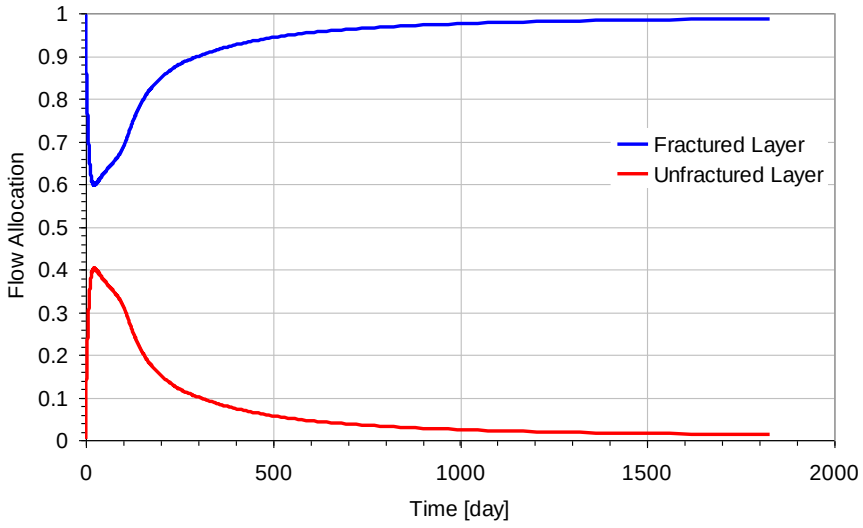

Figure 3.46: Flow allocation into the fractured and un-fractured layers in the fractured reservoir (*Case 2.2*)

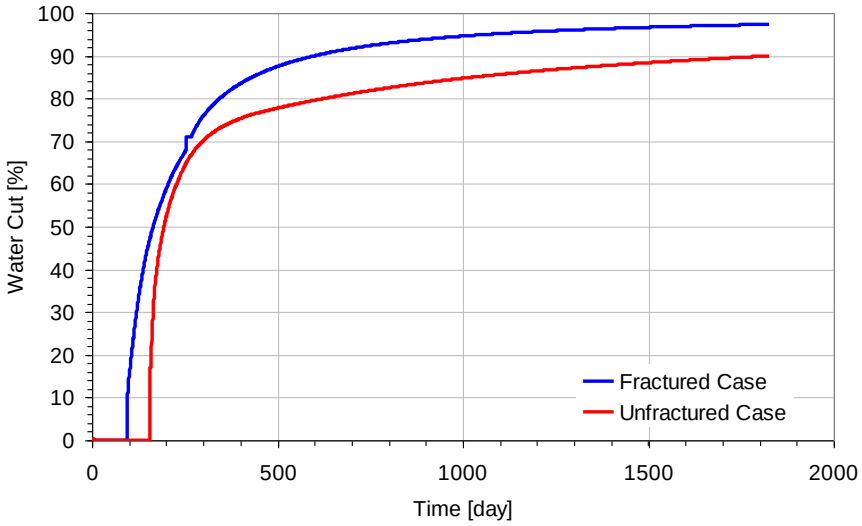

Figure 3.47: Water cut for fractured and un-fractured cases (*Case 2.2*)

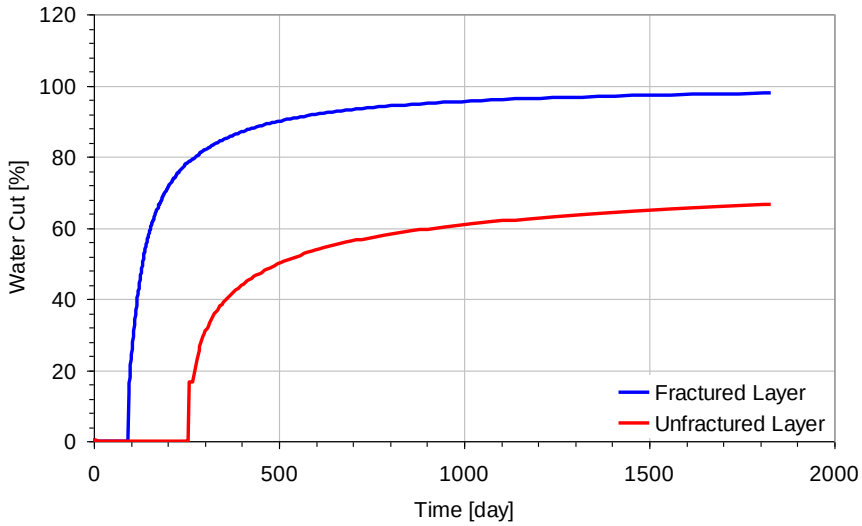

Figure 3.48: Water cut for the fractured and un-fractured layers in the fractured reservoir case (*Case 2.2*)

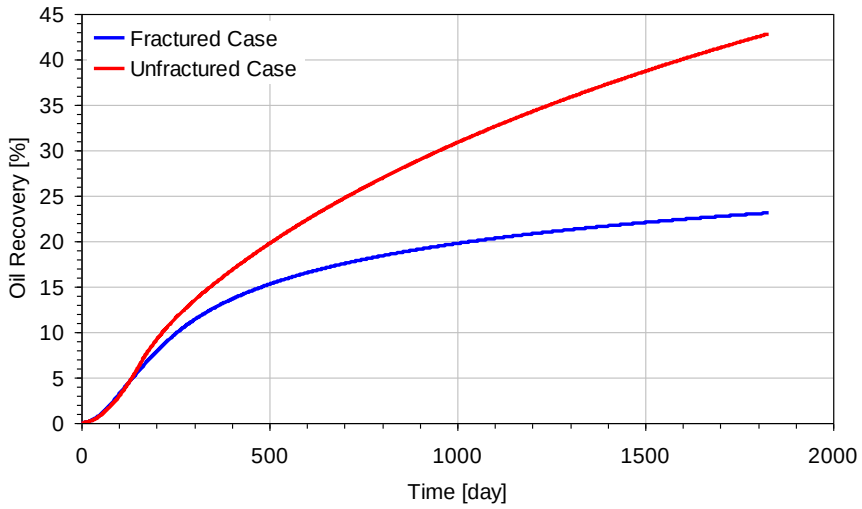

Figure 3.49: Oil recovery for fractured and un-fractured cases (*Case 2.3*)

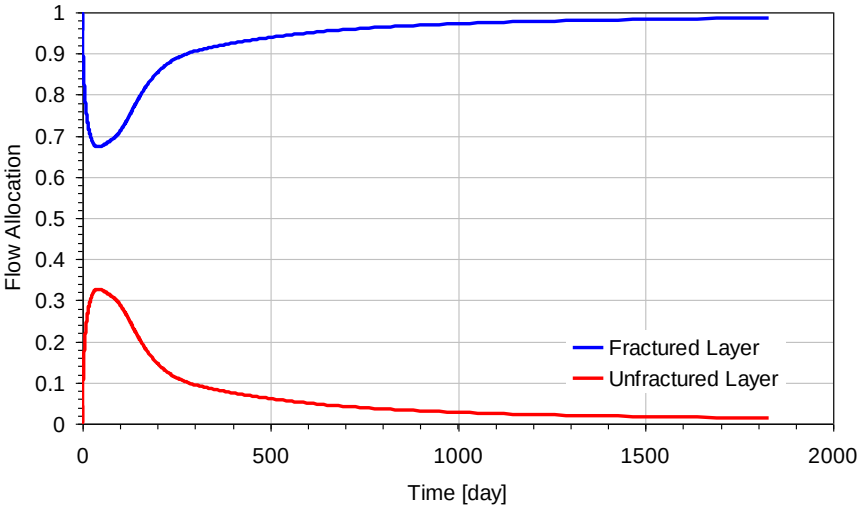

Figure 3.50: Flow allocation into the fractured and un-fractured layers in the fractured reservoir (*Case 2.3*)

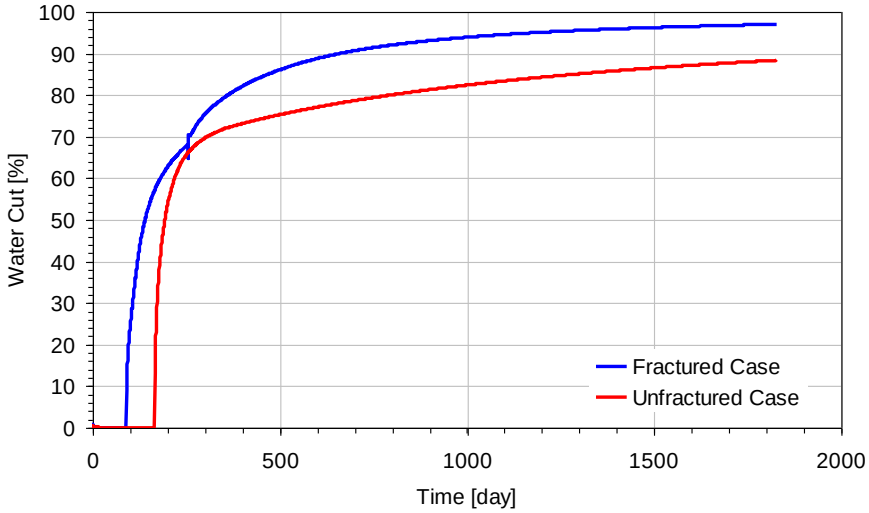

Figure 3.51: Water cut for fractured and un-fractured cases (*Case 2.3*)

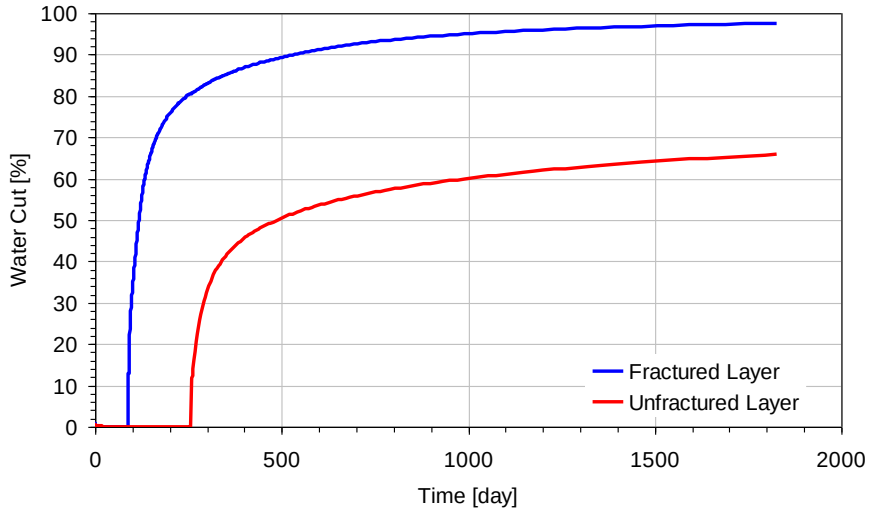

Figure 3.52: Water cut for the fractured and un-fractured layers in the fractured reservoir case (*Case 2.3*)

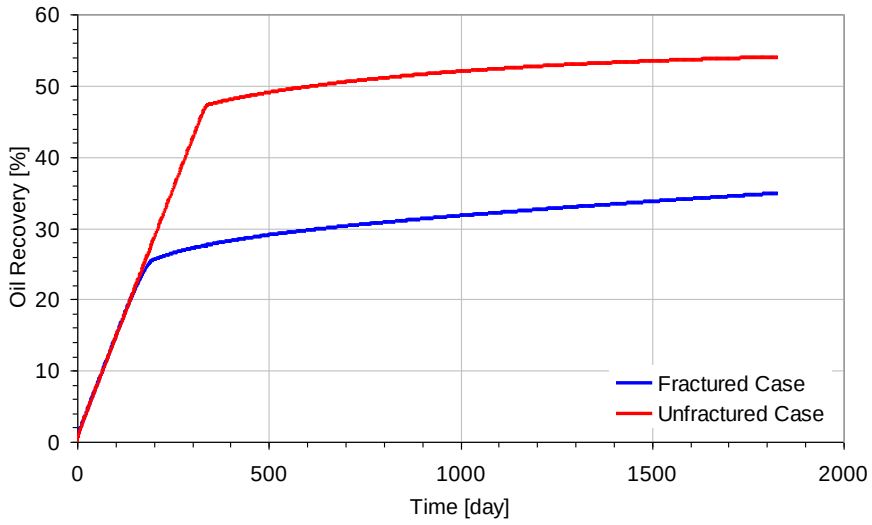

Figure 3.53: Oil recovery for fractured and un-fractured cases (*Case 2.4*)

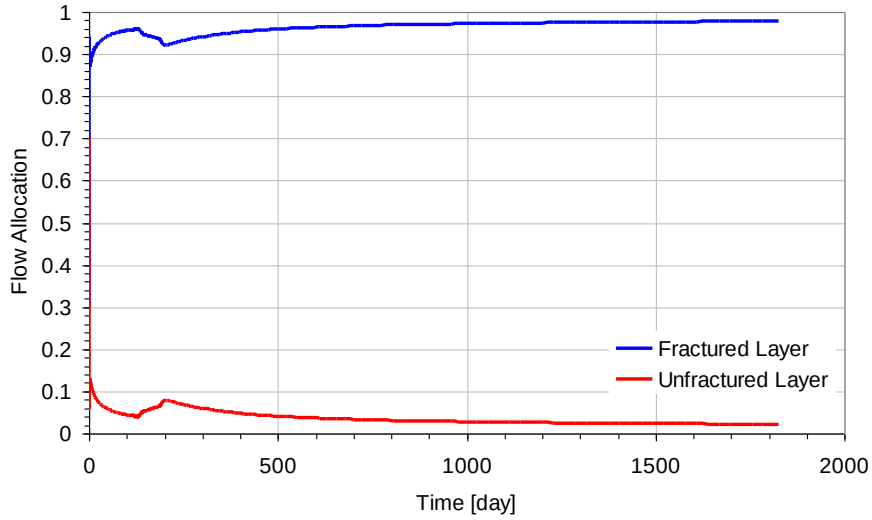

Figure 3.54: Flow allocation into the fractured and un-fractured layers in the fractured reservoir (*Case 2.4*)

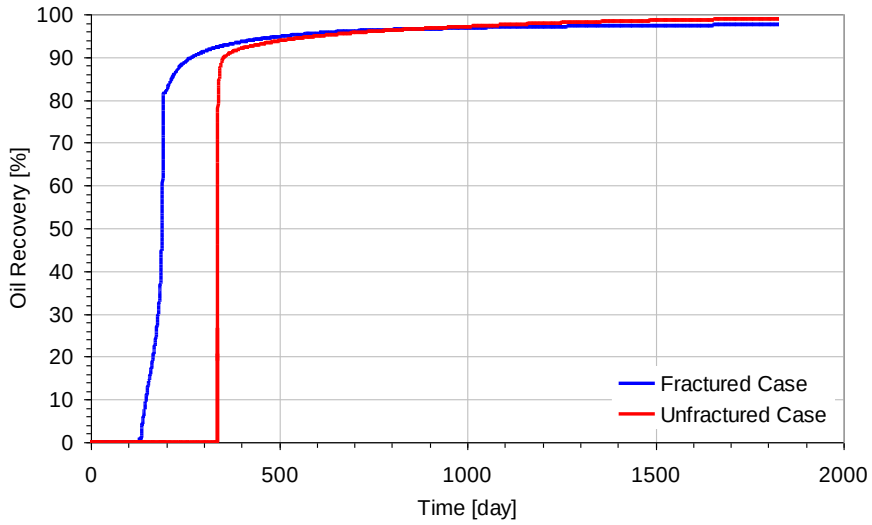

Figure 3.55: Water cut for fractured and un-fractured cases (*Case 2.4*)

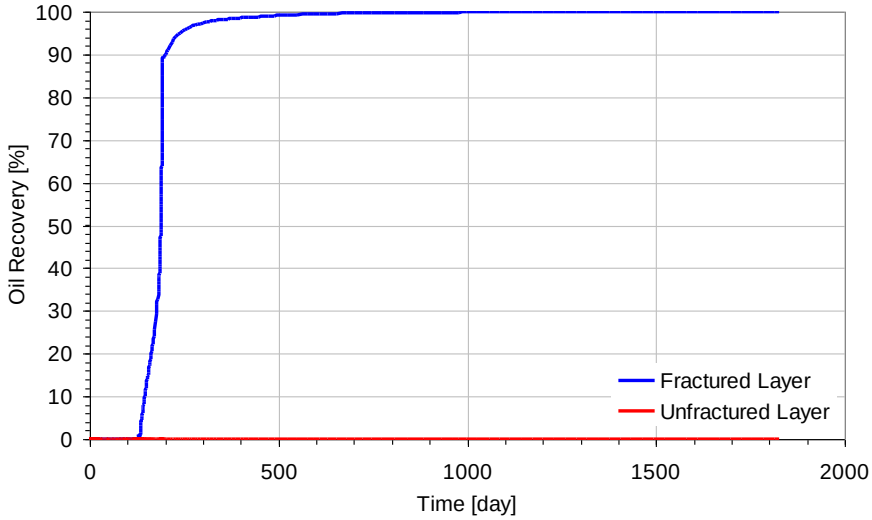

Figure 3.56: Water cut for the fractured and un-fractured layers in the fractured reservoir case (*Case 2.4*)

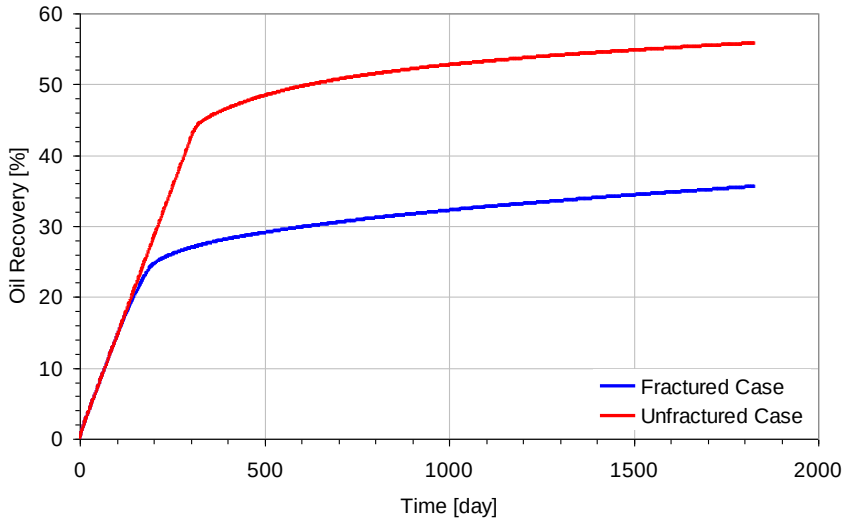

Figure 3.57: Oil recovery for fractured and un-fractured cases (*Case 2.5*)

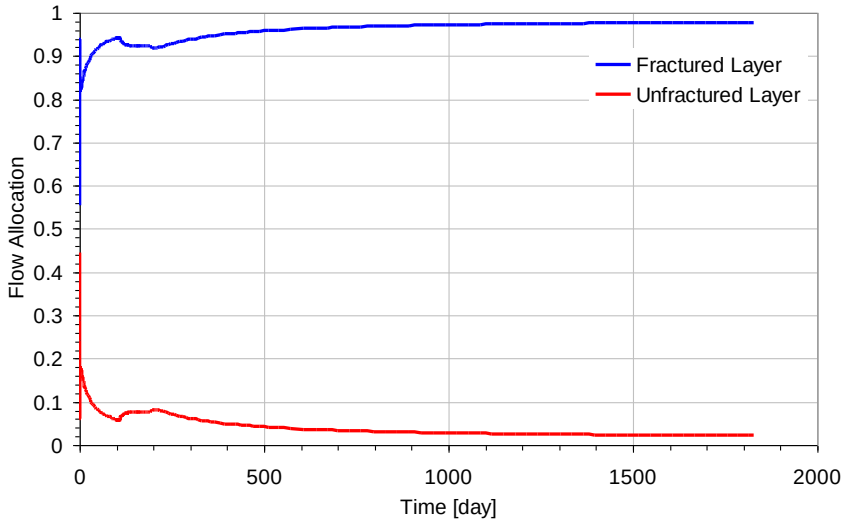

Figure 3.58: Flow allocation into the fractured and un-fractured layers in the fractured reservoir (*Case 2.5*)

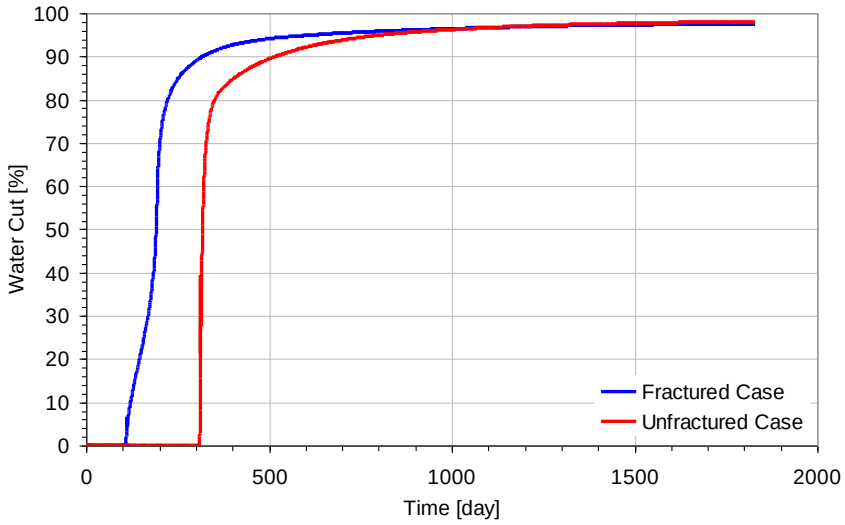

Figure 3.59: Water cut for fractured and un-fractured cases (*Case 2.5*)

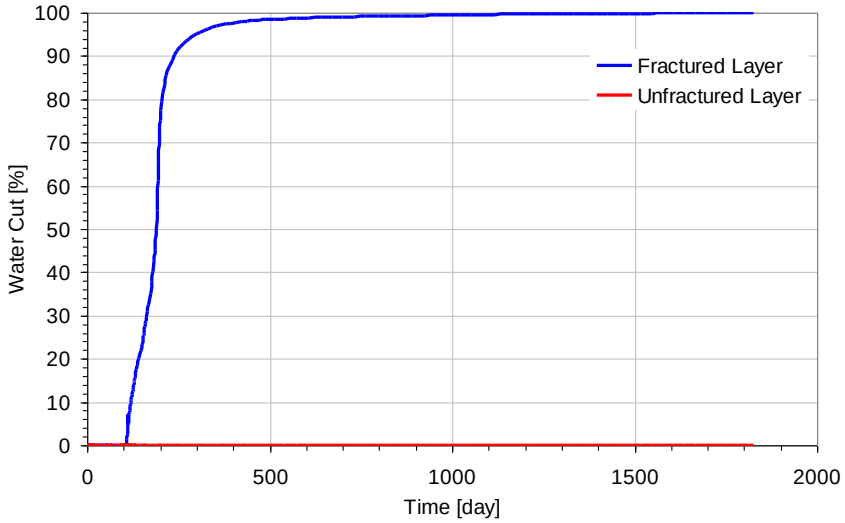

Figure 3.60: Water cut for the fractured and un-fractured layers in the fractured reservoir case (*Case 2.5*)

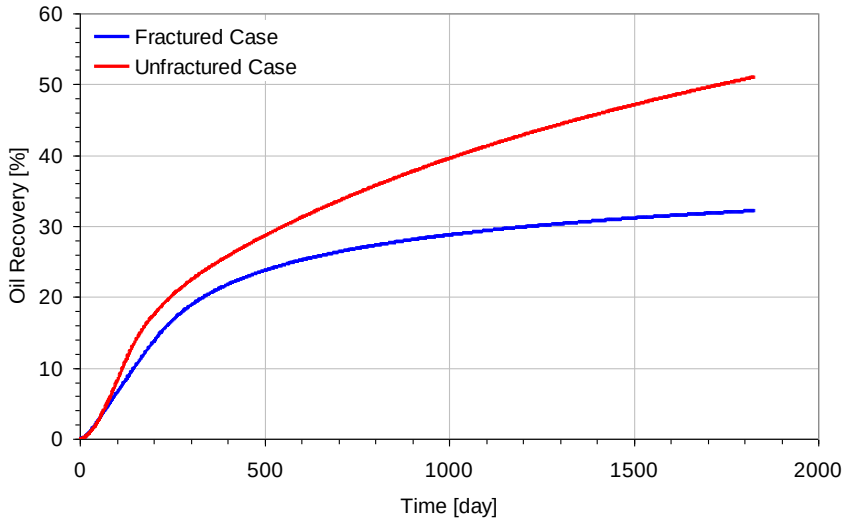

Figure 3.61: Oil recovery for fractured and un-fractured cases (*Case 2.6*)

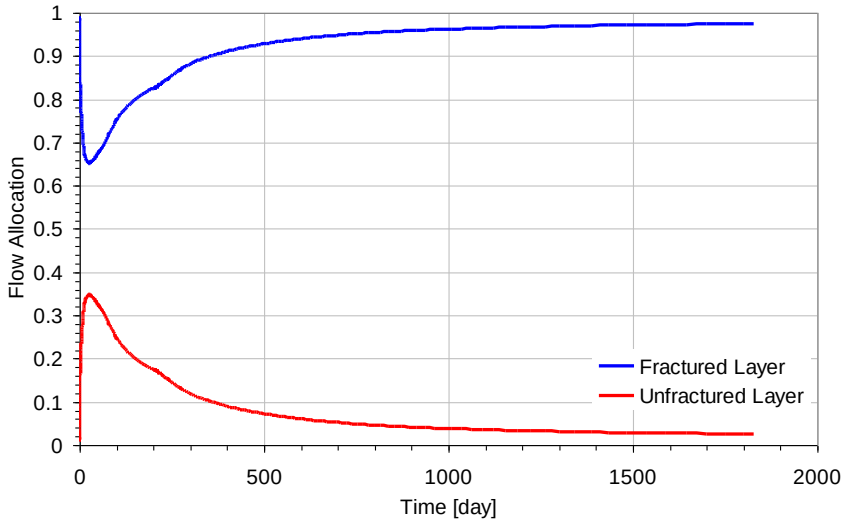

Figure 3.62: Flow allocation into the fractured and un-fractured layers in the fractured reservoir (*Case 2.6*)

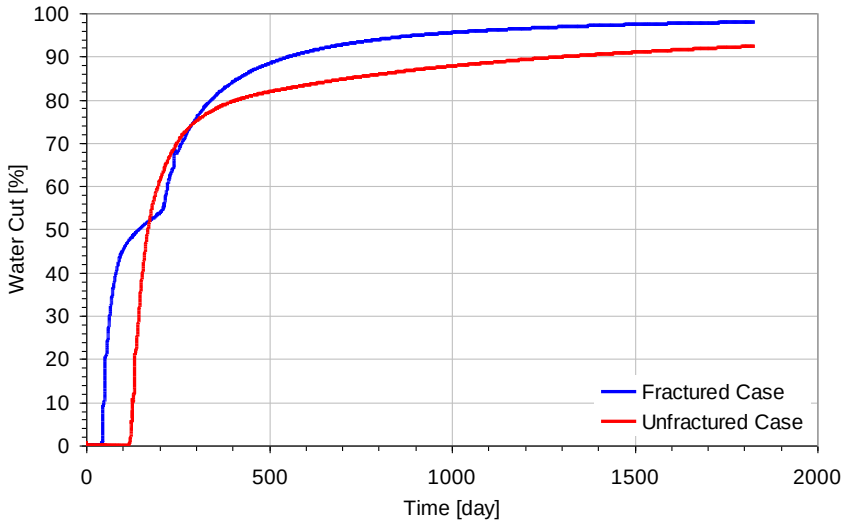

Figure 3.63: Water cut for fractured and un-fractured cases (*Case 2.6*)

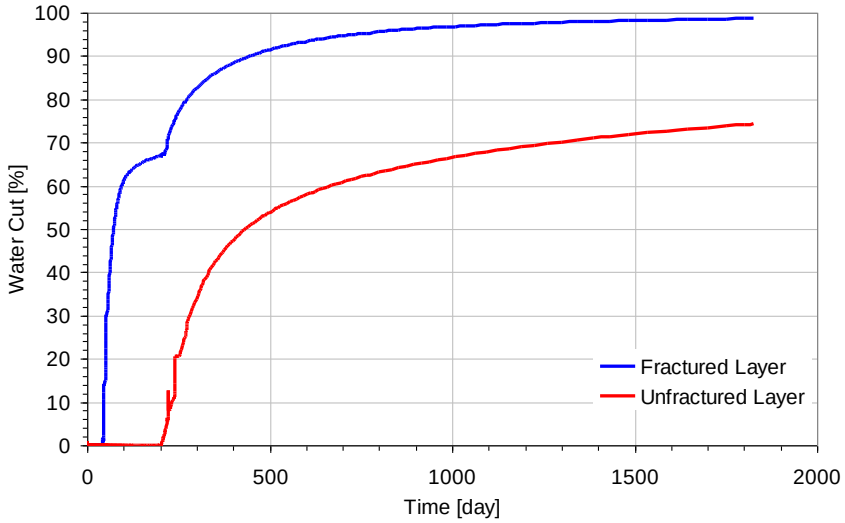

Figure 3.64: Water cut for the fractured and un-fractured layers in the fractured reservoir case (*Case 2.6*)

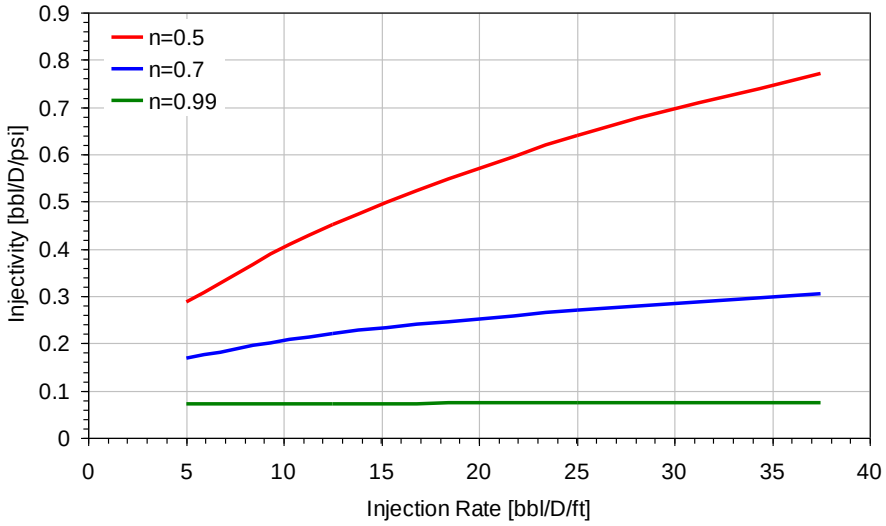

Figure 3.65: Injectivity with different power-law n values and injection rate, without fracture

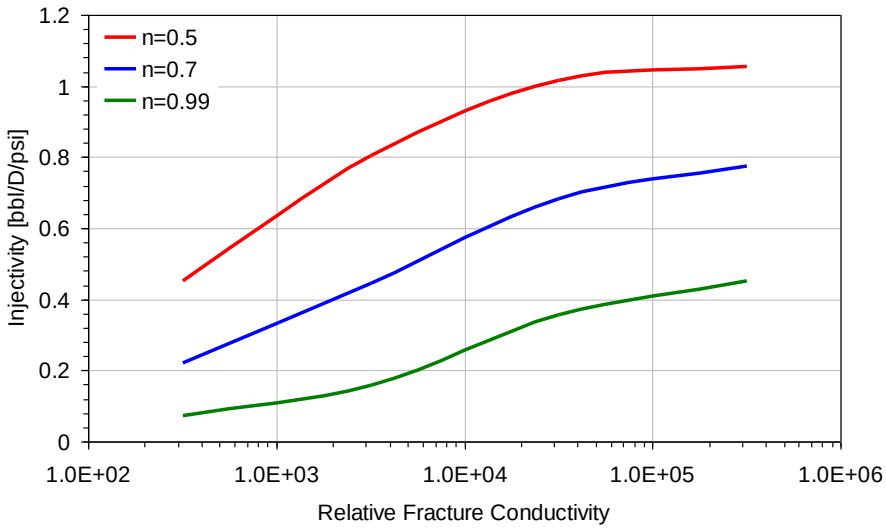

Figure 3.66: Injectivity with different power-law n values and fracture conductivity

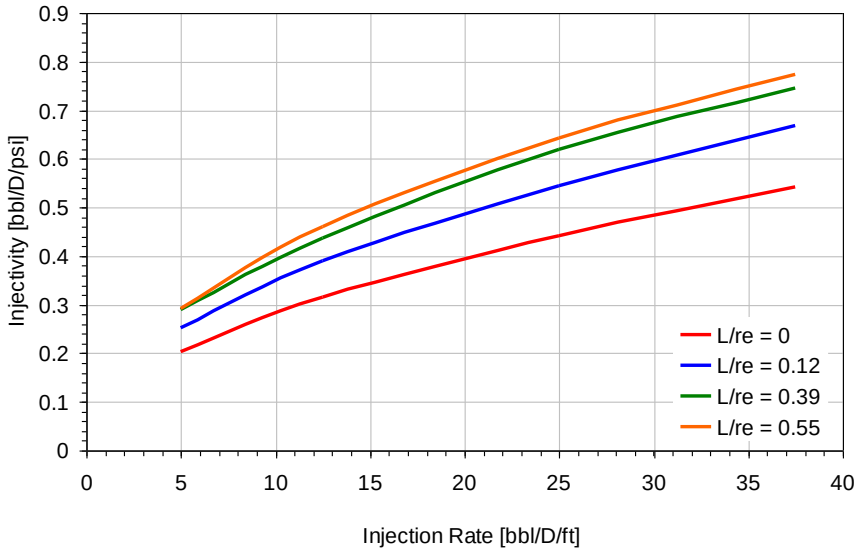

Figure 3.67: Injectivity of power-law fluid $\mu = 70\gamma^{-0.5}$, injection rate and fracture length

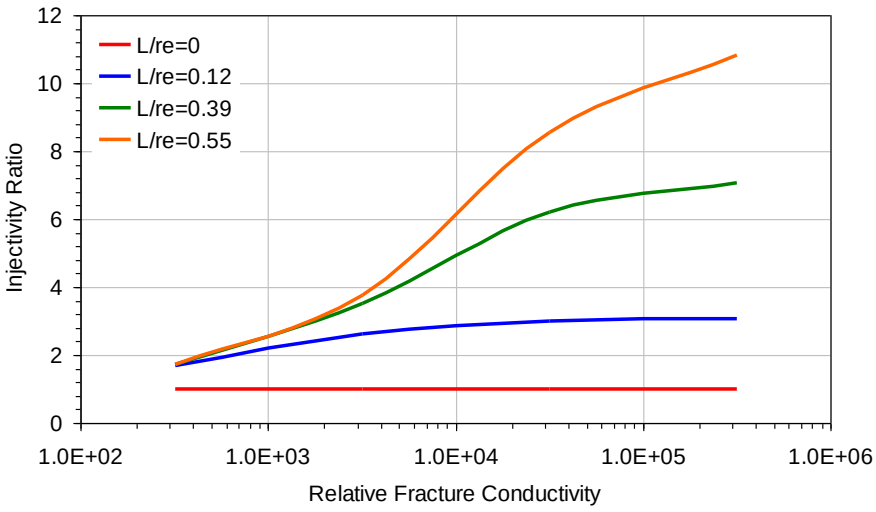

Figure 3.68: Injectivity of Newtonian fluid (70 cp) with different fracture conductivity and fracture length

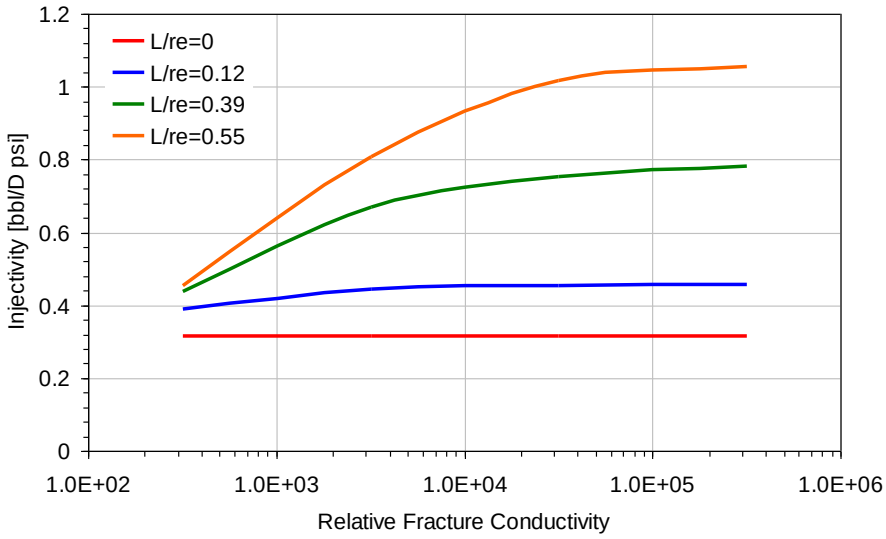

Figure 3.69: Injectivity of power-law fluid $\mu = 70\gamma^{0.5}$ with different fracture conductivity and fracture length

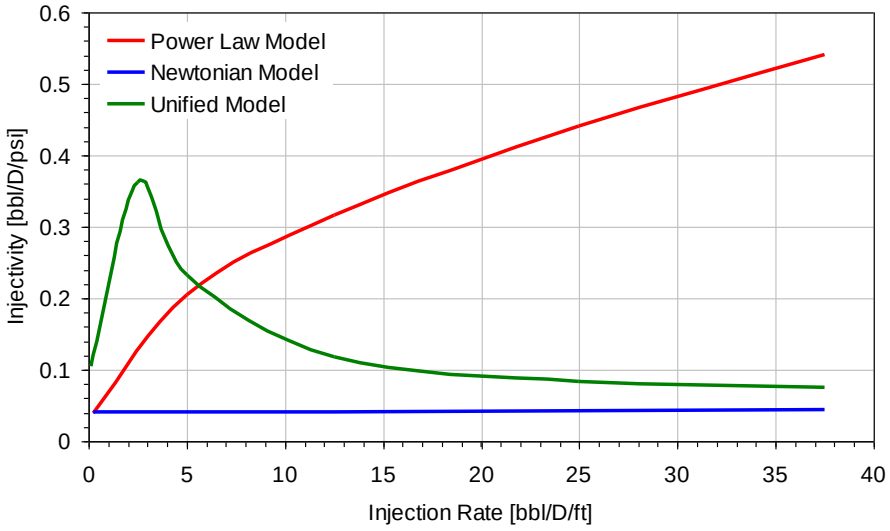

Figure 3.70: Injectivity of power-law, Newtonian, and unified model with different injection rate and without fracture

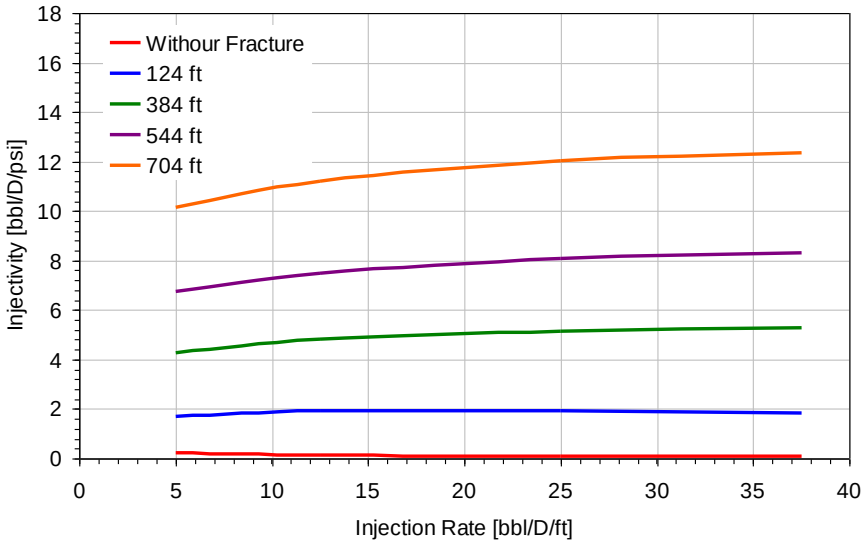

Figure 3.71: Injectivity of unified model with different injection rate and fracture length

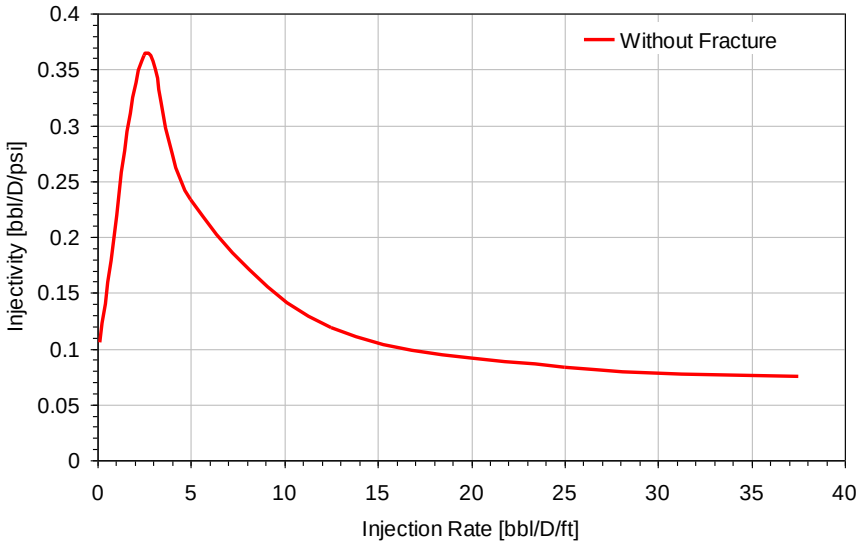

Figure 3.72: Injectivity of unified model with different injection rate and without fracture

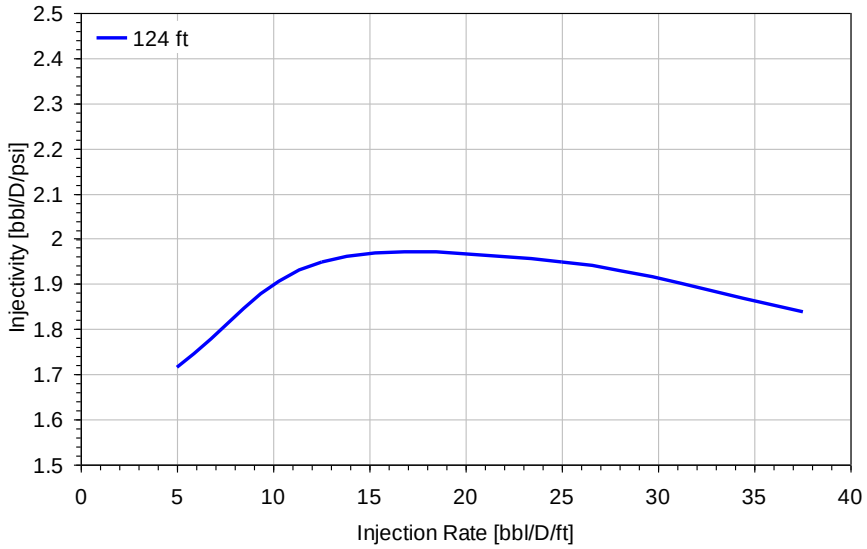

Figure 3.73: Injectivity of unified model with different injection rate and 124 ft fracture

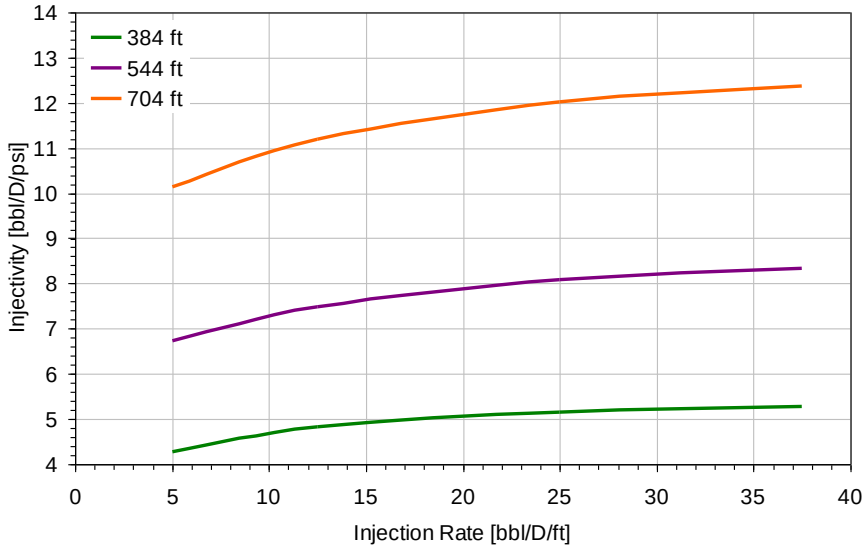

Figure 3.74: Injectivity of unified model with different injection rate and 384 ft, 544 ft, 704 ft fractures

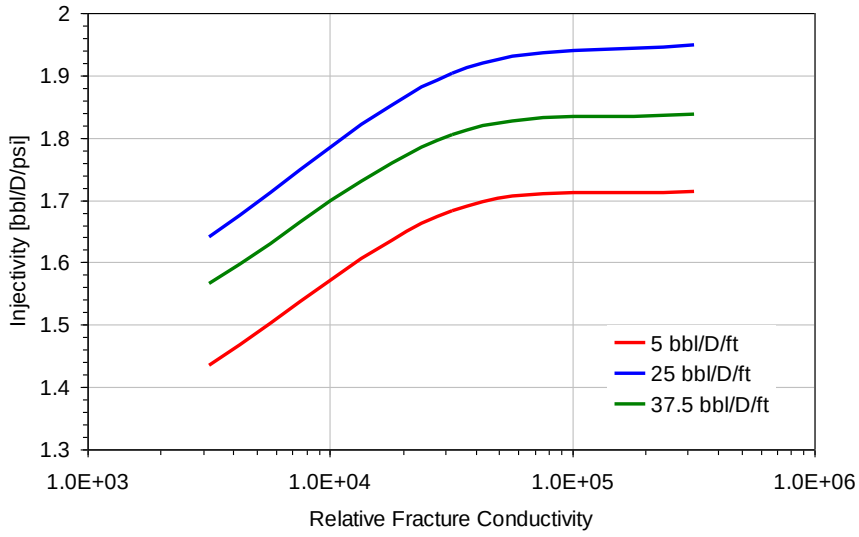

Figure 3.75: Injectivity of unified model with different injection rate and fracture conductivity, and 124 ft fracture length

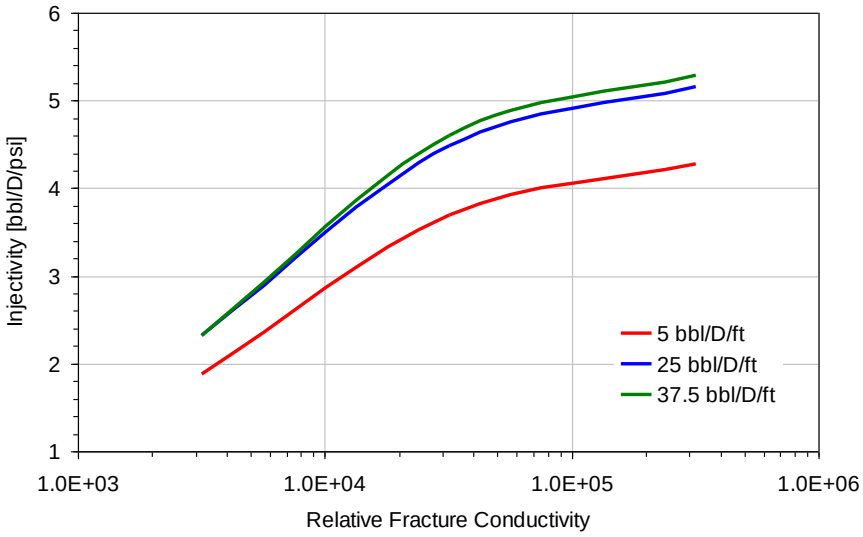

Figure 3.76: Injectivity of unified model with different injection rate and fracture conductivity, and 384 ft fracture length

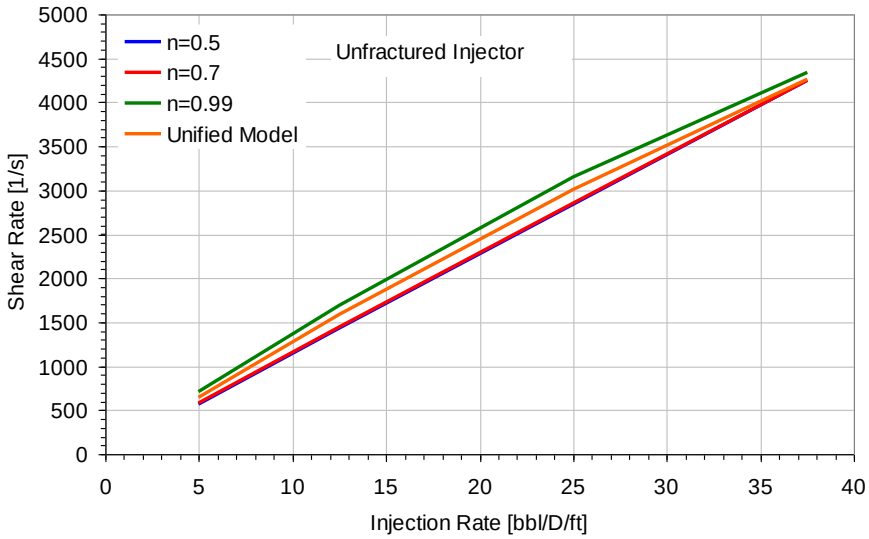

Figure 3.77: Relation between injection rate and shear rate with power-law different flow behavior index n values and unified model, un-fractured reservoir

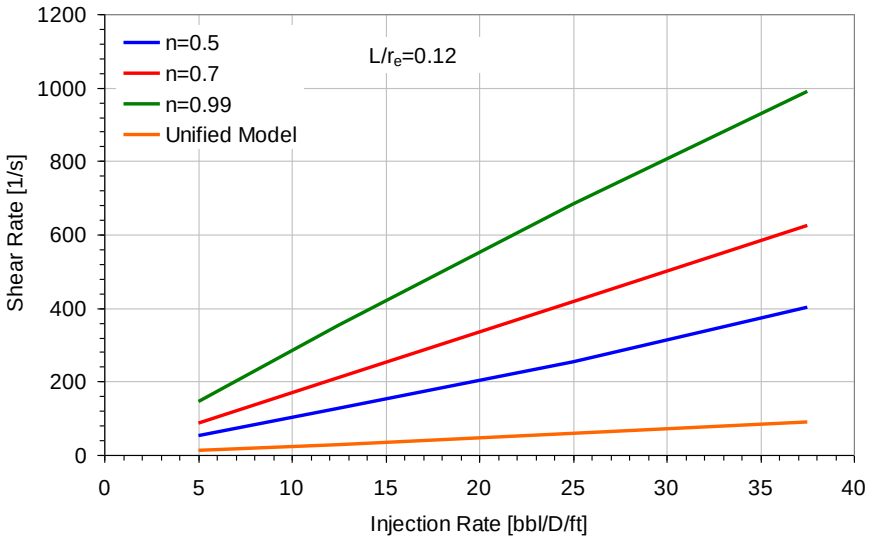

Figure 3.78: Relation between injection rate and shear rate with power-law different flow behavior index n values and unified model, $L/r_e = 0.12$

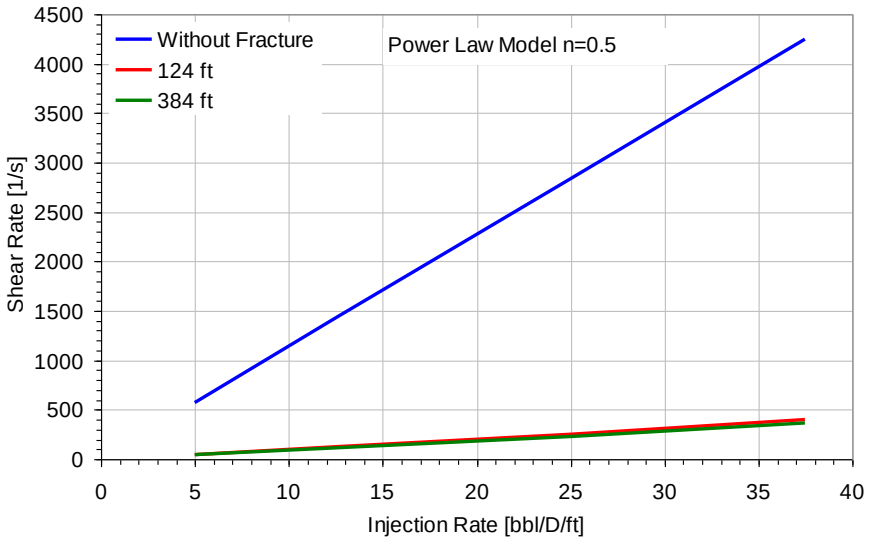

Figure 3.79: Relation between injection rate and shear rate with different fracture length, power-law fluid $\mu = 70\gamma^{-0.5}$

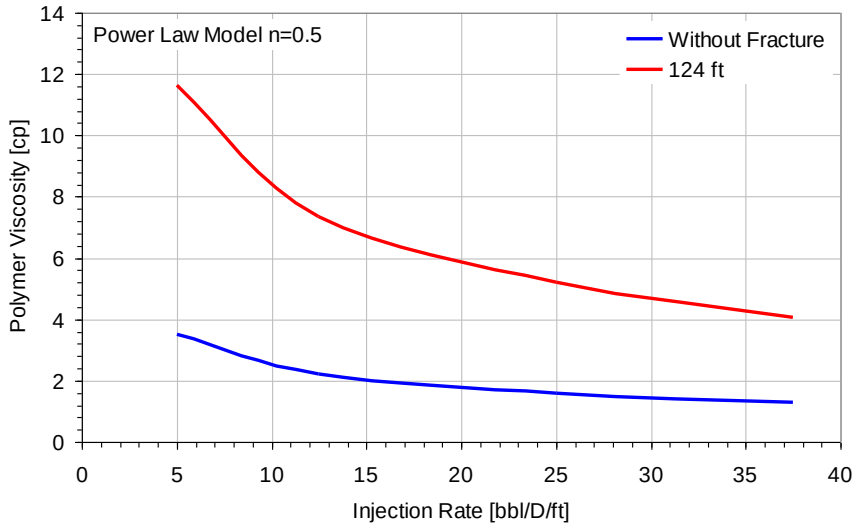

Figure 3.80: Relation between injection rate and polymer viscosity with different fracture length, power-law fluid $\mu = 70\gamma^{0.5}$

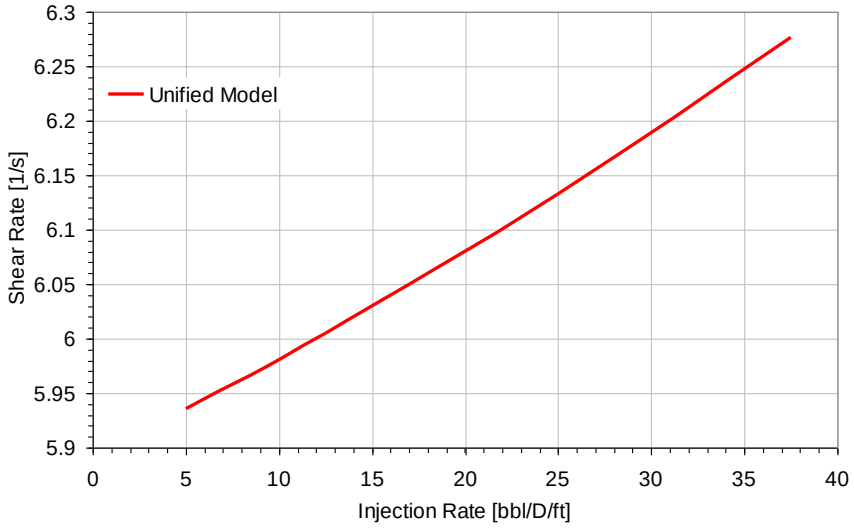

Figure 3.81: Relation between injection rate and shear rate, un-fractured case, unified model, Flopaam 3330S polymer (1,500 ppm; 1.6% NaCl; 25 ºC)

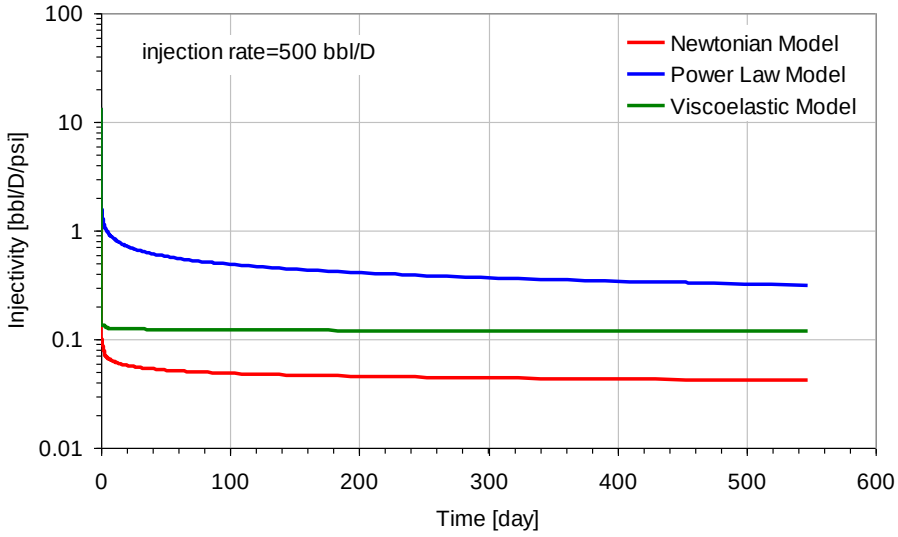

Figure 3.82: Injectivity of Newtonian, power-law, Viscoelastic model, injection rate = 500 bbl/D, without fracture, Newtonian model viscosity 70 cp, power-law model viscosity $\mu = 70\gamma^{0.5}$, unified model, Flopaam 3330S polymer (1,500 ppm; 1.6% NaCl; 25 ºC)

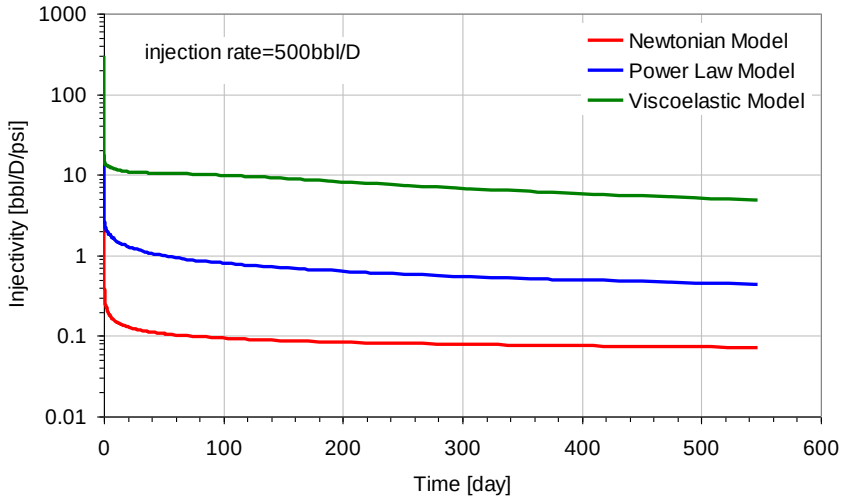

Figure 3.83: Injectivity of Newtonian, power-law, Viscoelastic model, injection rate = 500 bbl/D, fracture length 384 ft, Newtonian model viscosity 70 cp, power-law model viscosity $\mu = 70\gamma^{0.5}$, unified model, Flopaam 3330S polymer (1,500 ppm; 1.6% NaCl; 25 ºC)

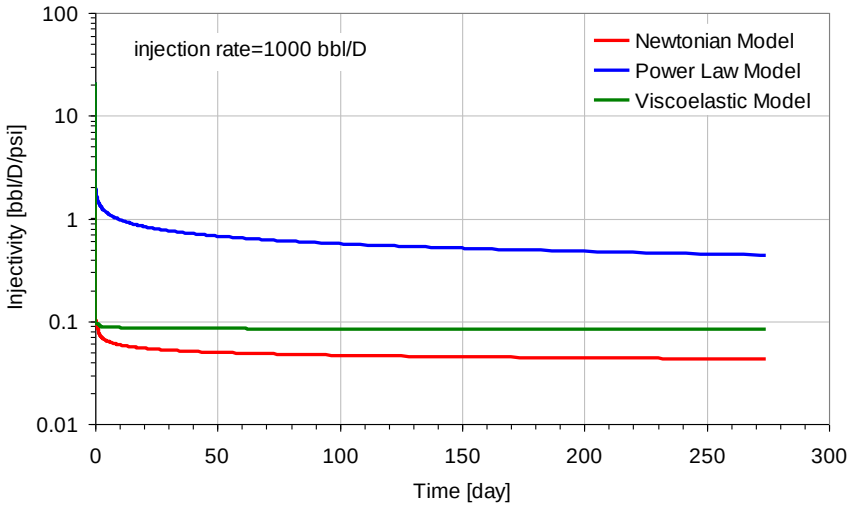

Figure 3.84: Injectivity of Newtonian, power-law, Viscoelastic model, injection rate = 1,000 bbl/D, without fracture, Newtonian model viscosity 70 cp, power-law model viscosity $\mu = 70\gamma^{0.5}$, unified model, Flopaam 3330S polymer (1,500 ppm; 1.6% NaCl; 25 ºC)

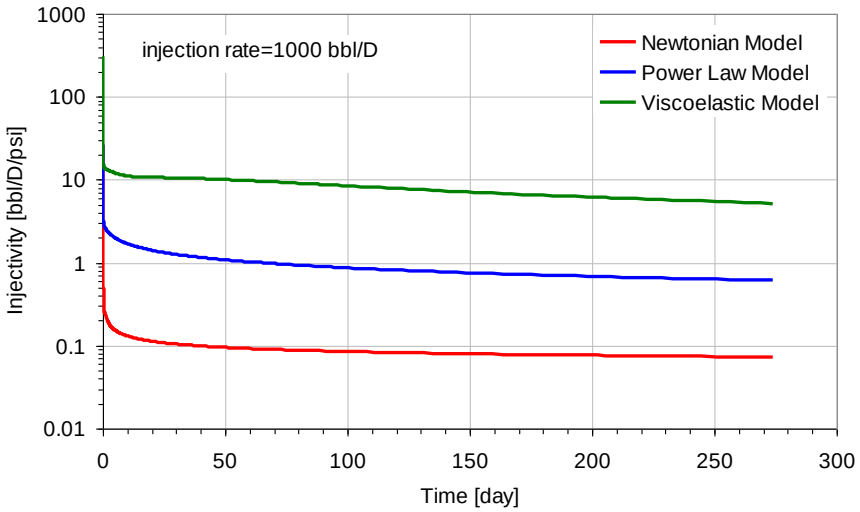

Figure 3.85: Injectivity of Newtonian, power-law, Viscoelastic model, injection rate = 1,000 bbl/D, fracture length 384 ft, Newtonian model viscosity 70 cp, power-law model viscosity $\mu = 70\gamma^{0.5}$, unified model, Flopaam 3330S polymer (1,500 ppm; 1.6% NaCl; 25 ºC)

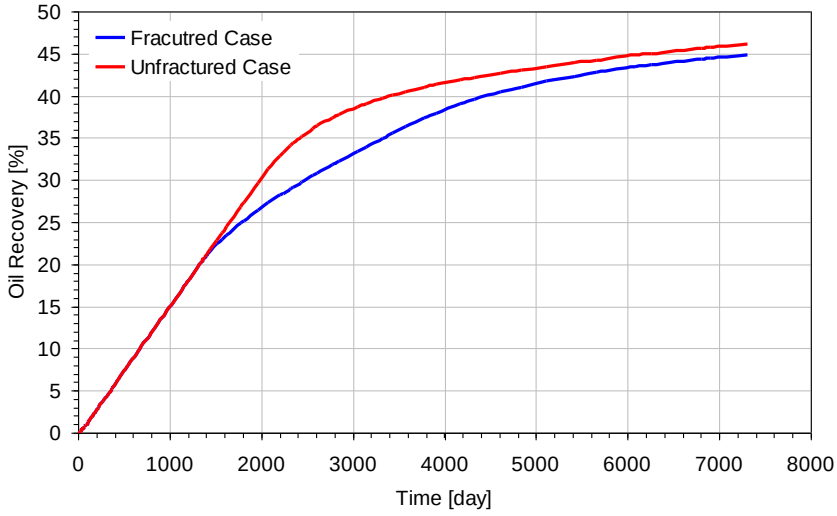

Figure 3.86: Oil recovery for fractured and un-fractured cases (*Case 3.1*), unified model Flopaam 3330S polymer (1,500 ppm; 1.6% NaCl; 25 ºC)

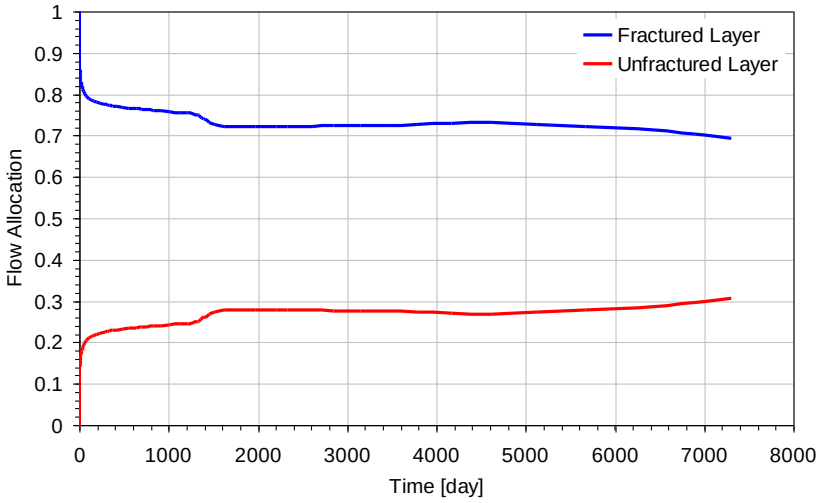

Figure 3.87: Flow allocation into the fractured and un-fractured layers in the fractured reservoir (*Case 3.1*), unified model Flopaam 3330S polymer (1,500 ppm; 1.6% NaCl; 25 ºC)

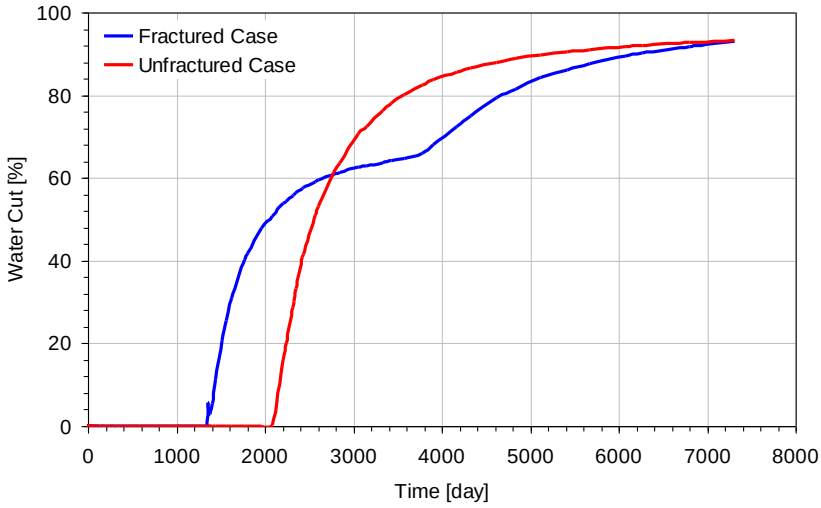

Figure 3.88: Water cut for fractured and un-fractured cases (*Case 3.1*), unified model Flopaam 3330S polymer (1,500 ppm; 1.6% NaCl; 25 ºC)

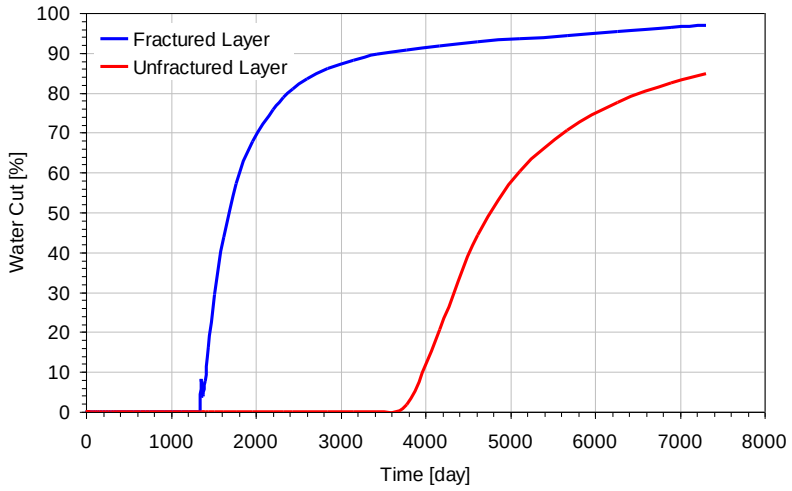

Figure 3.89: Water cut for the fractured and un-fractured layers in the fractured reservoir case (*Case 3.1*), unified model Flopaam 3330S polymer (1,500 ppm; 1.6% NaCl; 25 ºC)

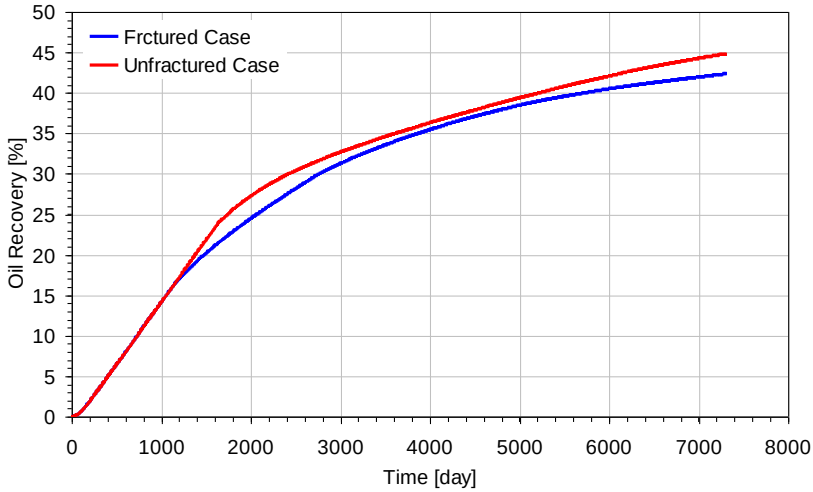

Figure 3.90: Oil recovery for fractured and un-fractured cases (*Case 3.2*), unified model Flopaam 3330S polymer (1,500 ppm; 1.6% NaCl; 25 ºC)

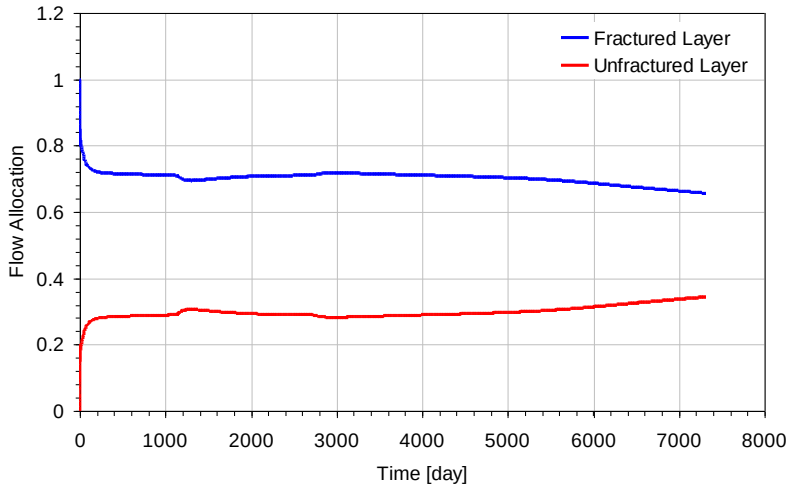

Figure 3.91: Flow allocation into the fractured and un-fractured layers in the fractured reservoir (*Case 3.2*), unified model Flopaam 3330S polymer (1,500 ppm; 1.6% NaCl; 25 ºC)

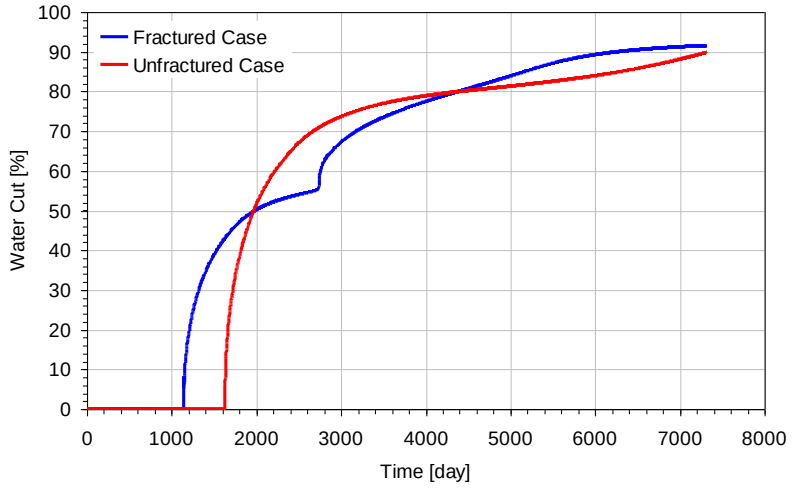

Figure 3.92: Water cut for fractured and un-fractured cases (*Case 3.2*), unified model Flopaam 3330S polymer (1,500 ppm; 1.6% NaCl; 25 ºC)

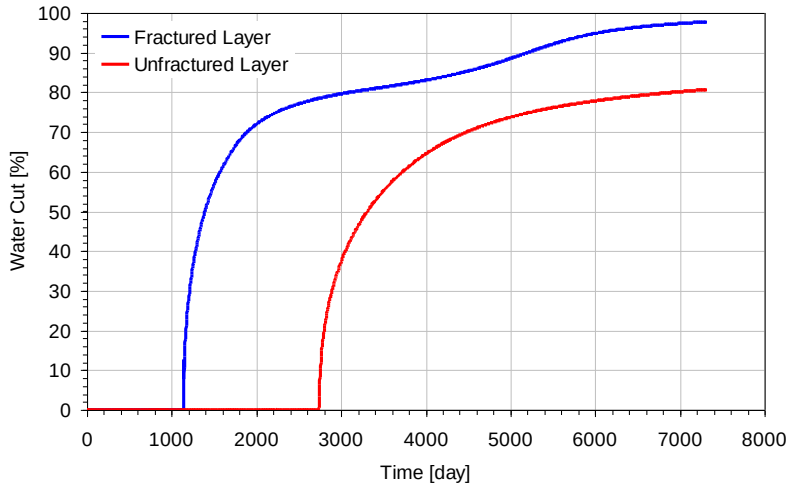

Figure 3.93: Water cut for the fractured and un-fractured layers in the fractured reservoir case (*Case 3.2*), unified model Flopaam 3330S polymer (1,500 ppm; 1.6% NaCl; 25 ºC)

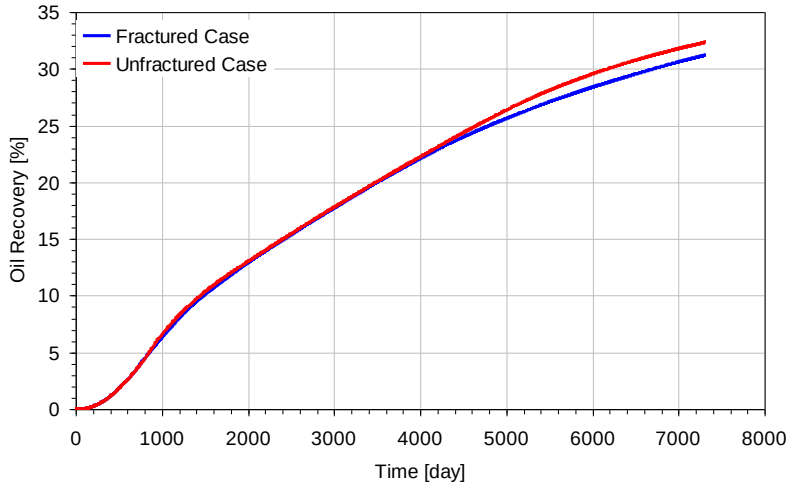

Figure 3.94: Oil recovery for fractured and un-fractured cases (*Case 3.3*), unified model Flopaam 3330S polymer (1,500 ppm; 1.6% NaCl; 25 ºC)

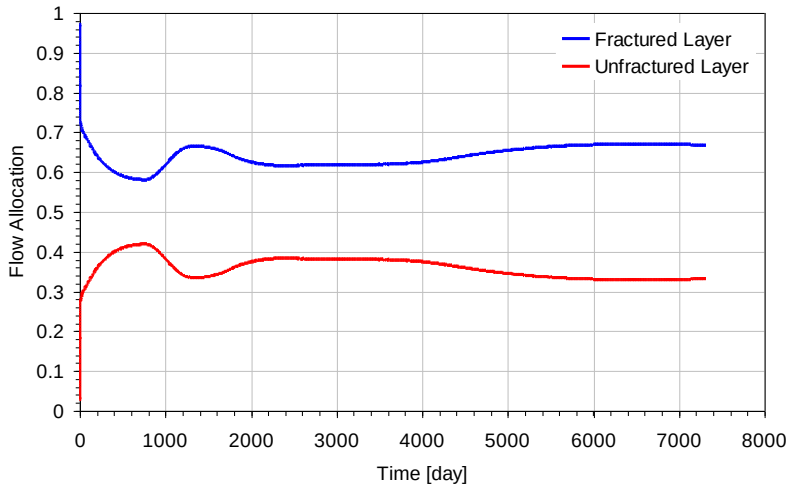

Figure 3.95: Flow allocation into the fractured and un-fractured layers in the fractured reservoir (*Case 3.3*), unified model Flopaam 3330S polymer (1,500 ppm; 1.6% NaCl; 25 ºC)

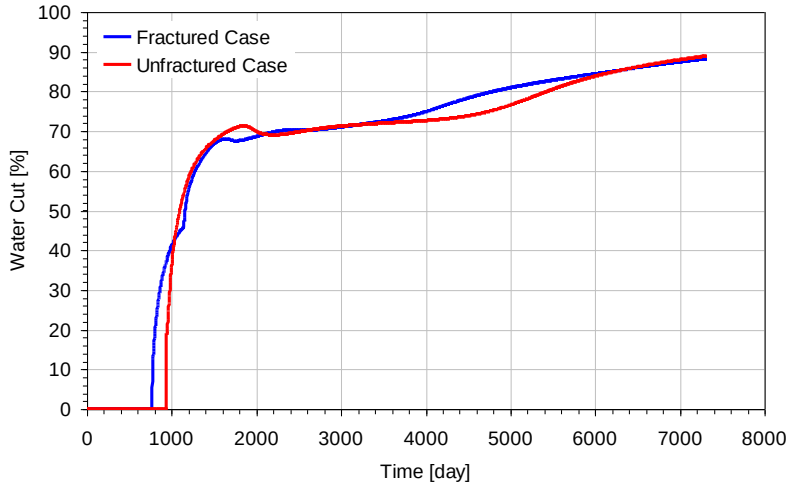

Figure 3.96: Water cut for fractured and un-fractured cases (*Case 3.3*), unified model Flopaam 3330S polymer (1,500 ppm; 1.6% NaCl; 25 ºC)

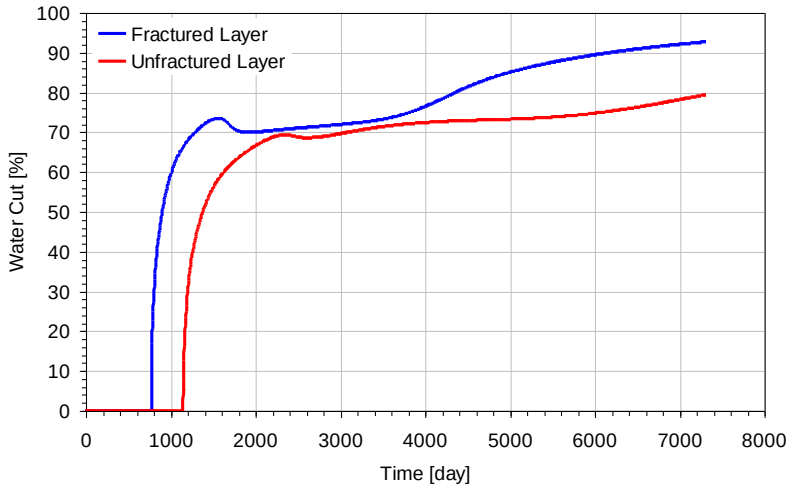

Figure 3.97: Water cut for the fractured and un-fractured layers in the fractured reservoir case (*Case 3.3*), unified model Flopaam 3330S polymer (1,500 ppm; 1.6% NaCl; 25 ºC)

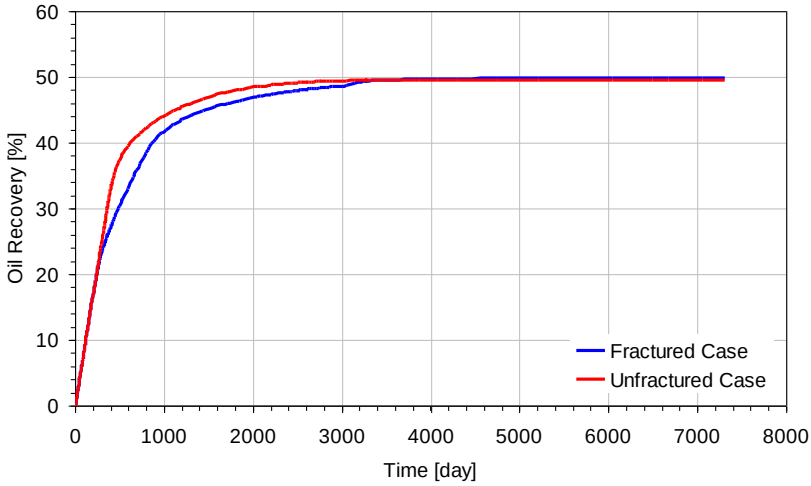

Figure 3.98: Oil recovery for fractured and un-fractured cases (*Case 3.4*), unified model Flopaam 3330S polymer (1,500 ppm; 1.6% NaCl; 25 ºC)

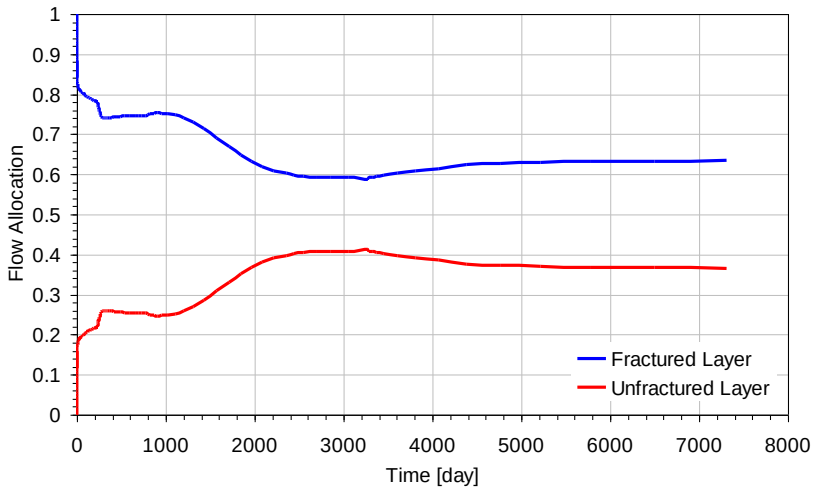

Figure 3.99: Flow allocation into the fractured and un-fractured layers in the fractured reservoir (*Case 3.4*), unified model Flopaam 3330S polymer (1,500 ppm; 1.6% NaCl; 25 ºC)

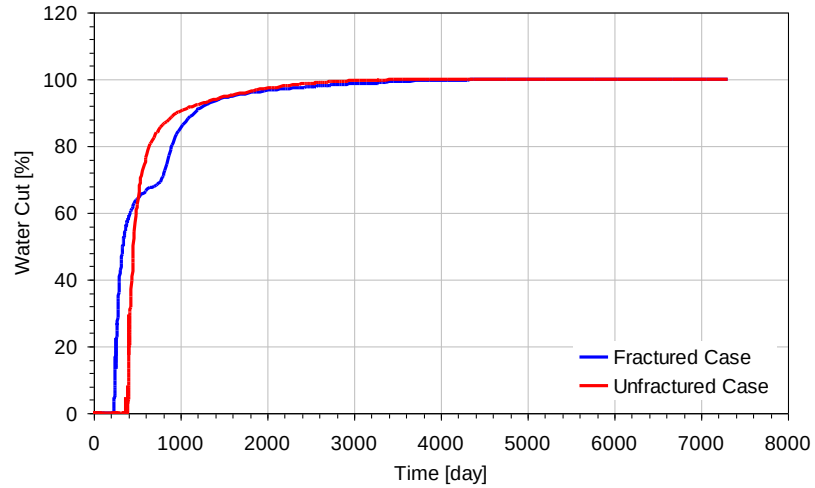

Figure 3.100: Water cut for fractured and un-fractured cases (*Case 3.4*), unified model Flopaam 3330S polymer (1,500 ppm; 1.6% NaCl; 25 ºC)

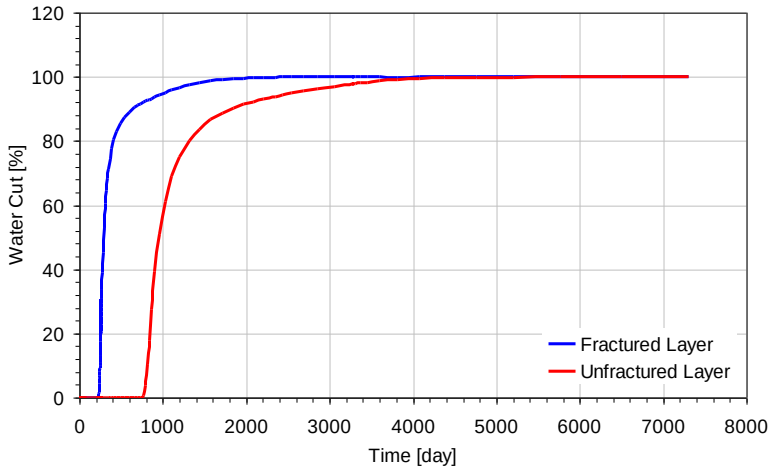

Figure 3.101: Water cut for the fractured and un-fractured layers in the fractured reservoir case (*Case 3.4*), unified model Flopaam 3330S polymer (1,500 ppm; 1.6% NaCl; 25 ºC)

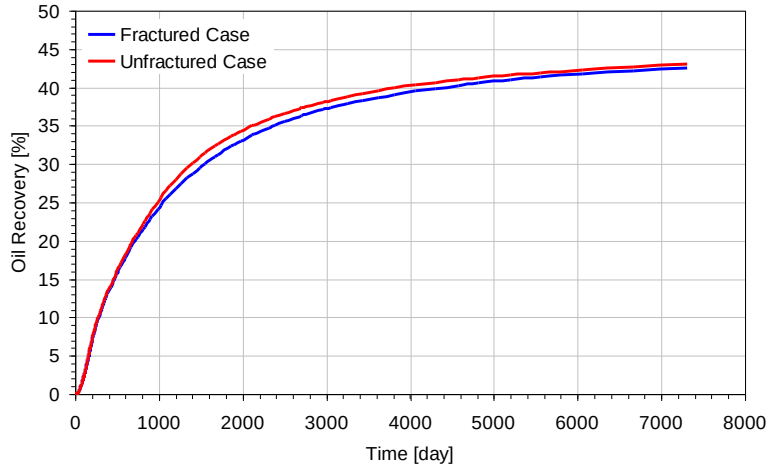

Figure 3.102: Oil recovery for fractured and un-fractured cases (*Case 3.5*), unified model Flopaam 3330S polymer (1,500 ppm; 1.6% NaCl; 25 ºC)

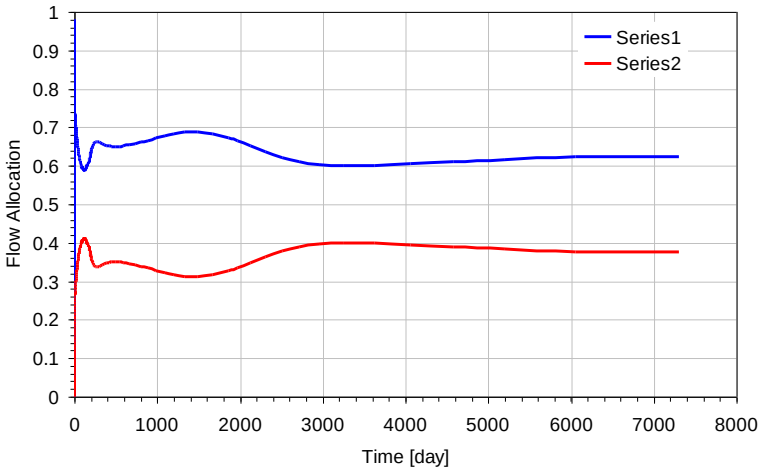

Figure 3.103: Flow allocation into the fractured and un-fractured layers in the fractured reservoir (*Case 3.5*), unified model Flopaam 3330S polymer (1,500 ppm; 1.6% NaCl; 25 ºC)

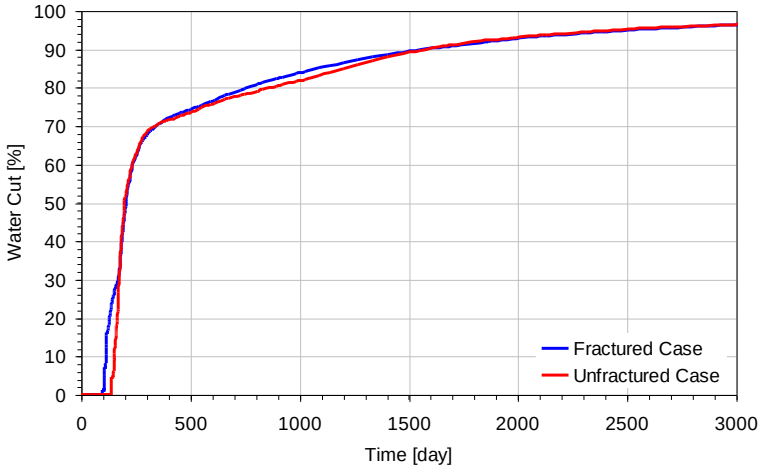

Figure 3.104: Water cut for fractured and un-fractured cases (*Case 3.5*), unified model Flopaam 3330S polymer (1,500 ppm; 1.6% NaCl; 25 ºC)

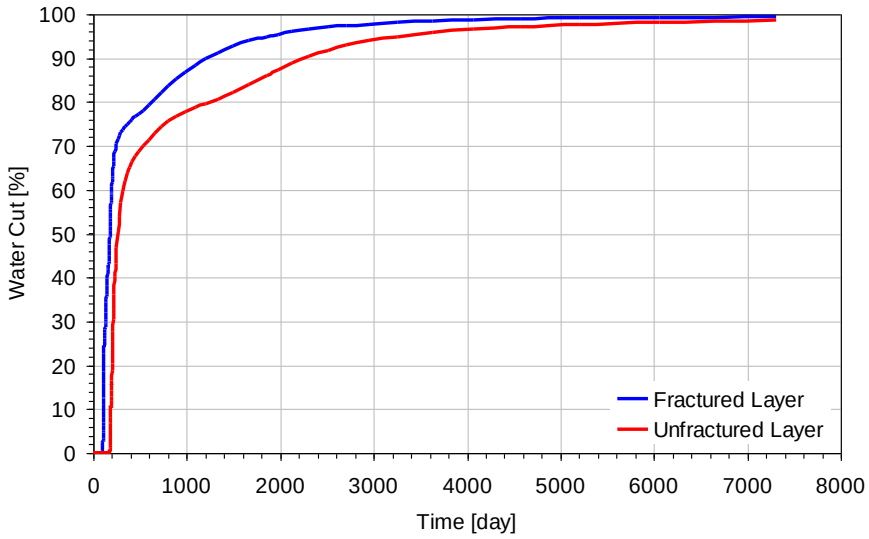

Figure 3.105: Water cut for the fractured and un-fractured layers in the fractured reservoir case (*Case 3.5*), unified model Flopaam 3330S polymer (1,500 ppm; 1.6% NaCl; 25 ºC)

Chapter 4: Water and Polymer Injectivity in Wells with Dynamic Fractures

4.1 INTRODUCTION

In Chapter 3, a series of waterflood and polymer flood simulations with a static fracture at the injection well were carried out to, (i) demonstrate the importance of the presence of fracture for those oil recovery processes; and (ii) identify the fracture, reservoir and flow parameters to which we need to pay special attention in assessing the performance of those processes during dynamic fracture generation.

This chapter first describes how a fracture develops at an injection well when water or polymer solution is injected, and how that fracture then grows. Waterflooding under dynamic induced fractures are investigated frequently (Chavez *et al.*, 2005; Dikken *et al.*, 1987; Hustedt *et al.*, 2006; Kuo *et al.*, 1984; Rod and Jorgensen, 2005; Souza *et al.*, 2005; Van den Hoek, 2004; Van den Hoek *et al.*, 2008; Wright *et al.*, 1999). Next, these mechanisms are incorporated into the injection simulation. The impact of induced dynamic fracture on well injectivity and reservoir sweep during waterflood and polymer flood is then examined with a series of simulations employing five-spot element models.

4.2 FRACTURE GENERATION/GROWTH MECHANISMS

4.2.1 Fracture Growth Mechanism during Water and Polymer Injection

Sea water and surface water are being used more and more during waterflooding in mature fields. Significant volumes of water are also produced from waterflood

operations, and this water must be re-injected into subsurface formations either for re-use or for disposal.

Quite frequently, there are colloidal particles and oil droplets in the produced water or sea water injected into the reservoir. Even though the injected particle concentration is usually very small (10~20 ppm), continuous injection of water (e.g. several hundred barrels per day for several years) damages and plugs the near-well formation. The reduced porosity and permeability near the injector, as described in detail in Chapter 2, increases injection BHP and reduces rock stress. When the effective stress of the rock in a certain direction becomes negative, tensile failure occurs. This is the main fracture generation and growth mechanism during water injection.

In the case of polymer injection, injection BHP increases because of high polymer viscosity. When a polymer solution is injected into the reservoir, its flow is initially radial. Because of the small radius of injector, fluid velocity and shear rate could be quite high, causing the fluid to exhibit shear-thickening behavior, as described in Chapter 2. High viscosity due to shear-thickening behavior increases injection BHP. With the consequent increase in pore pressure and decrease in effective rock stress, the fracture creation mechanism is exactly the same as for water injection.

After fracture creation, the fracture may grow away from the wellbore during continuous water or polymer injection. In the case of water injection, particle plugging (and the resulting damage) is concentrated at the zone near the fracture tip. This stress concentration at the fracture tip allows the fracture to continue to grow.

In the case of polymer injection, shear rate in the matrix with low permeability and porosity increases sharply near the fracture tip, because of the largest pressure

gradient. The increased shear rate at the fracture tip results in shear-thickening behavior and high polymer viscosity, which induces further fracture growth at the fracture tip. Continuous injection of water with particles and polymer thus facilitates both fracture initiation and fracture growth.

These dynamic fractures during water and polymer injection can have a significant impact on reservoir performance, as we can deduce from the simulations carried out in Chapter 3 with the simpler, static fracture cases. Fracture growth might be beneficial or harmful to reservoir sweep and oil recovery depending on wellbore-fracture geometry and reservoir heterogeneity. Also, fracture growth affects the improved injectivity during water and polymer injection. This complex, coupled process requires a careful investigation of fracture generation and growth during water and polymer injection. This chapter investigates the effects of injected fluid properties and the relation between injection BHP and fracture growth.

Reservoir simulators are generally not designed to simulate dynamic fracture growth with water and polymer injection. A new method for simulating fracture generation and growth during reservoir simulation is developed in this chapter. The primary problem in simulating reservoir flow behavior to account for a fracture at a well is that the processes controlling fracture growth occur at very small length scales (order of mm). However, it is not computationally efficient to simulate reservoir fluid displacements at this scale. Our proposed method to overcome this problem is to segment the problem (Yu *et al.*, 2005), with appropriate coupling and data transfer between the segments. This results in a significant improvement in computational efficiency. *CMG*-

STARS was used as the main flow simulator, and the fracture growth model was linked to it to provide fracture dynamics information.

Our proposed strategy to model fracture growth in a reservoir simulator is shown in **Figure 4.1**. The model makes the following assumptions:

1. The geo-mechanical properties are homogeneous during water and polymer injection.

The geo-mechanical properties are assumed to be homogeneous and isotropic during water and polymer injection. For example, the elastic modulus is assumed to be 3.95×10^7 psi and the Poisson ratio is 0.3 for fracture growth simulations in this chapter as shown **Table 4-1**.

2. Polymer rheology model is used to model polymer injection.

To model polymer injection with fracture growth, various polymer rheology models are used in this chapter including the Newtonian model, the power-law model, the Carreau model, and the visco-elastic (unified) model. In these polymer rheology models the polymer viscosity depends on the shear rate and polymer concentration. *CMG* was used to model the shear rate dependency of polymer viscosity. The limitation of *CMG* for shear rate dependent viscosity polymer injection is that the polymer viscosity in *CMG* depends on the fluid velocity instead of the shear rate. If the reservoir properties such as porosity and permeability are homogeneous, the correlation between the shear rate and the velocity is relatively simple. However, in the case of heterogeneous and time dependent reservoir properties (varying porosity and permeability), CMG can not model shear rate dependent polymer injection because the velocity and the shear rate cannot be matched one-to-one as shown in **Figures 4.2** and **4.3**. In order to model the shear rate

dependency of polymer viscosity in *CMG*, a subroutine was developed to transform shear rate dependent polymer viscosity to velocity dependent polymer viscosity. This transform was used in the case of fractured wells as well as in the case of un-fractured wells.

3. Fracture growth criterion

The mode of fracture growth criterion is assumed to be Mode I tensile failure. The fracture grows through every grid block for which the effective stress is negative and stops when the effective stress is positive. Another fracture criterion that has been extensively used for hard rocks is the stress intensity factor (Yew and Liu, 1993). The simulations conducted in this dissertation use the net pressure criteria which is more suitable for softer (lower Young's modulus) rocks.

4. Fracture growth does not change matrix permeability to fracture permeability.

To model fracture growth during water/polymer injection, reservoir grid block properties are updated in each time step. The permeability of each grid block is modified from that of a matrix to that of a fracture. However, the porosity of each grid block remains constant even in the case of fracture growth because changing of porosity for each grid block violates the material balance during simulation. Therefore, to represent the fracture growth, permeability is increased by 100 times or more, but the porosity stays constant.

These simplifying assumptions together with the external logic control shown in Figure 1 allow us to model fracture growth using a reservoir simulator.

In order to determine whether a fracture grows, shrinks (partially closes) or remains stationary during a given time step, a fracture propagation criterion based on an effective stress evaluation of all the fracture tips is incorporated as outlined below:

First, based on the pore pressure distribution in the reservoir at the current time step, *STARS* calculates the rock stress distribution in the reservoir. With water and polymer injection, the pore pressure (P_P) increases and the effective stress (σ) decreases with water and polymer injection as related by:

$$\sigma = S - \alpha_P P_P \tag{4.1}$$

Where *S* is the total stress and α_P is Biot's poroelastic constant.

When the effective stress becomes negative due to increasing pore pressure, tensile failure occurs near the injector. The fracture growth model checks the fracture propagation criterion at every grid block and at every time step to ensure that dynamic fracture growth is captured in every time step. The fracture can horizontal or vertical. If the minimum principal stress direction is vertical, a horizontal fracture is generated. On the contrary, a vertical fracture is generated when the minimum principal stress direction is horizontal. In the case of a vertical fracture, fracture orientation is determined by the direction of the minimum horizontal stress. Fracture orientation is always perpendicular to the minimum horizontal stress orientation. When the minimum horizontal stress becomes negative, a fracture starts to propagate perpendicular to the minimum horizontal stress direction. During water and polymer injection, the pore pressure (P_P) in the reservoir increases due to particle plugging and/or high polymer viscosity. The increased pore pressure results in negative effective stress (σ) and a fracture starts to form.

The width and height of dynamic fracture are determined by the pore pressure in the fracture. In this research, the fracture height is constant as a single grid block represents the layer thickness, similar to the KGD model. The fracture width in this simulation is assumed to be constant at 0.1 ft. A constant fracture width allows the local grid refinement to be much faster and more efficient than a dynamic grid refinement system.

After computing the fracture length and orientation, the fracture growth model updates the input data of STARS for next time step. By repeating this operation, the fracture growth during water/polymer injection is simulated.

The time step for fracture growth changes automatically with time to maximize the accuracy of fracture growth and minimize numerical errors. The simulation requires (i) initial reservoir properties such as porosity and permeability, (ii) initial injection conditions such as injection rate, injection fluid components, (iii) initial geo mechanical conditions such rock stress distribution, (iv) geo-mechanical properties such as elastic modulus, Poisson's ratio, and (v) shear rate dependent polymer viscosity during polymer injection or particle deposition rate during water injection as inputs. After one time step, initially 0.01 day, CMG shows the resulting rock stress distribution in each grid block. By transferring this information to the fracture growth model I wrote in Matlab, the fracture growth and orientation at a given time are determined. By using estimated fracture length and orientation, *CMG* runs subsequent simulation for another time step (for example, 0.01 day). Information between the reservoir simulator, *CMG*, and the fracture growth model is exchanged at every time step and allows us to dynamically model fracture growth during water/polymer injection.

For the case of water injection with suspended particle filtering, the fracture growth is driven by the deposition of particles near the fracture tip. In the case of polymer injection, increasing the viscosity near the fracture tip (because of its shear-rate dependence) may also induce fracture growth. In this research, the fracture width is fixed at 0.1 ft, and the grid block size increases with increasing distance from the injector. The injection well radius is 0.25 ft as shown in **Table 4-1**.

4.2.1.1 Fracture Growth due to Temperature Change

Temperature can also affect fracture growth. When a cool fluid such as water is injected into a hot reservoir, a growing region of cooled rock is established around the injection well. The rock matrix within the cooled region contracts and a thermoelastic stress field is induced around the well. For typical waterflooding of a moderately deep reservoir, horizontal earth stresses may be reduced by several hundred psi. As the fracture is generated and grows, the flow system evolves from an essentially radial geometry to one characterized more nearly as elliptical.

The volume of the cooled zone can be calculated by using following equation (Marx and Langenheim, 1959)

$$V_c = \frac{\rho_w C_w W_i}{\rho_{gr} C_{gr}(1-\phi) + \rho_w C_w \phi(1-S_{or}) + \rho_o C_o \phi S_{or}} \tag{4.2}$$

where V_c is the volume of the cooled zone, W_i is the total volume of injected water up to time t, ρ_w, ρ_o and ρ_{gr} are the densities of water, oil and mineral grains; C_w, C_o and C_{gr} are the specific heats of the water, oil and mineral grains respectively; ϕ is the

porosity; and S_{or} is the residual oil saturation (assuming all mobile oil has been displaced from the near-wellbore zone).

Stresses within the region of altered temperature, as well as stress in the surrounding rock that remains at its initial temperature, can change because of the expansion or contraction of the rock within the region of altered temperature. The thermoelastic stresses within an infinitely tall cylinder of elliptical cross section has been derived by Perkins and Gonzalez (1985), as briefly described below. The interior thermoelastic stresses, perpendicular ($\Delta\sigma_{1T}$) and parallel ($\Delta\sigma_{2T}$) to the major axes of the ellipse, are given by Equation (4.3) and Equation (4.4) respectively:

$$\frac{(1-\nu)\Delta S_{1T}}{E\beta\Delta T} = \frac{(b_o / a_o)}{1+(b_o / a_o)} \tag{4.3}$$

$$\frac{(1-\nu)\Delta\sigma_{2T}}{E\beta\Delta T} = \frac{1}{1+(b_o / a_o)} \tag{4.4}$$

where ν is the Poisson's ratio, a_0 and b_0 are the major and minor axes of the thermal front ellipse and β is the linear coefficient of thermal expansion, E is the Young's elastic modulus, and ΔT is the temperature difference between injected fluid and reservoir fluid. The sign convention used in the current study is that compressive stresses are positive and tensile stresses are negative.

Consider a waterflooding operation where a fluid which is significantly colder than the reservoir rock and fluids is injected into the reservoir. The rock stress distribution changes due to two principal factors: (i) injection water changes the reservoir pressure distribution; (ii) the temperature difference between the injected fluid and the

reservoir additionally changes stress. Plane strain ($\varepsilon_{yy} = 0$) horizontal stress is affected by vertical stress and pore pressure.

Two principal effective stress components can be defined by Equation (4.5) and Equation (4.6) (Zoback, 2006). One of the direction between x and y is minimum horizontal stress orientation.

$$S_{xx} = \frac{\nu}{1-\nu} \cdot S_v + \frac{1-2\nu}{1-\nu} \cdot \alpha_P P_P + \frac{E\varepsilon_{xx}}{1-\nu^2} + \frac{E\alpha_T \Delta T}{1-\nu} \tag{4.5}$$

$$S_{yy} = \frac{\nu}{1-\nu} \cdot S_v + \frac{1-2\nu}{1-\nu} \cdot \alpha_P P_P + \frac{\nu E\varepsilon_{xx}}{1-\nu^2} + \frac{E\alpha_T \Delta T}{1-\nu} \tag{4.6}$$

where S_v is the vertical stress and ε is the bulk strain.

If low temperature fluid is injected into a reservoir, ΔT becomes negative and the total and effective stresses decrease due to thermal effects. Pore pressure increase results in horizontal total stress increase as described by Equation (4.5) and Equation (4.6). However, effective horizontal stress with increasing pore pressure decreases as described by the next derivation.

Effective stress can be defined as

$$\sigma = S - \alpha_P P_P \tag{4.1}$$

A finite change in pore pressure can be represented as

$$P_P' = P_P + \Delta P_P \tag{4.7}$$

And a finite change in effective stress can be found by substituting Equation (4.1), Equation (4.5) and Equation (4.7) into next equation, as assuming there is no change of strain ($\varepsilon_{xx} = 0$) and the temperature (ΔT):

$$
\begin{aligned}
\sigma_{xx}'-\sigma_{xx} &= \left(S_{xx}'-\alpha_P P_P'\right)-\left(S_{xx}-\alpha_P P_P\right) \\
&= \left\{S_{xx}'-\alpha_P(P_P+\Delta P_P)\right\}-\left\{S_{xx}-\alpha_P P_P\right\} \\
&= \left\{\frac{\nu}{1-\nu}S_v+\frac{1-2\nu}{1-\nu}\alpha_P(P_P+\Delta P_P)-\alpha_P(P_P+\Delta P_P)\right\} \\
&\qquad -\left\{\frac{\nu}{1-\nu}S_v+\frac{1-2\nu}{1-\nu}\alpha_P P_P-\alpha_P P_P\right\} \\
&= \frac{1-2\nu}{1-\nu}\alpha_P(P_P+\Delta P_P)-\frac{1-2\nu}{1-\nu}\alpha_P P_P-\alpha_P\Delta P_P \\
&= -\frac{\nu}{1-\nu}\alpha_P\Delta P_P
\end{aligned}
\tag{4.8}
$$

A change in pore pressure of ΔP_P induces a change in effective stress of $-\frac{\nu}{1-\nu}\alpha_P\Delta P_P$. A negative effective stress due to high pore pressure induces tensile failure near the injector, which initiates a fracture. Other criteria for fracture propagation (e.g. stress intensity factor at the fracture tip) can be used as well.

Figure 4.4 and **Figure 4.5** show the impact of pore pressure increase and injected fluid temperature on effective stress and tensile failure. **Figure 4.4** and **Figure 4.5** obtained by using *STARS* in *CMG*. The distance in x-axis means the distance from the injector. The initial reservoir temperature is 175 °F. Water injection lasts for 5 years in this simulation. Over 5 years, the water injection decreases the effective stress according to Equation (4.5) and Equation (4.6). **Table 4.1** shows the initial conditions and geomechanical parameters used in this simulation.

Figure 4.7 shows that the cold injected fluid reduces effective minimum horizontal rock stress, which could be the cause of tensile failure. The blue line shows the effective normal stress with 175 °F injected fluid and the red line shows the stress with

75 °F. Because the injected fluid is so cold, the rock contracts, lowering the effective stress, and thus the stress difference, up to several hundreds psi.

4.3 WATER AND POLYMER INJECTION WELLS WITH A DYNAMIC FRACTURE IN A SINGLE LAYER

To investigate the mechanism and impact of fracture growth with water injection, a simple five-spot water injection model is used. There is an injector in the center and there are four producers, one in each corner as shown in **Figure 3.1**. We can specify two representative fracture growth orientations. The first one is the favorable fracture orientation, where the fracture is oriented through the center between two producers. The other one is the unfavorable orientation, where the fracture grows diagonally directly toward two producers.

During water and polymer flooding, particle plugging and shear-thickening behaviors initiate and propagate fracturing near the injector. Particle plugging occurs especially at the fracture tip, because the permeability of the fracture tip is much higher than the permeability of the already damaged fracture face near the injector. Also, during polymer injection, shear-thickening behavior can be observed near the fracture tip due to high fluid velocity. Thus particle plugging and shear-thickening are both driving forces for fracture growth.

In fracture growth model, local grid refinement method is applied to represent fracture near injector. The grid block size far from the injector is 40 ft and the grid block size near injector to represent fracture is 0.1 ft each.

The fracture growth depends on the injection rate, particle concentration in the injected water, and rock stress in the reservoir. A high injection rate and particle concentration in the injected water speeds up the formation damage near the injector, resulting in fast fracture growth. Lower reservoir stress also accelerates fracture growth. **Table 4.2** lists the parameters used in the fracture growth simulation.

4.3.1 Polymer Injection with Particle Plugging

Case 4.1
(a) Oil viscosity 1 cp, Newtonian polymer viscosity 5 cp (favorable mobility ratio)
(b) Favorable fracture orientation

The impact of fracture growth on reservoir sweep and oil recovery during polymer injection in a single-layer reservoir is small, because the favorable mobility ratio facilitates better reservoir sweep and late injected fluid breakthrough. Therefore, even when the fracture orientation is favorable, the oil recovery and the water breakthrough for both cases are almost the same (**Figure 4.9** and **Figure 4.10**). However, fracture growth does affect injectivity. The fracture growth after 2,000 days is about 25 ft and the fracture orientation is favorable. With fracture growth, injection BHP is lower, and injectivity is higher than without fracture growth (**Figure 4.10**). In real situations, effective stress can not decrease below 0 psi because the rock will fail in tension. Therefore, consideration of fracture growth is necessary during water injection and polymer injection to reflect more exact injection BHP, injectivity, reservoir sweep, and oil recovery.

Fracture growth during water injection is very similar to fracture growth during polymer injection. Water breakthrough, reservoir sweep, and oil recovery are almost the

same between fractured and un-fractured cases. Furthermore, the increase in water injectivity due to an induced fracture is very similar to that in the polymer injection case. Continuous fracture growth can stabilize the injection BHP and injectivity.

Case 4.2
(a) Oil viscosity 1 cp, Polymer injection (with unified rheology model) without particle plugging (favorable mobility ratio)
(b) Favorable fracture orientation

The unified polymer rheology model shows shear-thinning behavior in low shear rate regions and shear-thickening behavior in high shear rate regions as shown in sub-section 2.2.3. In the case of an initially un-fractured reservoir, low matrix permeability and porosity induces a high shear rate near the injector, which causes shear-thickening behavior before fracture initiation. The high viscosity subsequently generated could induce fracture creation. Furthermore, shear-thickening behavior can occur at the fracture tip after fracture initiation, which could be the main mechanism of fracture growth during unified polymer injection. For the example case shown in **Figure 4.11**, because of the favorable mobility ratio and favorable fracture orientation, the impact of dynamic fracture growth on oil recovery is negligible. Also, fracture growth prevents injection BHP from continuously increasing (**Figure 4.12**). Dynamic fracture growth causes injection well injectivity to stabilize, instead of decreasing continuously (**Figure 4.14)**. The reason the injectivity stabilization looks step-wise is the simulation numerical error with large grid block size (20 ft) and time step (1 day). Near the injector, the grid block size and initial time step are enough small (0.1 ft and 0.01 day), but the grid block size and time step increases far from the injector and after 1 month of simulation. **Figure 4.15** shows the

relation between shear rate and polymer viscosity in the matrix near the injector. When shear rate is lower than 100 s^{-1}, the fluid exhibits shear-thinning behavior. (lower shear rates increase polymer viscosity). Also, for high shear rates (above 150 s^{-1}), shear-thickening behavior can be observed (higher shear rates increase polymer viscosity).

4.4 WATER AND POLYMER INJECTION WELLS WITH DYNAMIC FRACTURE IN TWO LAYERS

When a fracture is generated and grows during water and polymer injection, geomechanical properties (e.g., elastic modulus, Poisson ratio, rock stress distribution) control its dynamics. When there are two layers which are impermeable each other, fracture can be generated and grown only in one layer or in both layers. Especially, in this research, we focus on the reservoir which has two layers with different rock stress distribution. Rock stress in one layer is lower than one in the other layer due to stress discontinuity. In this section, water and polymer injection with dynamic fractures in two layers are investigated, and the impact of dynamic fracture generation and growth during water and polymer injection on reservoir sweep and oil recovery is assessed.

4.4.1 Water Injection with Particle Plugging, Dynamic Fracture

Case 5.1
(a) Oil viscosity 10 cp (unfavorable mobility ratio)
(b) Favorable fracture orientation

During waterflooding, continuous particle plugging causes formation damage in the matrix. Reduced permeability and porosity could induce fracture creation and growth during water injection with particles. So far, there is no reservoir simulator which considers fracture growth during water and polymer flooding. Fracture growth model has the capability to update fracture growth due to water and polymer injection. **Figure 4.16** shows the oil recovery during water injection in a two layer reservoir. The blue line shows the oil recovery with fracture growth, and the red curve shows it without fracture growth. The initial effective stress in one layer is 1,000 psi and one in the other layer is 200 psi. The effective stress difference between two layers induces fracture growth in one layer, and no fracture in the other layer. Fracture growth in only one layer induces higher flow allocation into the fractured layer, which induces early water breakthrough and lower oil recovery. The fracture orientation is favorable in this simulation. On the other hand, if there is no fracture growth, which is possible with higher effective stress in both layers, flow allocation into both layers is exactly equal. This causes late water breakthrough and better reservoir sweep. Therefore, there is a critical difference in reservoir sweep and oil recovery between water injection with and without dynamic fracture growth.

4.4.2 Two Layers, Water Injection with Particle Plugging

Case 6.1
(a) Oil viscosity 10 cp (unfavorable mobility ratio)
(b) Favorable fracture orientation

Prior to investigating the impact of shear rate dependent polymer rheology on fracture growth, oil recovery, and reservoir sweep, a constant viscosity polymer model is investigated. Furthermore, a comparison between water and polymer injections is performed to show the impact of Newtonian polymer rheology on oil recovery (**Figure 4.21**). The red curve shows the oil recovery with polymer injection and the blue curve shows the oil recovery with water injection. The difference in oil recovery between water and polymer injection is due to the difference in their mobility ratios. Viscosities of water, polymer and oil are 1 cp, 30 cp, and 3 cp respectively. During polymer injection, a favorable mobility ratio delays water breakthrough and decreases injected fluid viscous fingering, which causes higher oil recovery. However, during water injection, the lower viscosity water exhibits fingering through the higher viscosity oil, which accelerates water breakthrough and lowers oil recovery.

4.4.3 Two Layers, Newtonian Polymer Injection with Particle Plugging

Case 7.1
(a) Oil viscosity 1 cp, Newtonian Polymer Viscosity 5 cp (favorable mobility ratio)
(b) Favorable fracture orientation

If there is different rock stress distribution in each of two layers during Newtonian polymer injection, there might be fracture growth in one layer but not in the other. This partial fracture growth affects the flow allocation, reservoir sweep, oil recovery, and injectivity. The fracture growth case shows early water breakthrough (**Figure 4.25** and **Figure 4.26**) and slightly lower oil recovery (**Figure 4.23**). After water breakthrough in both layers, overall oil recoveries are almost the same. However, at the point of

injectivity, the fracture case shows much higher injectivity than the un-fractured case (**Figure 4.22**). Also, the flow allocation into the fractured and the un-fractured layers are discontinuous at every time step due to dynamic fracture growth (**Figure 4.24**). The flow allocation into the fractured layer with fracture growth increases rapidly, because increased fracture length improves injectivity and flow allocation into the fractured layer. **Figure 4.27** shows the injectivity increase due to dynamic fracture growth. Injectivity does not decrease continuously but stabilizes. This is due to dynamic fracture growth, in spite of continuous particle plugging near the injector.

4.4.4 Two Layers, Unified Polymer Injection without Particle Plugging

Case 8.1
(a) Oil viscosity 1 cp (favorable mobility ratio)
(b) Favorable fracture orientation

In a single layer reservoir (*Case 4.2*), fracture growth does not significantly affect oil recovery. However, in the two-layer reservoir, dynamic fracture growth does affect reservoir sweep and oil recovery, because it induces unequal flow allocation into the fractured and the un-fractured layers (**Figure 4.29**).

When a fracture is created, more injected fluid flows into the fractured layer, which reduces reservoir sweep in the un-fractured layer. Therefore, due to high polymer viscosity, fracture can be generated and grown, which might be harmful to reservoir sweep and oil recovery. This harmful effect evident in a comparison of the water cut can be obtained for the fractured and un-fractured case (**Figure 4.30** and **Figure 4.31**).

Fracture growth in one layer increases the flow allocation into the fractured layer, which causes early water breakthrough in the fractured layer and late water breakthrough

in the un-fractured layer. Thus only a small amount of the injected fluid flows into the un-fractured layer. In **Figure 4.31,** water breakthrough in the un-fractured layer occurs at 2,050 days, while water breakthrough in the fractured layer occurs much later, after 4,000 days. Therefore, reservoir sweep in the un-fractured layer is delayed when there is fracture growth and higher flow allocation into the fractured layer.

Even though there is fracture growth in only one layer due to different rock stress distribution, dynamic fracture contributes to higher injectivity. **Figure 4.32** shows higher injectivity for the fractured reservoir and lower injectivity for the un-fractured reservoir. **Figure 4.29** shows the flow allocation into the fractured and the un-fractured layers. We can observe the flow allocation increase after dynamic fracture growth at each time step. Updated fracture growth affects the flow allocation into the fractured and the un-fractured layers, due to the shear-thickening behavior of the polymer.

4.5 SUMMARY

A model that allows us to simulate fracture growth in injectors using a conventional reservoir simulator is presented. This model takes into account particle plugging, pore pressure gradient, complex polymer rheology and thermal stresses. Based on the results from this model the following conclusions can be made.

- Injectivity decline may be expected in all injectors due to particle plugging and/or high polymer viscosity. However, fracture growth in injection wells during water and polymer flooding results in well injectivity in the field that is much higher and more stable than would be predicted if fracture growth were

not accounted for. This is primarily the result of fracture generation and growth.

- There are several key factors that affect fracture growth – particle concentration in the injected fluid, polymer rheology, injection rate, stress distribution of the reservoir, thermal effect, and reservoir heterogeneity.
- Injection of cold fluid intensifies the decrease of rock stress, which facilitates the fracture growth and increases injectivity.
- In homogeneous reservoirs, fracture growth does not have a significant impact on oil recovery and reservoir sweep. However, well injectivity with fracture growth is much higher than without fracture growth. The injectivity increases up to 5 times as high as the injectivity without fracture growth and the BHP stabilizes, and does not increase continuously, primarily due to fracture growth
- In layered reservoirs, fracture growth has a very significant effect on oil recovery and water cut. As a fracture grows in one layer, more and more injected fluid is injected into the fractured layer. It is shown that when injecting into a layered reservoir, fracture growth in one layer can result in the other layer being left almost entirely un-swept.
- When particle plugging is considered, the impact of fracture growth is even more pronounced, resulting in very poor sweep of the un-fractured layer.
- Polymer rheology is shown to play a critical role in determining injectivity and reservoir sweep. Shear-thickening behavior may be observed near the wellbore and at the fracture tip, resulting in significantly longer fractures.

Table 4.1: Input parameters for effective stress calculation

Initial Effective Minimum Horizontal Stress (psi)	1,000
Injection Rate (bbl/D)	900
Particle Concentration in the Injected Water (ppm)	20
Thermal Expansion Coefficient ($°F^{-1}$)	1×10^{-5}
Elastic Modulus	3.95×10^{7}
Poisson Ratio	0.3

Table 4.2: Input parameters for fracture growth simulation

Reservoir Properties

Reservoir Size (ft)	$300 \times 300 \times 140$
Reservoir Porosity and Permeability (md)	0.2; 100

Component Properties

Water Viscosity (cp)	1
Oil Viscosity (cp)	10

Rock and Component Properties

Irreducible Water Saturation	0.3
Residual Oil Saturation	0.3
Relative Permeability End Points for Water and Oil	0.3; 0.7

Initial Conditions

Pressure (psi)	3000
Oil Saturation	0.7

Geomechanical Properties

Initial Horizontal Minimum Stress (psi)	1000
Elastic Modulus (psi)	3.95×10^7
Poisson Ratio	0.3

Injection Well Properties

Injection Rate (bbl/D)	250
Injection Well Radius (inch)	3

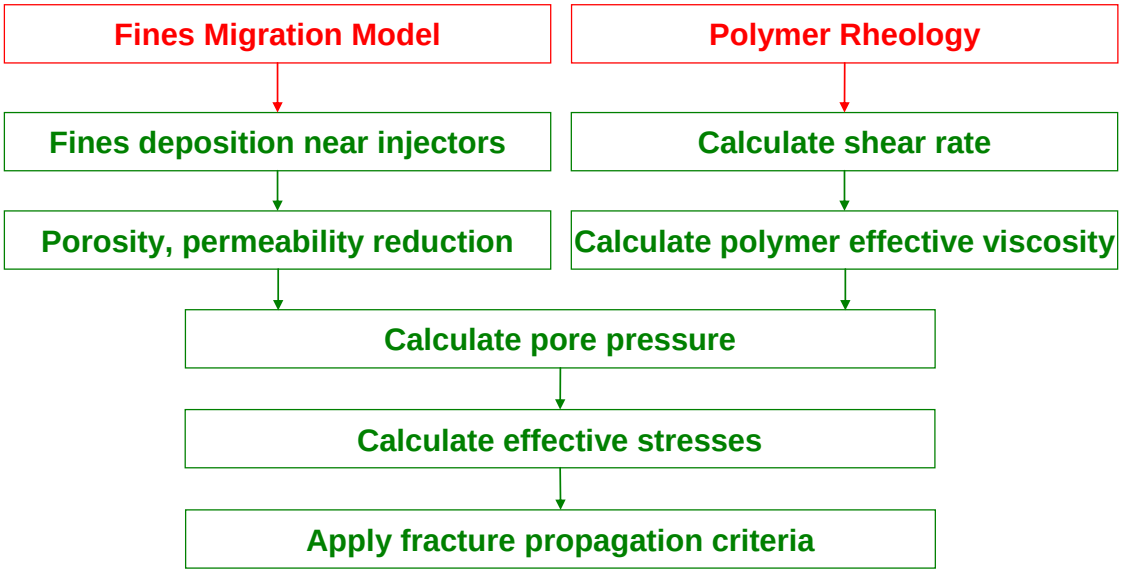

Figure 4.1: Fracture growth mechanism during water and polymer injection

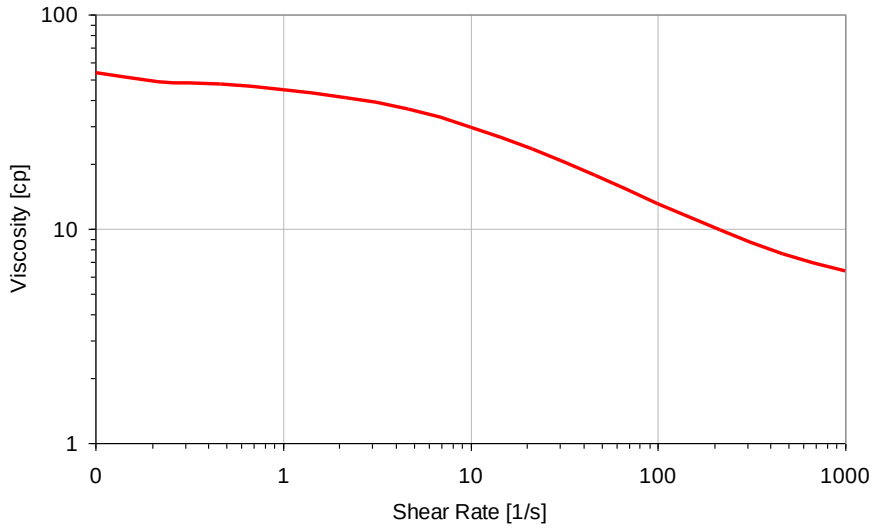

Figure 4.2: Shear rate dependent polymer viscosity, unified model, Flopaam 3330S polymer (1,500 ppm; 1.6% NaCl; 25 ºC)

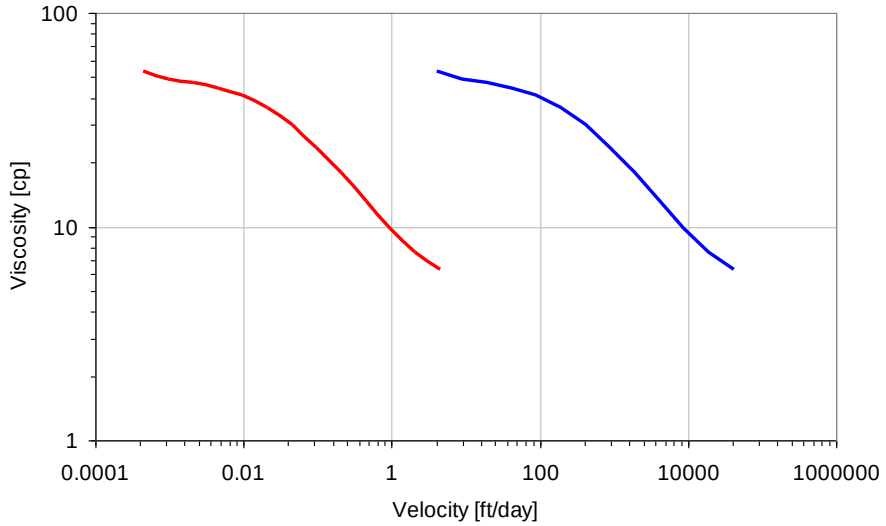

Figure 4.3: Polymer viscosity as a function of flow velocity in the fracture and matrix, unified model, Flopaam 3330S polymer (1,500 ppm; 1.6% NaCl; 25 ºC), fracture permeability 100D, matrix permeability 100mD

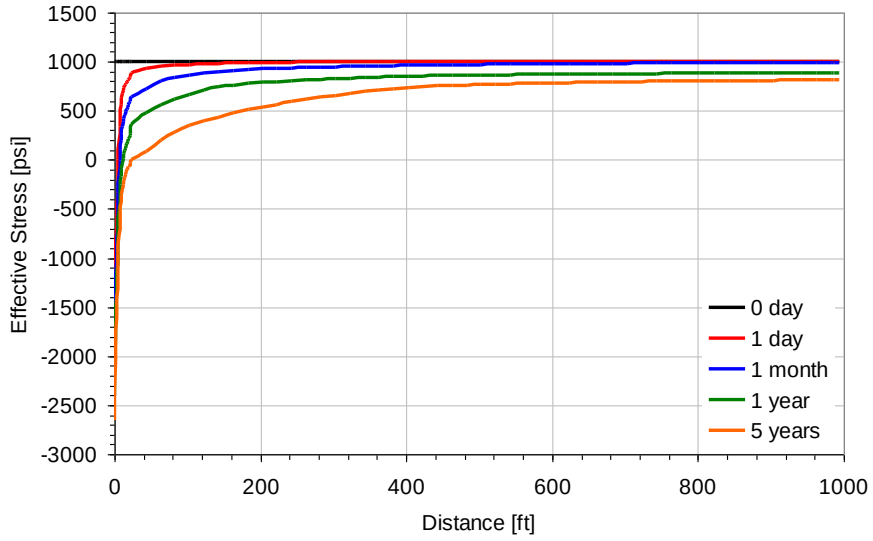

Figure 4.4: Effective stress distribution with fluid temperature 175 ºF, particle concentration 20 ppm, injection rate 900 bbl/D, reservoir temperature 175 ºF

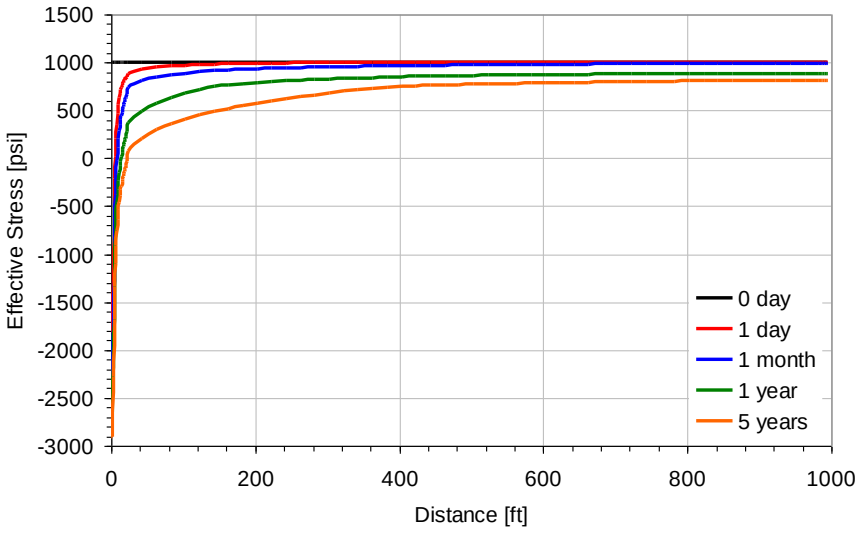

Figure 4.5: Effective stress distribution with fluid temperature 75 ºF, particle concentration 20 ppm, injection rate 900 bbl/D, reservoir temperature 175 ºF

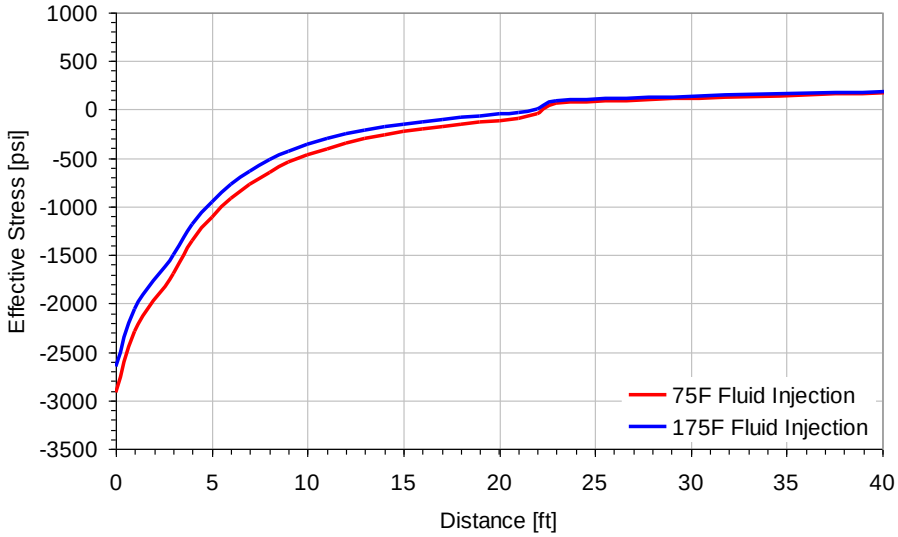

Figure 4.6: Effective stress distribution with different injection fluid temperature, particle concentration 20 ppm, injection rate 900 bbl/D, reservoir temperature 175 ºF

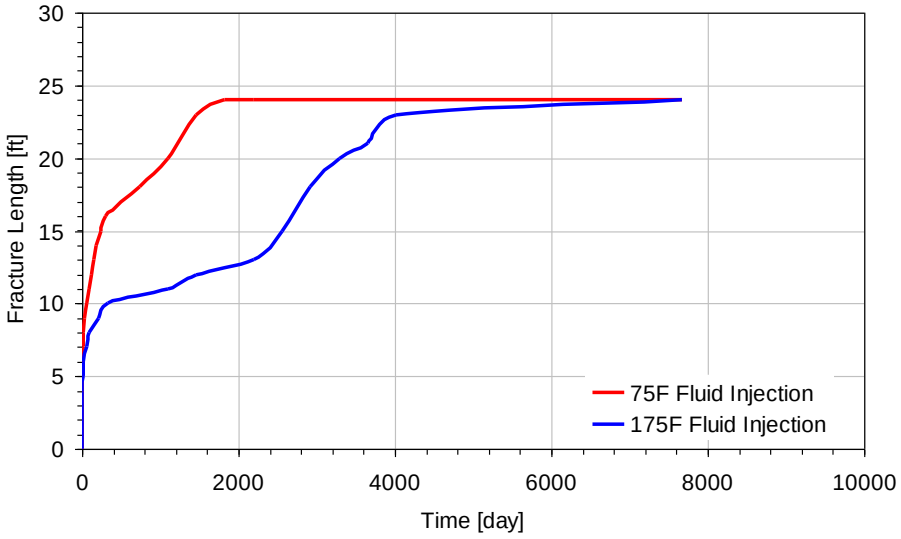

Figure 4.7: Fracture length with different injection fluid temperature, particle concentration 20 ppm, injection rate 900 bbl/D, reservoir temperature 175 ºF

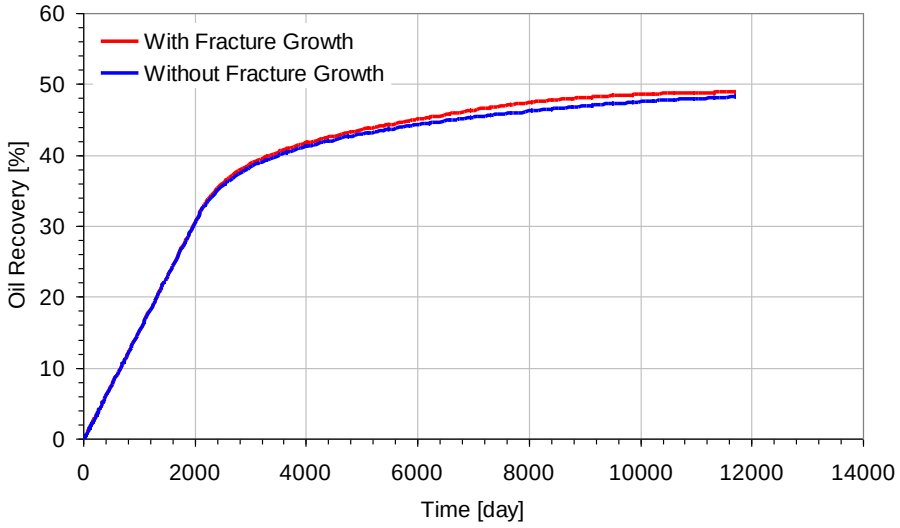

Figure 4.8: Oil recovery for fractured and un-fractured cases (*Case 4.1*)

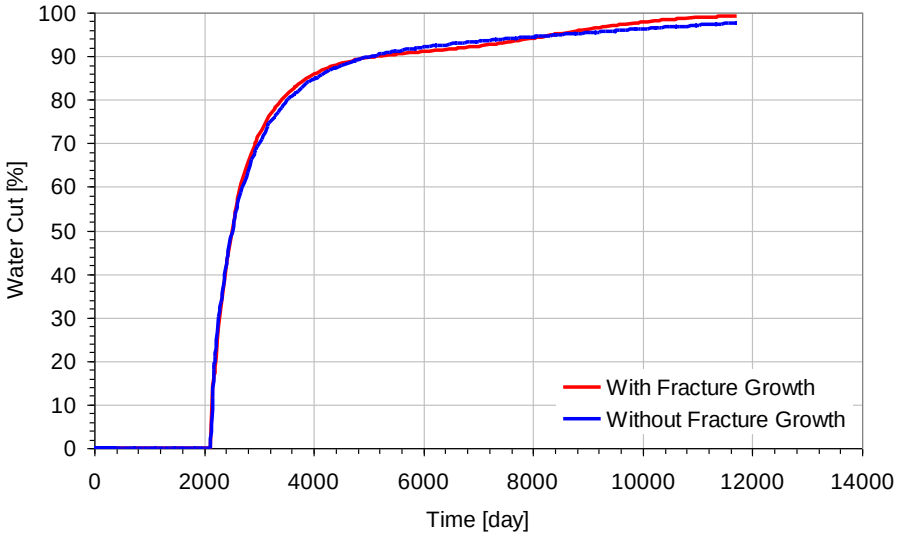

Figure 4.9: Water cut for fractured and un-fractured cases (*Case 4.1*)

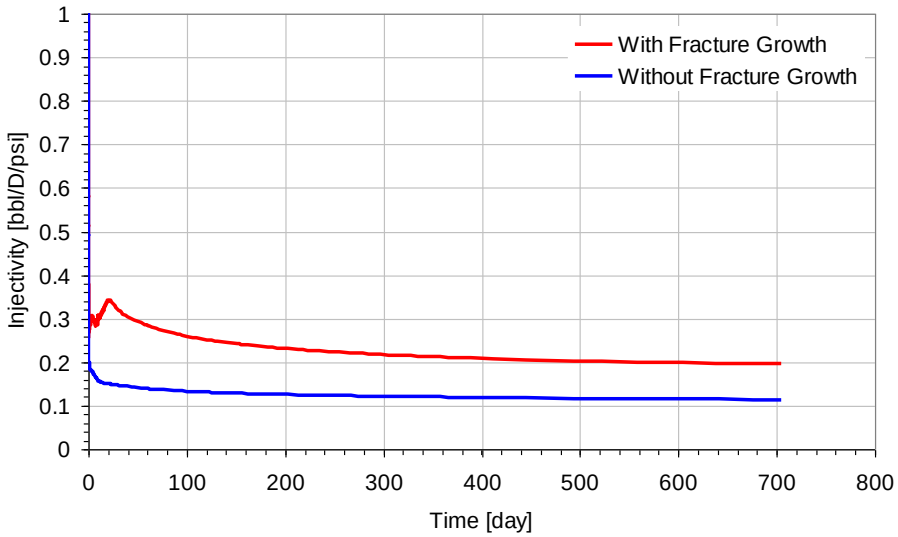

Figure 4.10: Injectivity for fractured and un-fractured cases (*Case 4.1*)

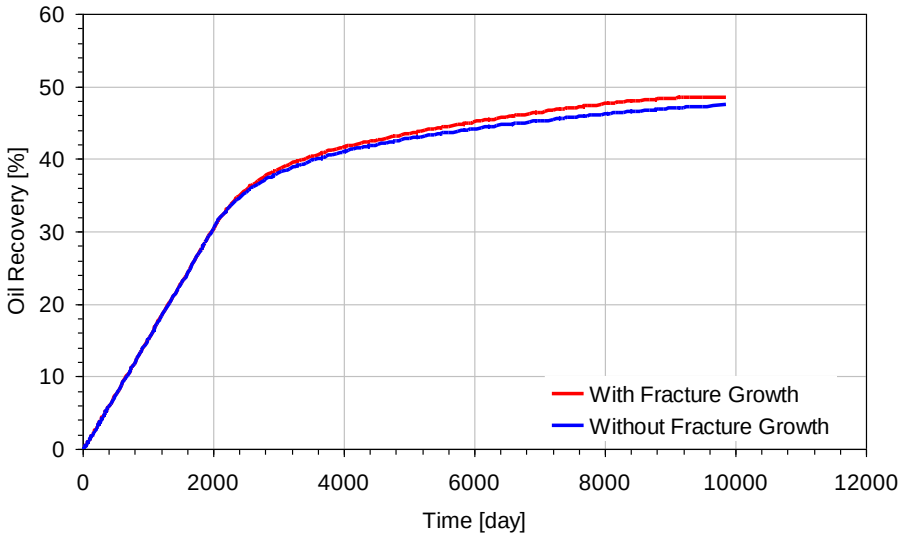

Figure 4.11: Oil recovery for fractured and un-fractured cases (*Case 4.2*), unified model, Flopaam 3330S polymer (1,500 ppm; 1.6% NaCl; 25 ºC)

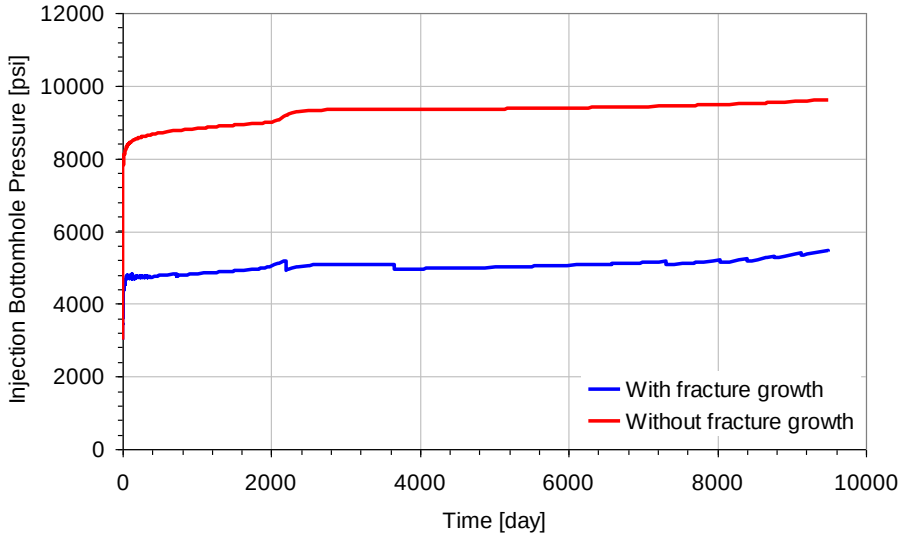

Figure 4.12: Injection BHP for fractured and un-fractured cases (*Case 4.2*), unified model, Flopaam 3330S polymer (1,500 ppm; 1.6% NaCl; 25 ºC)

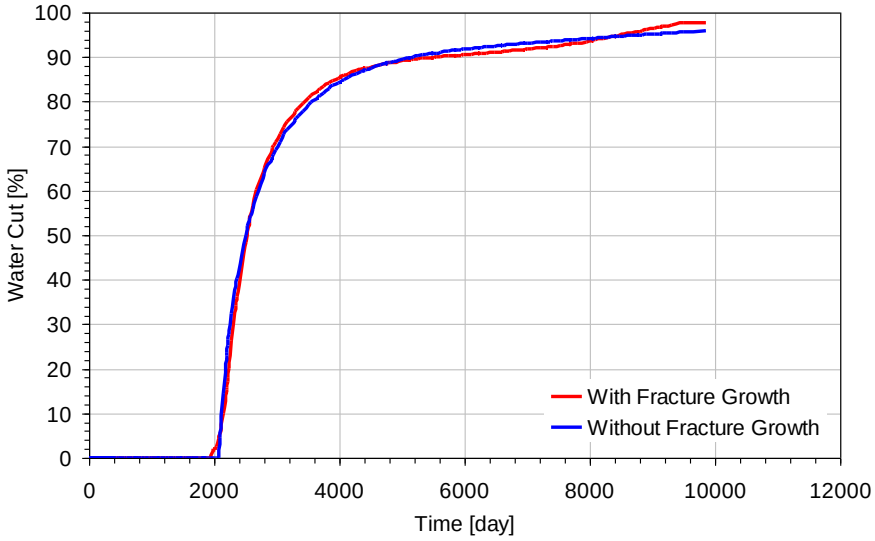

Figure 4.13: Water cut for fractured and un-fractured cases (*Case 4.2*), unified model, Flopaam 3330S polymer (1,500 ppm; 1.6% NaCl; 25 ºC)

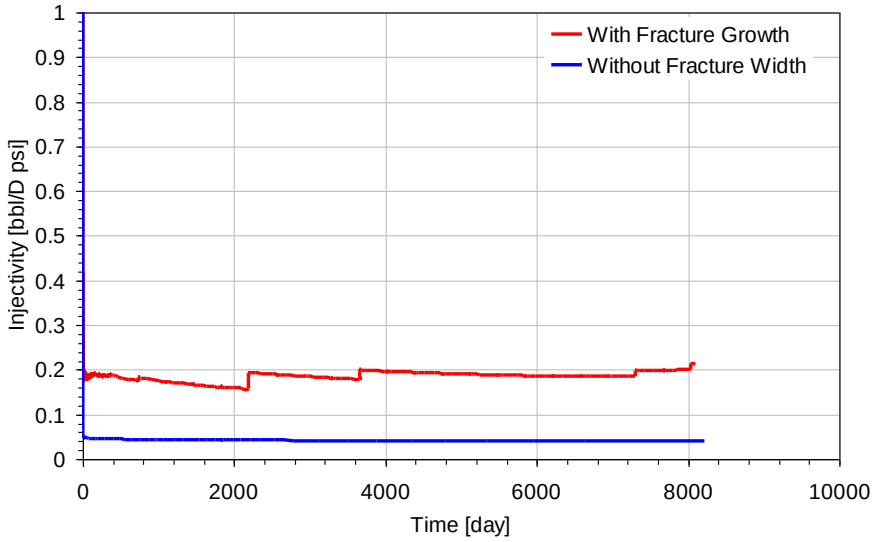

Figure 4.14: Injectivity for fractured and un-fractured cases (*Case 4.2*), unified model, Flopaam 3330S polymer (1,500 ppm; 1.6% NaCl; 25 ºC)

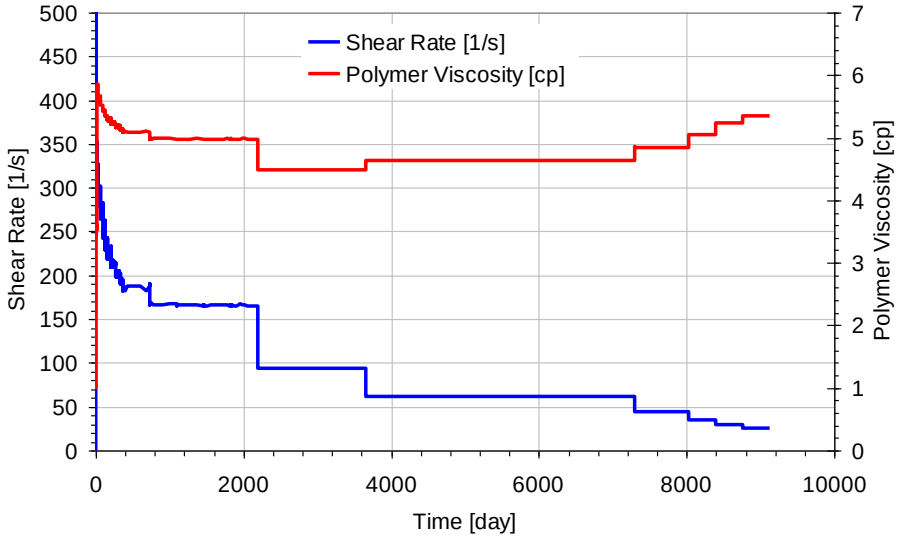

Figure 4.15: Relation between shear rate and polymer viscosity (*Case 4.2*), unified model, Flopaam 3330S polymer (1,500 ppm; 1.6% NaCl; 25 ºC)

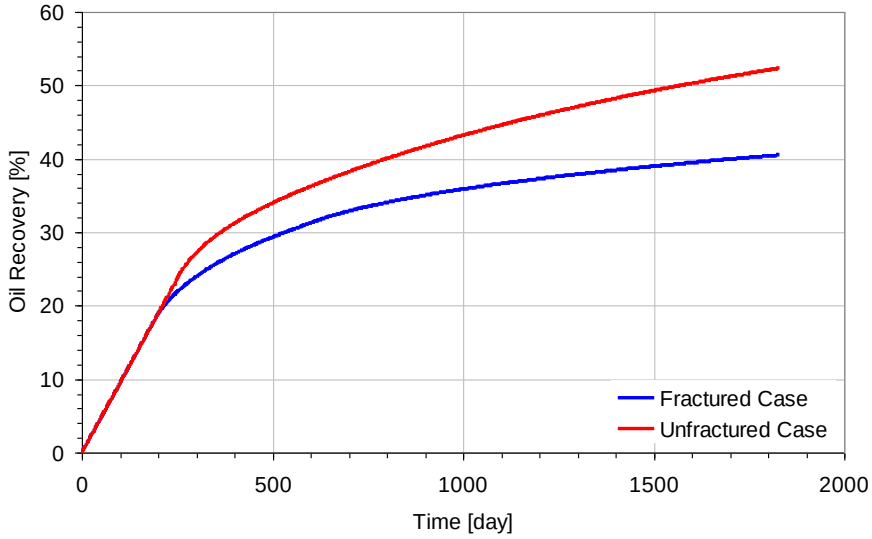

Figure 4.16: Oil recovery for fractured and un-fractured cases (*Case 5.1*)

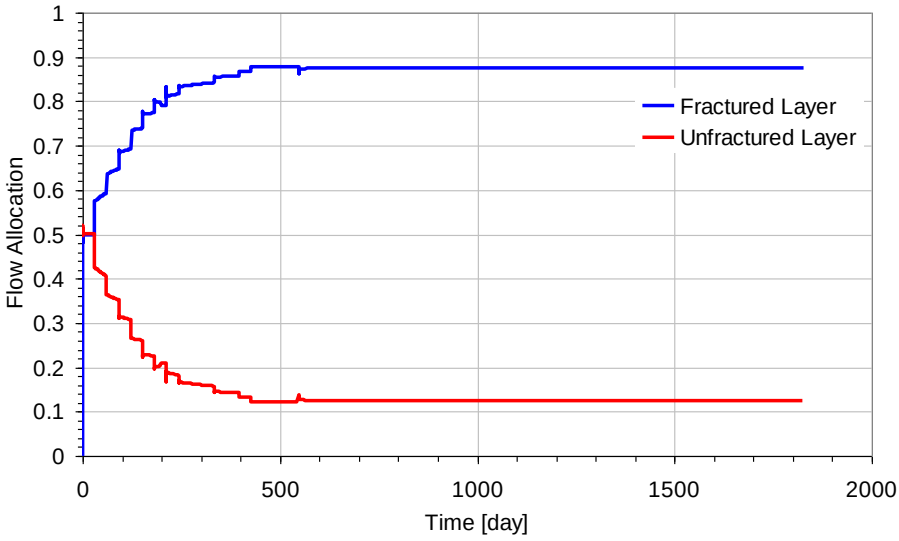

Figure 4.17: Flow Allocation for fractured and un-fractured layers (*Case 5.1*)

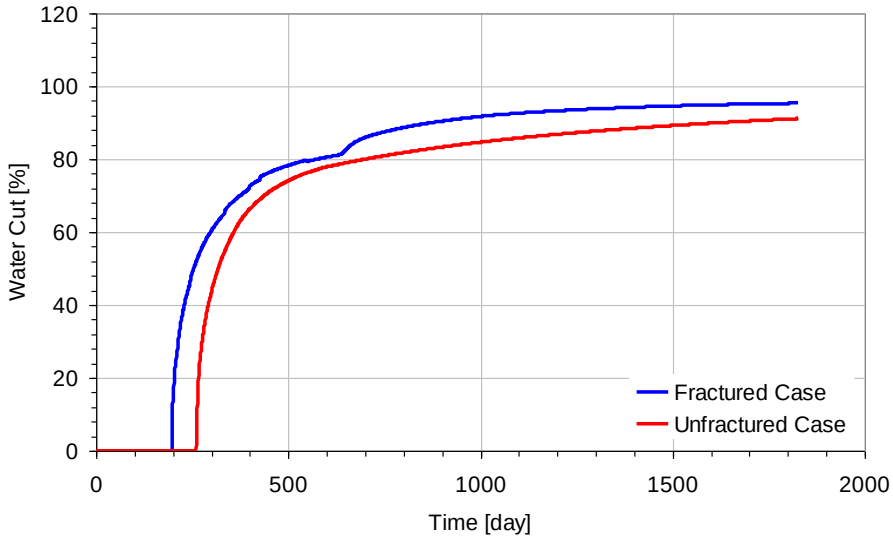

Figure 4.18: Water Cut for fractured and un-fractured cases (*Case 5.1*)

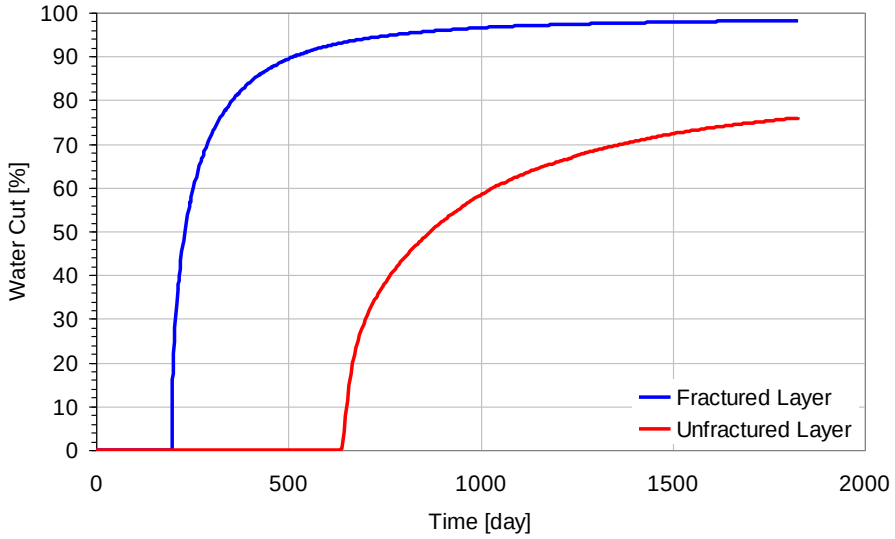

Figure 4.19: Water Cut for fractured and un-fractured layers (*Case 5.1*)

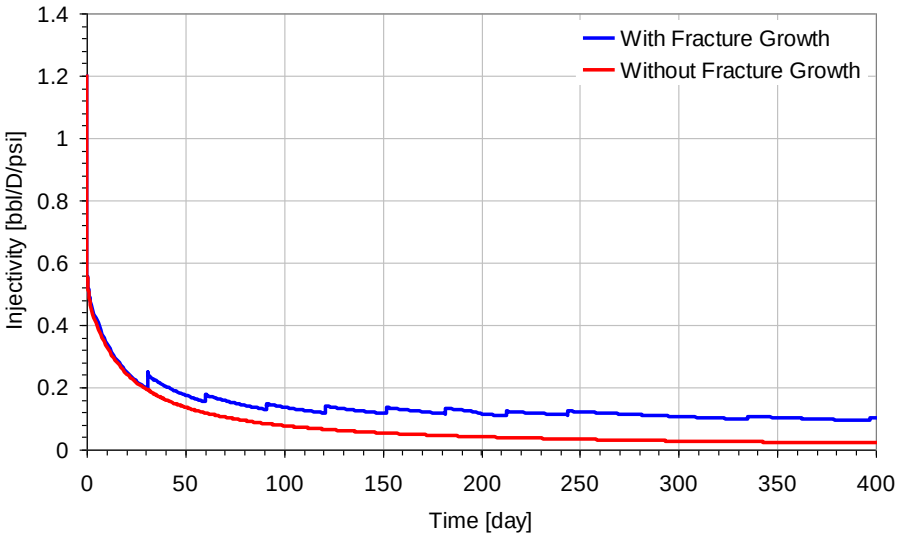

Figure 4.20: Injectivity for fractured and un-fractured cases (*Case 5.1*)

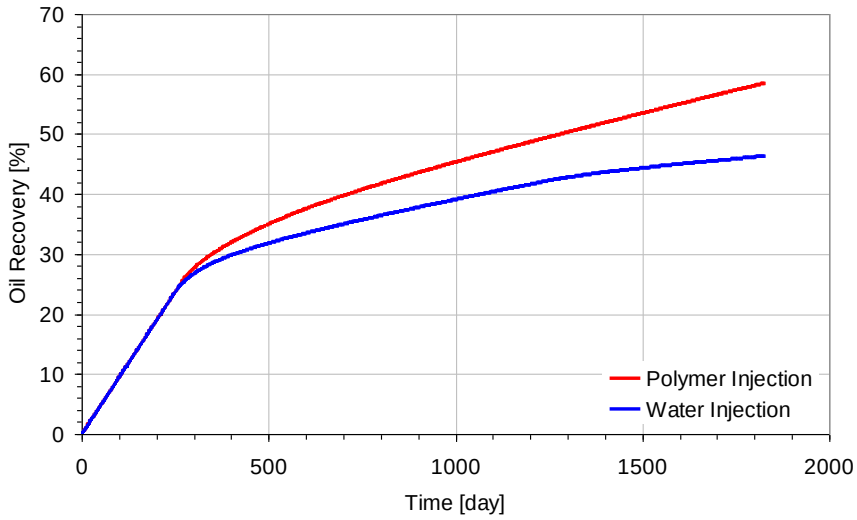

Figure 4.21: Oil recovery for polymer and water injection cases (*Case 6.1*)

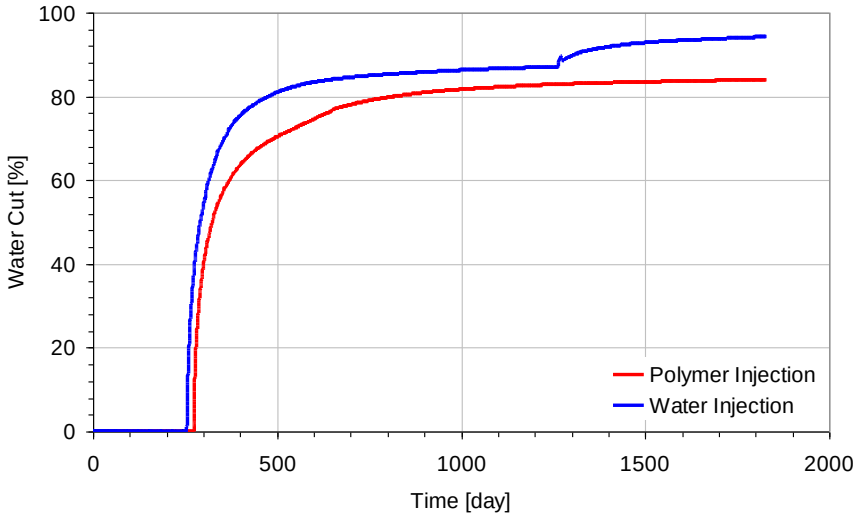

Figure 4.22: Water cut for polymer and water injection cases (*Case 6.1*)

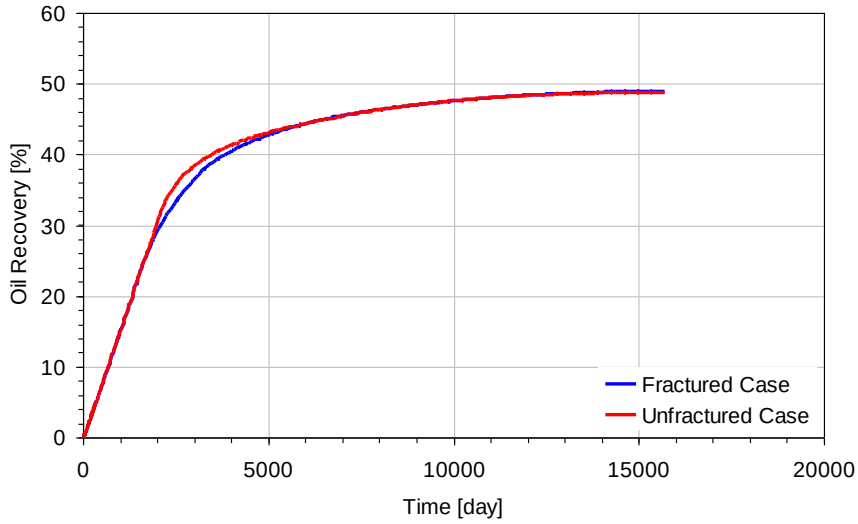

Figure 4.23: Oil recovery for fractured and un-fractured cases (*Case 7.1*)

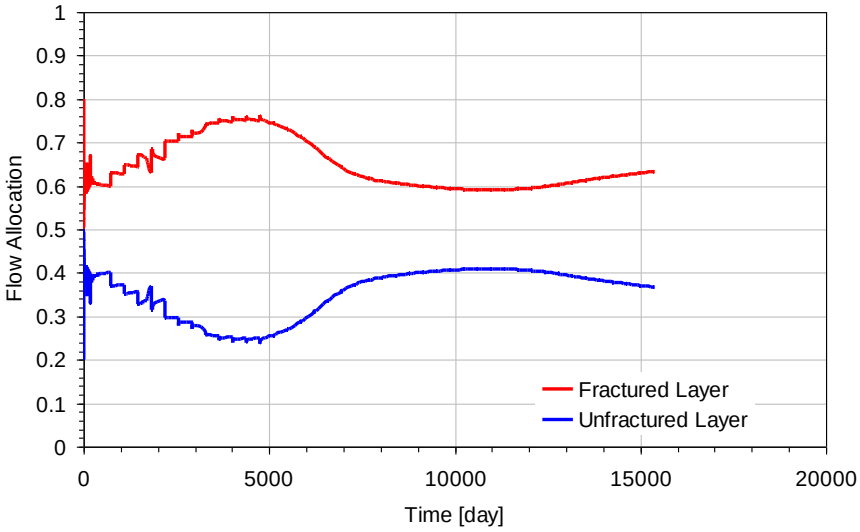

Figure 4.24: Flow allocation for fractured and un-fractured layers (*Case 7.1*)

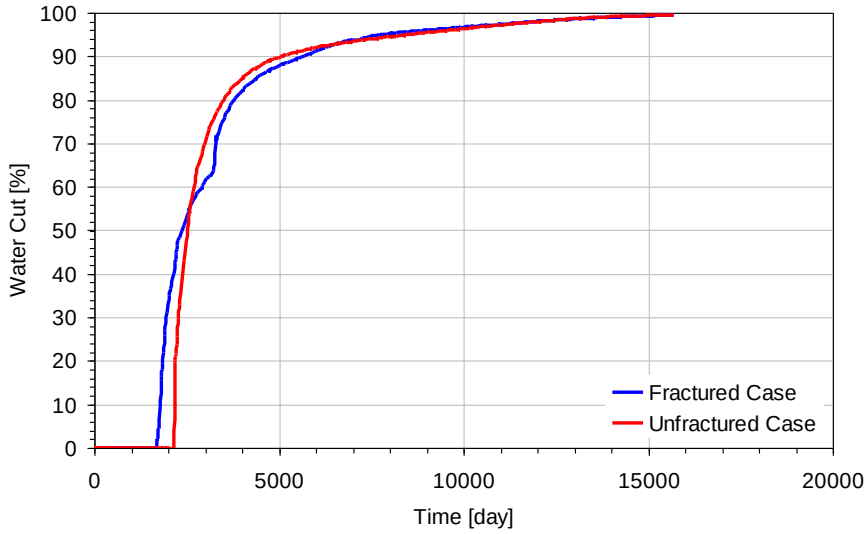

Figure 4.25: Water cut for fractured and un-fractured cases (*Case 7.1*)

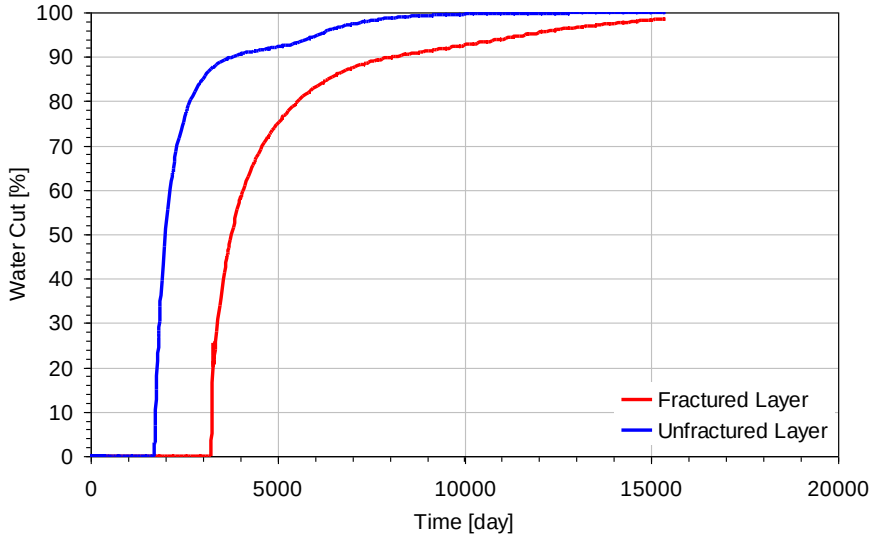

Figure 4.26: Water cut for fractured and un-fractured layers (*Case 7.1*)

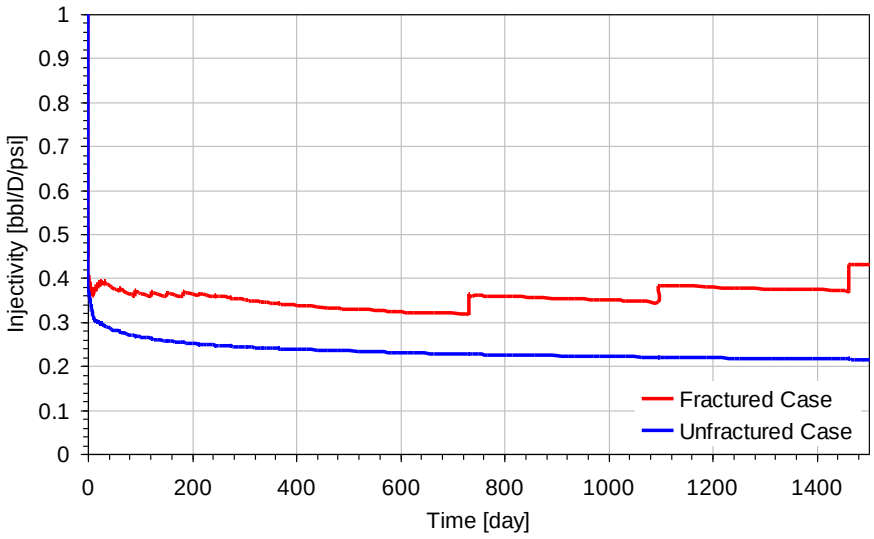

Figure 4.27: Injectivity for fractured and un-fractured cases (*Case 7.1*)

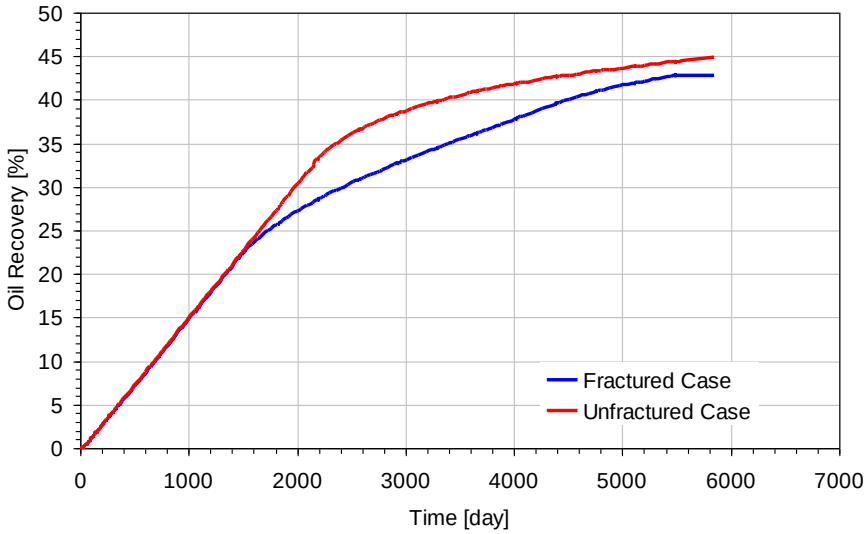

Figure 4.28: Oil recovery for fractured and un-fractured cases (*Case 8.1*), unified model, Flopaam 3330S polymer (1,500 ppm; 1.6% NaCl; 25 ºC)

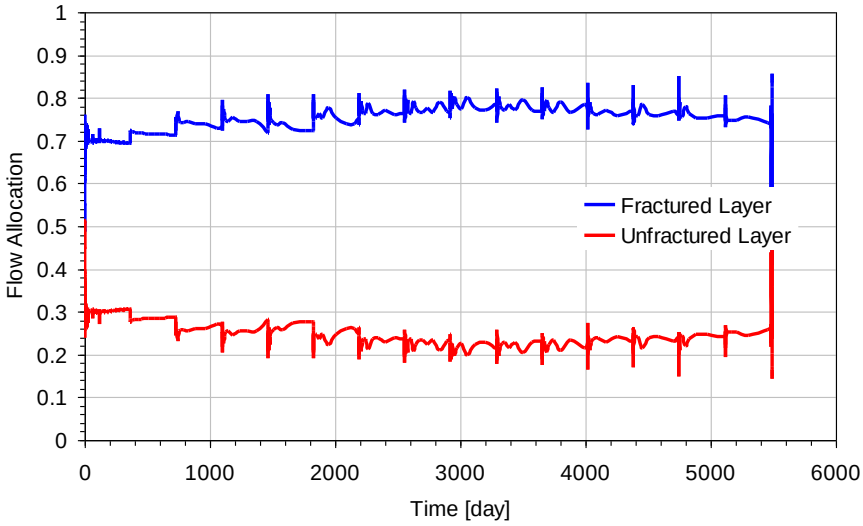

Figure 4.29: Flow allocation for fractured and un-fractured layers (*Case 8.1*), unified model, Flopaam 3330S polymer (1,500 ppm; 1.6% NaCl; 25 ºC)

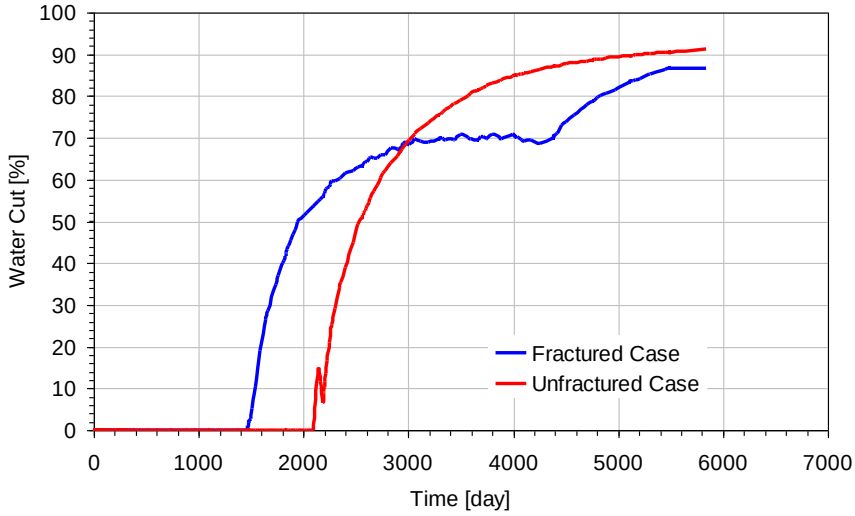

Figure 4.30: Water cut for fractured and un-fractured cases (*Case 8.1*), unified model, Flopaam 3330S polymer (1,500 ppm; 1.6% NaCl; 25 ºC)

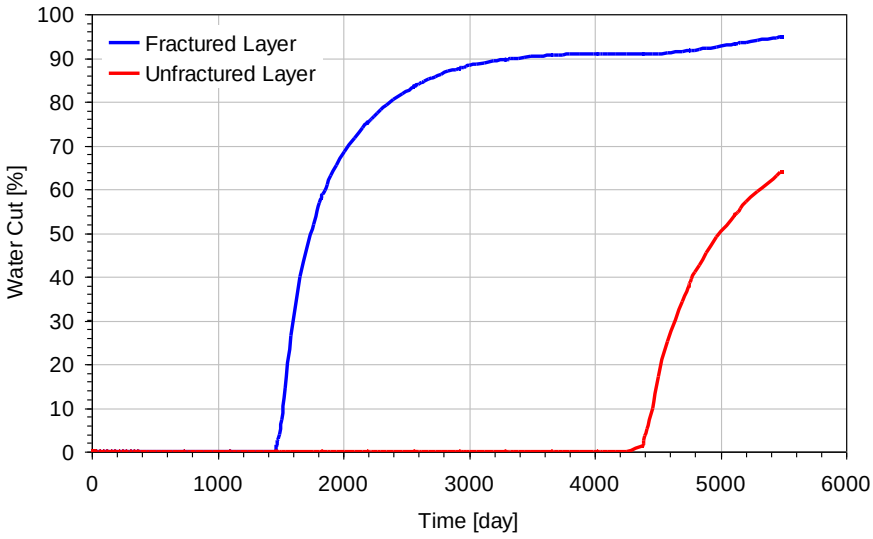

Figure 4.31: Water cut for fractured and un-fractured layers (*Case 8.1*), unified model, Flopaam 3330S polymer (1,500 ppm; 1.6% NaCl; 25 ºC)

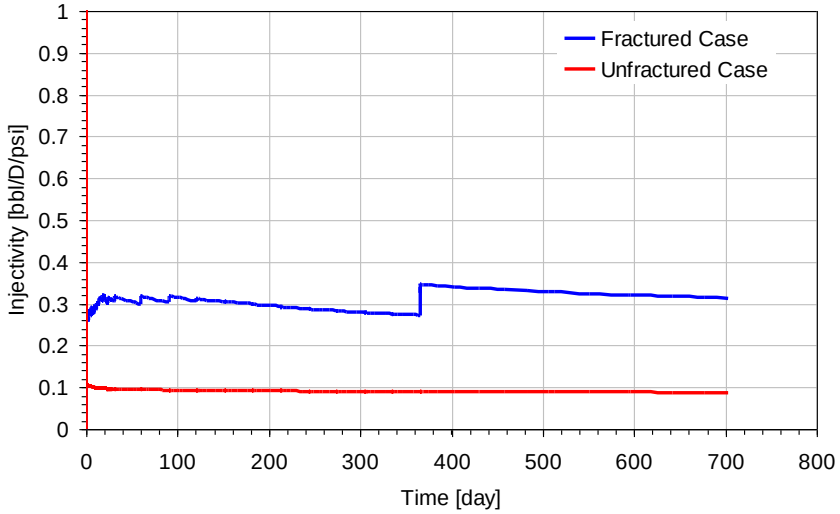

Figure 4.32: Injectivity for fractured and un-fractured layers (*Case 8.1*), unified model, Flopaam 3330S polymer (1,500 ppm; 1.6% NaCl; 25 ºC)

Chapter 5: Simulation of Water and Polymer Injection into Horizontal Wells

5.1 INTRODUCTION

For reservoirs with low vertical permeability and/or a large thickness, use of vertical injectors and producers (which cost less than horizontal wells) is adequate to obtain good oil recovery. On the other hand, if a reservoir has high vertical permeability or a thickness less than 100 ft, horizontal injectors and producers could produce much higher oil recovery than vertical wells. Therefore, it is necessary to investigate the effects of fracture initiation and growth at horizontal wells on oil recovery and reservoir sweep (Martini *et al.*, 2005; Owens *et al.*, 1992; Robinowitz *et al.*, 2004; Soliman and Boonen, 1997; Taber and Seright, 1992; Westermark *et al*., 2006). As was done for vertical well fractures in **Chapters 3** and **Chapter 4**, this chapter investigates the effects of static and induced dynamic fractures near horizontal wells during waterflood and polymer flood operations.

There are typically two different kinds of fracture geometry in horizontal wells, depending on the rock stress orientation near the well. If the minimum stress orientation is perpendicular to the horizontal injector, a longitudinal fracture is generated from the horizontal well, because the fracture plane must open in opposition to the minimum horizontal stress. If the minimum horizontal stress orientation is parallel to the horizontal injector, a transverse fracture is created near the well.

This chapter investigates the impacts of longitudinal and transverse fractures on well injectivity, reservoir sweep, and oil recovery. The key factors investigated are the

size of the fracture, the number of transverse fractures, the permeability of the fracture, and the type of injection well constraints (constant maximum injection BHP versus constant injection rate).

5.2 WATER INJECTION IN HORIZONTAL WELLS WITH STATIC TRANSVERSE FRACTURES

There are two extremes in fracture orientation with respect to the horizontal wellbore, transverse fractures and longitudinal fractures. The direction of fractures in horizontal wells is always perpendicular to the minimum horizontal stress. In this chapter, the impact of transverse and longitudinal fractures on well injectivity, reservoir sweep, and oil recovery is investigated under various injection constraints such as maximum injection rate or injection BHP. The conditions for the waterflood simulations are listed in **Table 5.1**.

5.2.1 Injection Constraint - Injection BHP

Transverse fractures can be generated near horizontal injection wells when the minimum horizontal stress orientation is parallel to the direction of the well. If there are transverse fractures near the horizontal injector, injectivity increases due to the high permeability of the fractures. Therefore, if there is an injection well transverse fracture, and the maximum injection BHP is held constant, the amount of fluid injected into the reservoir can be determined by injection well fracture length, permeability, and the number of fractures. A static fracture causes high injectivity, which in turn causes a large

amount of fluid to be injected into the reservoir. Because of the increased injectivity, oil recovery increases, as transverse fractures are generated and as the number of transverse fractures increases. **Figure 5.1** shows the amount of cumulative injected water for various numbers of transverse fractures. The transverse fracture plays an important role in increasing injectivity near the injector. Improved injectivity with injection well fractures induces improved oil recovery (**Figure 5.1** and **Figure 5.2**). In summary, at a constant BHP constraint, transverse injection well fractures improve oil recovery and injectivity; the amount of improvement is directly related to the number of fractures generated.

5.2.2 Injection Constraint - Injection Rate

The previous sub-section 5.2.1 describes how transverse injection well fractures improve well injectivity when maximum injection BHP is held constant. When the injection well constraint is an injection BHP, a transverse fracture increases the amount of cumulative injected fluid and oil recovery. On the other hand, if the injection well constraint is a constant injection rate, the transverse fracture can, if long enough, reduce the distance between the injection well fracture tip and the producer, thereby expediting water breakthrough, increasing the water-oil ratio, and increasing oil production rate. **Figure 5.3** shows that the number of transverse fractures has no observable effect on oil recovery at a constant injection rate for this well pattern. The transverse fractures cannot affect reservoir sweep and oil recovery in this particular model, because the distance between injector and producer is too large. However, the impact of the number of transverse fractures can be observed as a difference in injection BHP (**Figure 5.4**). The injection BHP increases very rapidly in the unfractured case, but more moderately in the

presence of more transverse fractures. Injection BHP increases more moderately with more transverse fractures due to improved well injectivity as shown in **Figure 5.4**. In summary, when injection rate is held constant, more transverse fractures result in a decreased injection BHP, but have a negligible effect on oil recovery.

5.2.3 Impact of Transverse Fractures on Well Injectivity and Reservoir Sweep

Sub-sections 5.2.1 and 5.2.2 investigate the impact of transverse fractures. In the case of a constant BHP constraint, the injection rate and oil recovery are determined by the number of transverse fractures as shown in **Table 5.2**.In the case of a constant injection rate, the number of fractures clearly affects injectivity and injection BHP, but has no observable effect on oil recovery (**Table 5.3**).

5.3 WATER INJECTION IN HORIZONTAL WELLS WITH STATIC LONGITUDINAL FRACTURE

5.3.1 Injection Constraint - Injection BHP

A longitudinal fracture can be generated when the minimum horizontal stress orientation is perpendicular to the horizontal injector. The constraint in this simulation is maximum injection BHP. Oil recovery and cumulative injected water increase as the size of the longitudinal fracture increases, because longitudinal fractures increase injectivity (**Figure 5.5** and **Figure 5.6**). The presence of a longitudinal fracture makes a noticeable difference in oil recovery; even the smallest fracture modeled in this simulation raised oil recovery from 4% to over 16%. The critical effect is that reservoir pressure is maintained

with waterflooding or polymer–flooding operations, which are affected by injectivity and a fracturing near the injector.

5.3.2 Injection Constraint - Injection Rate

Similar to the transverse fracture case, the size of the longitudinal fracture has a negligible effect on oil recovery. If there is no longitudinal fracture near the horizontal well, injection BHP increases rapidly when subject to a constant injection rate (**Figure 5.8**). However, if there is a longitudinal fracture, injection BHP increases much more slowly than in the unfractured case. **Figure 5.7** shows that the size of the longitudinal fracture has a negligible effect on oil recovery. Injection BHP, however, is significantly affected by longitudinal fracture as shown in **Figure 5.8**. In sub-section 5.6, increased injection BHP is discussed as a mechanism for fracture initiation, and is used to model dynamic fracturing.

5.3.3 Impact of Longitudinal Fractures on Well Injectivity and Reservoir Sweep

Similar to sub-section 5.2.3, in this section, the impact of longitudinal fracture on well injectivity and reservoir is summarized. In the case of a maximum injection BHP constraint, longitudinal fractures have a significant impact on well injectivity and oil recovery; oil recovery is much higher in the presence of a longitudinal fracture, and longer fractures yield higher oil recovery (**Table 5.4**).

In the case of a constant injection rate, a longitudinal fracture significantly decreases injection BHP increase, but does not significantly affect oil recovery. The size of the longitudinal fracture has a negligible effect on both injection BHP and oil recovery (**Table 5.5**).

5.4 WATER INJECTION IN HORIZONTAL WELLS WITH VARIOUS STATIC TRANSVERSE FRACTURE CONDUCTIVITIES

Fracture permeability is also an important parameter in this study; as fracture conductivity increases, well injectivity also increases. In this section, the impact of fracture conductivity on oil recovery and well injectivity is investigated.

5.4.1 Injection Constraint - Injection BHP

In this simulation, there are 3 transverse fractures in injector. At a constant maximum injection BHP, the increase in well injectivity leads to an increase in oil recovery and cumulative water injected (**Figure 5.9** and **Figure 5.10**). A ten-fold increase in fracture permeability results in a 1~2% increase in oil recovery after 150 years (**Table 5.6**).

5.4.2 Injection Constraint - Injection Rate

At a constant injection rate, injection BHP increases at a slower rate when fracture permeability is higher, and injectivity decreases slowly with increasing fracture permeability (**Figure 5.11** and **Figure 5.13**). The reason that the injectivity decreases during water injection is particle plugging. With higher fracture permeability, the rate of decreasing injectivity is much slower than with lower fracture permeability. Water breakthrough occurs earlier for a higher fracture permeability, and oil recovery is slightly lower (**Figure 5.12**).

5.4.3 Impact of Transverse Fracture Conductivity on Well Injectivity and Reservoir Sweep

Sub-sections 5.4.1 and 5.4.2 investigate the impact of transverse fracture conductivity on well injectivity and reservoir sweep. With a constant injection BHP constraint, higher transverse fracture conductivity induces higher oil recovery and injectivity (**Table 5.6**).

In the case of a constant injection rate constraint, higher transverse fracture conductivity results in much lower injection BHP and injectivity, but only somewhat lower oil recovery (**Table 5.7**).

5.5 WATER INJECTION IN HORIZONTAL WELLS WITH VARIOUS LONGITUDINAL FRACTURE CONDUCTIVITIES

5.5.1 Injection Constraint - Injection BHP

In the previous section (sub-section 5.4) we learned that transverse fracture conductivity can have a significant impact on well injectivity and injection BHP. This section makes a similar investigation for longitudinal fractures. **Figure 5.14** shows cumulative injected water as a function of time and longitudinal fracture conductivity at a constant injection BHP. A ten-fold increase in fracture conductivity from 100 D to 1,000 D results in a 72% increase in cumulative injected water at 50 years, while a ten-fold increase from 1,000 D to 10,000 D only results in a 5% increase in cumulative injected water. **Figure 5.15** indicates a similar trend for oil recovery. **Figure 5.16** shows

that higher fracture permeability slows the loss of injectivity (due to particle plugging) during injection with particle-laden water.

5.5.2 Injection Constraint - Injection Rate

The previous section (sub-section 5.5.1) investigates the effect of fracture conductivity on injectivity and oil recovery at a constant injection BHP. This section makes a similar investigation for a constant injection rate. Injectivity is expected to decline due to near-well particle plugging, but we observe that a fracture with a higher permeability slows the loss of injectivity, and also slows the increase of injection BHP (**Figure 5.17** and **Figure 5.18)**. In this case, with a constant injection rate, a fracture with a higher permeability facilitates earlier water breakthrough, which causes a slight decrease in oil recovery (**Figure 5.19**), although the volume of water injected is identical in each case.

5.5.3 Impact of Longitudinal Fracture Conductivity on Well Injectivity and Reservoir Sweep

Similar to transverse fractures, the conductivity of longitudinal fractures affects well injectivity and oil recovery depending on the type of injection well constraint. In the case of a constant injection BHP constraint, a higher permeability fracture increases the amount of water injected, increases the fraction of oil recovered, and slows the loss of injectivity during the injection of particle-laden water (**Table 5.8**). In the case of a constant injection rate constraint, a higher permeability fracture slows the increase of

injection BHP, slows the loss of injectivity, facilitates earlier water breakthrough, and has a negligible effect on the fraction of oil recovered (**Table 5.9**).

5.6 DYNAMIC LONGITUDINAL FRACTURE WITH HORIZONTAL WELL – WATER INJECTION

Sub-section 5.2 through sub-section 5.5 investigates phenomena associated with static fractures at horizontal injection wells. This section and those that follow investigate similar relationships during dynamic fracturing around horizontal wells with particle-laden water and with a unified model polymer.

Longitudinal fracturing occurs when the minimum horizontal stress acts perpendicular to the direction of the well, and when an injection process causes the injection BHP to exceed the breakdown pressure of the formation. If the injected water contains particles (i.e. particle plugging occurs), or if the injected polymer exhibits shear-thickening behavior, injection BHP increases rapidly, and quickly reaches the breakdown pressure (about 6,000 psi in this case). Once the fracture begins to grow, injectivity and injection BHP stabilize, with the injection BHP remaining lower than it would without a fracture, and with the injectivity remaining higher than it would without a fracture (**Figure 5.20**~**Figure 5.24**). The improvement in injectivity does not translate into a significant improvement in oil recovery; oil recovery with a longitudinal fracture is only 3% higher than without (**Figure 5.22**, unified model polymer).

5.7 DYNAMIC TRANSVERSE FRACTURE WITH HORIZONTAL WELL, DIFFERENT FRACTURE CONDUCTIVITY – WATER INJECTION

Transverse fracturing occurs when the minimum horizontal stress acts parallel to the direction of the well. Unlike a longitudinal fracture, the growth of a transverse fracture does not necessarily stabilize injection BHP and injectivity. **Figure 5.25** shows that, although injection BHP remains lower than it would without a transverse fracture, it still increases over time. Also, although injectivity remains higher than it would without a fracture, it still declines even while the fracture is still growing (**Figure 5.26**). A transverse fracture does not boost injectivity as much as a longitudinal fracture because it affects such a small fraction of the length of the well, whereas a longitudinal fracture affects the entire horizontal length. Therefore, even though transverse fracture growth continues during water and polymer injection, injection BHP increases, and injectivity cannot be stabilized.

5.8 SENSITIVITY STUDY FOR LOCATIONS OF HORIZONTAL INJECTOR AND PRODUCER

Horizontal (versus vertical) injection wells allow for much higher oil recovery in reservoirs that have a high vertical permeability, or that are relatively thin (less that 100 ft thickness). The capability of a horizontal well to deliver this higher oil recovery also depends on the geometry of the wellbore relative to the other injectors, producers, and the water-oil contact, as well as its height in the reservoir, its length, and the length and

height of the producers. This section explores these relationships under two conditions: a closed boundary (small) reservoir, and a (more realistic) open boundary (large) reservoir.

5.8.1 Closed Boundary Conditioned Reservoir (Small Reservoir Size)

As a first step towards understanding behavior in an unbounded reservoir, this section investigates the effects of wellbore geometry in a closed boundary conditioned reservoir. In this discussion, d represents the distance between the horizontal injector and producer, and L_f represents the transverse fracture half length (350 ft in this simulation). The fracture height is 360 ft and the injector is positioned 320 ft lower than the producer. As the distance between injector and producer decreases, L_f/d increases. **Figure 5.27** indicates that there is an optimal distance for this injector-producer arrangement: a ratio L_f/d of about 0.25. Too short a distance between injector and producer results in early water breakthrough, which decreases oil recovery. Too long a distance between injector and producer diminishes the beneficial effect of water injection on oil recovery.

A similar relationship exists between distance and oil recovery even when no fracture is present. As in the previous case, the injector is positioned 320 ft lower than the producer at every given distance d, but the distance is measured relative to the reservoir size because there is no fracture in this case. **Figure 5.28** shows that, without a fracture, the optimal well spacing between injector and producer is about 0.5 times the size of the reservoir.

The relative position of the water-oil contact (WOC) also affects oil recovery. WOC is the depth below which the water saturation in the reservoir is 99%. In this simulation, the reservoir thickness, h, is 960 ft; the reservoir ranges from 4040 ft to 5000

ft below the surface. WOC is represented by the variable h_{woc}, which represents the position of WOC above the bottom of the reservoir. The ratio h_{woc}/h is then a measure of how shallow the reservoir which contains oil, that is, how high WOC is located above the bottom of the reservoir. If the reservoir which contains oil is shallow, there is not enough oil to produce in the reservoir and oil recovery becomes low (**Figure 5.29**). **Figure 5.30** shows the vertical distribution of water saturation in the reservoir. The WOC is located 380 ft above the bottom of the reservoir. The water saturation below the WOC (0~380 ft) is 100%, and the water saturation above the WOC (380~920 ft) decreases to irreducible water saturation (about 30%) at the top of the reservoir. This water saturation distribution affects the impact of horizontal injector and producer placement as shown in **Figure 5.31**.

Figure 5.31 describes the effect of the position of the injector, h_{inj}, on oil recovery. In this simulation, the WOC is positioned at 480 ft ($h/h_{prod} = 0.6$); if the injector is positioned at lower than 480 ft, the horizontal injector is located in the 100% water saturated reservoir zone. When the fracture is located above the water column, oil recovery does increase and oil recovery increases more when the horizontal injector is located above the WOC. **Figure 5.32** shows a similar trend with respect to the position of the injector, but without a fracture.

Figure 5.33 shows the relationship between oil recovery and the distance between injector and producer. As with a transverse fracture, at too short a distance, early water breakthrough occurs, and oil recovery becomes lower. Too long a distance diminishes the beneficial effect of water injection on oil recovery. The optimal spacing in this case appears to be about 700 ft, after which increasing the distance yields negligible gains in oil recovery, and below which oil recovery rapidly declines.

Figure 5.34 is analogous to **Figure 5.31**, showing the effect of injector position on oil recovery for a horizontal injector with a longitudinal fracture. WOC is located at 480 ft and the injector is located lower than the producer. Interestingly, in the case of a longitudinal fracture, oil recovery decreases when the injector is located higher in the reservoir because of early water breakthrough and short distance between fracture and producer. Also, for a given distance between injector and producer, 400 ft, oil recovery is lower when the WOC is located higher (**Figure 5.35**).

Figure 5.36 shows the impact of horizontal well length on oil recovery. For this study, sensitivity to well length was tested in three ways: by increasing the length of both wells, by increasing the length of only the producer from 300 ft to 2,100 ft, and by increasing the length of only the injector from 300 ft to 2,100 ft. In all three cases, there is a positive correlation between well length and oil recovery. The impact of horizontal injector length is much more significant than the impact of producer length. When the horizontal injector length is half of its original length (2,100 ft), oil recovery decreases by 30%. However, when the horizontal producer length is half of its original length, oil recovery only decreases by 10%. Therefore, to maximize oil recovery, enough length of horizontal injector is necessary to maximize reservoir sweep.

Figure 5.37 and **Figure 5.38** show that the concentration of particles in injected water affects oil recovery significantly. In the **Figure 5.37**, the particle concentrations are 50 ppm and 0 ppm. In the **Figure 5.38**, the particle concentration is distributed from 0 ppm to 50 ppm and the oil recovery has been obtained at 15 years. The maximum injection BHP was kept constant at 4,500 psi, and the initial reservoir pressure is 3,000 psi. Oil recovery is much lower with higher particle concentrations, because particle

plugging occurs. Particle plugging causes injection BHP to increase rapidly, which decreases injectivity, and decreases oil recovery.

5.8.2 Opened Boundary Conditioned Reservoir (Large reservoir Size)

A reservoir with an opened boundary also exhibits a sensitivity to the parameters discussed in sub-section 5.8.1 (**Figure 5.39~Figure 5.46**). **Figure 5.39** (cp. **Figure 5.27**) shows the relationship between oil recovery and the distance between injector and producer for an injector with a transverse fracture. As distance decreases (L_f/d increases), oil recovery decreases because of early water breakthrough. As distance increases (L_f/d decreases), oil recovery increases, because reservoir pressure is maintained by water injection. Therefore, the peak which induces maximum oil recovery cannot be observed. When there is no fracture, the trend is similar (**Figure 5.40**, cp. **Figure 5.28**). When an injector with a longitudinal fracture is closer to a producer, oil recovery is lower, because water breakthrough occurs earlier and reservoir sweep is less efficient (**Figure 5.44).** Also, when WOC is positioned too high, there is not enough oil in the reservoir and oil recovery decreases significantly with both a transverse and a longitudinal fractures (**Figure 5.41** cp. **Figure 5.29**, and **Figure 5.45** cp. **Figure 5.35**). When an injector with a transverse fracture is located higher in the reservoir, it induces a higher pressure near the producer, which increases oil recovery as shown in **Figure 5.42**. When injector and transverse fracture near injector are located below the WOC (h_{woc}/h=0.5 and h_{inj}/h=0.25), oil recovery decreases significantly. The trend is similar for an injector without a fracture (**Figure 5.43**). When an injector with a longitudinal fracture is closer (L_f/d is higher) to a

producer, oil recovery is lower, because water breakthrough occurs earlier, and reservoir sweep is less efficient (**Figure 5.44).**

5.9 SUMMARY

As in vertical injection wells, horizontal injection wells can be used for water and polymer injection. Furthermore, particle-plugging during water injection and high polymer viscosity during polymer injection are the main factors which induce injection well fractures. This chapter investigates the sensitivity of reservoir sweep, injectivity, and oil recovery to several parameters: the size of transverse and longitudinal fractures, the number of transverse fractures along a horizontal injector, the conductivity of transverse and longitudinal fractures, the concentration of particles in injected water, and the arrangement within the reservoir of the injector, the producer, and the WOC. Horizontal wells with dynamically growing fractures have also been investigated. These sensitivity studies are conducted with several combinations of the following constraints: constant injection BHP, constant injection rate, closed reservoir boundary, and open reservoir boundary.

In the case of static fractures with constant injection BHP, horizontal injection well fractures (both transverse and longitudinal) increase injectivity, thereby increasing the amount of injected fluid and the fraction of oil recovered. At a constant injection rate, horizontal injection well fractures increase injectivity, but do not significantly affect reservoir sweep or oil recovery.

In the case of dynamic fractures, there is no fracture growth with constant injection BHP because injection rate decreases when the injection pressure increases up to the BHP constraint. However, the fracture is created and grows with a constant injection rate constraint. This increases well injectivity and stabilizes the injection BHP.

By performing a dimensionless study of horizontal wells, the impact of the position of the WOC and the injectors and producers, longitudinal vs transverse fractures, and lengths of horizontal injector and producer on oil recovery and reservoir sweep has been investigated. This dimensionless representation is useful for deciding on the position of the horizontal injector and producer to maximize reservoir performance.

Table 5.1: Input data for water injection with static fracture

Reservoir Properties

Reservoir Size (ft)	$2,400 \times 2,500 \times 600$
Reservoir Porosity and Permeability (md)	0.2; 100
Reservoir Pressure (psi) at 4700 ft depth	3,000

Rock and Fluid Data

Relative Permeability End Points for Water and Oil	0.3; 0.7
Irreducible Water Saturation	0.3
Residual Oil Saturation	0.35
Compressibility of Formation, Water, and Oil (psi^{-1})	6.7×10^{-7}; 3.03×10^{-6}; 8.32×10^{-6}
Particle Concentration in the Injected Water	50 ppm

Well Properties

Well Type	Horizontal
Injection Well Radius (in)	3

Table 5.2: Impact of transverse fractures on well injectivity and oil recovery with constant injection BHP constraint (4,500 psi)

	Cumulative Injected Water at 100 years (bbl)	Oil Recovery at 100 years (%)
Without Fracture	6.1×10^{7}	5.7
With 3 Transverse Fractures	6.3×10^{7}	6.1
With 7 Transverse Fractures	6.7×10^{7}	6.6

Table 5.3: Impact of transverse fractures on well injectivity and oil recovery with constant injection rate constraint (30,000 bbl/D)

	Injection BHP at 10 years (psi)	Oil Recovery at 10 years (%)
Without Fracture	5.2×10^{4}	8.6
With 3 Transverse Fractures	3.8×10^{4}	8.6
With 7 Transverse Fractures	2.8×10^{4}	8.6

Table 5.4: Impact of longitudinal fractures on well injectivity and oil recovery with constant injection BHP constraint (4,500 psi)

	Injection BHP at 27 years (psi)	Oil Recovery at 27 years (%)
Fracture Height 0 ft	4.1×10^{7}	3.5
Fracture Height 200 ft	2.6×10^{8}	14.8
Fracture Height 300 ft	3.2×10^{8}	16
Fracture Height 400 ft	3.6×10^{8}	-
Fracture Height 500 ft	4.0×10^{8}	-

Table 5.5: Impact of longitudinal fractures on well injectivity and oil recovery with constant injection rate constraint (30,000 bbl/D)

	Injection BHP at 16 years (psi)	Oil Recovery at 16 years (%)
Without Fracture	1.5×10^{5}	12.4
Fracture Height 300 ft	1.1×10^{8}	12.2
Fracture Height 400 ft	1.1×10^{8}	12.2
Fracture Height 500 ft	1.1×10^{8}	12.1

Table 5.6: Impact of transverse fracture conductivity on well injectivity and oil recovery with constant injection BHP constraint (4,500 psi)

	Cumulative Injected Water at 30 years (bbl)	Oil Recovery at 30 years (%)
With Fracture (k_f = 100 D)	3.7×10^{7}	3.5
With Fracture (k_f = 1,000 D)	4.8×10^{7}	4.7
With Fracture (k_f = 1,0000 D)	6.0×10^{7}	5.6

Table 5.7: Impact of transverse fracture conductivity on well injectivity and oil recovery with constant injection rate constraint (30,000 bbl/D)

	Injection BHP at 50 years (psi)	Oil Recovery at 50 years (%)	Well Injectivity at 50 years (bbl/D/psi)
With Fracture (k_f = 100 D)	1.4×10^{4}	20.5	0.7
With Fracture (k_f = 1,000 D)	8.8×10^{3}	19.5	0.8
With Fracture (k_f = 10,000 D)	6.8×10^{3}	19	0.95

Table 5.8: Impact of longitudinal fracture conductivity on well injectivity and oil recovery with constant injection BHP constraint (4,500 psi)

	Cumulative Injected Water at 50 years (bbl)	Oil Recovery at 50 years (%)
With Fracture (k_f = 100 D)	4.4×10^7	5.6
With Fracture (k_f = 1,000 D)	7.6×10^7	7.8
With Fracture (k_f = 10,000 D)	8.0×10^7	8.2

Table 5.9: Impact of longitudinal fracture conductivity on well injectivity and oil recovery with constant injection rate (30,000 bbl/D)

	Injection BHP at 50 years (psi)	Oil Recovery at 50 years (%)	Well Injectivity at 50 years (bbl/D/psi)
With Fracture (k_f = 100 D)	1.4×10^4	20.5	9.0
With Fracture (k_f = 1,000 D)	8.8×10^3	19.5	6.5
With Fracture (k_f = 10,000 D)	6.8×10^3	19	2.5

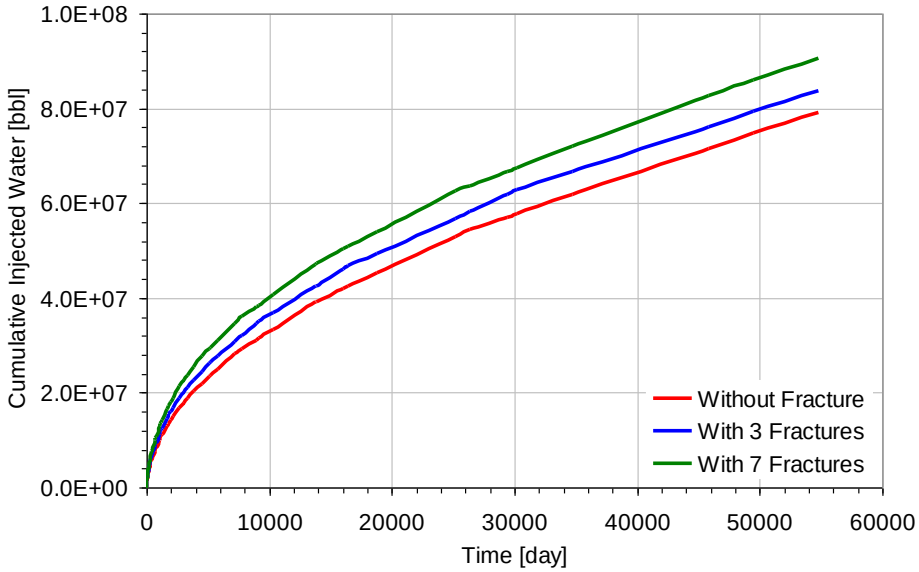

Figure 5.1: Cumulative injected water as a function of the number of transverse fractures at constant injection BHP 4,500 psi, fracture height 325 ft, fracture half length 300 ft

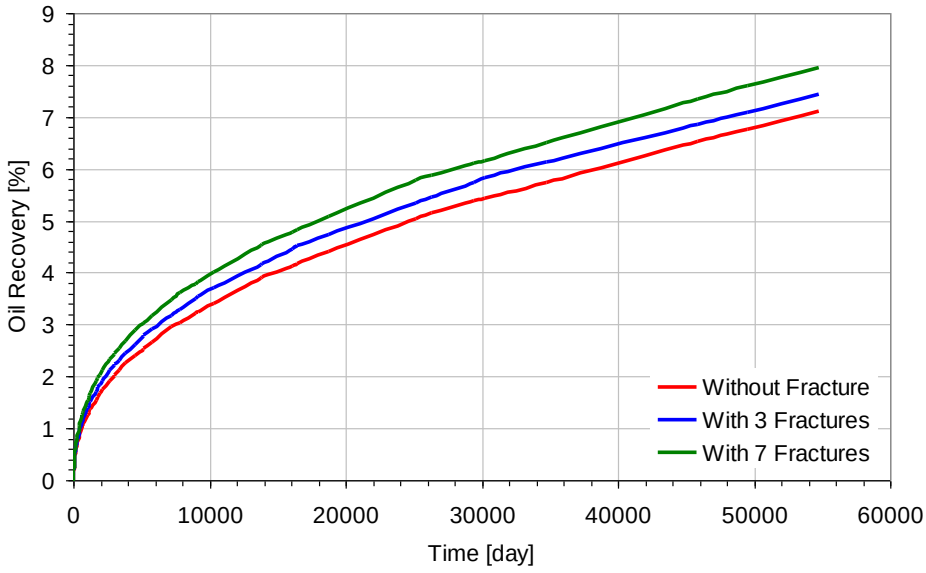

Figure 5.2: Oil recovery as a function of the number of transverse fractures at a constant injection BHP 4500 psi, fracture height 325 ft, fracture half length 300 ft

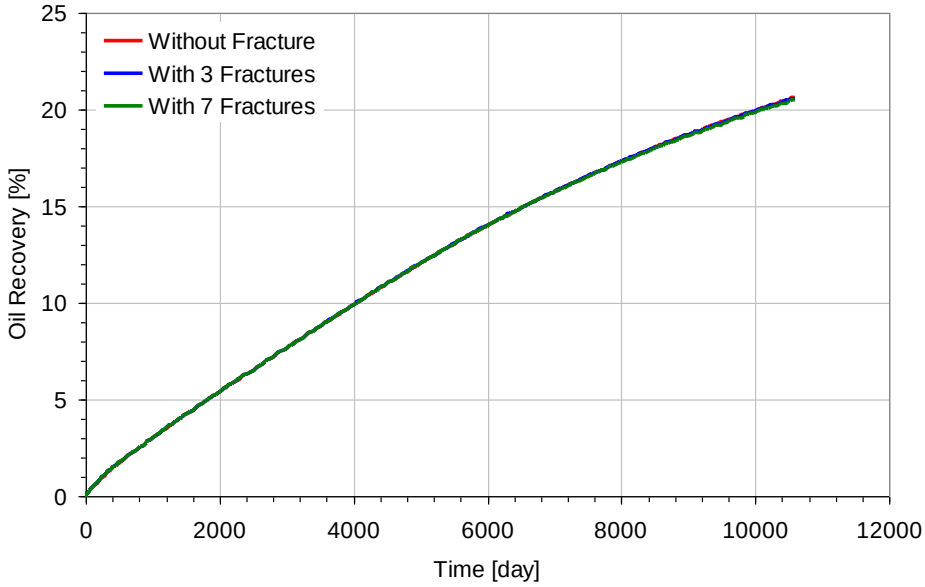

Figure 5.3: Oil recovery as a function of the number of transverse fractures at a constant injection rate 30,000 bbl/D, fracture height 325 ft, fracture half length 300 ft

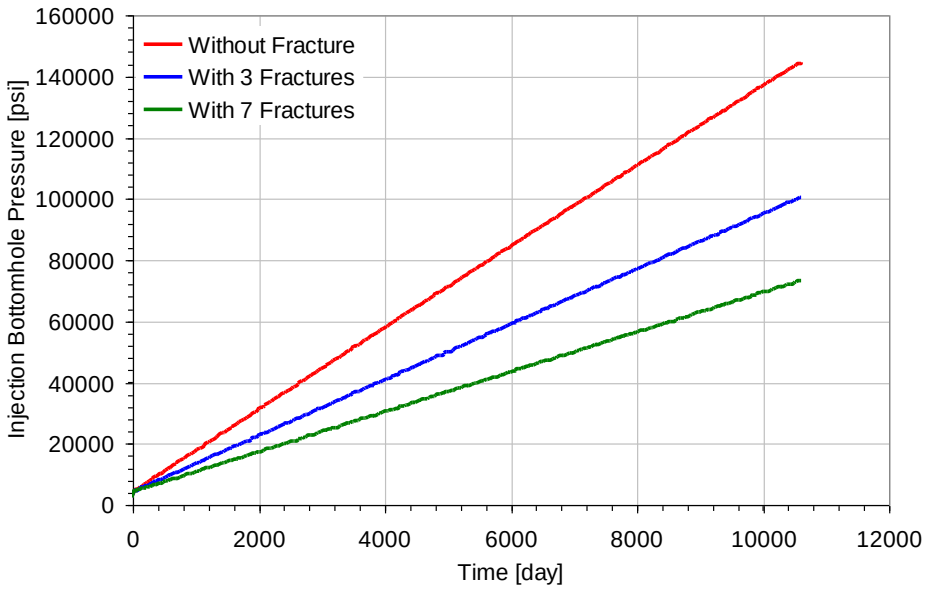

Figure 5.4: Injection BHP as a function of the number of transverse fractures at a constant injection rate 30,000 bbl/D, fracture height 325 ft, fracture half length 300 ft

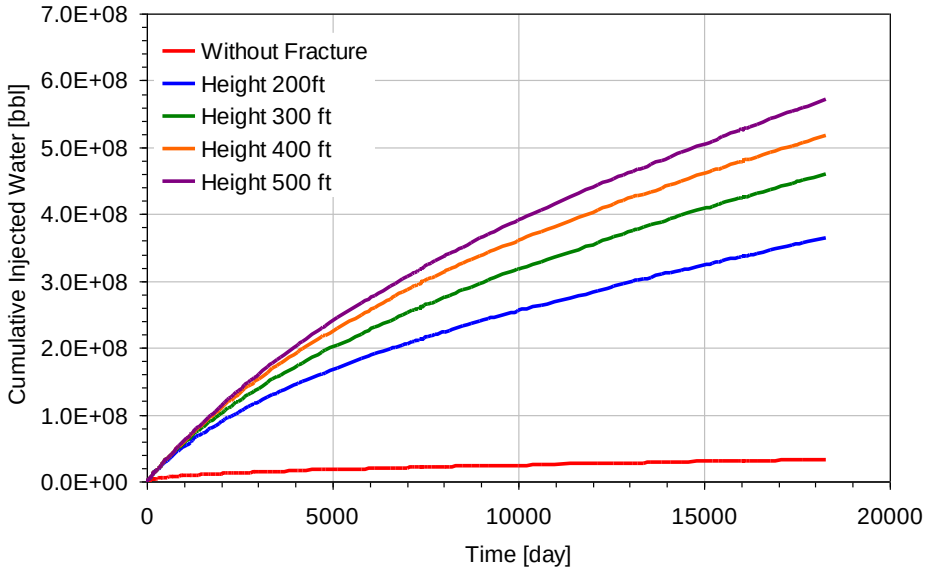

Figure 5.5: Cumulative injected water as a function of longitudinal fracture height at a constant injection BHP 4,500 psi

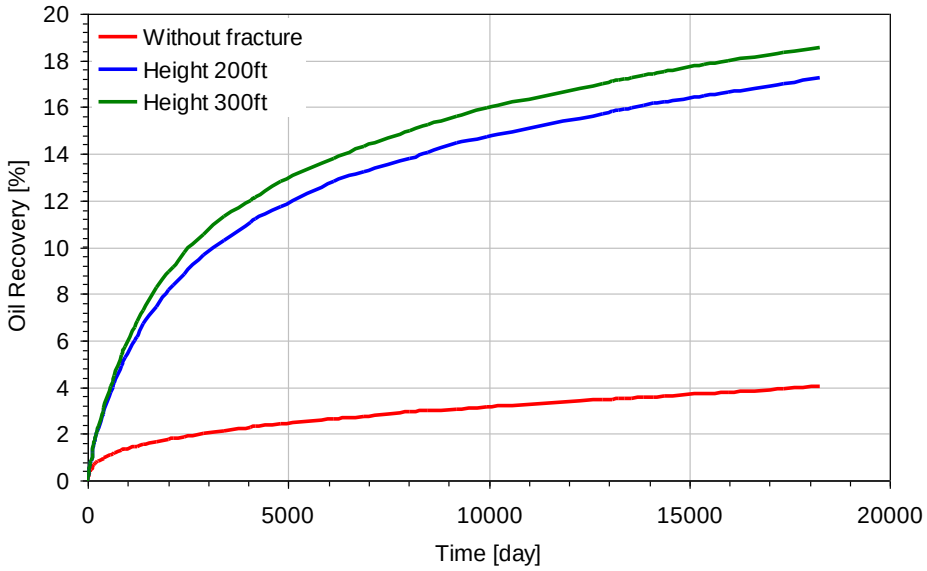

Figure 5.6: Oil recovery as a function of longitudinal fracture height at a constant injection BHP 4,500 psi

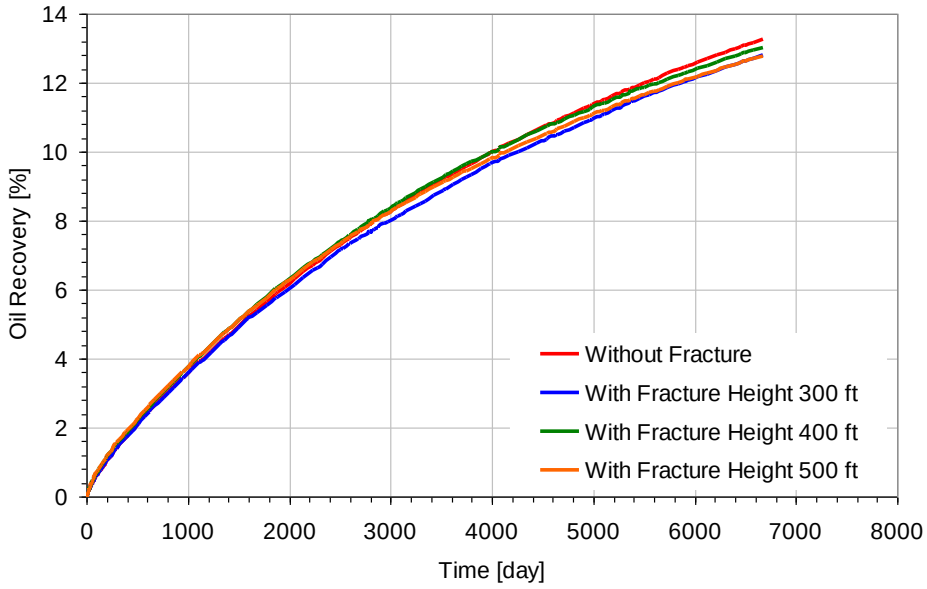

Figure 5.7: Oil recovery as a function of longitudinal fracture height at a constant injection rate 30,000 bbl/D

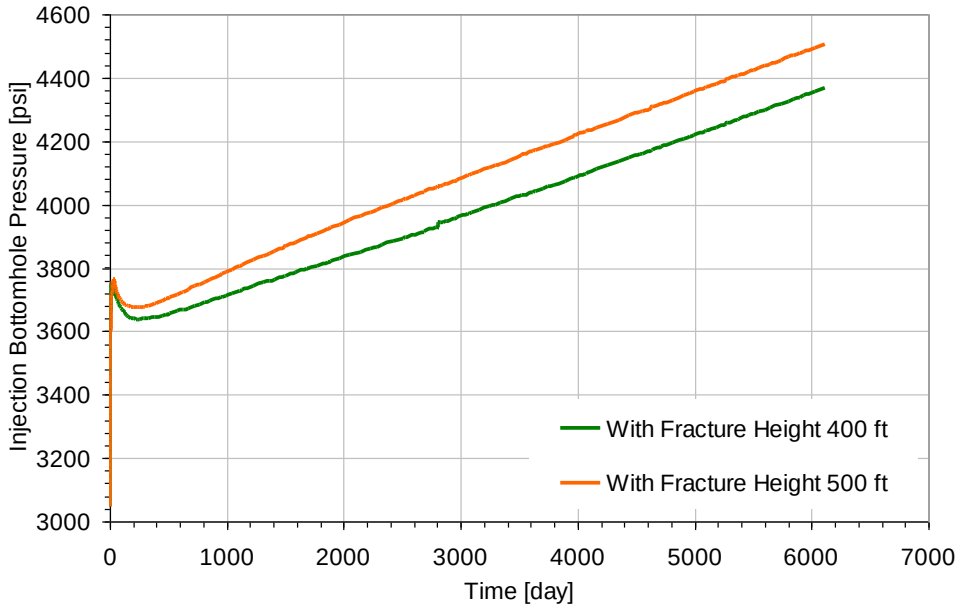

Figure 5.8: Injection BHP as a function of longitudinal fracture height at a constant injection rate 30,000 bbl/D

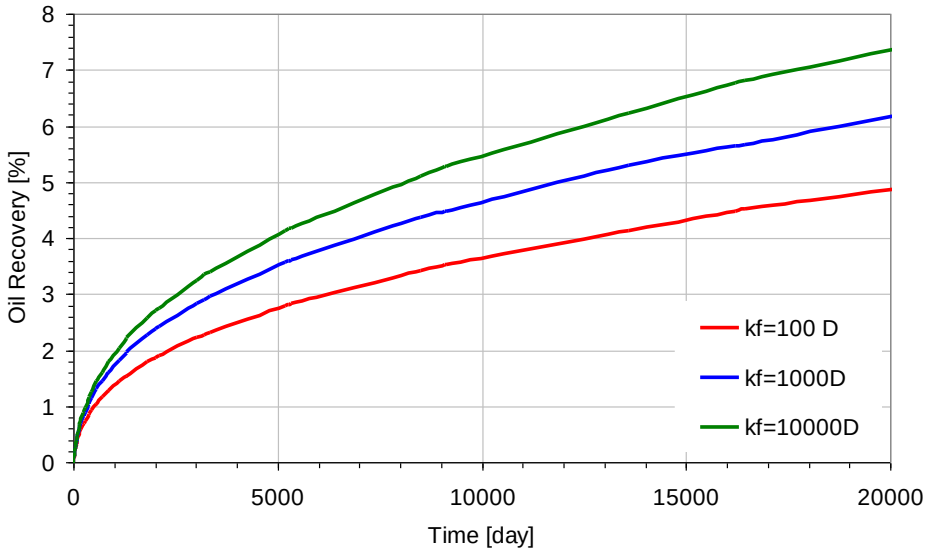

Figure 5.9: Oil recovery as a function of transverse fracture conductivity at a constant injection BHP 4,500 psi, fracture height 325 ft, fracture half length 300 ft

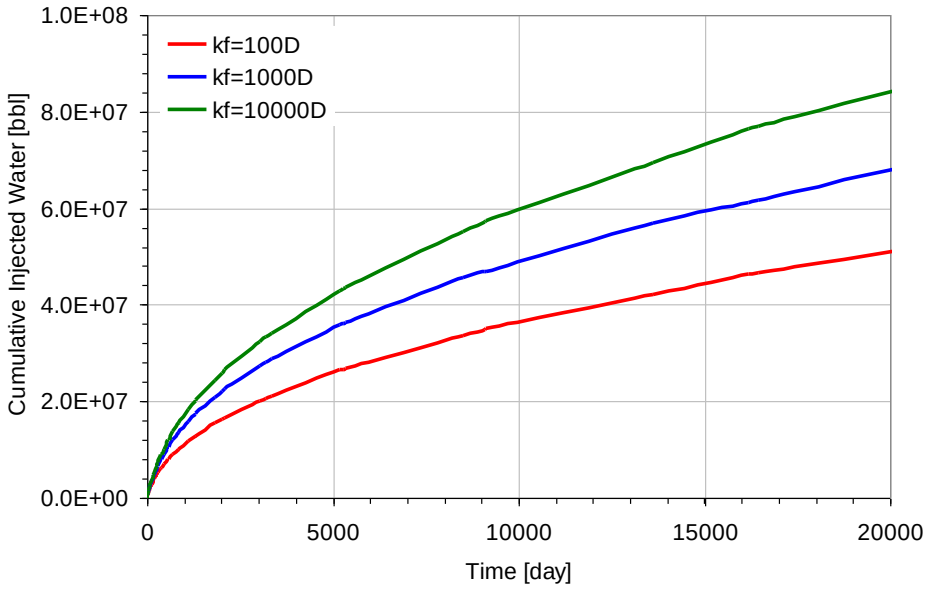

Figure 5.10: Cumulative injected water as a function of transverse fracture conductivity at a constant injection BHP 4,500 psi, fracture height 325 ft, fracture half length 300 ft

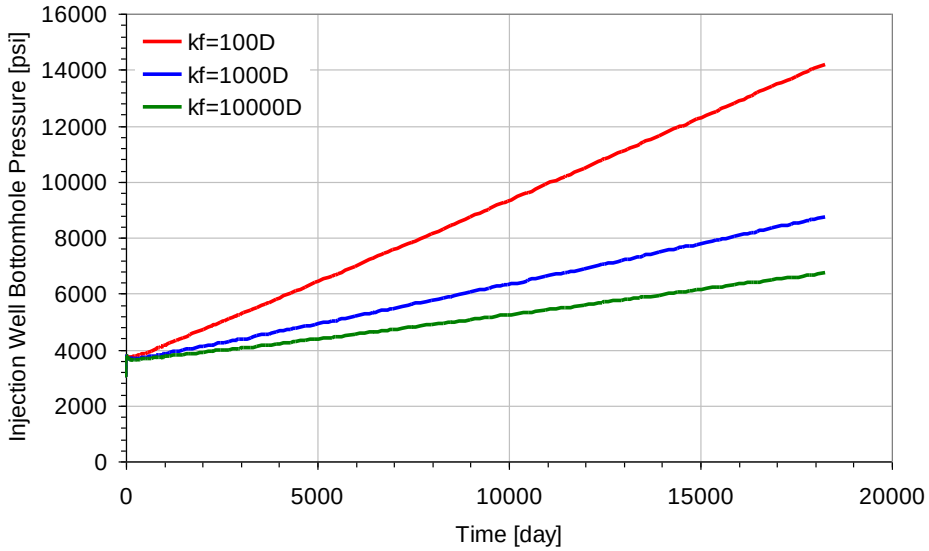

Figure 5.11: Injection BHP as a function of transverse fracture conductivity at a constant injection rate 30,000 bbl/D, fracture height 325 ft, fracture half length 300 ft

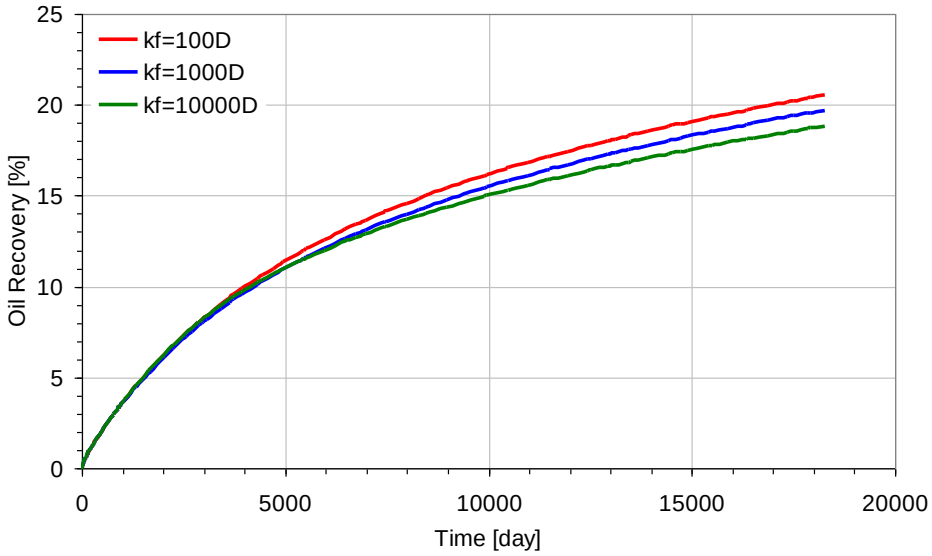

Figure 5.12: Oil recovery as a function of transverse fracture conductivity at a constant injection rate 30,000 bbl/D, fracture height 300 ft

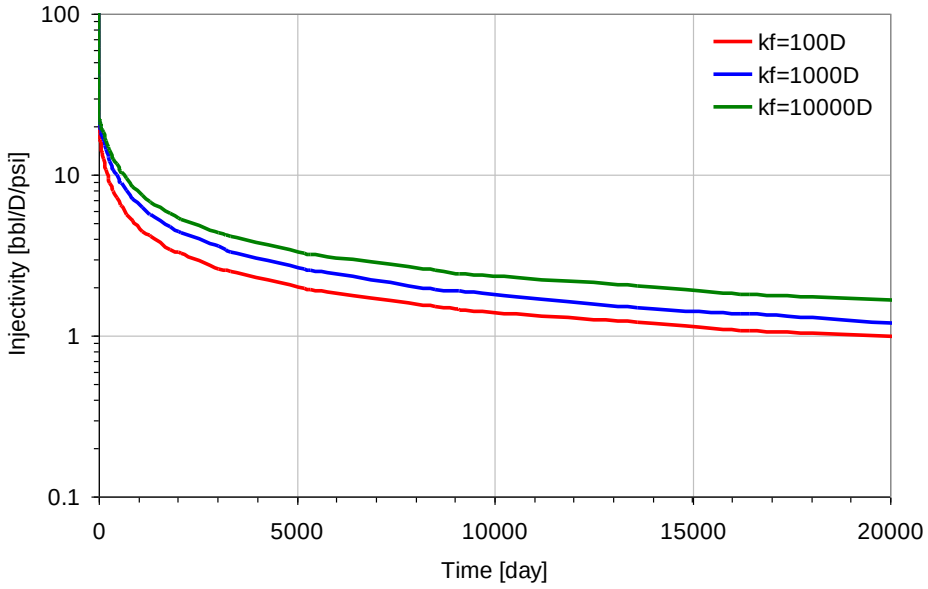

Figure 5.13: Injectivity as a function of transverse fracture conductivity at a constant injection rate 30,000 bbl/D, fracture height 300 ft

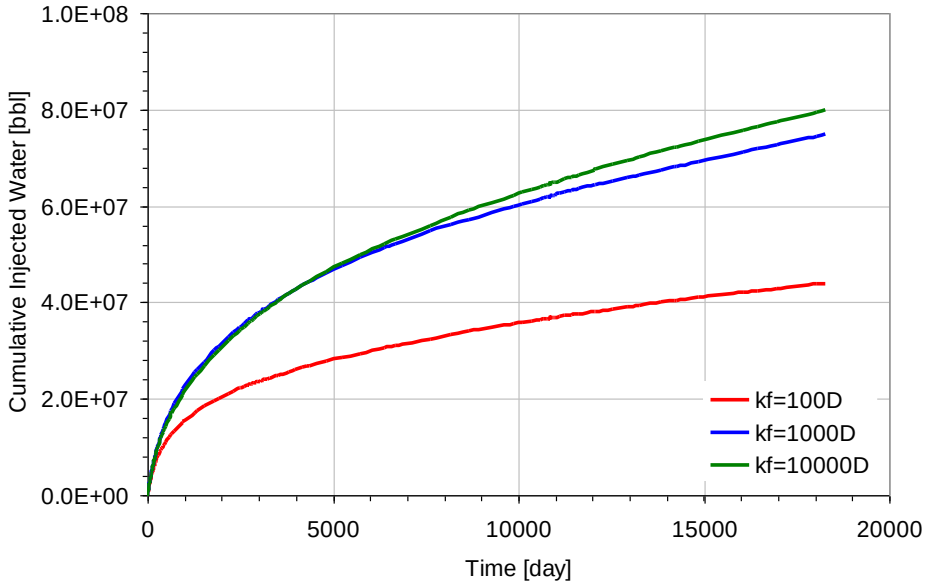

Figure 5.14: Cumulative injected water as a function of longitudinal fracture conductivity at a constant injection rate 30,000 bbl/D, fracture height 300 ft

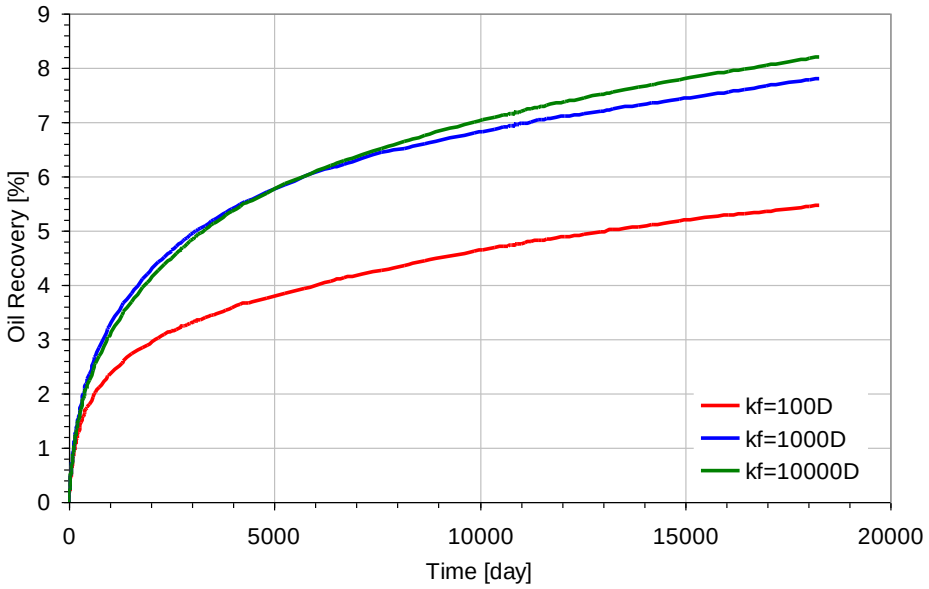

Figure 5.15: Oil recovery as a function of longitudinal fracture conductivity at a constant injection BHP 4,500 psi, fracture height 325 ft, fracture half length 300 ft

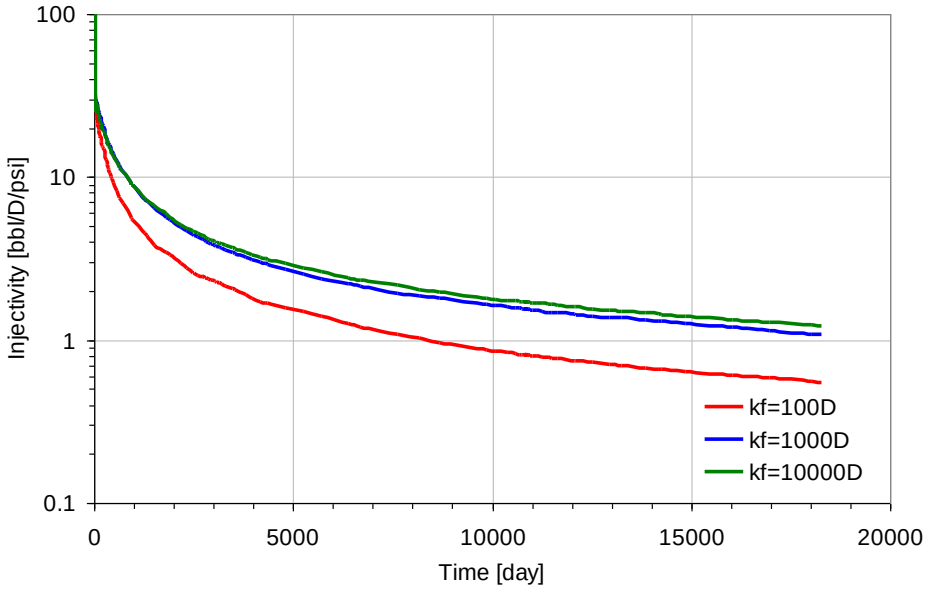

Figure 5.16: Injectivity as a function of longitudinal fracture conductivity at a constant injection BHP 4,500 psi, fracture height 325 ft, fracture half length 300 ft

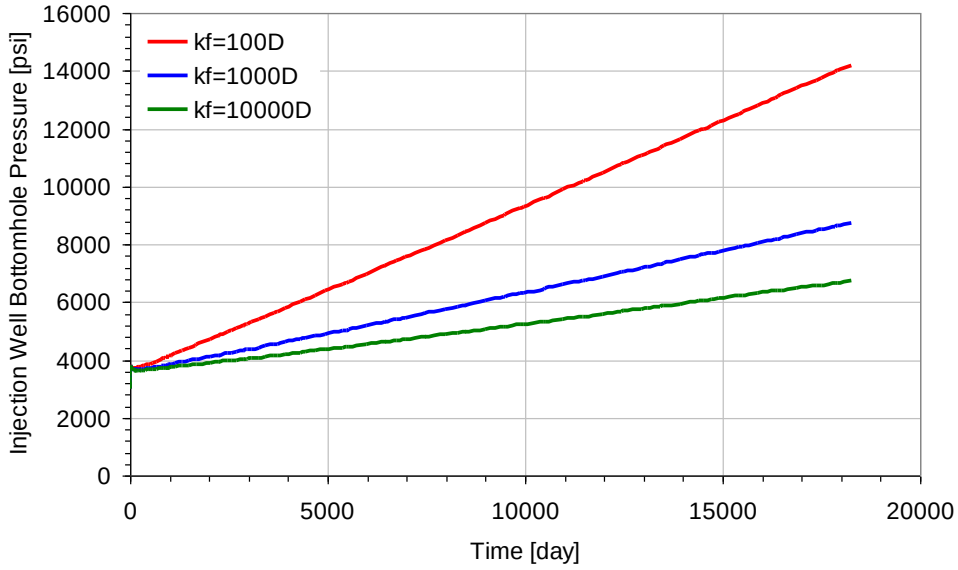

Figure 5.17: Injection well BHP as a function of longitudinal fracture conductivity at a constant injection rate 30,000 bbl/D, fracture height 300 ft

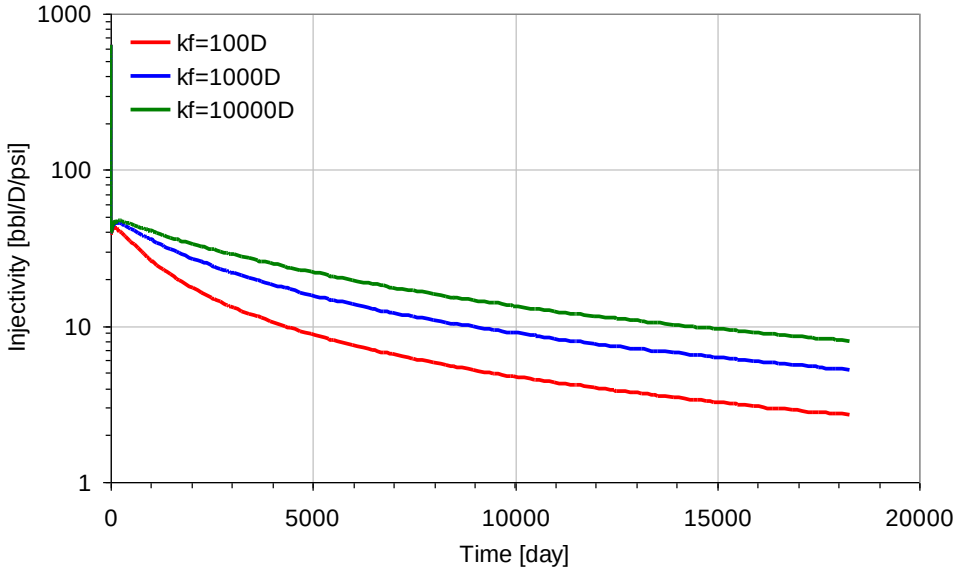

Figure 5.18: Injectivity as a function of longitudinal fracture conductivity at a constant injection rate 30,000 bbl/D, fracture height 300 ft

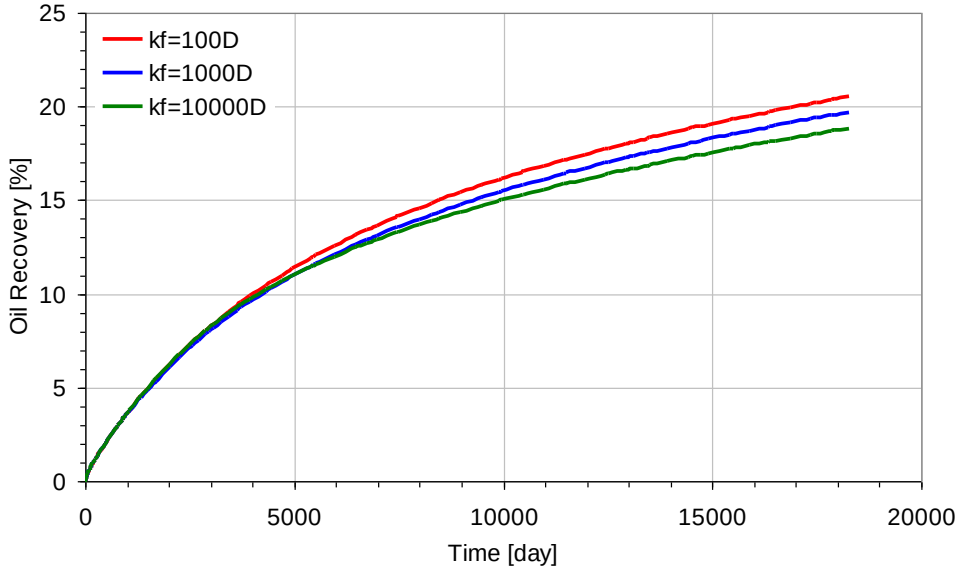

Figure 5.19: Oil recovery as a function of longitudinal fracture conductivity at a constant injection rate 30,000 bbl/D, fracture height 300 ft

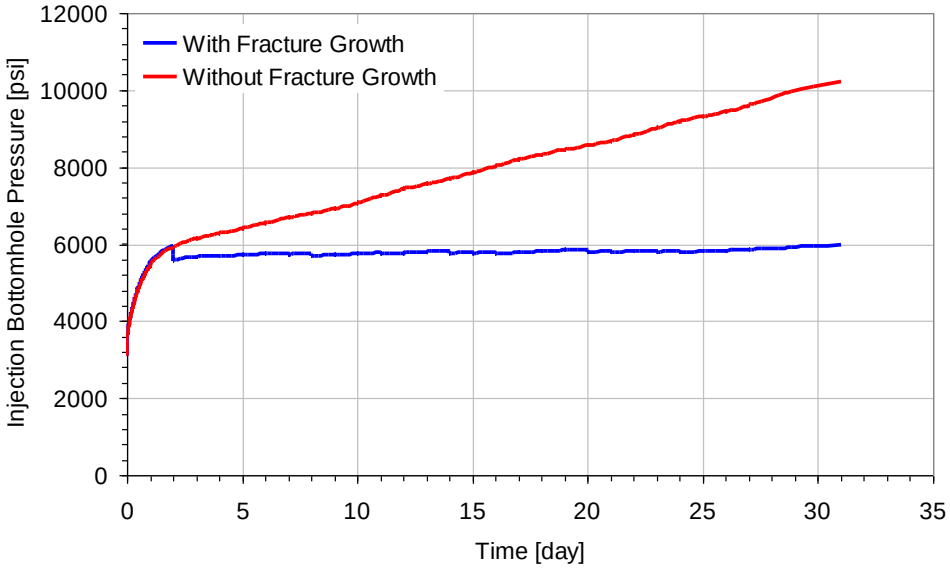

Figure 5.20: Injection BHP for longitudinally fractured and unfractured reservoirs at a constant injection rate 30,000 bbl/D

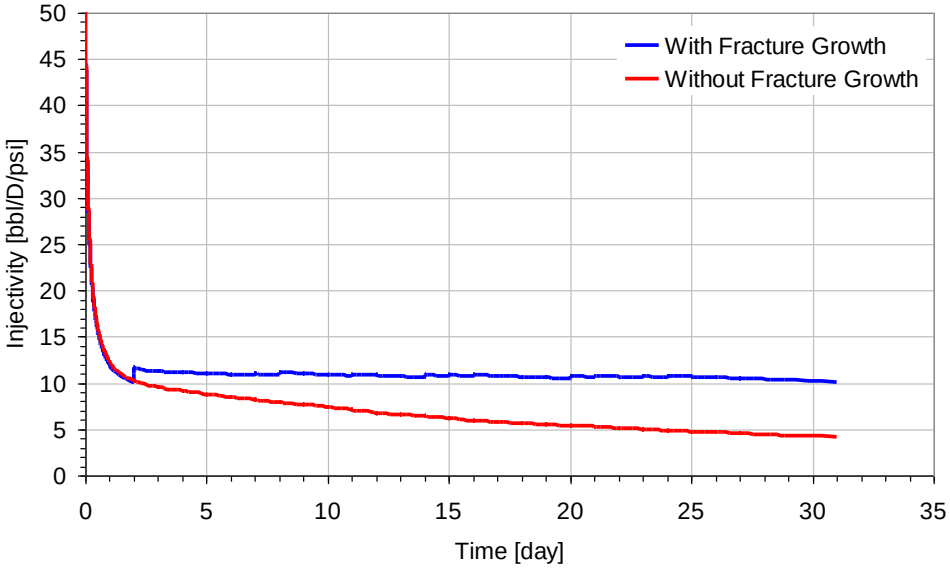

Figure 5.21: Injectivity for longitudinally fractured and unfractured reservoirs at a constant injection rate 30,000 bbl/D

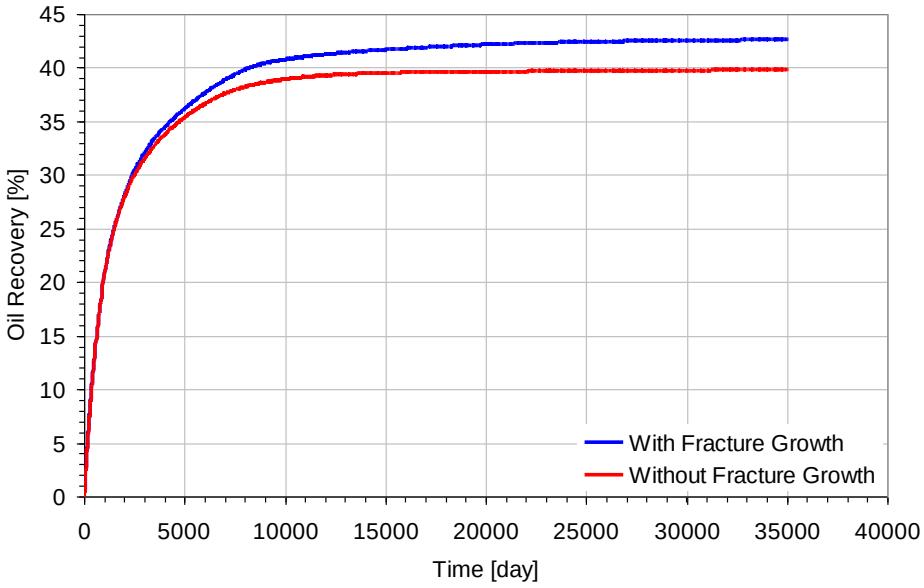

Figure 5.22: Oil recovery for longitudinally fractured and unfractured reservoirs at a constant injection rate 30,000 bbl/D

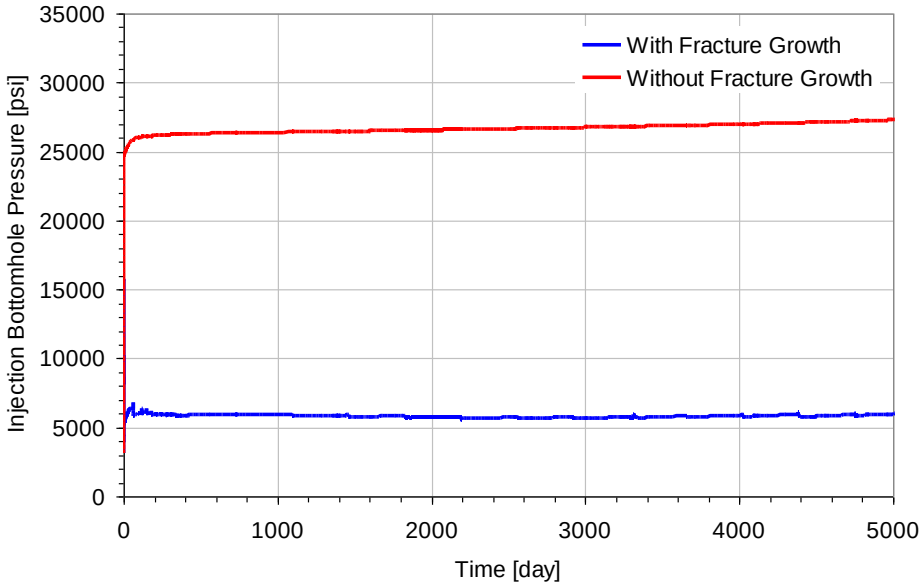

Figure 5.23: Injection BHP for longitudinally fractured and unfractured reservoirs at a constant injection rate 30,000 bbl/D

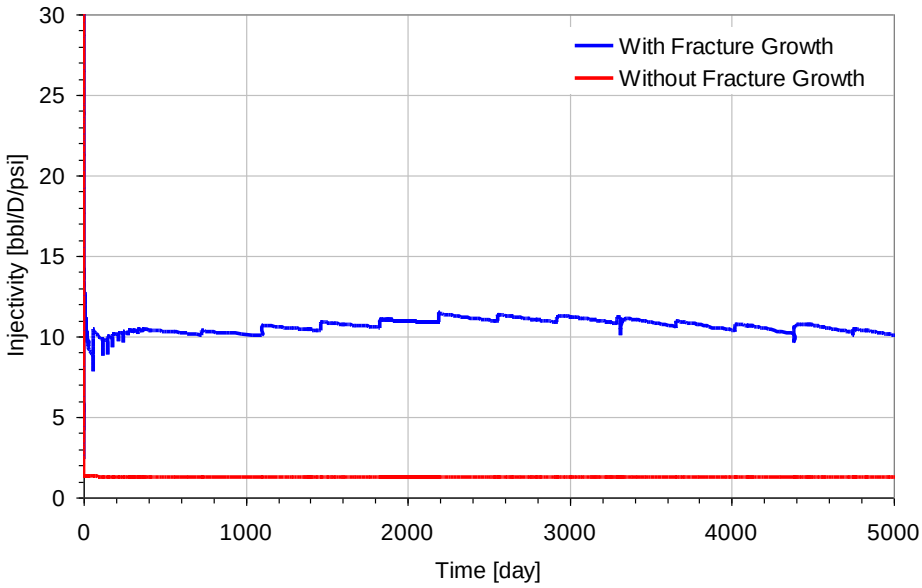

Figure 5.24: Injectivity for longitudinally fractured and unfractured reservoirs at a constant injection rate 30,000 bbl/D

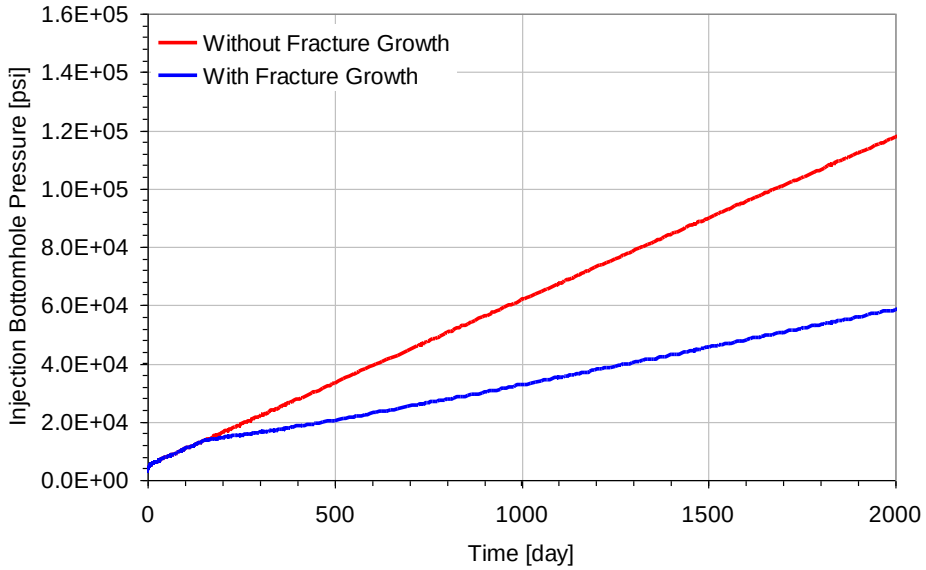

Figure 5.25: Injection BHP for transversely fractured and unfractured reservoirs at a constant injection rate 30,000 bbl/D

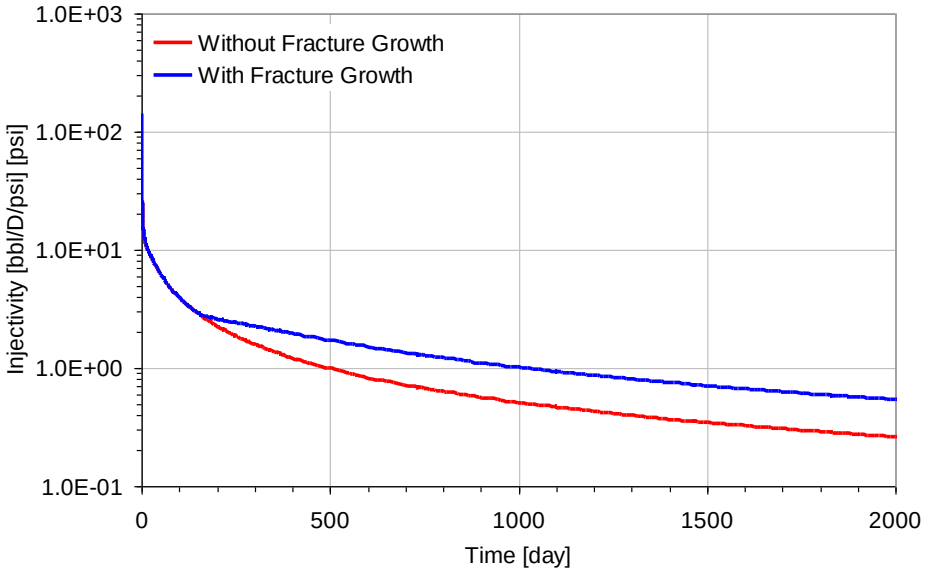

Figure 5.26: Injectivity for transversely fractured and unfractured reservoirs at a constant injection rate 30,000 bbl/D

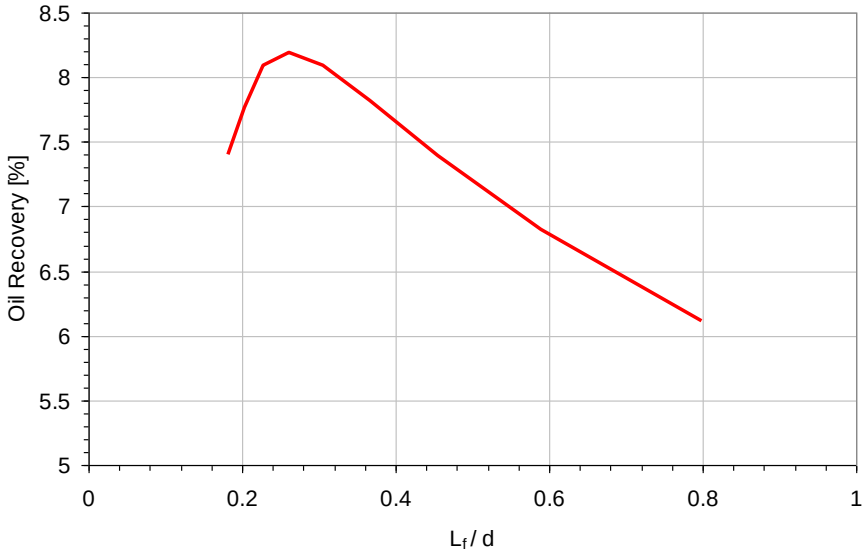

Figure 5.27: Impact of distance between horizontal injector and producer. *d*: distance between injector and producer, L_f: transverse fracture half length 350 ft, fracture height 360 ft, height difference between injector and producer 320 ft

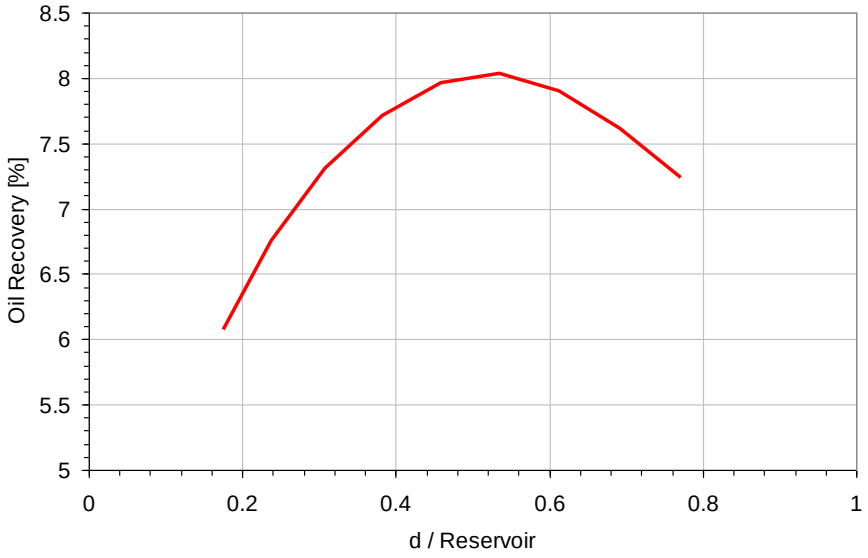

Figure 5.28: Impact of distance between horizontal injector and producer (unfractured and dimensionless case)

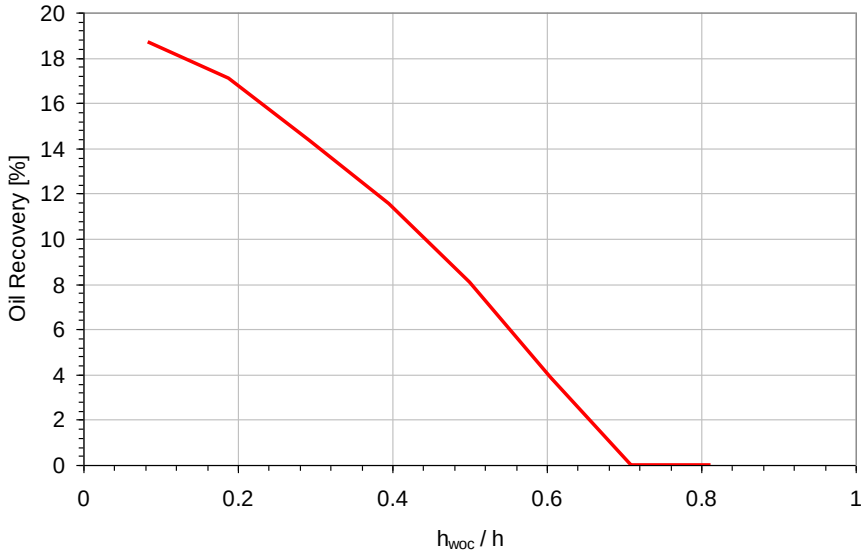

Figure 5.29: Impact of Water-Oil contact on oil recovery at 50 years, fracture half length 350 ft, fracture height 360 ft, distance of height between injector and producer 320 ft

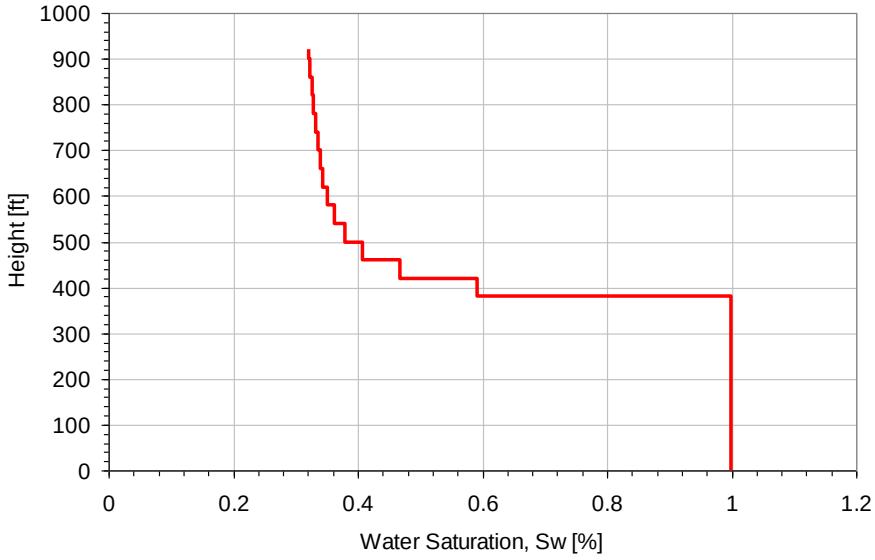

Figure 5.30: Vertical equilibrium of water saturation, WOC 380 ft, and irreducible water saturation 0.3

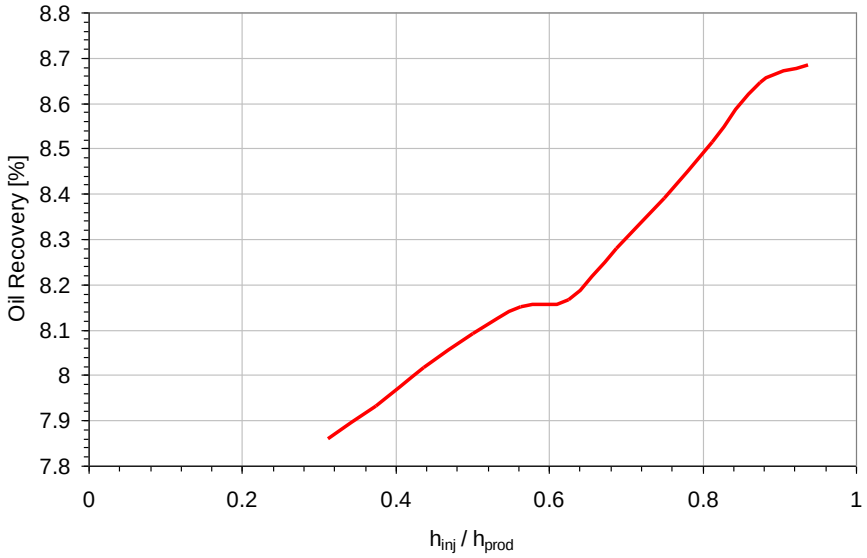

Figure 5.31: Impact of injector well height on oil recovery at 50 years, with transverse fracture, fracture half length 350 ft, fracture height 360 ft, WOC 480 ft

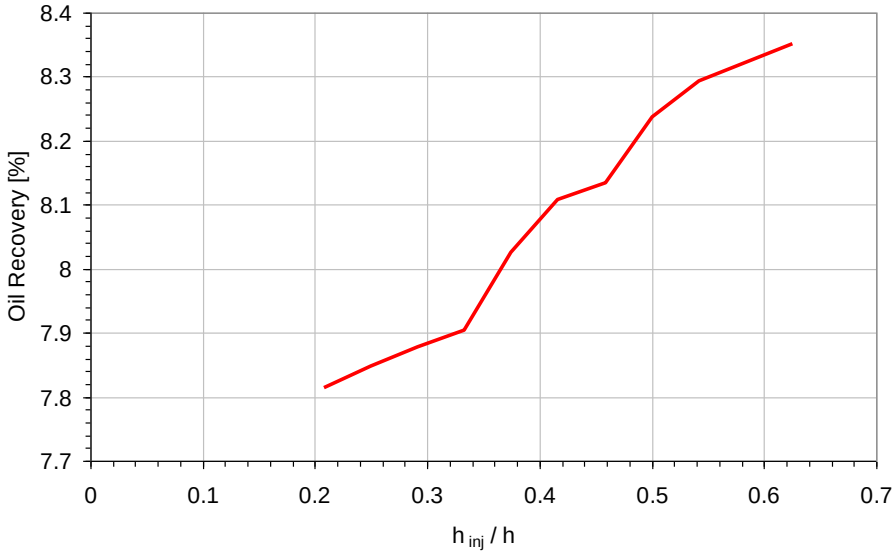

Figure 5.32: Impact of injector height on oil recovery at 50 years, unfractured case, WOC 480 ft

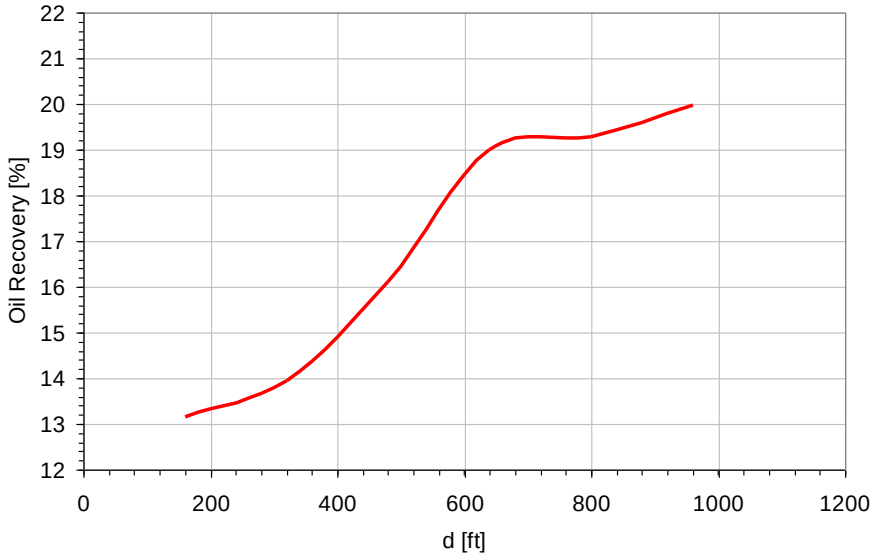

Figure 5.33: Impact of distance between horizontal injector and producer with longitudinal fracture on oil recovery at 50 years, fracture height 100 ft

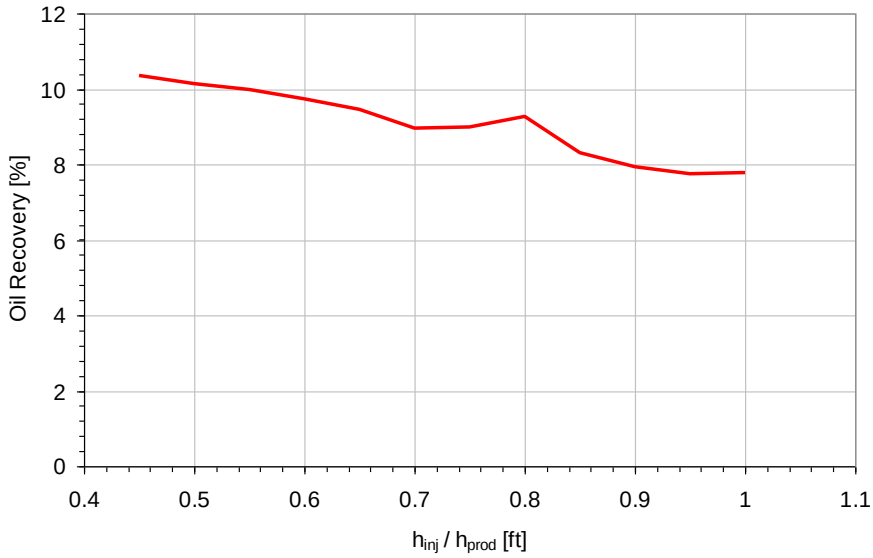

Figure 5.34: Impact of injector height on oil recovery, height of horizontal producer 400 ft, longitudinal fracture height 100 ft

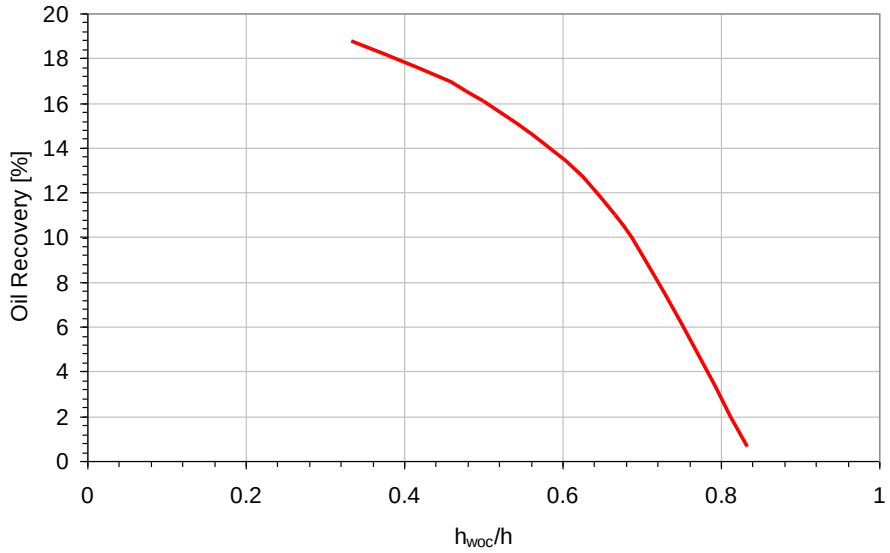

Figure 5.35: Impact of WOC on oil recovery. Longitudinal fracture on horizontal injector

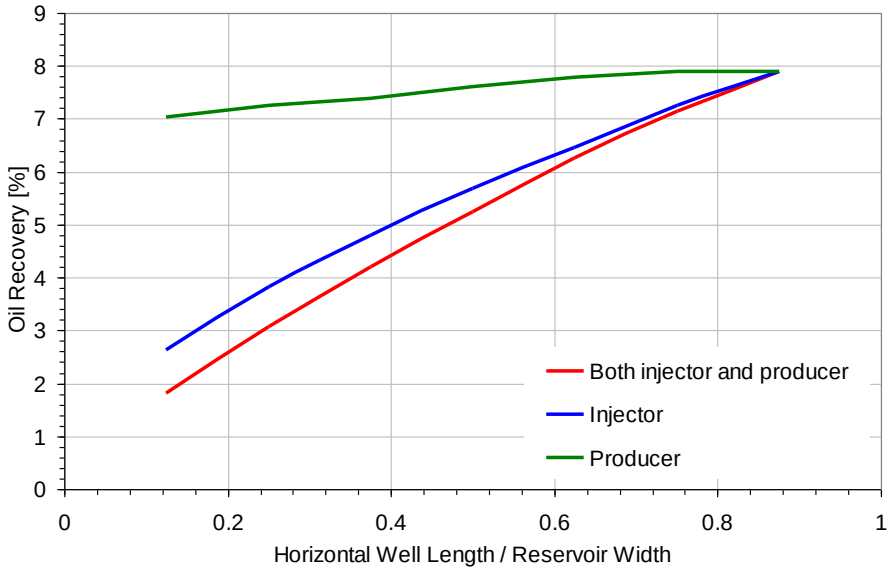

Figure 5.36: Impact of horizontal well length including injector and producer

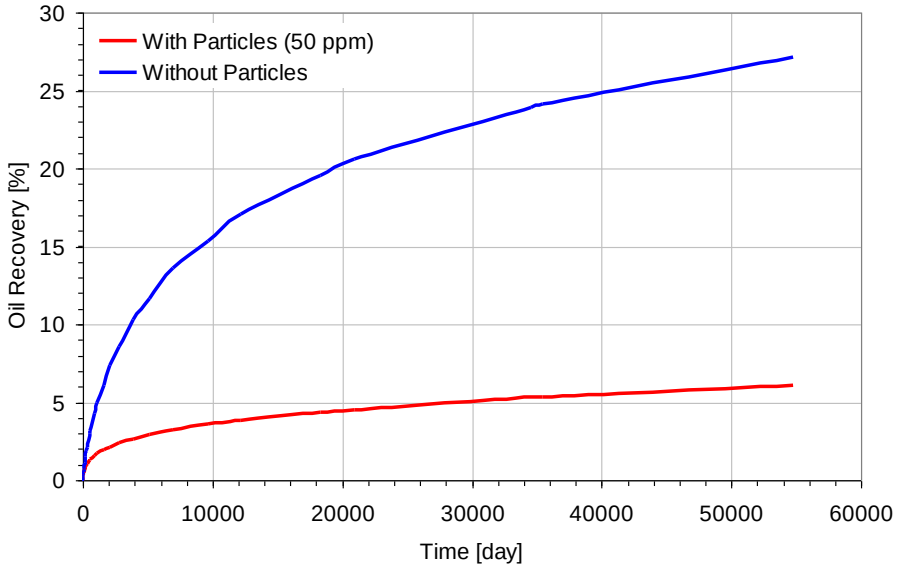

Figure 5.37: Impact of particle plugging on oil recovery with constant injection BHP constraint

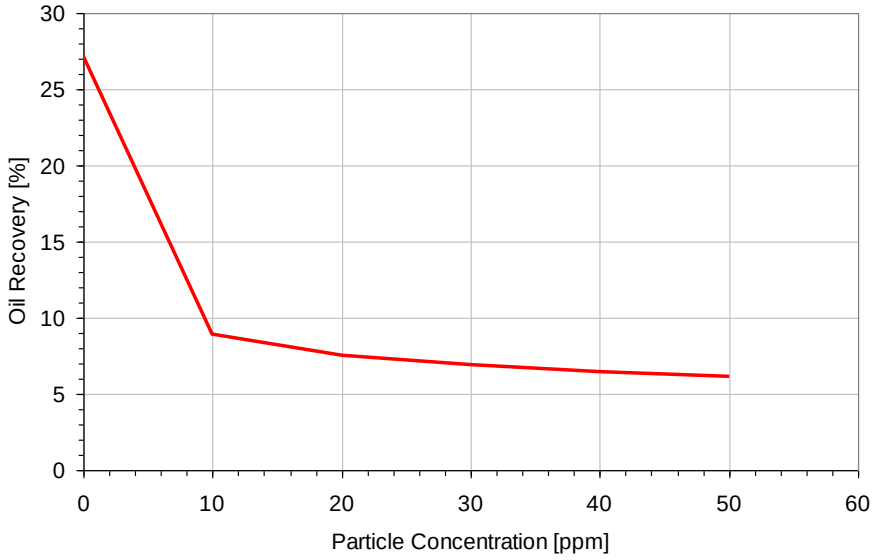

Figure 5.38: Impact of particle plugging on oil recovery with constant injection BHP constraint

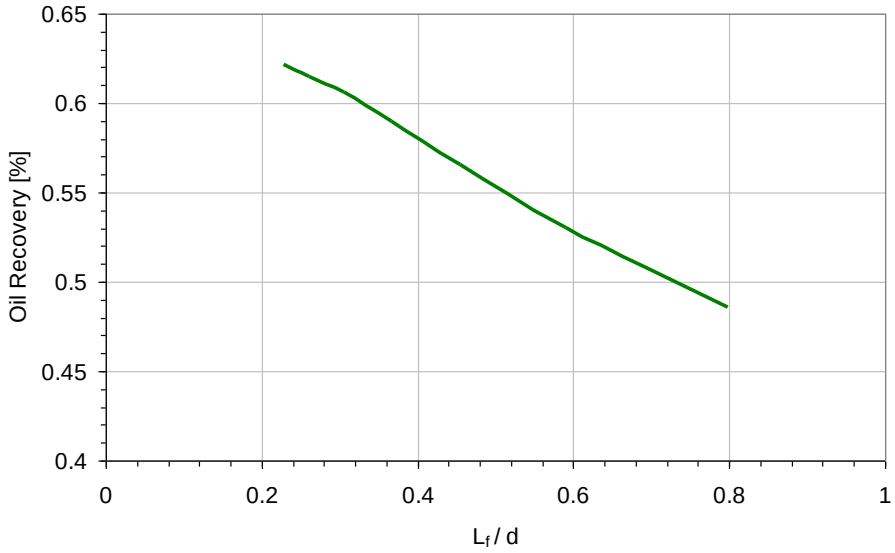

Figure 5.39: Impact of distance between horizontal injector and producer. *d*: distance between injector and producer, L_f: transverse fracture half length

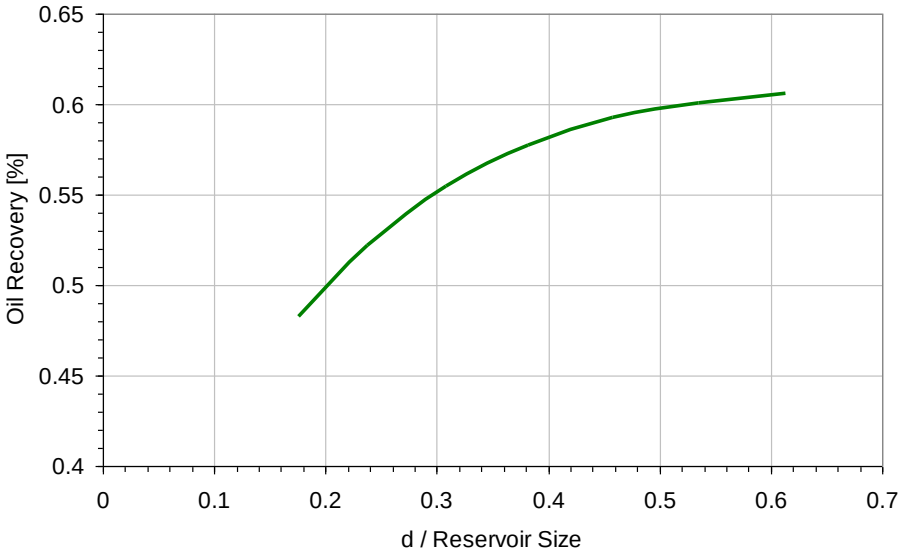

Figure 5.40: Impact of distance between horizontal injector and producer

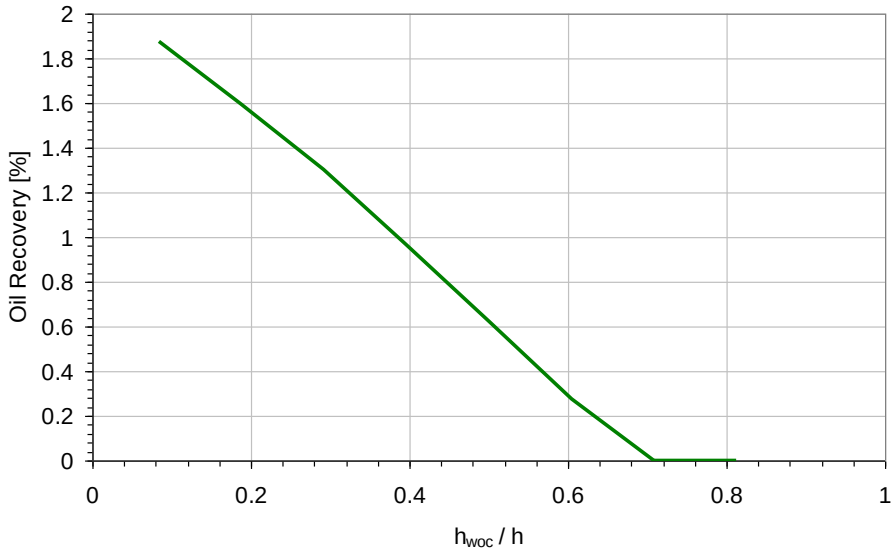

Figure 5.41: The impact of WOC on oil recovery at 50 years, fracture half length 350 ft, distance of height between injector and producer 320 ft, transverse fracture height 360 ft

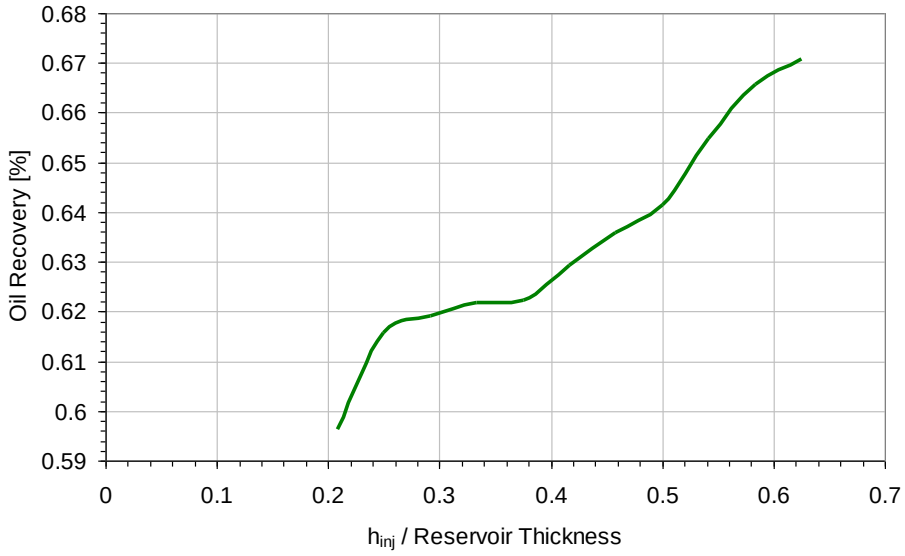

Figure 5.42: Impact of injector height on oil recovery at 50 years, with transverse fracture, half length 350 ft, height 360 ft, water oil contact 480 ft

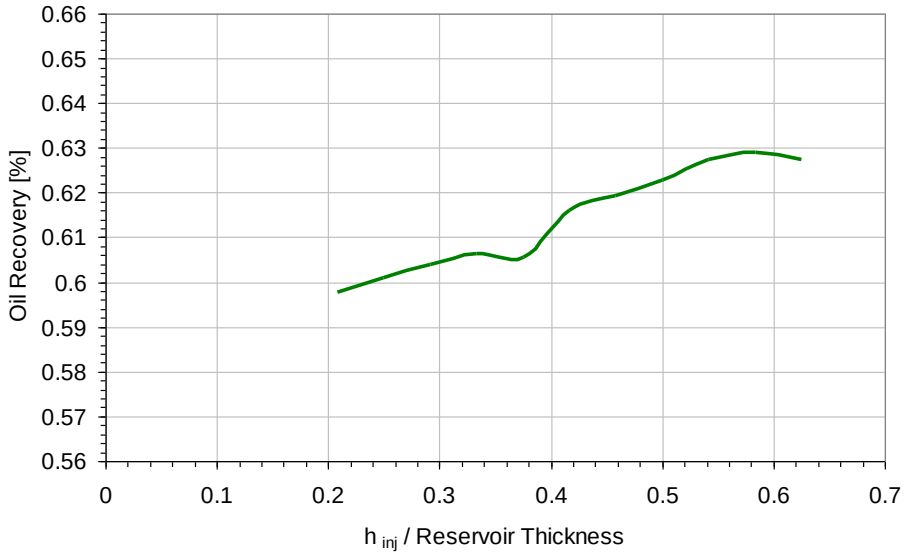

Figure 5.43: Impact of injector height on oil recovery at 50 years, without transverse fracture, water oil contact 480 ft

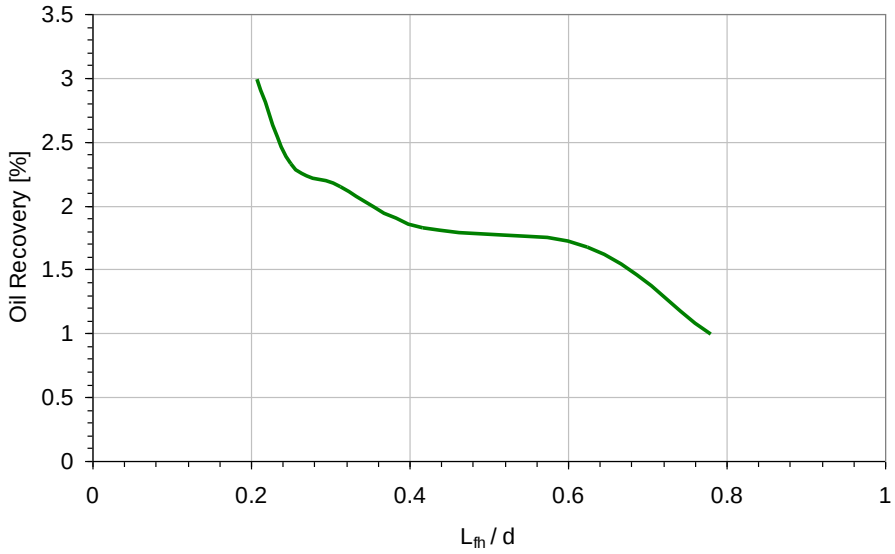

Figure 5.44: Impact of distance between horizontal injector and producer with longitudinal fracture on oil recovery at 50 years, fracture height 100 ft

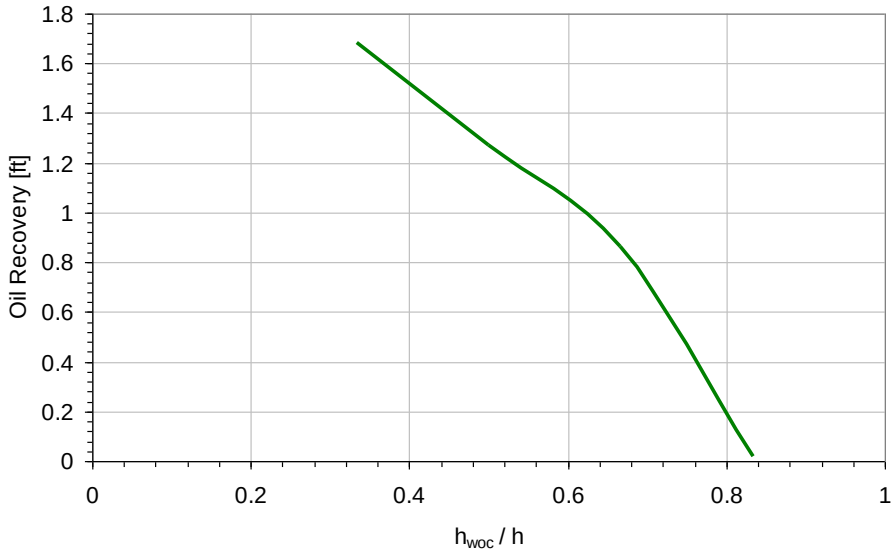

Figure 5.45: The impact of water oil contact on oil recovery. Longitudinal fracture on horizontal injector, fracture height 100 ft

Chapter 6: Comparison with Field Data

6.1 INTRODUCTION

The main objective of this chapter is to compare model predictions to actual field injection data. A successful match of the field data with the fracture growth model developed in this research serves to validate the model and demonstrate its utility.

It is necessary to fully understand the reservoir properties and the process conditions to perform history matching simulations. The reservoir which is modeled for simulation in this chapter is a 15-acre sandstone reservoir which has 6 five-spot patterns, with 12 injectors and 6 producers in this reservoir section. We will call the injectors as Well #1 to Well #12 in order. There are 9 layers in the reservoir model which have different porosities and permeabilities. The upper four layers have similar geological characteristics (porosity and permeability) and the lower five layers have similar geological properties. The average porosities of the upper and lower layers are 0.17 and 0.20, respectively. Also, the average permeability of the upper layers is 137 md compared to 203 md for the lower five layers. For the base case, the injection rate of all injectors is 125 bbl/D and the production rate of all producers is 250 bbl/D, which maintains the injection and production balance. In all figures that compare field and simulated data in this chapter, the dotted curves are the field data and the solid lines represent the simulation predictions. The blue and pink color curves represent pressure and injection rates, respectively.

By conducting history matching with field data, in addition to the validation of the fracture growth model, the optimization of injection conditions for better future oil production could be attempted.

6.2 COMPARISON OF FIELD DATA WITH SIMULATION RESULTS

In this section, the history matching simulation is carried out to match actual reservoir data from pilot scale surfactant polymer flood. Polymer injection has been performed after water injection and fracture generation/growth during polymer injection has been assessed with this simulation. Sharma *et al.* (2011) performed history matching for this field but they assumed the static fracture during polymer injection. In this chapter, water and polymer injection has been modeled with fracture generation/growth to match the field data more accurately. Latest injection and pressure data from the field is compared with simulated results. Based on this history matching, the future injection responses could be predicted and the remedial actions could be implemented if needed. For the history matching, a heterogeneous sandstone reservoir model was first built. Field injectivity behavior was simulated with *CMG-STARS* and the fracture growth model described in **Chapter 4**. The simulation results with the fracture growth model and *CMG-STARS* match the field data well. Also, several injection conditions (injected particle concentration, polymer concentration, and the injection rate that can cause shear-thickening behavior) can be deduced from the best-fit parameters for the history matches of the injection BHP data. That is, the rate of increase in pressure due to particle plugging during water injection, and high polymer viscosity during polymer injection, can provide

information about particle concentration and polymer viscosity. The rock stress distribution can also be predicted near the injection well by observing the fracture pressure.

The fracture growth model is therefore useful not only for predictive process simulations when well fracture occurs due to particle plugging or high polymer viscosity, but also for fracture diagnosis during the field injection operation.

Table 6.1 shows the properties of the reservoir. Because of the unfavorable mobility ratio between injected water and reservoir oil, polymer injection was performed after water injection for improved oil recovery. In the actual field operation, polymer was injected together with surfactant. However, for our preliminary attempt to match the injectivity data, the effect of surfactant was neglected in this simulation. This may be partially justified from the observations that the viscosity of the injection surfactant formulation is usually close to the viscosity of its polymer content.

Figure 6.1 shows the relative permeability curves for water and oil. The irreducible water saturation and residual oil saturation are both 0.28, and the end point relative permeability of water and oil are 0.268 and 0.788, which indicates a water-wet reservoir. **Figure 6.2** shows the relationship between viscosity and shear rate for the injected polymer that was used in this study. The dots show the viscosity observed in the lab, and the red line shows the polymer viscosity in the reservoir simulator, *CMG STARS*.

In the simulation, water and polymer injection rates are prescribed same as the field data, and the injection BHP is simulated. **Figure 6.3** shows the injection BHP and flow rate as a function of time for Well #1. Water injection occurs for the first 105 days. At the 105^{th} day, a shut in to remove skin near wellbore is simulated. After this

stimulation, a short injection well fracture seems to have occurred because the injection BHP that dropped to zero when the well is shut in is now temporarily stabilized. Water injection (with particles) resumes again, and BHP increases again. At the 132nd day, shear rate dependent polymer injection was started. The high polymer viscosity induced a sudden increase in BHP, and the stabilization of the injection BHP at approximately 1,000 psi indicates the fracture initiation and growth. This occurred about the 147th day, when the horizontal stress is maintained around about 0 psi because of tangential failure. In **Figure 6.3**, three important trends are observed: (i) injection BHP increases during water injection due to particle plugging, (ii) injection BHP increases during polymer injection due to shear-thickening behavior, and (iii) BHP remains constant after fracture creation and during fracture growth.

Figure 6.4 describes the injectivity during water and polymer injection for Well #1. Injectivity decreases during water injection because of continuous particle plugging. At the 106th day, the injectivity decreases rapidly because of the gun shot stimulation. After this, injectivity of water increases slightly because skin damage has been removed. At the 128th day, the polymer injection begins and the injectivity decreases sharply due to shear-thickening behavior. However, polymer injectivity does not decrease any further once it drops to 0.1 bbl/D/psi. The match between field injectivity data and simulation match suggests that the fracture generation and growth during polymer injection stabilized the polymer injectivity.

The history matching between field data and simulation results has been performed for wells #2, #3, and #4 also. **Figure 6.5** shows the injection BHP and flow rate as a function of time for Well #2. Field data for injection BHP are matched very

accurately with simulation results. Because injection and production balance is maintained in this reservoir, the increase of injection BHP during water injection indicates particle plugging during water injection. The slope of injection BHP increase depends on the particle concentration in the injected water. High particle concentration increases the slope of injection BHP. Therefore, by performing sensitivity study at various particle concentrations, the slope of injection BHP can be matched, and injected particle concentration can be predicted. During polymer injection from the 132nd day, the rate of increase in injection BHP is related to the extent of shear-thinning and shear-thickening behavior. Also, the stabilized injection BHP during polymer injection at the 142nd day depends on initial rock stress distribution. From the match of the stabilized injection BHP using the fracture growth model, the actual initial rock stress can be estimated. **Figure 6.6** shows the injectivity decline for Well #2. The overall trend of injectivity is very similar to the previous injectivity decline curve for Well #1. Particle plugging and high polymer viscosity decrease injectivity, while fracture creation and growth stabilize injectivity. **Figures 6.6~Figure 6.9** show the history matching results for Well #3 and Well #4. The fracture growth model can match injection well conditions (particle concentration and polymer rheology), and reservoir conditions (rock stress, matrix permeability, porosity, pressure, etc.). History matching suggests that every well has a different fracture pressure, which suggests that the initial rock stresses are different for each injection well and that each well will experience a different fracture growth rate and length.

The stabilized injection BHP and injectivity can be important clue in fracture diagnosis. Initial effective rock stress and fracture generation/growth characteristics can

be predicted from injection BHP and injectivity data by using the fracture growth model. The model can also compute the impact of fracture generation/growth during water/polymer injection, as shown below. **Figure 6.11** shows the impact of injection well fractures on well injectivity during injection of a Newtonian polymer (27 cp viscosity). Without fracture generation, the injectivity with water injection is about 0.2 bbl/D/psi and the injectivity with polymer injection is 0.007 bbl/D/psi. The injectivity with polymer injection (0.007 bbl/D/psi) is roughly 27 times lower than one with water injection (0.2 bbl/D/psi) because the viscosity of the Newtonian polymer is 27 times higher than the viscosity of water. The impact of a fracture on polymer injectivity can be investigated by comparing polymer injectivity with and without fracture. The polymer injectivity with a fracture is about 0.1 bbl/D/psi, which means that the injection well fracture improves injectivity up to 15 times. In the Newtonian fluid case, the difference is very significant. However, in the case of a unified viscosity model polymer (**Figure 6.12**), the difference is rather small. Without a fracture, shear rate is high, so viscosity remains low; with a fracture, shear rate is lower, so viscosity is higher, which somewhat counters the beneficial effect of the fracture. Because of this type of polymer rheology, there is not a big difference in injectivity between a fractured well (0.1 bbl/D/psi) and an un-fractured well (0.075 bbl/D/psi).

Dynamic fracture growth affects shear rate in the matrix near the injector. As the fracture grows, the velocity and shear rate in the matrix decrease, which affects the viscosity of the shear rate dependent polymer. **Figure 6.13** shows the transition in shear rate, and the resulting transition in polymer viscosity. Fracture growth makes the velocity in the matrix near the injector decrease, which causes the polymer viscosity to increase to

about 15 to 18 cp. As a consequence, fracture growth does not boost injectivity as much as expected. Dynamic fracture growth boosts injectivity by increasing absolute permeability (fracture permeability), but the resulting increase in polymer viscosity in the matrix suppresses injectivity; the effects counter each other, and there is not a significant difference in injectivity with and without a fracture.

Because of shear rate dependent polymer behavior, injectivity is also related to injection rate (**Figure 6.14**). The injectivity of this polymer injection model has a maximum (0.2 bbl/D/psi) at 100 bbl/D. At injection rates greater than 100bbl/D, injectivity decreases as injection rate increases because of shear-thickening behavior. At injection rates lower than 100 bbl/D, injectivity decreases as injection rate decreases because of shear-thinning behavior.

Figure 6.15 compares injectivity with and without fracture. Injectivity without dynamic fracture growth shows the effect of shear-thinning and shear-thickening behavior. However, in the case of dynamic fracture, injectivity increases monotonically with increasing injection rate, because fracture creation pressure is independent of injection rate; fracture creation pressure is related only to the initial rock horizontal stress. If bottom-hole pressure, P_{btp}, and reservoir pressure, P_{res}, are constant, injectivity is directly proportional to injection rate:

$$injectivity = \frac{q}{P_{btp} - P_{res}} \tag{6.1}$$

Fluid viscosity affects the rate of fracture growth, as well as injectivity and injection BHP. Injection of a fluid with a higher viscosity induces earlier fracture growth. **Figure 6.16** shows fracture growth during water and polymer injection. Fracture growth

occurs much sooner during the injection of a high viscosity polymer. Injectivity also decreases more rapidly during polymer injection than during water injection (**Figure 6.17**), although injectivity does eventually stabilize at the same value for both fluids once the fracture is fully developed.

Figure 6.18 shows the injection BHP during water and polymer injection. Fracture growth near the injector prohibits injection BHP from increasing. If there is no fracture generation near the injector, the injection BHP increases continuously. Dynamic fracture growth stabilizes the injection BHP and well injectivity.

6.3 SHEAR RATE DEPENDENT POLYMER INJECTION IN BROOKSHIRE DOME FIELD

One more history match has been performed for Brookshire Dome Field, 35 mile west of Houston, Texas. Well spacing in this field is 2 to 5 acre and 2.0 MMBO has been produced. Reservoir temperature is 130 ºF and oil viscosity is 28 cp. Shear rate dependent polymer injection has been performed and simulation was carried out to match the injection pressure by using injection rate, polymer rheology, and given reservoir properties. The objective in this chapter is to investigate the impacts of polymer rheology, polymer concentration, shear rate coefficient (C), perforation densities, and grid block size on well injectivity as well as to match the simulated injection pressure to field data.

6.3.1 Introduction to the Field Data

In addition to the history matching described in sub-section 6.2, a history match with the Brookshire Dome Field has been performed. Injection well conditions are listed in **Table 6.2**. The reservoir permeability varies for each of five layers as shown in **Figure 6.3**. Reservoir size for simulation is 1,500×1,500×72 ft and the end point permeabilities of water and oil are 0.2 and 0.8. The viscosity of polymer used in this injection is related to shear rate as shown in **Figure 6.19**. **Figure 6.20** shows the tubing head pressure and injection rate during polymer injection. Pressure fluctuates in time with injection rate.

6.3.2 Development of the Simulation Model

The simulation model to match Brookshire Dome Field data has been developed by using *STARS* in *CMG*. The shear rate dependent polymer model has been used in this simulation and assumption that there is no fracture in this field is given. The polymer rheology data and injection rate for polymer injection as shown in **Figure 6.19** and **Figure 6.20** were used to match the injection BHP.

6.3.3 Screening Simulations before History Match

To investigate the impact of simulation parameters on well injection BHP, several sensitivity studies are preformed. **Figure 6.21** shows the sensitivity of well head pressure to perforation density. The variable *ff* refers to the number of perforations per grid block. When perforation density is very low (0.25 shots/ft), well head pressure increases rapidly. In contrast, at a high perforation density (6 shots/ft) well head pressure increases more slowly. The shear rate coefficient also has an effect on well head pressure, as shown in **Figure 6.22**:

$$\dot{\gamma}_{fac} = C\left[\frac{3n+1}{4n}\right]^{\frac{n}{n-1}} \tag{3.3}$$

The shear rate coefficient, *C*, relates flow velocity and shear rate. The shear rate coefficient can be determined if the remaining values in Equation 3.3 are known. All other things being equal, shear rate is directly proportional to fluid velocity via the shear rate coefficient. Usually, shear rate coefficient varies from 1 to 100, but it is hard to evaluate and predict it for each polymer injection simulation. For the sake of simplicity, a coefficient of 6 is often used in polymer injection simulations, but this value is not necessarily accurate for every simulation. **Figure 6.22** and **Figure 6.23** show the sensitivity of well head pressure and polymer viscosity during injection to shear rate coefficient. For a shear-thinning fluid, a high shear rate coefficient corresponds to a higher shear rate, and thus a lower polymer viscosity (**Figure 6.23**), which decreases well head pressure (**Figure 6.22**). Reservoir thickness also affects well head pressure as shown in **Figure 6.25**. When the reservoir thickness is small, the rate of increase of injection pressure is higher than with a thicker reservoir.

Figure 6.26 shows that well head pressure increases more slowly when shear rate coefficient is high, perforation density is high, and reservoir thickness is large. A higher shear rate coefficient corresponds to a higher shear rate, which induces shear-thinning behavior (lower polymer viscosity). At a lower polymer viscosity, injection pressure decreases. Even without changing shear rate coefficient, injection BHP increases more slowly for a higher perforation density and a thicker reservoir.

Grid block size can also significantly affect polymer viscosity. Because polymer viscosity plays very important role in well injectivity during polymer injection, this study makes a careful investigation of the effect of grid block size on polymer viscosity. **Figure 6.27** shows the different grid block refinement schemes. "Unrefined" means that there is no grid block refinement near the injector, and the gird block size is 5 ft. In the scheme labeled "Refined", the 5-foot grid block containing the injector is split into nine 1.6-foot blocks. In the scheme labeled, "More Refined", the nine 5-foot grid blocks surrounding and including the injector are all split into nine 1.6-foot grid blocks. Grid block size and refinement play a significant role in well injectivity. Smaller grid blocks induce a higher fluid velocity and shear rate near the injector, which reduces polymer viscosity and increases injectivity. **Figure 6.28** shows the sensitivity of injection BHP to shear rate coefficient and grid block refinement. When the shear rate coefficient is 6 and the grid block is unrefined, injection BHP increases to 2,950 psi after 1 month of polymer injection. On the other hand, when the shear rate coefficient is higher, and the 200 square ft area near the injection well is refined, the injection BHP increases to only 2,320 psi. Injectivity is also affected by shear rate coefficient and grid block refinement. Because the viscosity of the polymer decreases with a more refined grid or with a higher shear rate coefficient, polymer injectivity also increases for a more refined grid or for a higher shear rate coefficient (**Figure 6.28**). For example, at a shear rate coefficient of 50 and with a more refined grid, injectivity is 50% higher than with a shear rate coefficient of 6 and an unrefined grid.

Figure 6.30 shows the impact of grid block size on well injection rate during shear rate dependent polymer injection. Because the injection wells are pressure

constrained, the injection rate depends on the time and injectivity. The larger grid block size induces lower injectivity than the smaller grid block size, because a smaller grid block size induces lower polymer viscosity and higher polymer injectivity. For example, after 15 days, polymer injection with larger grid block, 5 ft, shows 80 bbl/D of injection rate. However, with smaller grid block size, 0.7 ft, the injection rate is about 150 bbl/D; decreasing the grid block size by 86% results in an 87% increase in injection rate. This relationship can be used to estimate the injectivity at a given grid block size. As mentioned earlier, a smaller grid block size corresponds to higher well injectivity (**Figure 6.31**). For example, at 15 days, polymer injectivity with a 0.7-foot grid block is 50% higher than with 5-foot grid block. To more accurately simulate polymer injection, it is important to carefully consider the choice of grid block size. A smaller grid block size will result in more accurate simulation results, but will take longer than a simulation with a large grid block size. To show the impact of grid block size and shear rate coefficient on well injectivity, several simulations with different grid block sizes and shear rate coefficients have been performed. **Figure 6.32** shows that injectivity increases as grid block size decreases and shear rate coefficient increases. The injectivity with a smaller grid block (0.7 ft) and higher shear rate coefficient (C = 50) is two times higher than with a coarse grid block (5 ft) and low shear rate coefficient (C = 6).

6.3.4 History Matching Simulations

To match injection BHP, various approaches has been performed during polymer injection. The assumption that there is one fracture or two fractures near injector. The wellhead pressure with/without fracture has been simulated in **Figure 6.25** but the

difference between field and simulation injection pressure is still rather large. The trend of the injection pressure is assessed with this history matching; field injection pressure is still lower than simulation data, which should be investigated with more investigation in the future.

So far, polymer injection history matching with Brookshire Dome Field has been investigated. The simulation results from **Figure 19** to **Figure 32** are obtained at early and initial polymer injection. From now on, polymer injection history matching has been performed after 5 months polymer injection. Therefore, the injection rate and injection BHP are stabilized in this period. **Figure 6.33** shows the field data of polymer injection rate and wellhead pressure. Injection rate ranges from 500 to 1,400 bbl/D and wellhead pressure does not increase too much and ranges up to 600 psi. To model polymer injection accurately, polymer concentration should be informed in detail. **Figure 6.34** shows the polymer concentration as a function of time. Polymer concentration ranges from 1,000 ppm to 3,500 ppm. The high polymer concentration induces high viscosity. As well as polymer concentration, polymer shear rate is a critical parameter to determine polymer viscosity. **Figure 6.35** shows the shear rate dependent polymer viscosity. As explained, higher polymer concentration increases polymer viscosity at 1 s^{-1} shear rate, polymer viscosity is about 100 cp with 4,000 ppm polymer concentration. On the other hand, with 2,000 ppm polymer concentration, polymer viscosity at 1 s^{-1} is about 45 cp. Therefore, the information of polymer viscosity as functions of polymer concentration and shear rate is extremely important. One more thing we have to observe is shear-thinning behavior of polymer. As shear rate increases polymer viscosity decreases. As explained in **Figure 6.35**, shear rate is critical parameter to determine polymer viscosity

and injection pressure. In polymer injection simulation, shear rate is a function of injection rate, reservoir permeability/porosity, etc.

One more important parameter to determine shear rated in polymer injection simulation is grid block size. Near injector, the injection rate and shear rate changes sharply, careful modeling of grid block size is very important. When grid block size is too large, fluid velocity and shear rate can be obtained by average values. Therefore, the detailed and realistic shear rate values can not be obtained with large grid block size. In **Figure 6.36**, 0.7 ft grid with refinement means that the grid block which includes injector is 0.7 ft and the near wellbore region's grid block size is 0.2 ft. Fine grid block can induce more realistic polymer velocity and shear rate, which brings accurate estimation of polymer viscosity. In **Figure 6.36**, the difference of the wellhead pressure due to different grid block size is up to 600 psi.

To support the importance of grid block sizes, **Figure 6.37** provides the polymer viscosity as a function of grid block size. When grid block size is 5 ft, polymer viscosity can be higher than 7 cp because of lower shear rate and less shear-thinning behavior. On the contrary, 0.7 ft grid block sizes induce much lower polymer viscosity due to higher shear rate and more shear-thinning behavior. **Figure 6.37** indicates the polymer viscosity in near injector. As explained sub-section 6.3, shear rate coefficient is very critical to determine polymer viscosity as shown in **Figure 6.38**. The higher shear rate coefficient induces more shear-thinning behavior and lower polymer viscosity. Therefore, the injection pressure with higher shear rate coefficient values should be much lower than with lower shear rate coefficient. The injection pressure difference between 6 and 50 shear rate coefficient values is more than 1,000 psi. Polymer concentration is the other

parameters to determine wellhead pressure as shown in **Figure 6.39**. The lower polymer concentration induces much lower injection pressure due to much lower polymer viscosity. Therefore, accurate calculation of polymer viscosity as a function of polymer concentration, shear rate, and grid block size is very critical. In this dissertation, polymer model has capability to calculate and consider these parameters accurately, which can be used for accurate polymer injection simulation.

In this sensitivity study, the effect of polymer concentration, polymer rheology, shear rate coefficient, and grid block size has been performed. However, the field injection pressure is much lower than simulation results. There might be several reasons. The first one could be reservoir heterogeneity. We assume five different permeability layers reservoir, but actual reservoir might have much more heterogeneous reservoir properties including minor natural fractures. The other factor is the shear rate coefficient as explained in sub-section 6.3. We assume shear rate coefficient is 6 but it might be various from 1 to several hundreds. The sensitivity study has been performed in **Figure 6.39**.

6.4 SUMMARY

Data simulated by using the fracture growth model developed in this research can match field data during water and polymer injection. Injection conditions such as the water quality and polymer rheology can be evaluated by using this model. Also, reservoir conditions such as rock stress distribution, reservoir permeability and porosity can be

predicted also. Furthermore, a history match can provide optimum injection conditions for waterflooding and polymer EOR processes.

This fracture growth model can also investigate the impact of dynamic fracturing on well injectivity and reservoir performance. Because the fracture growth model can simulate complicated polymer rheology and reservoir heterogeneities (layering, fractures, etc), it can predict reservoir sweep and oil recovery more accurately during water and polymer injection.

By performing sensitivity study in polymer injection, the impact of shear rate coefficient, polymer concentration, perforation density, and grid block sizing can be investigated. High shear rate coefficient induces more shear-thinning behavior of polymer, which decreases polymer viscosity and injection BHP. If perforation density is high in injection well, the injection BHP increase decreases also. Lastly, grid block size is also very important to assess injection BHP because grid block size determines shear rate of polymer, which affects polymer viscosity and injection BHP. To model the fracture growth, shear rate dependence of polymer viscosity, particle plugging during water injection, accurate consideration of these parameters are very important.

Table 6.1: Reservoir properties for history matching

Initial Reservoir Pressure	75 psi
Arithmetic Average Porosity	0.19
Arithmetic Average Permeability	174 md
Initial Water Saturation	0.35
Reservoir Salinity	0.33 meq/ml
Water Viscosity	0.933 cp
Oil Viscosity	10.9 cp

Table 6.2: Injection Well Properties for Brookshire Dome Field

Tubing Diameter	2.875 inch
Perforation Location	2118~2190 ft
Perforation Density	6 shots / ft
Perforation Diameter	0.5 inch

Table 6.3: Reservoir Permeability in Brookshire Dome Field

Layer	Thickness (ft)	Permeability (md)
1	8	250
2	4	500
3	12	167
4	24	100
5	24	20

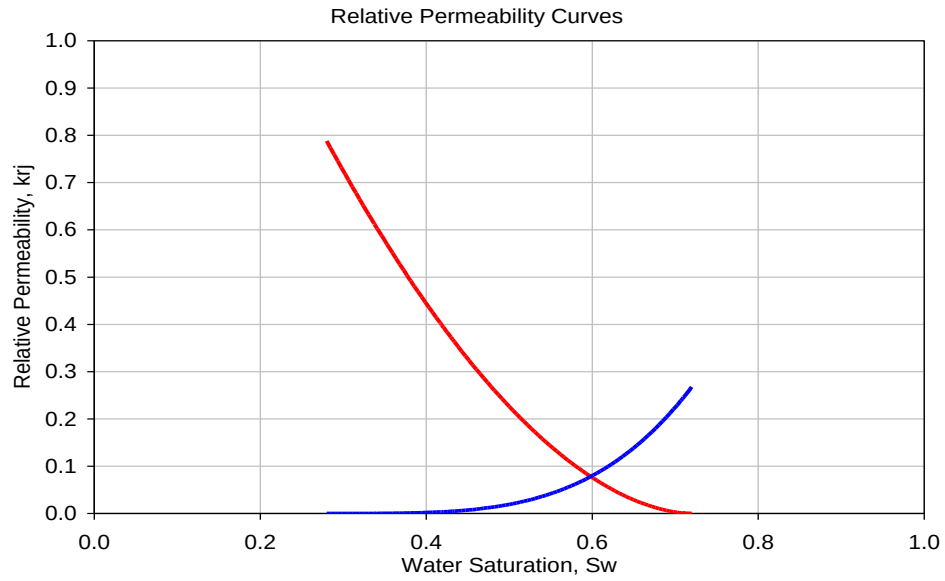

Figure 6.1: Relative permeability curves for water and oil

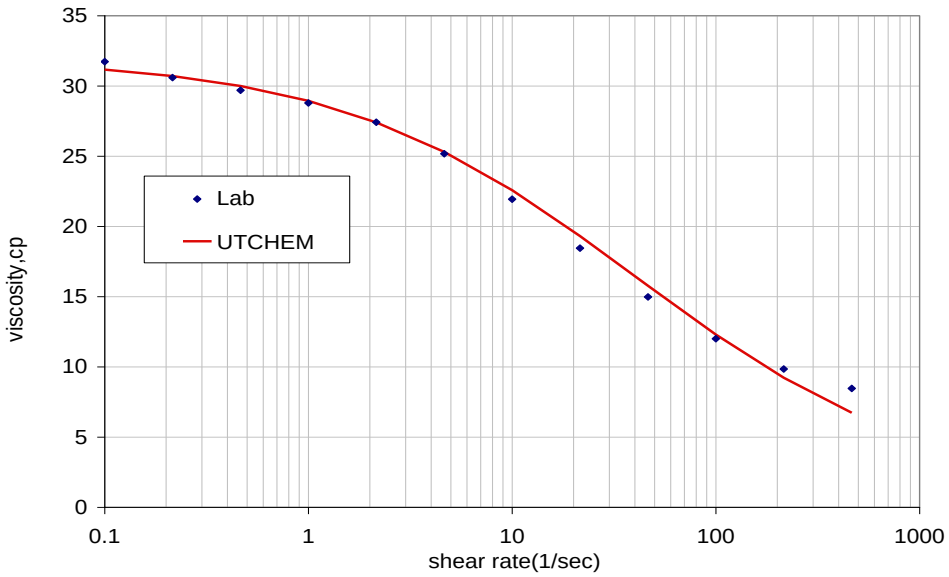

Figure 6.2: Shear rate dependent polymer viscosity, unified model: Flopaam 3330S polymer viscosity vs. shear rate (1500 ppm; 1.6 % NaCl; 25 ºC)

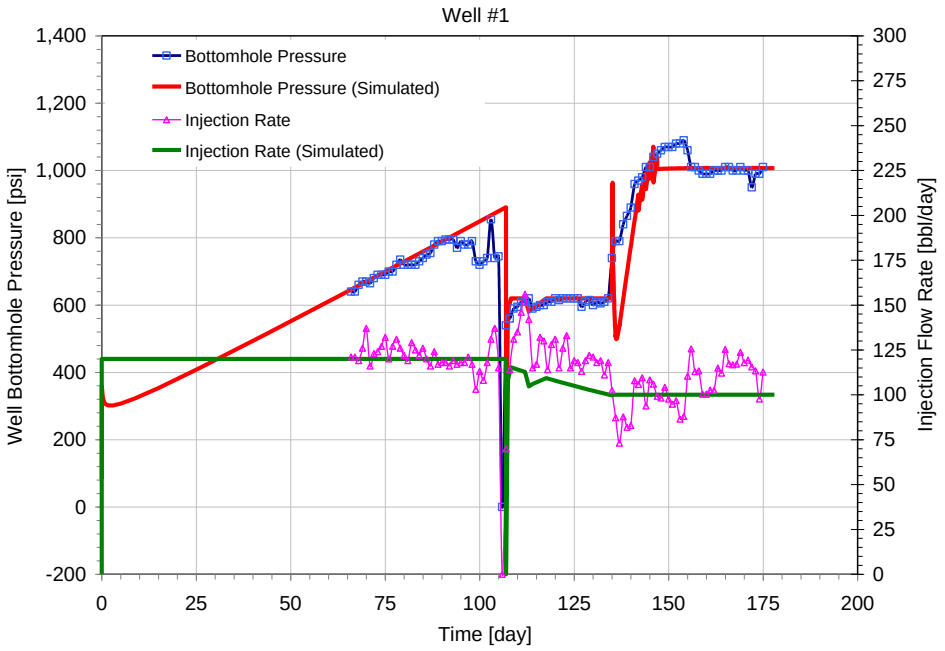

Figure 6.3: Field data comparison with simulated results of Well #1

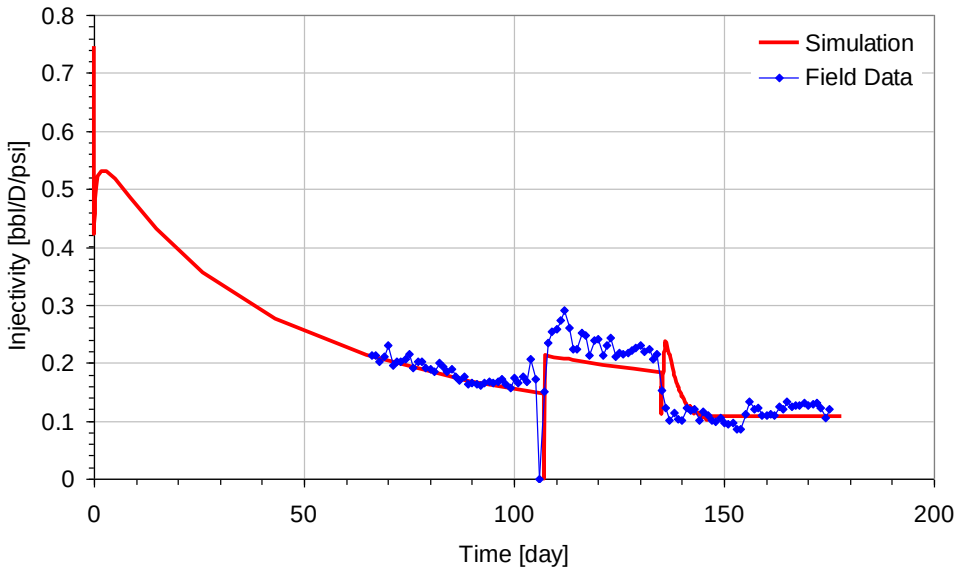

Figure 6.4: Field data (Injectivity) comparison with simulated results of Well #1

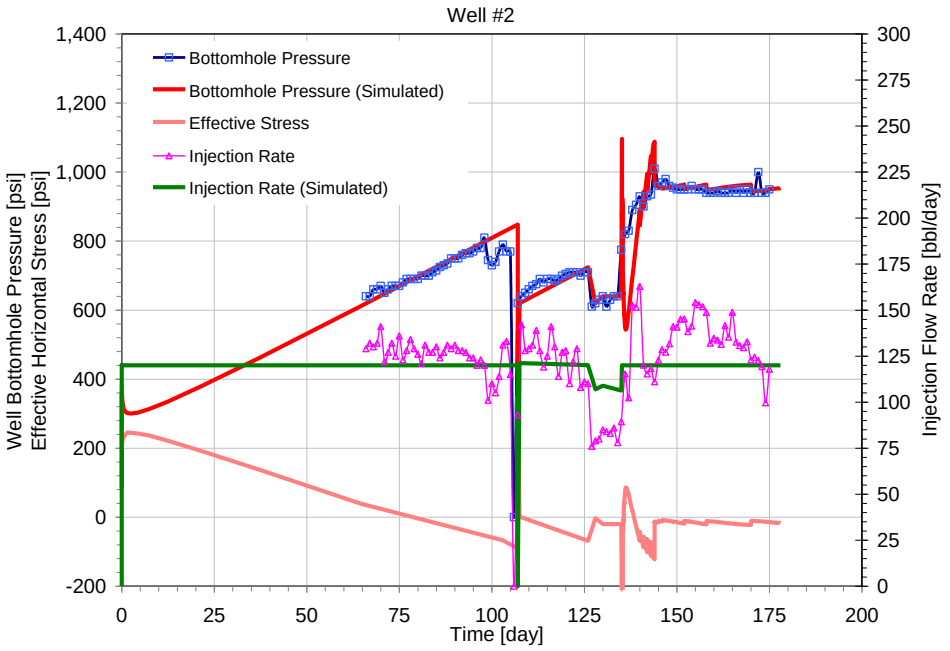

Figure 6.5: Field data comparison with simulated results of Well #2

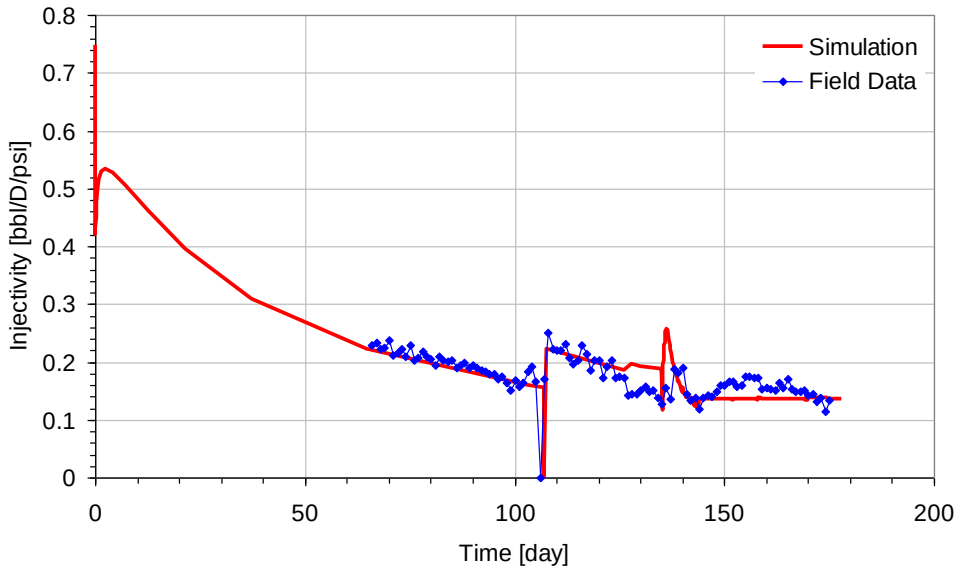

Figure 6.6: Field data (Injectivity) comparison with simulated results of Well #2

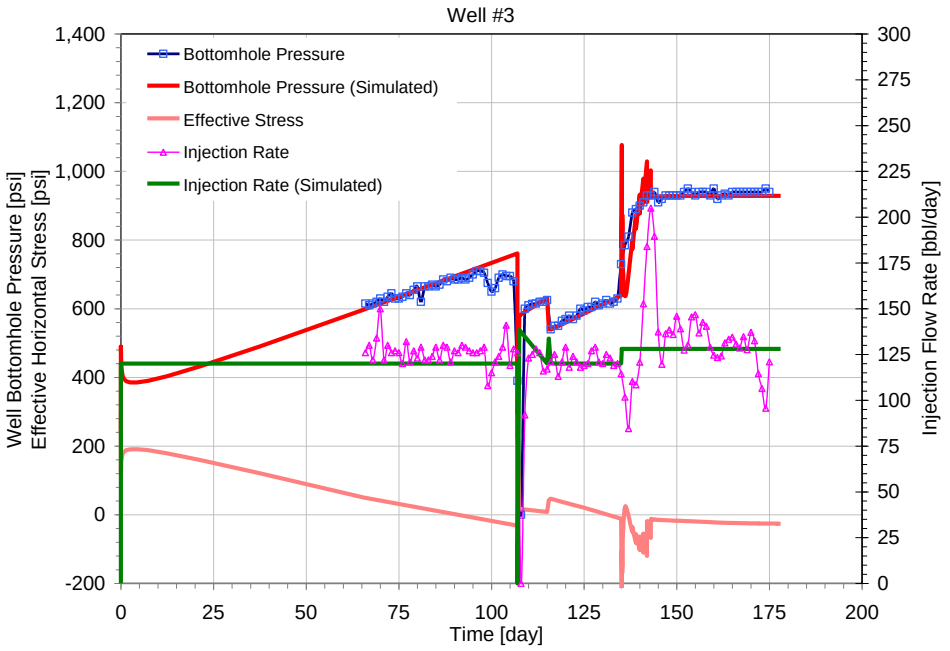

Figure 6.7: Field data comparison with simulated results of Well #3

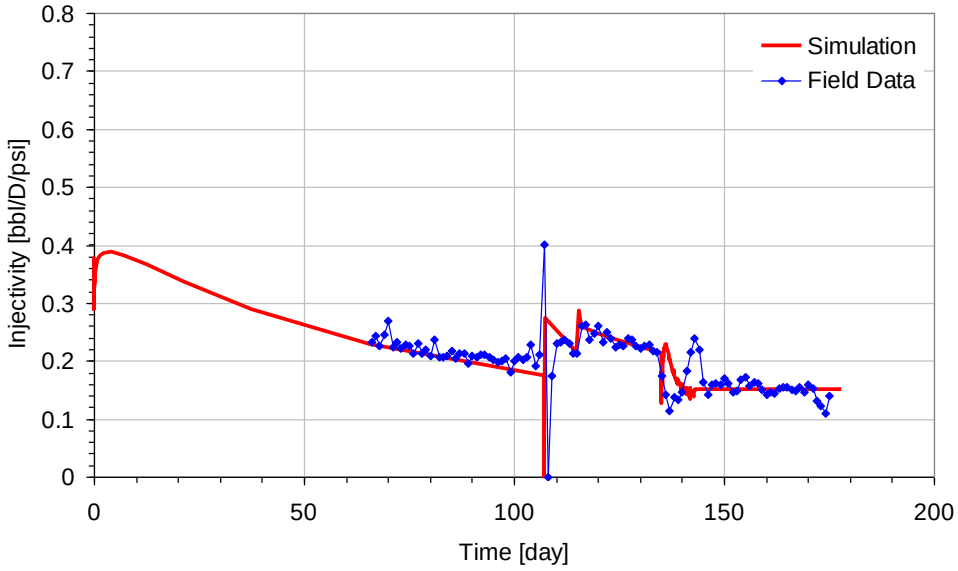

Figure 6.8: Field data (Injectivity) comparison with simulated results of Well #3

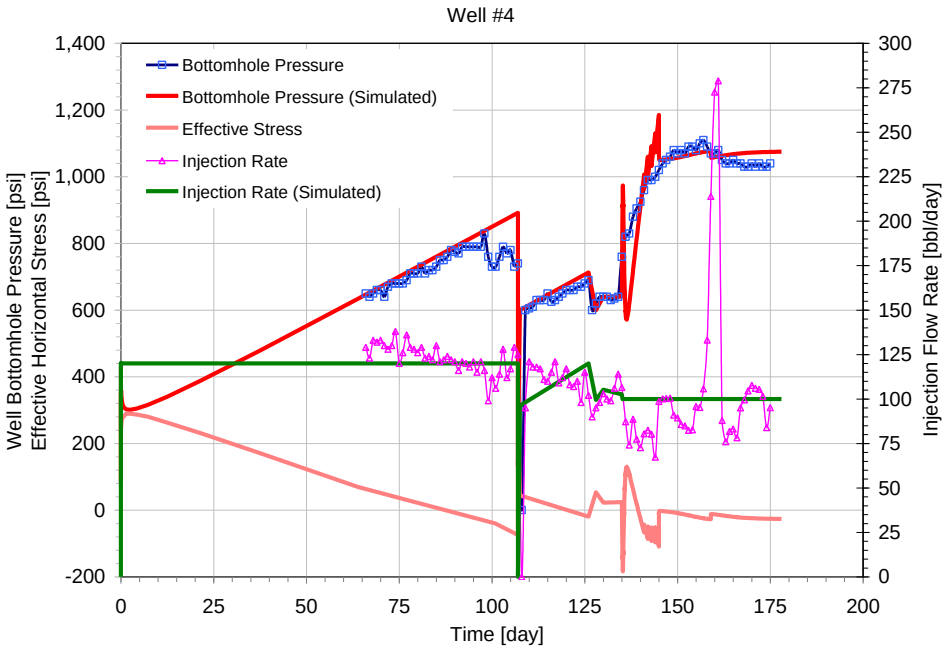

Figure 6.9: Field data comparison with simulated results of Well #4

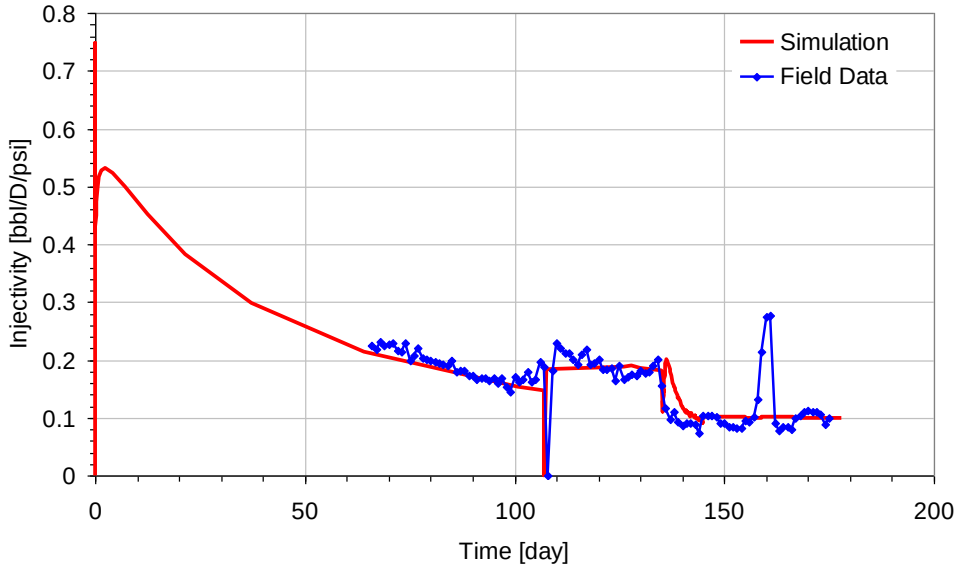

Figure 6.10: Field data (Injectivity) comparison with simulated results of Well #4

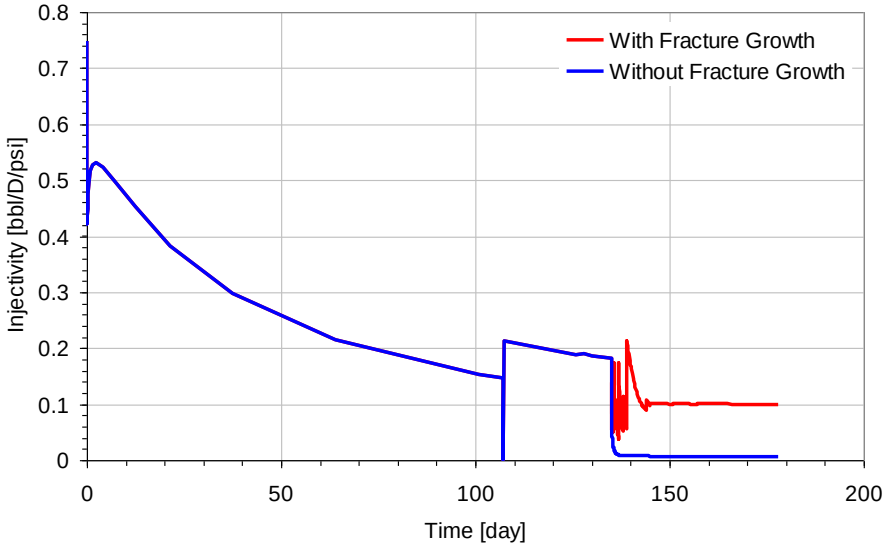

Figure 6.11: Impact of dynamic fracture growth on well injectivity, Newtonian polymer, polymer viscosity 27 cp

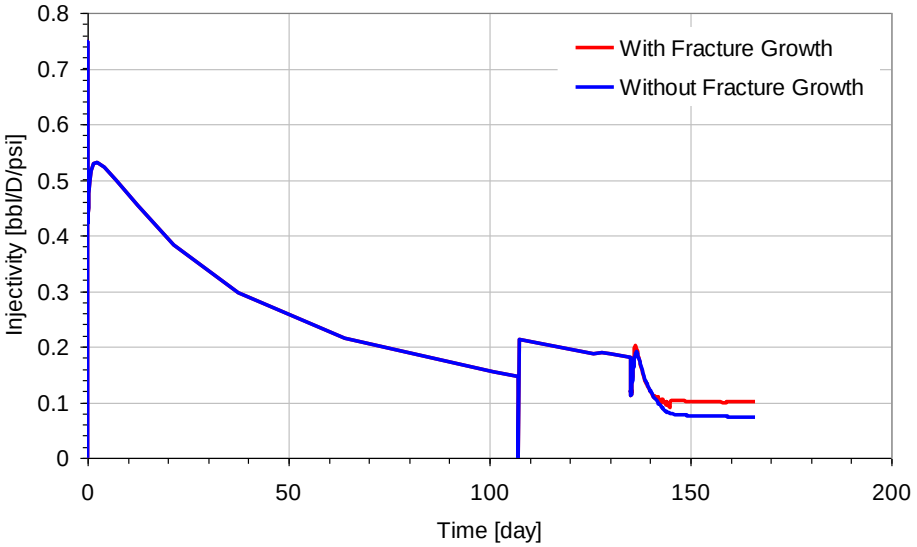

Figure 6.12: Impact of dynamic fracture growth on well injectivity, unified polymer model: Flopaam 3330S polymer viscosity vs. shear rate (1500 ppm; 1.6 % NaCl; 25 ºC)

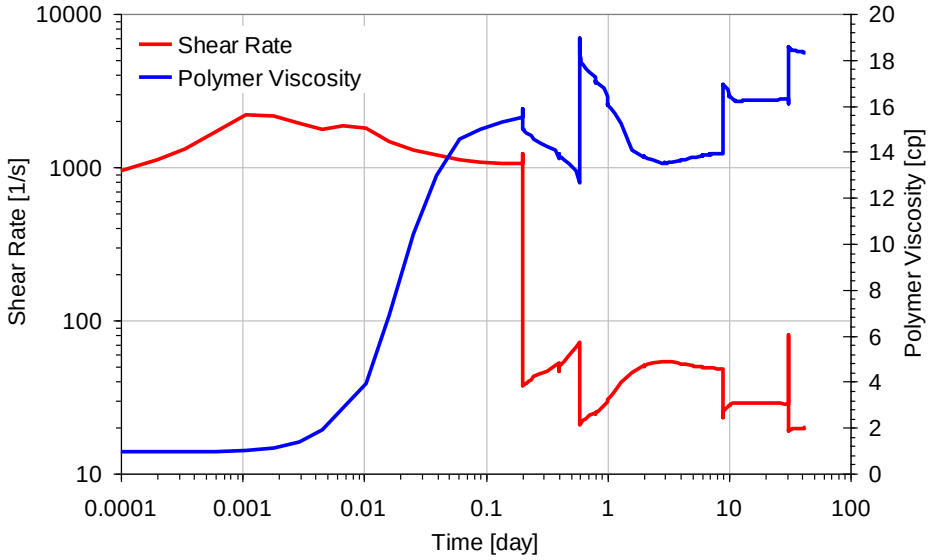

Figure 6.13: Relation between shear rate and polymer viscosity, unified polymer model: Flopaam 3330S polymer viscosity vs. shear rate (1500 ppm; 1.6 % NaCl; 25 ºC)

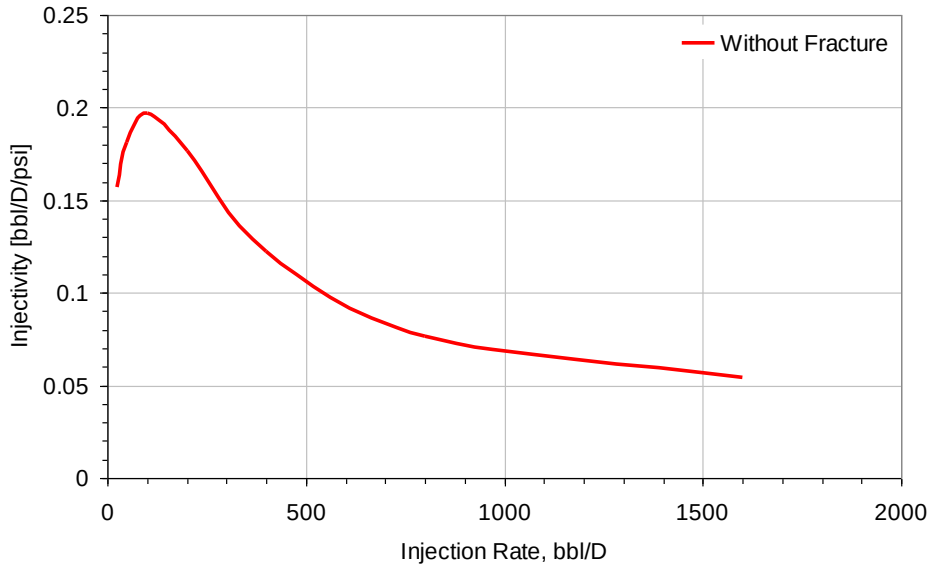

Figure 6.14: Injectivity with different injection rate, unified polymer model: Flopaam 3330S polymer viscosity vs. shear rate (1500 ppm; 1.6 % NaCl; 25 ºC)

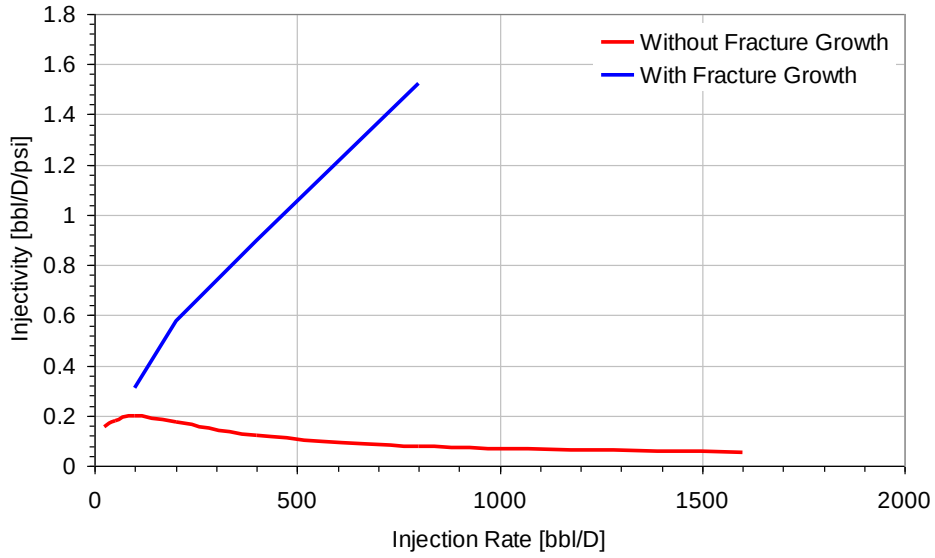

Figure 6.15: Injectivity with different injection rate with/without fracture growth, unified polymer model: Flopaam 330S polymer viscosity vs. shear rate (1500 ppm; 1.6 % NaCl; 25 ºC)

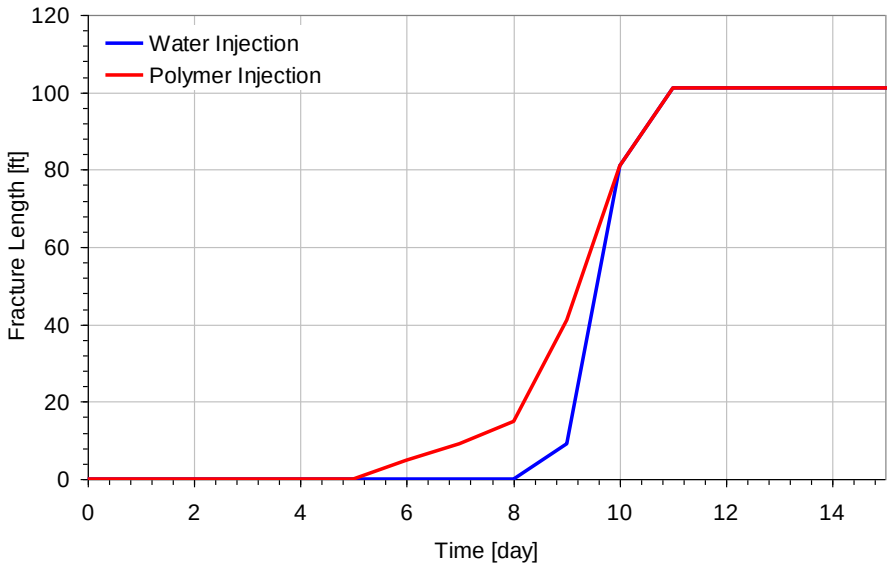

Figure 6.16: Fracture growth during water and polymer injection, unified polymer model: Flopaam 330S polymer viscosity vs. shear rate (1500 ppm; 1.6 % NaCl; 25 ºC)

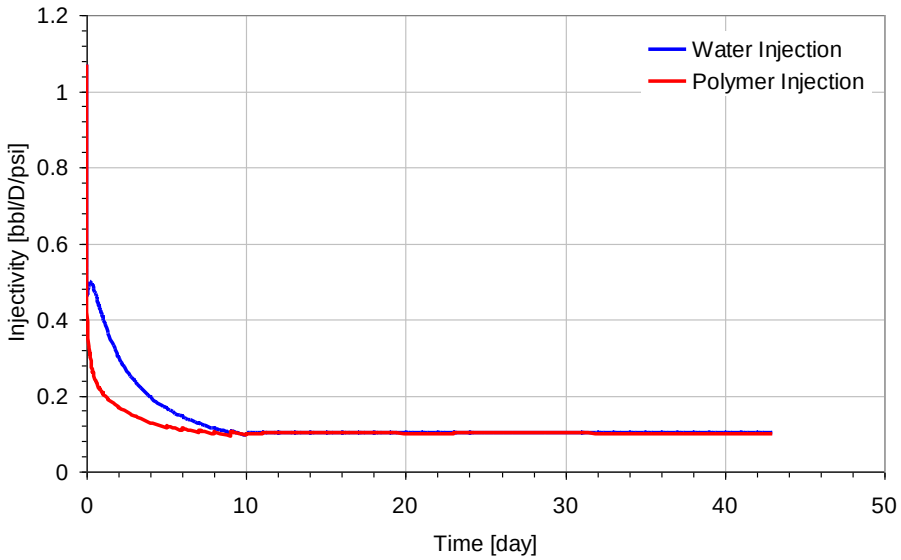

Figure 6.17: Injectivity decline during water and polymer injection, unified polymer model: Flopaam 3330S polymer viscosity vs. shear rate (1500 ppm; 1.6 % NaCl; 25 ºC)

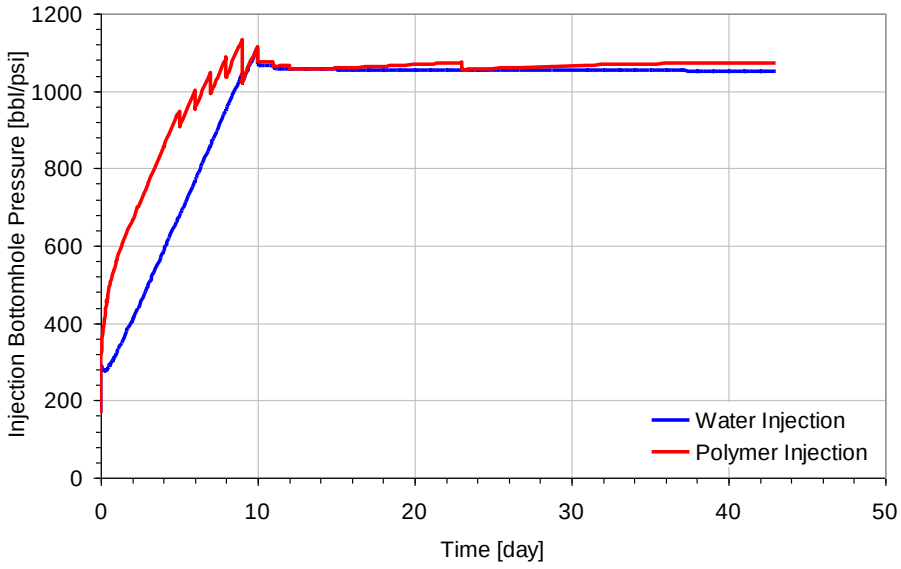

Figure 6.18: Injection BHP increase during water and polymer injection, unified polymer model: Flopaam 3330S polymer viscosity vs. shear rate (1500 ppm; 1.6 % NaCl; 25 ºC)

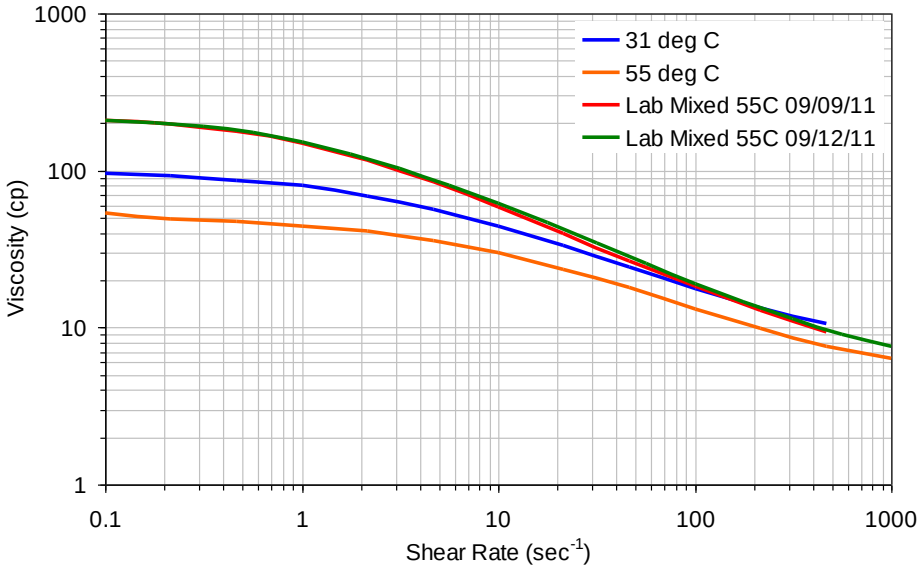

Figure 6.19: Shear rate dependent polymer viscosity with different temperature and shear rate

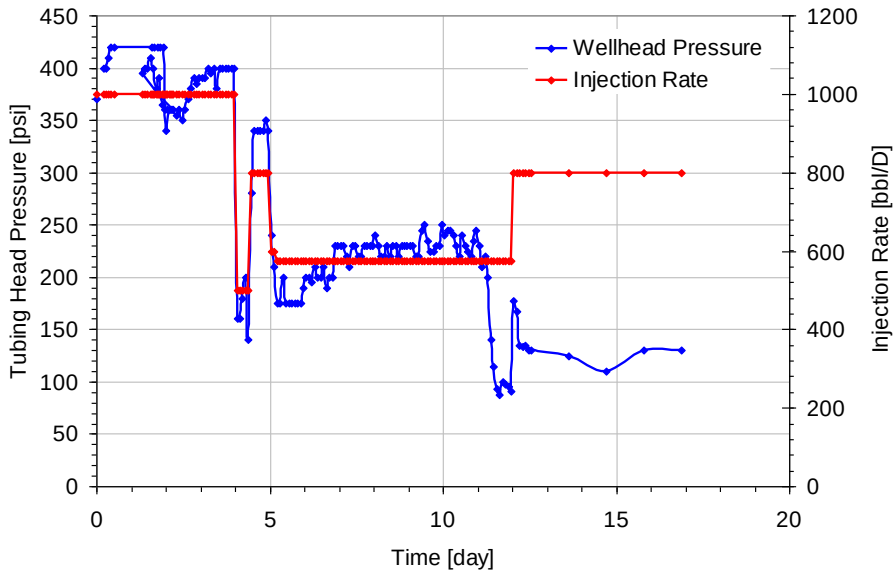

Figure 6.20: Shear rate dependent polymer viscosity with different temperature and shear rate

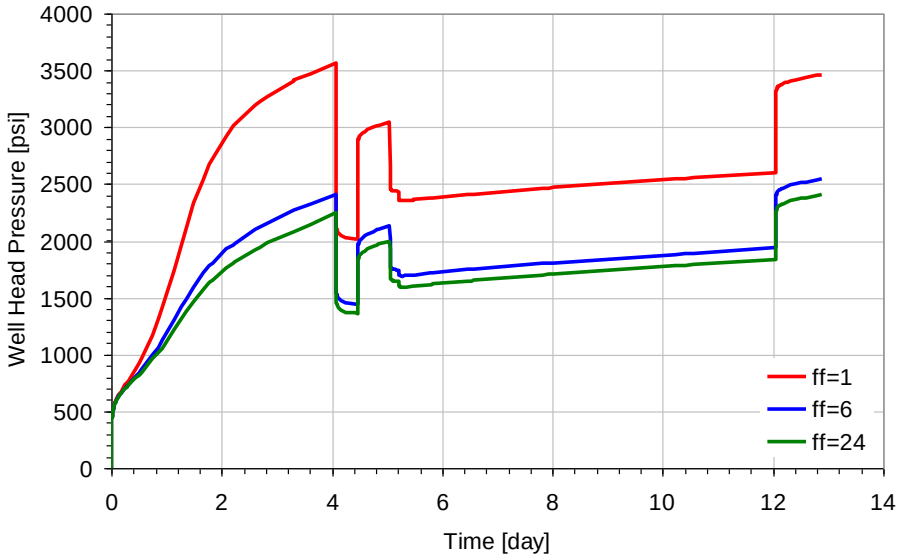

Figure 6.21: Well Head Pressure with various perforation densities

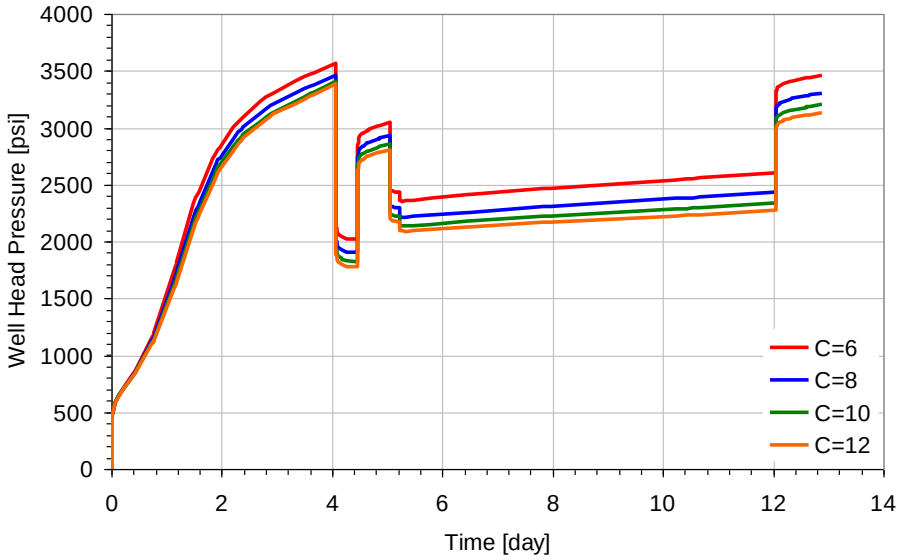

Figure 6.22: Impact of shear rate coefficient on well head pressure

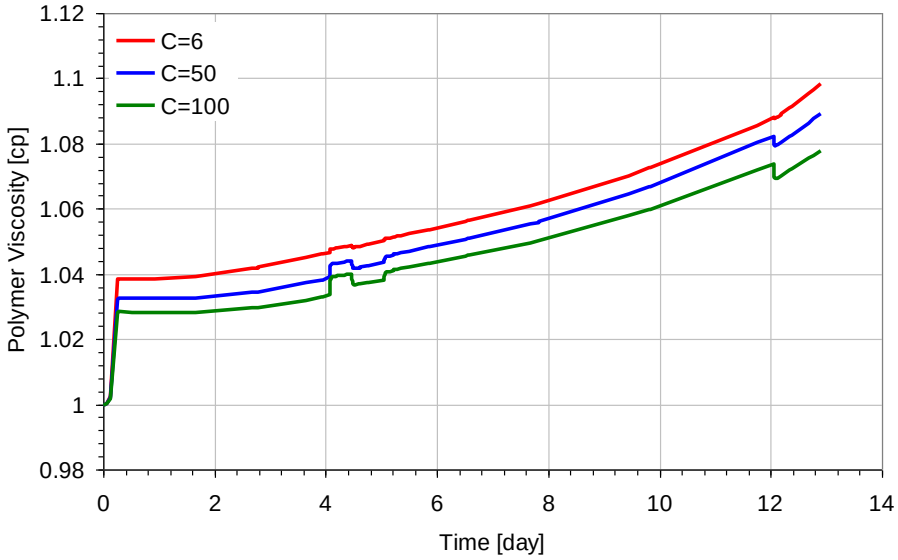

Figure 6.23: Impact of shear rate coefficient on polymer viscosity

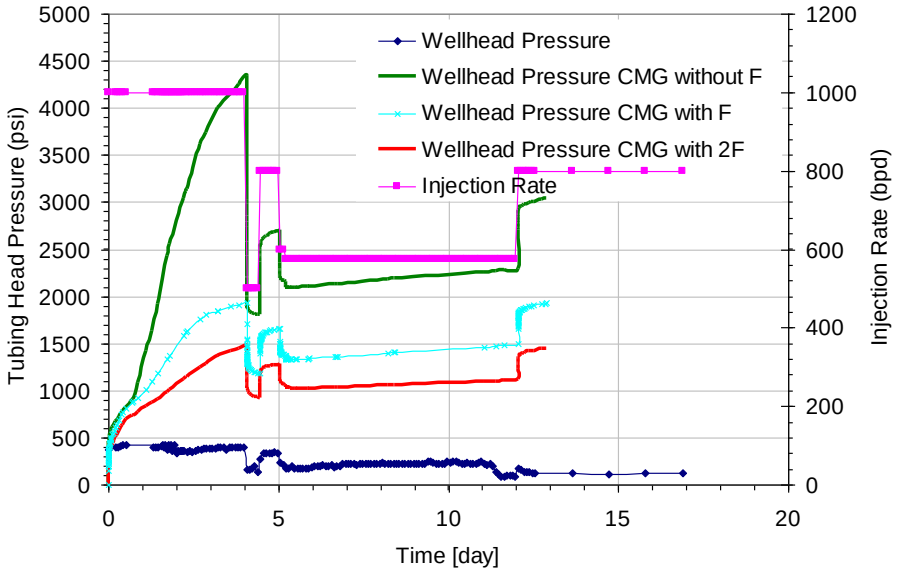

Figure 6.24: Tubing head pressure and injection rate during polymer injection with difference C value and fracture

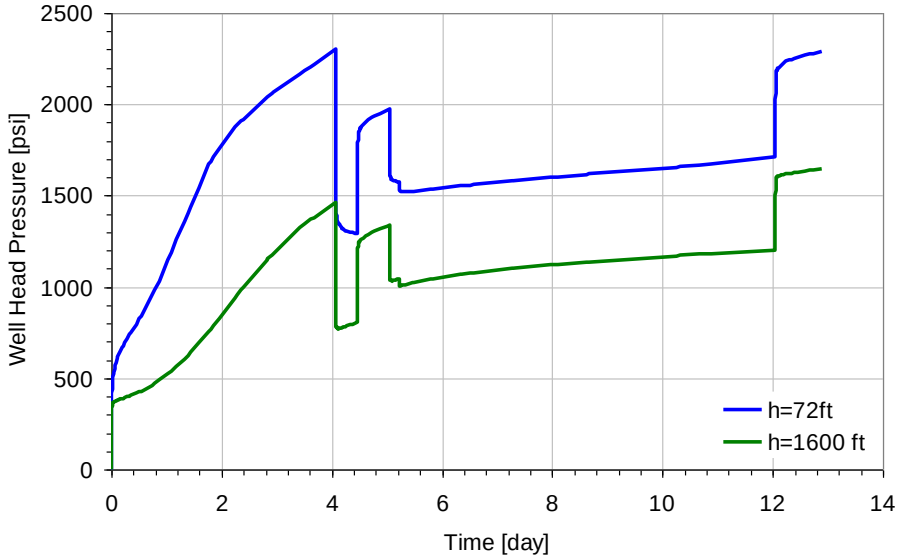

Figure 6.25: Impact of reservoir thickness on well head pressure

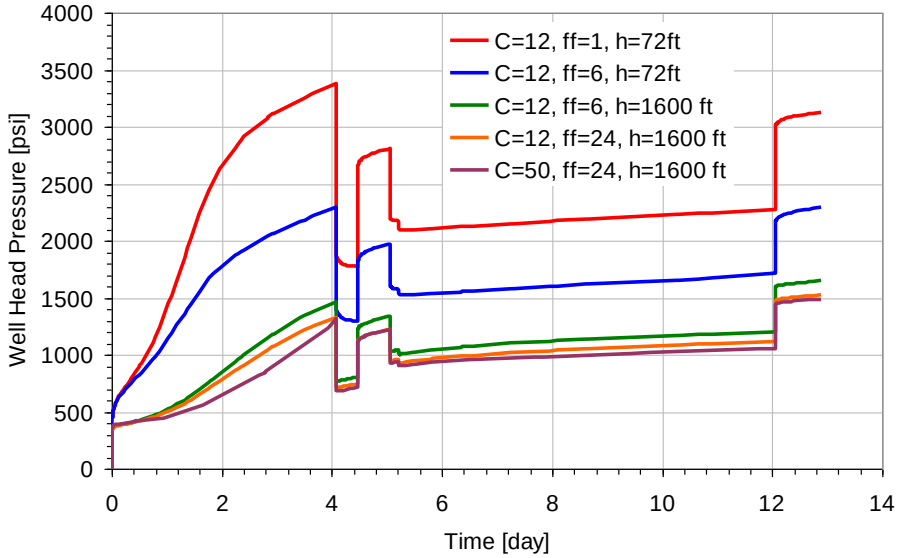

Figure 6.26: Impact of shear rate coefficient, perforation density, and reservoir thickness

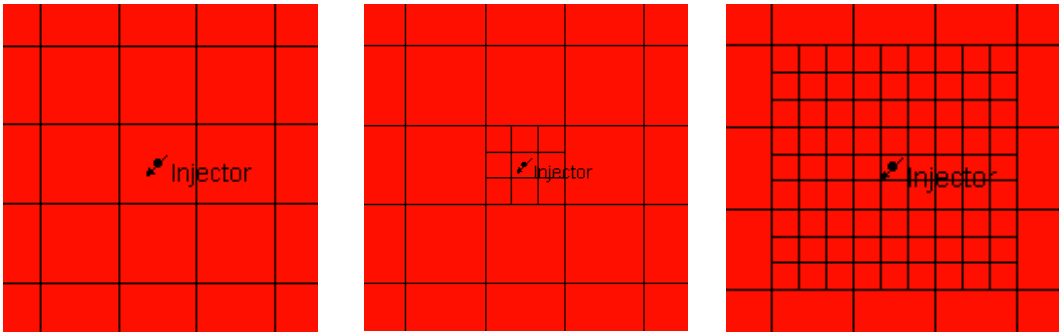

Figure 6.27: Grid block refinement near injector

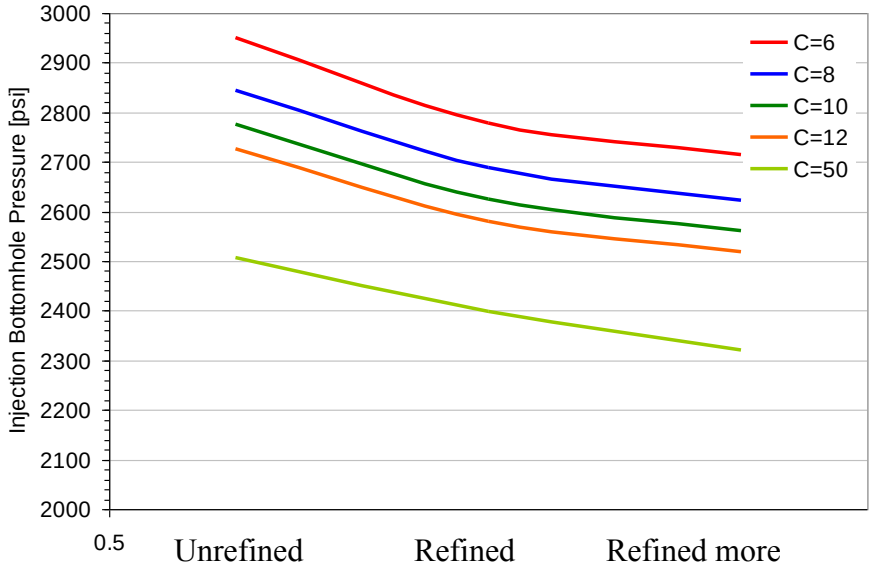

Figure 6.28: Impact of grid block refinement on injection BHP

Unrefined

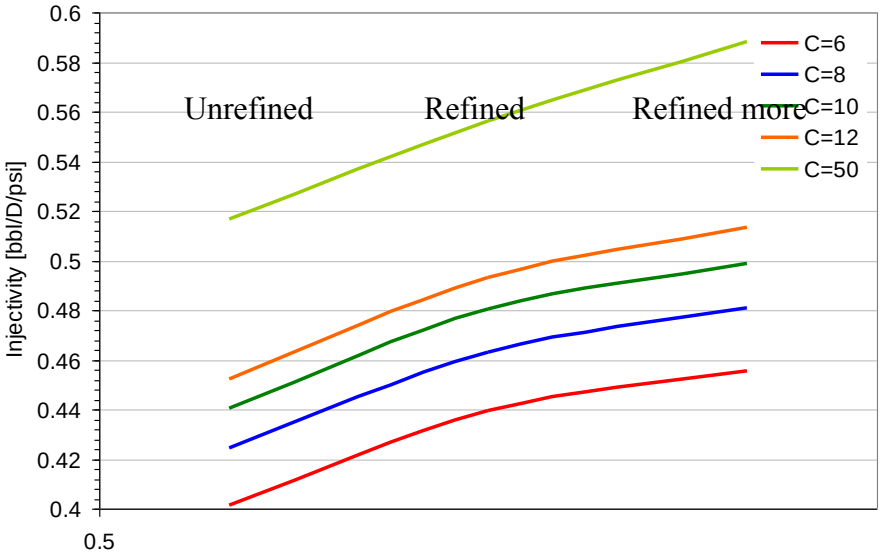

Figure 6.29: Impact of grid block refinement on well injectivity during polymer injection

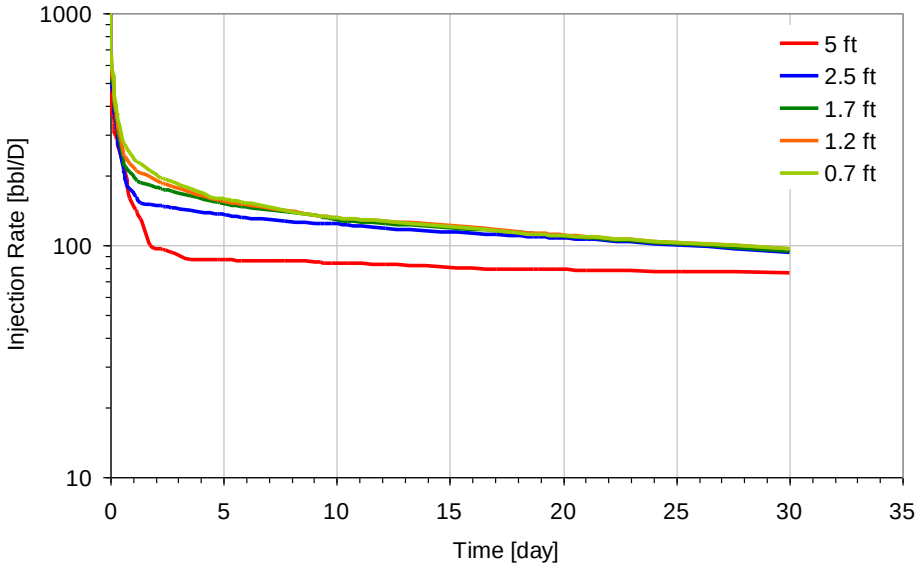

Figure 6.30: Impact of grid block size on polymer injection rate

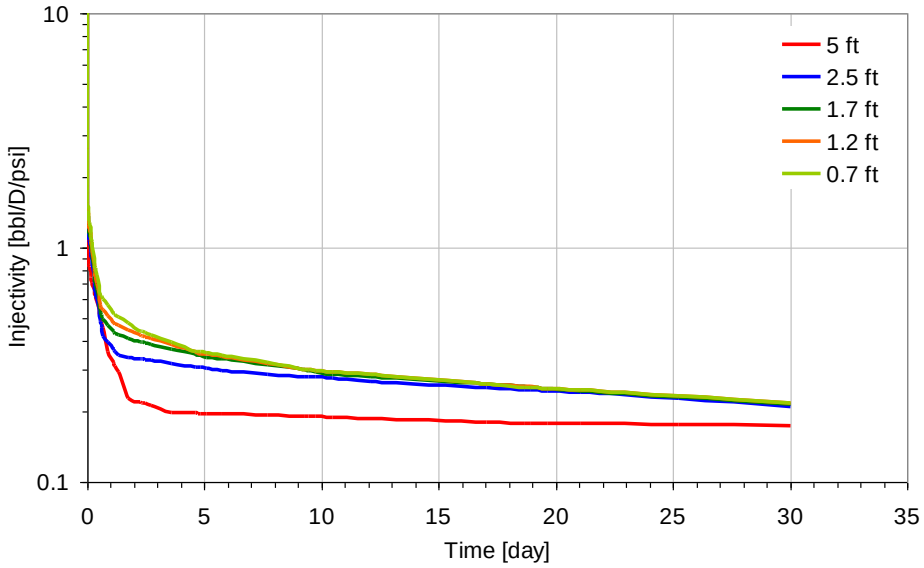

Figure 6.31: Impact of grid block size on well injectivity during polymer injection

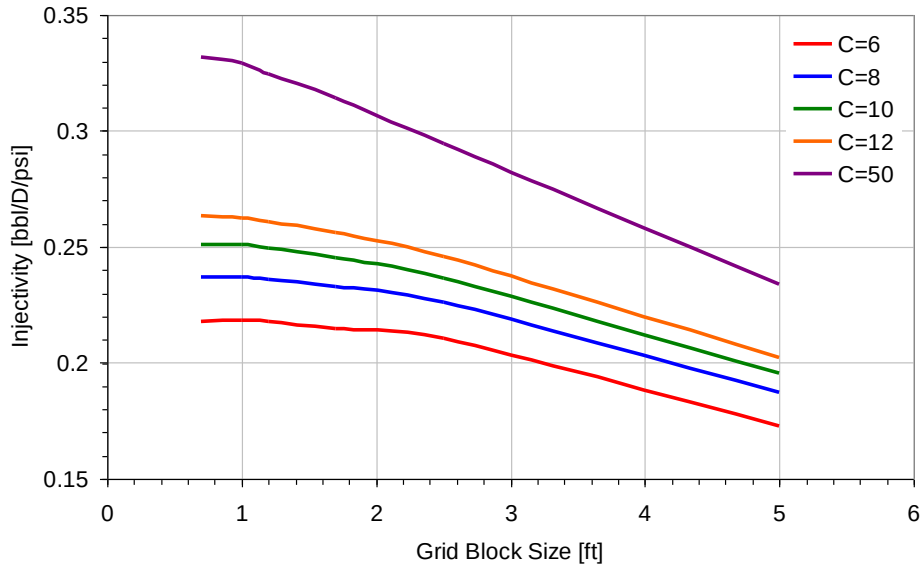

Figure 6.32: Impact of grid block size and shear rate coefficient on well injectivity during polymer injection

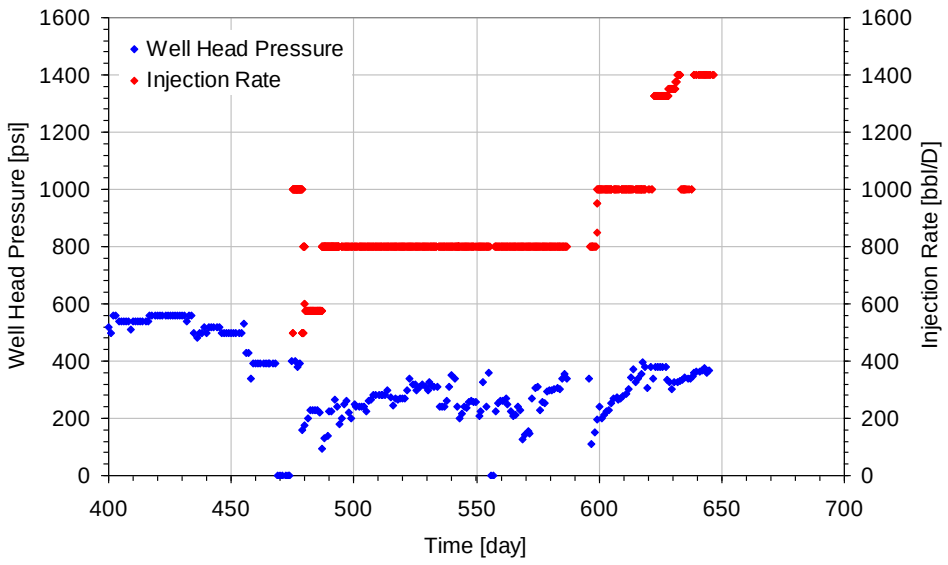

Figure 6.33: Injection Rate and well head pressure field data in Brookshire Dome Field

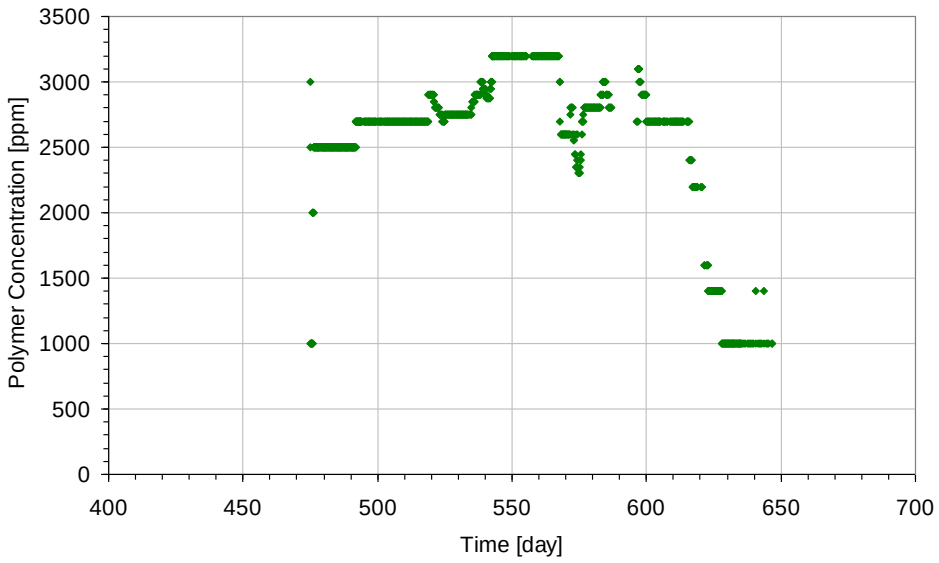

Figure 6.34: Polymer concentration profile in Brookshire Dome Field

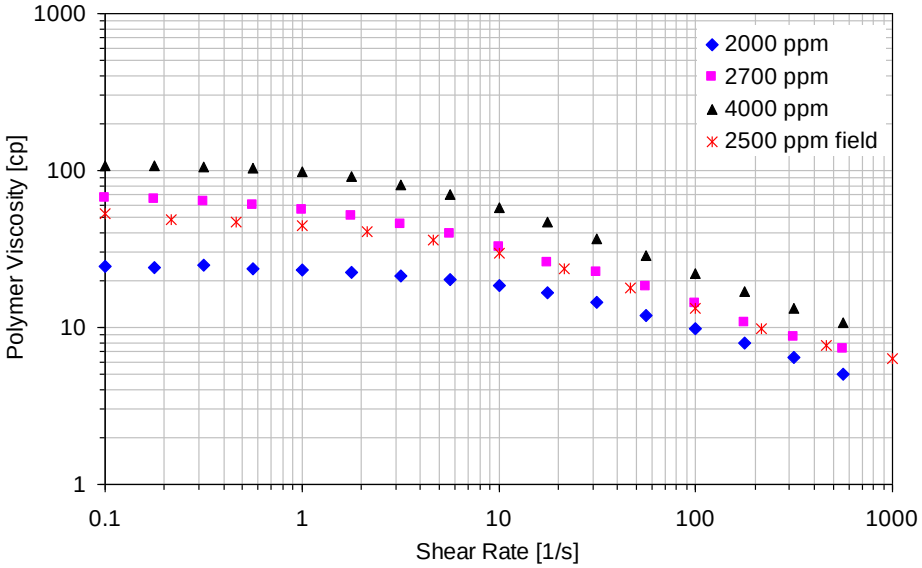

Figure 6.35: Shear rate dependent polymer viscosity with different polymer concentration

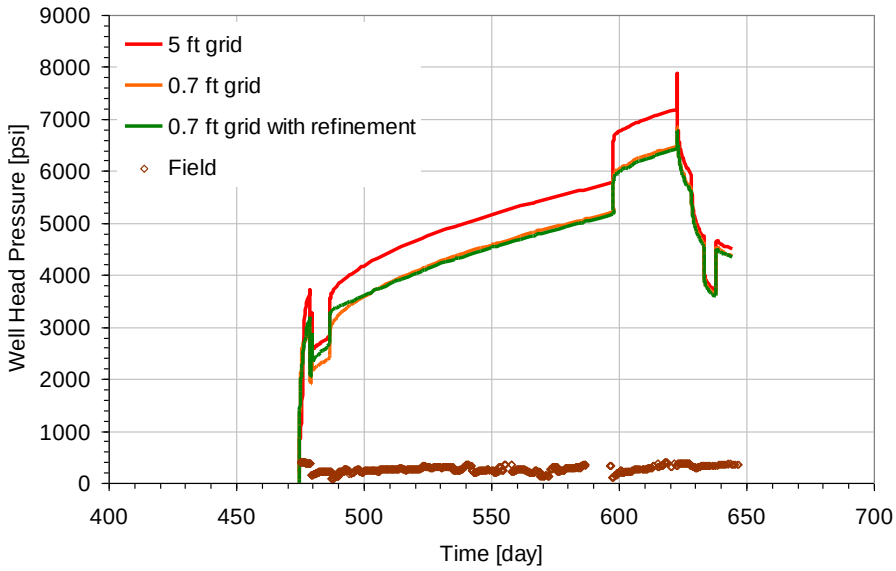

Figure 6.36: Well head pressure with different grid block sizes

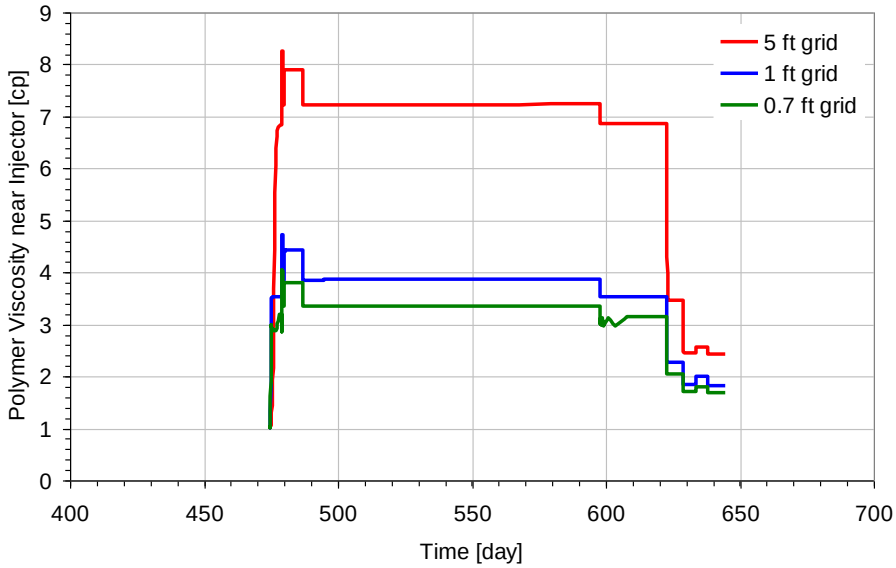

Figure 6.37: Polymer viscosity near injector with different grid block sizes

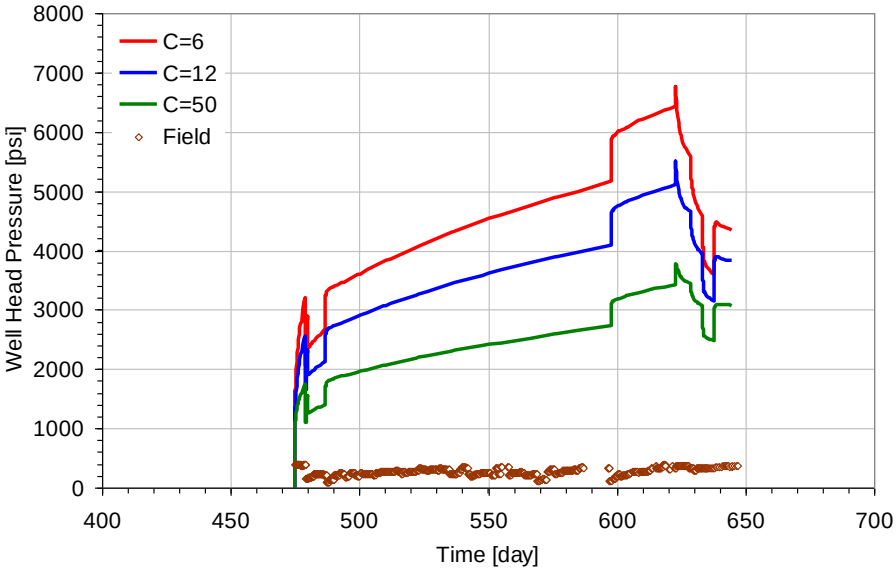

Figure 6.38: Wellhead pressure with different shear rate coefficients

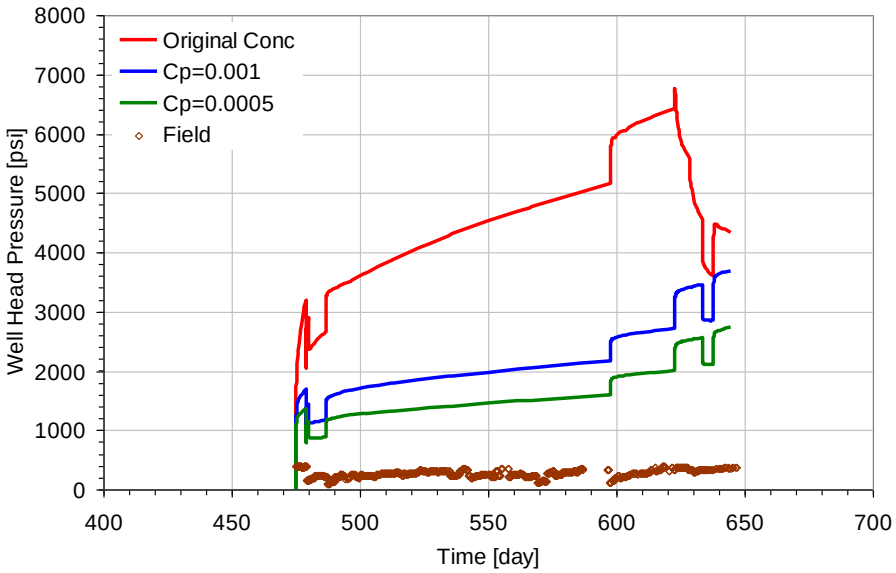

Figure 6.39: Wellhead pressure with different polymer concentrations

Chapter 7: Conclusions and Recommendations for Future Work

7.1 CONCLUSION

Fractures can be initiated and propagated during water and polymer injection. Particle plugging during water injection causes injectivity to decline, which induces fracture generation and growth. To improve sweep efficiency, polymer injection can be used to improve oil recovery. The injection of a high-viscosity polymer may decrease injectivity, which facilitates fracture initiation and growth during polymer injection. Our ability to simulate fracture generation and growth is critical in all aspects of reservoir simulation. So far, fracture generation and growth during water and shear rate dependent polymer injection have not been studied in great detail. In this dissertation we combine a fracture growth model that can model fracture generation and growth during water and shear rate dependent polymer injection with a reservoir simulator to investigate the impact of fracture growth on oil recovery. Important parameters that affect the performance of a waterflood or a polymer flood are identified. These include: fracture orientation, reservoir heterogeneity, particle concentration in the injected water, polymer concentration, and polymer rheology.

The problem of polymer injectivity has been studied in some detail in this research. Several parameters which can affect well injectivity such as polymer rheology, fracture length/conductivity, reservoir heterogeneity, and particle concentration have been investigated. It is found that despite accounting for polymer rheology and fracture

growth several questions remain about how polymer flow in porous media should be simulated.

Chapter 2 presents a model for particulate plugging during water injection, and shear rate dependent polymer behavior during polymer injection; it describes particle deposition in porous media during water injection, and shear-thinning and shear-thickening behavior during polymer injection. Even though the concentration of particles or oil droplets is usually small (about 20 ppm), the impact of particle trapping on porosity and permeability is significant after an extended period of injection. Reduced porosity and permeability increase injection BHP during water injection. The high fluid viscosity during polymer injection also increases injection BHP. When the injection rate is high enough to show shear-thickening behavior near the injector, polymer viscosity can increase significantly, and this also increases injection BHP. To investigate the impact of injection well fractures on well injectivity and reservoir sweep during waterflooding and chemical EOR processes, Chapter 3 investigates water injection and polymer injection in the presence of a static injection well fracture. The investigation includes a study of the sensitivity of oil recovery, injectivity and oil cut to several parameters: static fracture length, injection rate, degree of shear rate dependence, and fracture conductivity. The simulations were done for a homogeneous (single-layer) reservoir and for a heterogeneous (two-layer) reservoir. Some key conclusions can be summarized as follows:

- A static fracture with favorable mobility ratio has a negligible effect on water breakthrough and oil recovery in a one-layer reservoir. However, when the mobility ratio is unfavorable, a fracture has a significant effect. In the presence

of a fracture, water breakthrough occurs earlier, and oil recovery is lower than without a fracture.

- The oil recovery and reservoir sweep with and without a fracture in a two-layer reservoir show significant differences. As the viscosity of the resident fluid in the reservoir increases, the flow distribution into the fractured layer decreases. For example, flow into the fractured layer is 95% with a 0.1 mobility ratio, whereas the flow allocation into the fractured layer is 55% with a mobility ratio of 10. A lower mobility ratio increases the effect of a static fracture on flow distribution in a two layer reservoir. This can significantly lower reservoir sweep and oil recovery.
- Particle plugging intensifies the impact of a static fracture in a two-layer reservoir on oil recovery and reservoir sweep. The flow allocation into the fractured layer is up to 99% of the injected fluid. Therefore, reservoir sweep in the un-fractured layer is minimal and most of oil in the un-fractured layer cannot be recovered unless a down-hole flow control device is installed. As a result, a static fracture in only one layer induces poor reservoir sweep and low oil recovery.
- Injectivity during polymer injection depends on polymer rheology because the mobility ratio between the injected polymer and oil in the reservoir is a function of injection rate and reservoir properties. Injectivity increases with increasing injection rate during injection of a shear-thinning polymer. As the degree of shear-thinning and the fracture conductivity increases, injectivity also increases.

- Viscoelastic fluid rheology, which shows shear-thinning behavior at low shear rate and shear-thickening behavior at high shear rate, affects well injectivity. In the high shear rate region, injectivity decreases with increasing injection rate due to shear-thickening behavior, but in the low shear rate region, well injectivity increases with increasing injection rate. High shear-rates, above several thousands psi, can be observed near wells injecting at reasonable injection rates, for example 20 bbl/D/ft. In such instances shear-thickening behavior and consequent high effective polymer viscosity will play an important role in determining the fracture generation.

To extend the study of the impact of injection well fractures during waterflooding and chemical EOR processes, Chapter 4 investigates dynamic fracture growth. This chapter models fracture initiation and growth during waterflooding and chemical EOR processes by introducing a fracture growth model. Particle plugging and shear-thickening behavior around a new fracture tip have been investigated; these phenomena are key factors for fracture propagation during continuous water and polymer injection. Key findings in Chapter 4 can be summarized as follows:

- Injectivity decline may be expected in all injectors due to particle plugging and/or high polymer viscosity. However, fracture growth in injection wells during water and polymer flooding results in well injectivity in the field that is much higher and more stable than would be predicted if fracture growth were not accounted for. This is primarily the result of fracture generation and growth. Shear-thickening behavior of polymers induces fast fracture growth, but this may not be manifested in lower injectivity.

- Injection of cold fluid intensifies the decrease of rock stress, which facilitates the fracture growth and increases injectivity. This is the well-known phenomenon of thermal fracturing that has been observed in many fields.
- Well injectivity with fracture growth is much higher than without fracture growth. The injectivity increases up to 5 times as high as the injectivity without fracture growth and the BHP stabilizes, and does not increase continuously, primarily due to fracture growth
- In homogeneous reservoirs, fracture growth does not have a significant impact on oil recovery and reservoir sweep. However, in layered reservoirs, fracture growth has a very significant effect on oil recovery and water cut. As a fracture grows in one layer, more and more injected fluid is injected into the fractured layer.

Chapter 5 explores the behavior of both longitudinal and transverse horizontal injection well fractures under static and dynamic conditions. In the case of static fractures with constant injection BHP, horizontal injection well fractures (both transverse and longitudinal) increase injectivity, thereby increasing the amount of injected fluid and the fraction of oil recovered. At a constant injection rate, horizontal injection well fractures increase injectivity, but do not significantly affect reservoir sweep or oil recovery. In the case of dynamic fractures, there is no fracture growth with constant injection BHP because injection rate decreases when the injection pressure increases up to the BHP constraint. However, the fracture is created and grows if the injection rate is held constant. This increases well injectivity and stabilizes the injection BHP. This chapter investigates the sensitivity of reservoir sweep, injectivity, and oil recovery to several

parameters: the size of transverse and longitudinal fractures, the number of transverse fractures along a horizontal injector, the conductivity of transverse and longitudinal fractures, the concentration of particles in injected water, and the arrangement within the reservoir of injector, producer, and WOC. These sensitivity studies are conducted with several combinations of the following constraints: constant injection BHP, constant injection rate, closed reservoir boundary, and open reservoir boundary.

- Horizontal injection well fractures increase injectivity and stabilize the injection pressures needed to inject at a given rate.
- The increase in injectivity with longitudinal fractures is generally more favorable than with transverse fractures.
- The number, the size, and the permeability of transverse/longitudinal fractures affect the well injectivity and the injection BHP. The increase in BHP for un-fractured horizontal wells is two times faster than a horizontal well with transverse fractures. The injectivity decreases faster when the fracture conductivity is lower.
- In the case of dynamic fractures, the dynamic fracture increases the well injectivity and stabilizes the injection BHP.
- The injectivity of fractured horizontal injectors decreases much more slowly with time than for vertical injectors.

In Chapter 6, history matches with field data were performed for two case studies. In Field Case study 1, the fracture growth model matches the field data well when growing fractures are considered. Injection conditions, such as the water quality and

polymer rheology, and reservoir conditions, such as rock stress distribution, reservoir permeability and porosity, have been estimated. In Field Case study 2, large differences in polymer injectivity between field data and model predictions were observed, when no fracture was assumed to be present. If a fracture was assumed to be present, the injectivity match was better but the differences were still significant.

In an attempt to improve the agreement between the simulations and the field data, the impact of shear rate coefficient in the polymer viscosity model, and grid block sizing on injectivity, was investigated with simulation. The grid block size is very important in assessing the injection BHP because the grid block size determines the shear rate of the polymer near the wellbore in radial flow. A very small (of the order of inches) grid block size is needed to accurately model polymer injection accurately. Smaller grid block sizes result in higher injectivities being computed.

A high shear rate coefficient (C) increases the estimated shear rate in the rock and results in more shear-thinning, i.e., lower polymer viscosity and injection BHP. This may be one reason for the discrepancy between the field observations and the simulations. Another possible reason is that our estimates of shear rate are incorrect because we are assuming that all the perforations are open. This may not be the case. If only a fraction of the perforations are open, this would result in a much higher shear rate near wellbore and provide a better match with the high injectivities observed in the field. More reliable methods for estimating shear rates in porous media are needed.

7.2 RECOMMENDATIONS FOR FUTURE WORK

To complete more realistic and generally applicable modeling of water and polymer injection and fracture generation and growth during injection, the following are some recommendations for future work:

1. Our understanding of polymer flow in porous media is incomplete. Injectivities obtained with the simulator are still too low compared to those observed in the field. Empirical fits to the field data can be obtained by adjusting estimates of the shear rate, but this is clearly not justified by theory. A better understanding of how laboratory measurements of polymer rheology should be applied to flow in porous media should be developed.
2. Simulation of shear rate dependent polymer injection into a heterogeneous reservoir requires a shear rate dependent polymer model. Some of the reservoir models relate the fluid velocity to polymer viscosity. This makes it very difficult to simulate injection into a heterogeneous reservoir where the porosity and permeability may be changing with time. It would be very useful instead to have the polymer viscosity depend on the shear rate (rather than fluid velocity).
3. Fracture growth has been modeled using a planar fracture growth model. It has been documented in the literature that these injection induced fractures can re-orient in response to changes in in-situ stresses (induced by injection and production). It may be important to take into account the changes in the stresses in the earth due to injection and production of fluids (poro-elastic stresses).

Abbreviations and Nomenclature

a_o	=	major semi-axis of the elliptical cool region
b_o	=	minor semi-axis of the elliptical cool region
C	=	polymer-specific empirical constant
d_g	=	grain diameter
d_p	=	particle diameter
F_{CD}	=	relative fracture conductivity
ff	=	partial completions factor
h	=	formation thickness / fracture height
k	=	matrix permeability
K	=	consistency index
k_{dp}	=	permeability reduction due to reduced porosity
k_{ds}	=	permeability reduction due to increased surface area
k_{dt}	=	permeability reduction due to increased tortuosity
k_f	=	fracture permeability
K_K	=	Kozeny constant
k_o	=	initial permeability
k_{rw}	=	water relative permeability
M	=	mobility ratio
n	=	power-law exponent
n_1	=	polymer-specific empirical constant
n_2	=	empirical constant
P_{btp}	=	bottom-hole pressure
P_P	=	pore pressure

P_{res} = reservoir pressure

S = total stress

S_S = specific surface area

S_w = water saturation

T = temperature

u = Darcy velocity

u_w = Darcy velocity of the polymer-containing water phase

w = fracture width

x_f = fracture half length

y = distance in y direction

α = polymer-specific empirical constant

α_P = Biot's poroelastic constant

β = damage factor

β = linear coefficient of thermal expansion

γ_{eff} = effective shear rate

$\dot{\gamma}_{fac}$ = shear rate factor

λ = polymer-specific empirical constant

λ_2 = empirical constant

μ_{app} = apparent viscosity

$\mu_{\max}$ = shear-thickening plateau viscosity

μ_p^o = limiting Newtonian viscosities at the low shear limit

μ_∞ = limiting Newtonian viscosities at the high shear limit

ν = Poisson's ratio

σ = effective stress

σ_d = specific deposit (volume of deposited particles per unit bulk volume)

$\Delta\sigma_{1T}$ = change (final-initial) in average interior stress perpendicular to the major axis of the ellipse resulting from a temperature difference ($T - T_R$) between the elliptical cylinder and the surroundings

$\Delta\sigma_{2T}$ = change (final-initial) in average interior stress parallel to the major axis of the ellipse resulting from a pressure difference ($T - T_R$) between the elliptical cylinder and the surrounding, psi

τ = tortuosity

τ_r = relaxation time for a polymer molecule

ϕ = porosity

ϕ_o = initial porosity

Bibliography

Aboousleiman, Y., Bai, M., and Roegiers, J.C.: "Thermoporoelastic Coupling in Hydraulic Fracturing", ISRM International Symposium – EUROCK 96 held in Turin, Italy, September 2-5, 1996.

Azeemuddin, M., Ghori, S.G., Saner, S., and Khan, M.N.: "Injection-Induced Hydraulic Fracturing in a Naturally Fractured Carbonate Reservoir: A Case Study from Saudi Arabia", SPE 73784 presented at 2002 SPE International Symposium & Exhibition on Formation Damage Control held in Lafayette, Louisiana, February 20-21, 2002.

Barkman, J.H. and Davidson, D.H.: "Measuring Water Quality and Predicting Well Impairment", *Journal of Petroleum Technology*, **24** (7): 865-873, 1972.

Cannella, W. J., Huh, C., and Seright, R. S.: "Prediction of Xanthan Rheology in Porous Media", SPE 18089 presented at the SPE Annual Technical Conference and Exhibition held in Houston, Texas, October 2-5, 1988.

Chavez, J.C., Carruthers, J., and McCurdy, P.: "Water Flooding Efficiency in a Scenario of Multiple Induced Fractures, an Applied Geomechanical Study", SPE 97526 presented at the SPE International Improved Oil Recovery Conference in Asia pacific held in Kuala Lumpur, Malaysia, December 5-6, 2005.

Delshad, M., Kim, D., Magbagbeola, O., Huh, C., and Pope, G.A.: "Mechanistic Interpretation and Utilization of Viscoelastic Behavior of Polymer Solutions for Improved Polymer-Flood Efficiency", SPE 113620 presented at the 2008 SPE Improved Oil Symposium held in Tulsa, Oklahoma, April 19-23, 2008.

Dikken, B.J. and Niko, H.: „Waterflood-Induced Fractures: A Simulation Study of Their Propagation and Effects on Waterflood Sweep Efficiency", SPE 16551 presented at Offshore Europe 87, Aberdeen, United Kingdom, September 8-11, 1987.

Fernando, R.H., Glass, J.E., and Burnett, D.A. "Extensional Viscosity Correlation with Mobility Control Buffer Flow Behavior in Berea Cores", SPE 13584 presented at the International Symposium on Oilfield and Geothermal Chemistry held in Phoenix, April 9-11, 1985.

Gadde, P.B. and Sharma, M.M.: "Growing Injection Well Fractures and their Impact on Waterflood Performance", SPE 71614 presented at the 2001 SPE Annual Technical Conference and Exhibition of SPE held in New Orleans, Louisiana, September 20-October 3, 2001.

Garrouch, A.A.: "A Viscoelastic Model for Polymer Flow in Reservoir Rocks", SPE 54379 presented at the 1999 SPE Asia Pacific Oil and Gas Conference and Exhibition held in Jakarta, Indonesia, April 20-22, 1999.

Genbao, Q., Xiaohui, J., and Hongmei, Z.: "Numerical Simulation Study of Water Injection Development in an Extra-low-permeability Fractured Reservoir, Xiaoguai Oilfield", SPE 64794 presented at the SPE International Oil and Gas Conference and Exhibition in China held in Beijing, China, November 7-10, 1999.

Han, X., Wang, W., and Xu, Y.: "The Viscoelastic Behavior of HPAM Solutions in Porous Media and its Effects on Displacement Efficiency", SPE 30013 presented at the International Meeting on Petroleum Engineering held in Beijing, PR China, November 14-17, 1995.

Heemskerk, J., Rosmalen, R.J., Holtslag, R.J., and Teeun, D.: "Quantification of Viscoelastic Effects of Polyacrylamide Solutions", SPE/DOE 12652 presented at the SPE/DOE Fourth Symposium on Enhanced Oil Recovery held in Tulsa, Oklahoma, April 15-18, 1984.

Huh, C. and Rossen, W.R.: "Approximate Pore-Level Modeling for Apparent Viscosity of Polymer-Enhanced Foam in Porous Media", *SPE Journal* **13** (1): 17-25, 2008.

Hustedt, B., Qui, Y., Zwarts, D., and van den Hoek, P.J.: "Modeling Water-Injection-Induced Fractures in Reservoir Simulation", SPE 95726 presented at the 2005 SPE Annual Technical Conference and Exhibition held in Dallas, Texas, October 9-12, 2005.

Hustedt, B., Zwarts, D., Bjoerndal, H.-P., Masfry, R., and van den Hoek, P.J.: "Induced Fraturing in Reservoir Simulations: Application of a New Coupled Simulator to Waterflooding Field Examples", SPE 102467 presented at the 2006 SPE Annual Technical Conference and Exhibition held in San Antonio, Texas, September 24-27, 2006.

Ji, L., Settari, A., Sullivan, R.B., and Orr, D.: "Methods for Modeling Dynamic Fractures in Coupled Reservoir and Geomechanics Simulation", SPE 90874 presented at the SPE Annual Technical Conference and Exhibition held in Houston, Texas, September 26-29, 2004.

Kuo, M.C.T., Hanson, H.G., and DesBrisay, C.L.: "Prediction of Fracture Extension during Waterflood Operations", SPE 12769 presented at the 1984 California Regional Meeting held in Long Beach, California, April 11-13, 1984.

Lee, K., Huh, C., and Sharma, M.M.: "Impact of Fracture Growth on Well Injectivity and Reservoir Sweep during Waterflood and Chemical EOR Processes", SPE 146778 presented at the 2011 SPE Annual Technical Conference and Exhibition held in Denver, Colorado, October 30-November 2, 2011.

Liu, J. and Seright, R.S.: "Rheology of Gels Used for Conformance Control in Fractures", SPE 59318 presented at the 2000 SPE/DOE Improved Oil Recovery Symposium held in Tulsa, Oklahoma, April 3-5, 2000.

Liu, Z., Yue, X., Hou, J., and Zhang, L.: "Comparison of Displacement Oil Mechanism of Polymer, ASP and Foam of ASP in Micro Pores and Dead Ends of Pores", SPE 77876 presented at the SPE Asia Pacific Oil and Gas Conference and Exhibition held in Melbourne, Australia, October 8-10, 2002.

Maerker, J.M. and Sinton, S.W.: "Rheology Resulting from Shear-induced Structure in Associating Polymer Solutions", *Journal of Rheology* **30** (1): 077-099, 1984.

Martini, R.F., Bonet, E.J., and Schiozer, D.J.: "Water Injection in Viscous Oil through Horizontal Well", SPE/PS-CIM/CHOA 97740 presented at the SPE International Thermal Operations and Heavy Oil Symposium held in Calgary, Alberta, Canada, November 1-3, 2005.

Mukherjee, H. and Economides, M.J.: "A Parametric Comparison of Horizontal and Vertical Well Performance", *SPE Formation Evaluation* **6** (2): 209-216, 1997.

Munoz Mazo, E.O., Montoya Moreno, J.M., and Schiozer, D.J.: "Study of Sweep Efficiency of Water Injection under Fracturing-Conditions Process", SPE 107846 presented at the 2007 SPE Latin American and Caribbean Petroleum Engineering Conference held in Buenos Aires, Argentina, April 15-18, 2007.

Owens, K.A., Andersen, S.A., and Economides, M.J.: "Fracturing Pressures for Horizontal Wells", SPE 24822 presented at the 67th SPE Annual Technical Conference and Exhibition held in Washington, DC, October 4-7, 1992.

Pang, S. and Sharma, M.M.: "A Model for Predicting Injectivity Decline in Water Injection Wells", *SPE Formation Evaluation* **12** (3): 194-201, 1997.

Perkins, T.K. and Gonzalez, J.A.: "The Effect of Thermoelastic Stresses on Injection Well Fracturing", *SPE Journal* **25** (1): 78-88, 1985.

Ranjbar, M., Rupp, J., Pusch, G., and Meyn, R.: "Quantification and Optimization of Viscoelastic Effects of Polymer Solutions for Enhanced Oil Recovery", SPE/DOE 24154 presented at the SPE/DOE Eighth Symposium on Enhanced Oil Recovery held in Tulsa, Oklahoma, April 22-24, 1992.

Robinowitz, S. and Weyland, H.V.: "Enhance Oil Recovery with Horizontal Waterflooding, Osage County, Oklahoma", SPE 89373 presented at the 2004 SPE/DOE Fourteenth Symposium on Improved Oil Recovery held in Tulsa, Oklahoma, April 17-21, 2004.

Rod, M.H. and Jorgensen, O.: "Injection Fracturing in a Densely Spaced Line Drive Waterflood – The Halfdan Example", SPE 94049 presented at the SPE Europec/EAGE Annual Conference held in Madrid, Spain, June 13-16, 2005.

Saripalli, P.K., Bryant, S.L., and Sharma, M.M.: "Role of Fracture Face Plugging in Injection Well Fracturing and Injectivity Decline", SPE 52731 presented at the 1999 SPE/EPA Exploration and Production Environmental Conference held in Austin, Texas, February 28-March 3, 1999.

Schechter, R.S.: "Oil Well Stimulation", 262. Englewood Cliffs, New Jersey, USA: Prentice-Hall, 1992.

Sharma, A.: "Assessment of Polymer Injectivity during Chemical Enhanced Oil Recovery Process", MS Thesis, The University of Texas at Austin, December 2010.

Sharma, M.M., Pang, S., Wennberg, K.E., and Morgenthaler, L.N.: "Injectivity Decline in Water Injection Wells-An Offshore Gulf of Mexico Case Study", SPE 38180 presented at the SPE European Formation Damage Conference held in Hague, Netherlands, June 2-3, 1997.

Soliman, M.Y. and Boonen, P.: "Review of Fractured Horizontal Wells Technology", SPE 36289 presented at the SPE Asia Pacific Oil and Gas Conference and Exhibition held in Kuala Lumpur, Malaysia, April 14-16, 1997.

Sorbie, K.S.: "Polymer-Improved Oil Recovery", Blackie and Son Ltd, Glasgow, 1991.

Souza, A.L.S., Fernandes, P.D., Mendes, R.A., Rosa, A.J., and Furtado, C.J.A.: "The Impact of Injection with Fracture Propagation during Waterflooding Process", SPE 94704 presented at the SPE Latin American and Caribbean Petroleum Engineering Conference held in Rio de Janeiro, Brazil, June 20-23, 2005.

Suarez-Rivera, R., Stenebraten, J., Gadde, P.B., and Sharma, M.M.: "An Experimental Investigation of Fracture Propagation during Water Injection", SPE 73740 presented at the SPE International Symposium and Exhibition on Formation Damage Control held in Lafayette, Louisiana, February 20-21, 2002.

Suri, A. and Sharma, M.M.: "A Model for Water Injection into Frac-Packed Wells", SPE 110084 presented at the SPE Annual Technical Conference and Exhibition held in Anaheim, California, November 11-14, 2007.

Suri, A. and Sharma, M.M.: "Fracture Growth in Horizontal Injectors", SPE 119379 presented at the SPE Hydraulic Fracturing Technology Conference, Woodlands, Texas, January 19-21, 2009.

Taber, J.J. and Seright, R.S.: "Horizontal Injection and Production Wells for EOR or Waterflooding", SPE 23952 presented at the 1992 SPE Permian Basin Oil and Gas Recovery Conference held in Midland, Texas, March 18-20, 1992.

Taber, J.J. and Martin, F.D.: "EOR Screening Criteria Revisited – Part 1: Introduction to Screening Criteria and Enhanced Recovery Field Projects", *SPE Reservoir Engineering* **12** (3): 189-198, 1997.

Van den Hoek, P.J., Matsuura, T., de Kroon, M., and Gheissary, G.: "Simulation of Produced Water Re-Injection under Fracturing Conditions", SPE 36846 presented at the SPE European Petroleum Conference held in Milan, Italy, October 22-24, 1996.

Van den Hoek, P.J.: "Impact of Induced Fractures on Sweep and Reservoir Management in Pattern Floods", SPE 90968 presented at the SPE Annual Technical Conference and Exhibition held in Houston, Texas, September 26-29, 2004.

Van den Hoek, P.J., Al-Masfry, R., Jansen, J.D., Hustedt, B., and van Schijndel, L.: "Waterflooding under Dynamic Induced Fractures: Reservoir Management and Optimization of Fractured Waterfloods", SPE 110379 presented at the SPE/DOE Improved Oil Recovery Symposium held in Tulsa, Oklahoma, April 19-23, 2008.

Van den Hoek, P.J., Matsuura, T., de Kroon, M., and Gheissary, G.: "Simulation of Produced Water Re-Injection under Fracturing Conditions", SPE 36846 presented at the SPE European Petroleum Conference held in Milan, Italy, October 22-24, 1996.

Vossoughi, S.: "Profile modification using in situ gelation technology-a review", *Journal of Petroleum Science and Engineering* **26**: 199-209, 2000.

Wang, D., Cheng, J., Yang, Q., Gong, W., Li, Q., and Chen, F.: "Viscous-Elastic Polymer Can Increase Microscale Displacement Efficiency in Cores", SPE 63227 presented at the 2000 SPE Annual Technical Conference and Exhibition held in Dallas, Texas, October 1-4, 2000

Wang, D., Han, P., Shao, Z., Chen, J., and Seright, R.S.: "Sweep Improvement Options for the Daqing Oil Field", SPE 99441 presented at the 2006 SPE/DOE Symposium on Improved Oil Recovery held in Tulsa, Oklahoma, April 22-26, 2006.

Wang, D., Seright, R. S., Shao, Z., and Wang, J.: "Key Aspects of Project Design for Polymer Flooding", SPE 109682 presented at the SPE Annual Technical Conference and Exhibition held in Anaheim, California, November 11-14, 2007.

Westermark, R.V., Schmeling, J., Dauben, D.L., Robinowitz, S., Weyland, H.V.: "Application of Horizontal Waterflooding to Improve Oil Recovery from Old Oil Fields", SPE 99668 presented at the 2006 SPE/DOE Symposium on Improved Oil Recovery held in Tulsa, Oklahoma, April 22-26, 2006.

Wright, C.A., Weijers, L., Davis, E.J., and Mayerhofer, M.: "Understanding Hydraulic Fracture Growth: Tricky but Not Hopeless", SPE 56724 presented at the 1999 Annual Technical Conference and Exhibition in Houston, Texas, October 3-6, 1999.

Xia, H., Yue, X., Wang, D., Li, Q., and Zhang, X.: "Prediction of IPR Curve of Oil Wells in Visco-Elastic Polymer Solution Flooding Reservoirs", SPE 72122 presented at the SPE Asia Pacific Improved Oil Recovery Conference held in Kuala Lumpur, Malaysia, October 8-9, 2001.

Xia, H., Wang, D., Wu, J., Kong, F.: "Elasticity of HPAM Solutions Increases Displacement Efficiency under Mixed Wettability Conditions", SPE 88456 presented at the SPE Asia Pacific Oil and Gas Conference and Exhibition held in Perth, Australia, October 18-20, 2004.

Yang, F., Wang, D., Yang, X., Sui, X., Chen, Q., and Lei, Z.: "High Concentration Polymer Flooding is Successful", SPE 88454 presented at the SPE Asia Pacific Oil and Gas Conference and Exhibition held in Perth, Australia, October 18-20, 2004.

Yang, F., Wang, D., Wu, W., Wu, J., Liu, W., Kan, C., and Chen, Q.: "A Pilot Test of High-Concentration Polymer Flooding to Further Enhance Oil Recovery", SPE 99354 presented at the 2006 SPE/DOE Symposium on Improved Oil Recovery held in Tulsa, Oklahoma, April 22-26, 2006.

Yew, C.H., Liu, G.F., "The Fracture Tip and Critical Stress Intensity Factor of a Hydraulically Induced Fracture", SPE production & Facilities ***8*** (3): 171-177, 1993.

Yin, H., Wang, D., and Zhong, H., "Study on Flow Behaviors of Viscoelastic Polymer Solution in Micropore with Dead End", SPE 101950 presented at the 2006 SPE Annual Technical Conference and Exhibition held in San Antonio, Texas, September 24-27, 2006

.

Yu, M., Gadde, P., and Sharma, M.M.: "Process-Based Decomposition on Distributed Systems-A Strategy to Solve Large Scale Simulation Problems", SPE 77721 presented at the SPE Annual Technical Conference and Exhibition held in San Antonio, Texas, September 29-October 2, 2002.

Zerpa, L.E., Queipo, N.V., Pintos, S., and Salager, J.L.: "An Optimization Methodology of Alkaline-Surfactant-Polymer Flooding Processes using Field Scale Numerical Simulation and Multiple Surrogates", *Journal of Petroleum Science and Engineering* **47** (3-4): 197-208, 2005.